Thèse de doctorat

Pour obtenir le grade de Docteur de Mécanique

UNIVERSITE POLYTECHNIQUE HAUTS-DE-FRANCE

par Andrés MALO-ESTEPA

Soutenue le 18 Décembre 2018 à Valenciennes

Ecole doctorale Sciences Pour l'Ingénieur (ED SPI 072)

Laboratoire d'Automatique, de Mécanique et d'Informatique Industrielles et Humaines, LAMIH - UMR 8201

Numéro d'ordre: 18/45

Prise en compte de la variabilité des caractéristiques de suspension d'un bogie pour l'optimisation des opérations de maintenance

JURY

Président du jury: FOND, Christophe. Professeur des Universités. Université de Strasbourg

Rapporteur: AUBRY, Evelyne. Professeur des Universités. ENSISA - Université de Haute Alsace
Rapporteur: MÉO, Stéphane. Professeur des Universités. Université François Rabelais de Tours

Co-directeur de thèse : BOUKAMEL, Adnane. Directeur Scientifique. IRT Railenium
Co-directeur de thèse : TISON, Thierry. Professeur des Universités. UPHF - LAMIH
Co-encandrant de thèse : MASSA, Franck. Maître de Conférences. UPHF - LAMIH

Membre invité: WOLF, Andreas. Senior suspension engineer. Bombardier Transportation
Membre invité: CHAMPAGNE, Philippe. Maître de Conférences. UPHF - LMCPA

Acknowledgements

The acknowledgements page is perhaps the space on a manuscript where one can find some of traits of the person behind the writing. A PhD is rarely a single person's endeavour, but rather the community of many efforts, I hope that these words may recall and thank all the people which have contributed to the achievement of the project.

This PhD has been a joint undertaken between Bombardier Transportation, the LAMIH laboratory of the Université Polytechnique Hauts-de-France in Valenciennes and the IRT Railenium. I would like to thank them all for their technical and financial support, as well as the FEDER funding, which made the thesis possible.

I would like to address my gratitude to Professor Christophe Fond, who has honoured me by chairing the Jury as its President, as well as for his remarks and suggestions during the subsequent discussion. I would like to thank Professor Evelyne Aubry and Professor Stéphane Méo for accepting to report and evaluate my research works. Their thorough reports, accurate questions and scientific rigour enriched the discussions during the jury and pointed out possible subjects of interest for future works. I am grateful to all of them for "braving" the reviewing of the manuscript without faltering, in spite of its length.

Should someone have asked me whether I would undertake a PhD some four years ago, my answer would have been "no way". Yet sometimes it is a matter of gathering the right pieces together: a thrilling subject and sound, watching advisors and reliable partners.

It is with my warmest gratitude that I would like to thank my three advisors for their unfaltering support during these three years. Dr. Adnane Boukamel for thinking of me and trusting my skills to undertake this works. His patience and availability in spite of a heavily loaded schedule made me change my mind over elastomers and get a new taste of them. This gratitude is equally shared with Professor Thierry Tison, who accepted embarking on this endeavour. I strongly appreciated his frankness and clear points of view, which helped me to stay straight and upright during the thesis. I would like to thank Professor Frank Massa for his contribution, as well as for permanently follow the evolution of the works, proposing valuable points of view and

making sure that work and deadlines could be kept.

The works which were undertaken would not have reached this point without Bombardier's support. Many efforts have been gathered in this thesis: Bertrand Deleval has been a permanent presence in Crespin, ensuring an everyday follow and awareness of the practical outcomes of the project, and Johannes Picht in Siegen, who backed my efforts in learning SIMPACK and getting it to work properly. I thank Georg Edlbacher, former RAMS responsible in Zürich, for his confidence and advice regarding quality and safety aspects and for presenting me Andreas Wolf, Bombardier's senior suspension engineer. Andreas has enthusiastically supported this project, opening contacts with suppliers and operators, without which the elastomer part of the manuscript would not exist. Along him, Lukasz Krzanowski, Jan-Philip Jensen and Nicolas Wertebach from Siegen contributed to our MARC simulations and component testing, thank you all.

The PhD being a scientific endeavour, a part of the works and experimenting took place in the LAMIH and other laboratories. I would like to thank Benjamin Bourel, to whom I booked the ageing stove for long periods and Remi Delille, who willingly answered many questions regarding testing. My gratitude goes as well to Denis Lesueur: after one of my tests had yellow-tainted a wall, he reassured my concerns and advised me to get in touch with the LMCPA laboratory in my quest for chemical analysis. All the tests of the aged rubber samples were done thanks to the generosity and efforts of Pascal Laurent, Benoît Jorgowski and Professor Philippe Champagne. The samples needed a series of characterization tests, which were performed in the LMR laboratory at Tours. I renew my thanks to Professor Stéphane Méo, who let us "squatter" the test machines, always carefully prepared by Mathieu Venin.

Pursuing my first contract with Railenium with a PhD would have never crossed my mind if I hadn't been so warmly welcome in Valenciennes, upon my arrival from Spain. My first project manager Dr. Carlota Pons, and my first colleague, now Dr. Julie Chalon, have a great deal on it. My fellow colleagues in LAMIH have been an example and helped me out during these years: doctors Colin Debras, Camille Durand, Benoît Fontenier, Kévin Lemercier, Jérémy Wouts, Alexandre Hiricoiu, Anthony Bracq, Anthony Graziani, as well as the future doctors: Xavier Roothaer, Oussama Filali, Hans Boungoumba, Camille Bataille... I will not forget my colleagues from Railenium, thank you for being along this journey during these four and a half years: Andrea Díaz, the two Nicolas, Mohammed, Seb', Émilie, Diego, Rudy... My greatest thanks go to the CERMEL students as well, which eagerly "adopted" me during my journeys to Tours: Daphné, Clémence, Oumaima, Julien.

Last, but not least, I my deepest gratitude is for my family, which has followed this three-year project in all circumstances (good, worrying and stressing). They have fostered (and been patient) with my taste for trains, always encouraging it: from railway magazines to trainspotting sessions,

through unexpected holiday stops "just to see that station/train". To my parents, thank you for your unconditional support, enthusiasm and encouragements at any time, this work is also an achievement of yours. To my sister - soon a doctor too -, thank you for your presence and encouragements at any time, any place, even while facing a wild ride on your side. Finally, I would like to thank my partner, Lucas, for his support, patience, comprehension... His presence by my side every day has undoubtedly contributed to the achievement of this manuscript and been a source of tranquillity during stressful times.

After this personal words... May I invite you to a brief journey on railways, trains and suspensions? Lets turn the page!

Résumé étendu

Introduction

De nos jours, le transport ferroviaire joue un rôle primordial dans la mobilité au cœur des sociétés des pays industrialisés. Que ce soit pour le transport des marchandises ou le transport de passagers entre les grandes métropoles, le chemin de fer contribue au développement socio-économique avec une moindre empreinte environnementale en comparaison à d'autres moyens de transport. Dans le cadre européen, les dernières directives de la Commission Européenne imposent un changement de paradigme dans la définition de la filière ferroviaire [EU, 2014]. Traditionnellement structurés autour de grands monopoles à propriété publique, les réseaux européens ont basculé sur un modèle de gestion bipartite. L'infrastructure demeure sous gestion d'une agence nationale décernant des sillons sous une logique équitable, tandis que les opérateurs traditionnels peuvent être concurrencés par des nouveaux acteurs issus du secteur privé.

L'entrée de ces nouveaux opérateurs a des conséquences pour le fonctionnement de la filière. Face aux anciennes entreprises, disposant de services internes avec la maîtrise de la gestion de la maintenance et du matériel roulant, les nouveaux opérateurs privilégient les contrats "clé en main". Cette philosophie s'articule autour du fournisseur du matériel roulant choisi, qui prend en charge la construction des entrepôts pour les trains, ainsi que la gestion et l'exécution des activités de maintenance du parc des véhicules, pour le compte de l'opérateur. Pouvant chiffrer jusqu'à 30 % des coûts du cycle de vie, les activités de maintenance et les coûts opérationnels qui lui sont associés deviennent un enjeu majeur à définir lors d'un appel d'offre, afin d'assurer la meilleure attractivité d'un fournisseur de matériel roulant vis-à-vis des autres constructeurs du marché.

Une optimisation soigneuse des cycles d'entretien, par la réduction des interventions (moindres pertes par immobilisation, gain en main d'œuvre et en pièces de rechange) est donc un atout majeur dans le nouveau horizon de la filière.

La plupart des matériels roulants actuels existant sur le marché comporte, dans leur conception, l'utilisation d'un sous-système comprenant les organes de roulement: le bogie. Ce sous-système est apparu à la première moitié du XIX^{ème} siècle pour répondre à deux besoins simultanés: la

perte de stabilité des véhicules à essieux fixes, suite à l'augmentation des vitesses commerciales [Wickens, 1965] et la longueur des véhicules, ainsi que la *difficulté d'inscription en courbe* de ces matériels suite à leur allongement [Iwnicki, 2006]. Le bogie est le résultat de l'union de deux essieux sur un cadre rigide, à plus faible empattement, connectés à la caisse par des liaisons de type traverse-pivot. Ce système a montré un grand succès et demeure, de nos jours, une solution optimale pour tous les types de matériels roulants ferroviaires. Cependant, de par son rôle clé pour assurer la sécurité du véhicule en roulement, ainsi que le confort des passagers éventuels, il est soumis à des protocoles d'entretien strictes. La plupart de ces opérations comportant le démontage et/ou la dépose des organes (de roulement, suspension ou structuraux) pour examen, les véhicules sont contraints de passer en atelier pour extraire les bogies. Le passage nécessitant un soulèvement du train ou du wagon pour accéder aux bogies, puis le démontage des organes, le véhicule se voit immobilisé pendant des périodes de plusieurs jours. Pour pallier à cela, les opérateurs disposent d'un stock de bogies prêts à l'usage, qui sont incorporés directement au véhicule après extraction des bogies à entretenir. En dépit de la réduction des temps d'immobilisation de la rame, les coûts liés à l'entretien des bogies demeurent toujours importants.

Dans ce contexte, une réduction des coûts liés à l'entretien devient d'un intérêt majeur pour les acteurs de la filière, notamment pour les fournisseurs de matériel roulant offrant des contrats "clé en main". Ce nouveau cadre a porté le constructeur de matériel roulant Bombardier Transport France à s'approcher de l'Institut de Recherche Technologique (IRT) Railenium et de l'Université Polytechnique Hauts-de-France, à travers son laboratoire LAMIH. L'intérêt du partenaire industriel est de disposer d'une méthodologie visant à optimiser la maintenance du sous-système bogie. Pour ce faire, il est envisagé d'évaluer la possibilité d'un allongement du cycle de vie de certains composants du bogie. La stratégie adoptée pour évaluer cette possibilité comporte les étapes suivantes:

- Un premier travail a consisté à déterminer les composants du bogie pertinents pour cette étude, en utilisant des outils-métier et les pratiques de qualité présentes au sein de l'organisation de Bombardier. Une étude de la criticité (fréquence de défaillance + gravité des défaillances) des composants de suspension, de leurs modes de défaillance et de leur couplage a été effectuée. À l'issue de cette étude, **le choix de certains éléments de suspension à base élastomère a été établi**.
- Ces éléments ont fait ensuite l'objet d'une étude de leurs constituants de base et des possibles défaillances au long du cycle de vie. **Une analyse** des matériaux et des mécanismes menant à **des changements de propriétés** permet d'apporter des modèles de vieillissement et d'évolution des caractéristiques des composants, **ainsi qu'une quantification de la variabilité** des propriétés mécaniques.
- L'enjeu principal du travail est de procurer une amélioration des performances de mainten-

ance, tout en préservant **les niveaux de qualité et de sécurité** fixés à l'heure actuelle pour les modèles de bogie de Bombardier. Ces critères **peuvent être évalués à partir d'une étude du comportement dynamique du véhicule ferroviaire**. L'impact des variations des caractéristiques des organes sur les indicateurs sécuritaires d'usage dans la filière est étudié. Ces résultats permettent une évaluation de la conformité du véhicule sous conditions "dégradées" envisageables à partir des modèles de vieillissement.

Aspects de sécurité et maintenance ferroviaire

Le **second chapitre du manuscrit** s'intéresse à l'évaluation des aspects sécuritaires du matériel roulant ferroviaire par le biais de la norme EN-50126. Elle codifie la méthodologie et les instruments nécessaires pour assurer la sécurité, notamment la FDMS (Fiabilité, Disponibilité, Maintenance et Sécurité). L'instrument clé dans la FDMS est l'AMDEC (acronyme d'Analyse des Modes de Défaillance et Étude de la Criticité), qui donne une liste exhaustive de l'ensemble des composants d'un sous-système déterminé, ainsi que tous les modes de défaillance propres à chaque élément. Chaque mode de défaillance se voit attribuer une qualification en termes de gravité et de la fréquence d'apparition du défaut. L'acceptabilité du défaut est définie par une matrice de criticité, regroupant toutes les combinaisons des différents scénarios possibles [EN50126, 2010].

Une confrontation de l'AMDEC du bogie aux modèles numériques du matériel roulant a été effectuée, afin de déterminer les éléments participant à la modélisation d'un véhicule ferroviaire. Ensuite, les modes de défaillance ont été classés par leurs niveaux de gravité et leurs taux d'occurrence. Cela a permis de construire des tableaux de probabilité d'apparition simultanée d'incidences sur deux éléments. **Aucune combinaison d'événements à forte gravité n'a été considérée comme plausible**, ne revêtant pas d'intérêt pour les travaux. Cependant, il a été constaté que les données de l'AMDEC (notamment les taux d'occurrence des modes de défaillance) sont fondées sur une base empirique (retour d'expérience, essais) référée aux cycles de vie actuels. Par conséquent, étant donné que l'étude portera sur une extension du cycle de vie des pièces, il apparaît peu pertinent de fonder le choix des éléments d'intérêt sur la seule base de leur taux de défaillance.

Afin de faire intervenir des notions complémentaires à la criticité des éléments, un arbre décisionnel a été mis en place en collaboration avec les services FDMS de Bombardier. Cet instrument a pour but de parcourir une AMDEC de façon exhaustive, triant les organes du système en fonction de leur importance et intérêt. Ensuite, les composants sélectionnés sont soumis à un examen de leurs modes de défaillance. Les organes de suspension seront ainsi sélectionnés à partir de certaines défaillances dont les mécanismes physiques nécessitent d'être maîtrisés (défaillances à criticité/conséquences non-négligeables). L'application de cet instrument au bogie FLEXX Compact de Bombardier a permis de choisir plusieurs défaillances d'intérêt

pour l'étude: augmentation de la raideur mécanique des *éléments primaires de guidage* (PSi) en métal-caoutchouc et des *ressorts secondaires auxiliaires* (SSE) en métal-caoutchouc; perte de capacité dissipative sans fuite d'huile sur les *amortisseurs hydrauliques*. **Le choix final a été de se focaliser sur les éléments de type PSi.**

Caractérisation du vieillissement du caoutchouc

Composants métal-caoutchouc dans l'industrie ferroviaire

Le **troisème chapitre du manuscrit** traite des aspects liés aux matériaux élastomères et à leur application dans l'industrie ferroviaire. L'utilisation des élastomères comme composant de base sur le matériel roulant date du XIX^{ème} siècle [Jones, 2012], pour la réalisation des tampons et des ressorts de suspension primaire [Macbeth, 1939]. L'utilisation des composants stratifiés en métal et caoutchouc apparaît dans les années 1960 et 1970: métro profond de Londres [M.E.C, 1983], nouvelles séries de locomotives de la SNCF (BB 7200 - 15000 - 22000, "nez cassées"), etc. Les principes constructifs demeurent sensiblement les mêmes: une ou plusieurs couches de caoutchouc sont adhérées à des armatures métalliques les encadrant. L'élastomère prend ainsi un rôle structurel, assurant la liaison et le transfert des efforts, tout en apportant son aptitude dissipative, permettant de filtrer les vibrations. Aujourd'hui, les éléments métal-caoutchouc sont largement répandus dans l'industrie ferroviaire, ayant des applications aussi bien sur des suspensions primaires et secondaires que sur des butées ou petits composants.

Caractérisation et modélisation du comportement des élastomères

Le comportement des élastomères, de par ses caractéristiques fortement non-linéaires, est abordé dans le cadre de l'hyperélasticité. L'hyperélasticité est due au comportement entropique du réseau caoutchoutique [Treloar, 1975], composé d'un mélange de chaînes moléculaires enchêvetrées. La vulcanisation confère au caoutchouc ses propriétés mécaniques par la réticulation des chaînes, entre elles-mêmes (vulcanisation au peroxide [Loan, 1967]) ou par des agents comme le soufre [Akiba and Hashim, 1997]. L'ajout des charges (noir de carbone, silice) joue aussi un rôle sur la tenue mécanique du mélange, notamment la capacité d'amortissement et la résistance à la fatigue [Guth, 1945] [Kraus, 1965].

La modélisation du comportement hyperélastique est abordée dans le cadre des grandes déformations [Sidoroff, 1982] [Holzapfel, 2000]. Ce comportement appartient au domaine de l'élasticité non-linéaire, en absence de phénomènes dissipatifs, et peut être défini par la donnée d'une *fonction d'énergie libre* spécifique [Boukamel, 2006] [Lejeunes, 2006]. L'enjeu de la caractérisation du matériau est donc de trouver une forme d'énergie traduisant la réponse du matériau. Dans le

cadre ce ces travaux, une approche *phénoménologique* a été privilégiée avec le choix d'un modèle de type Mooney-Rivlin généralisé [Rivlin and Saunders, 1951], avec cinq paramètres (modèle de James [Boukamel, 2006]).

Évolution du matériau: vieillissement thermique et caractérisation mécanique

Parmi les verrous technologiques de ces travaux, nous trouvons l'absence de retour d'expérience sur le comportement des pièces ciblées en service, notamment de par la mise en service récente du matériel roulant faisant l'objet de ces travaux. D'un point de vue formel, il est connu que le matériau est soumis à plusieurs phénomènes concurrentiels au long de la vie des pièces: la *fatigue mécanique*, le *vieillissement* du matériau, enfin le *fluage* de la pièce dû à l'élastomère. Les phénomènes de fatigue conduisent à un affaiblissement des propriétés mécaniques, tandis que le fluage, dépendant du temps (phénomène viscoélastique), conduit à un affaissement des pièces. Le vieillissement de l'élastomère a comme conséquence un raidissement de la pièce. Compte tenu du cadre de travail et des modes de défaillance extraits de l'AMDEC (augmentation de la raideur mécanique), nous ne nous intéresserons par la suite qu'aux phénomènes liés au vieillissement du matériau et à son impact sur le comportement hyperélastique.

Les effets de vieillissement au long d'un cycle de vie ont été déjà abordés dans la littérature [Mott and Roland, 2001] [Le Saux, 2010]. La difficulté principale de ces études étant d'obtenir des échantillons de matière suffisamment vieillie, le vieillissement accéléré apparaît comme une technique utile [Le Huy and Evrard, 2001]. Le traitement des résultats par le biais d'une loi de type Arrhenius permet d'extrapoler les résultats ainsi obtenus à la durée de vie du matériau [Gillen and Clough, 1997] [Gillen and Celina, 2000]. Une campagne de vieillissement a été mise en place (voir Tableau 1), inspirée de plusieurs travaux [Woo and Kim, 2006] [Le Saux, 2010] [Chang Su and Hyun Sun, 2015].

Les essais de vieillissement thermique ont été conduits sur des échantillons de cautchouc (ISO37 - H1 [ISO37, 2012]), placés dans une étuve avec renouvellement d'air, puis stockés et stabilisés. La caractérisation mécanique des éprouvettes a été effectuée par des essais de traction uniaxiale mesurant la courbe stabilisée du matériau et les propriétés à rupture. Les résultats des essais montrent l'influence du vieillissement thermique sur le matériau: *diminution de la déformation et de l'effort maximum à rupture*, ainsi qu'une *augmentation de la raideur sécante* mesurée à 200 % de déformation. L'application d'une méthode de type Arrhenius a permis d'extrapoler les courbes maîtresses de ces grandeurs à la température d'opération habituelle.

Des essais complémentaires visant la caractérisation de l'état physicochimique de l'élastomère vieilli ont été effectués. Il s'agit d'une courte série d'essais de gonflement [ASTM-D6814-02, 2002], inspirée de [Barbosa et al., 2017], dont l'objectif est d'évaluer la variation du taux de réticulation

	Température					
Amb	50 ° C	60 ° C	70 ° C	75 ° C	80 ° C	90 ° C
∞	-	-	-	-	1 jour	1 jour
-	-	*2 jours*	2 jours	*2 jours*	2 jours	2 jours
-	-	-	5 jours	-	5 jours	5 jours
-	-	*10 jours*	10 jours	*10 jours*	10 jours	10 jours
-	15 jours	*15 jours*	15 jours	*15 jours*	15 jours	-
-	30 jours	-	30 jours	-	-	-
-	45 jours	-	-	-	-	-

Table 1: Les configurations en rouge ont eu un taux de casses prématurées élevé lors de la caractérisation mécanique. Les cas en italique correspondent aux tests avec un faible nombre d'éprouvettes (< 3), moins représentatifs.

du caoutchouc au cours des vieillissements. **La densité de réticulation de l'élastomère augmente avec le vieillissement thermique. Certains paramètres mécaniques**, comme la raideur sécante, **montrent une dépendance linéaire avec le taux de réticulation**. Le taux de réticulation a été traduit par une loi d'Arrhenius, composant une courbe maîtresse de son évolution au cours du temps.

Les courbes de comportement des essais de traction ont été traitées avec une routine développée dans le logiciel Mathematica, permettant ainsi d'identifier les paramètres d'un modèle analytique basé sur une forme d'énergie libre de type Mooney-Rivlin généralisée à cinq paramètres. **Plusieurs ensembles de coefficients C_{ij} ont été obtenus, caractérisant le comportement matériau pour chacun des états de vieillissement**. Ces données permettront l'évaluation de la raideur de la pièce globale dans une étape ultérieure.

Variabilité des propriétés de suspension

Le **quatrième chapitre de la thèse** est consacré à l'étude et la quantification de la variabilité, étape clé dans la caractérisation complète d'un problème. Selon [Bouchon-Meunier, 2007], le niveau de connaissance sur un phénomène est généralement imparfait . Cette *incertitude* peut être *épistémologique*, donc liée à l'état global de connaissance d'un sujet précis, ou liée à la *nature* (environnement, société, etc.) [Walker et al., 2003]. Notre intérêt s'est porté sur les incertitudes naturelles, qui peuvent être *irreductibles* et *reductibles*, selon leurs sources et les moyens disponibles pour les quantifier et les gérer [Moens and Vandepitte, 2005]. Le *management des incertitudes* commence par leur *quantification* et s'appuie sur plusieurs familles de méthodes pour étudier leur

propagation dans le cadre du problème étudié.

La quantification de l'incertitude dépend fortement de l'information disponible: une approche *probabiliste* est conseillée lorsque la base de données de départ est riche; le cas échéant, des méthodes type *intervalles* [Moore et al., 2009] ou l'*approche floue* [Zadeh, 1965] permettent de construire un ensemble, pondéré ou non, représentatif de la variabilité. Quant à la propagation des incertitudes, la façon d'aborder le problème est aussi conditionnée par la connaissance de celui-ci. Si les paramètres incertains sont représentés par des quantités aléatoires, des méthodes probabilistes comme les *simulations Monte-Carlo* (MCS) [Metropolis and Ulam, 1949] ou le *Chaos Polynomial* [Ghanem and Spanos, 1990] peuvent s'appliquer. Si le formalisme de départ est flou, le *Principe d'Extension de Zadeh* (ZEP) [Zadeh, 1975] permet de propager l'incertitude sur la base d'un DOE [Hanss, 2002]. Les *analyses de sensibilité* [McWilliam, 2001] ou des *algorithmes d'optimisation* [Massa et al., 2009] sont aussi des alternatives plus efficaces.

La modélisation de systèmes ayant des nombreux degrés de liberté est souvent difficilement abordable d'une façon directe, notamment avec des méthodes demandant beaucoup de calculs (MCS, ZEP). Pour pallier à cette limitation, deux approches sont généralement utilisées. Les *Modèles d'ordre Réduit* projettent le problème original à grande dimension dans une dimension plus faible (POD, PGD, Hyperreduction) [Ryckelynck, 2005] [David et al., 2012] [Chinesta et al., 2010] [Rutzmoser and Rixen, 2017]. Si la manipulation des équations gouvernant le problème n'est pas possible, les *modèles de substitution* comme la *Méthode des Surfaces de Réponse*, les *Fonctions à Base Radiale* ou le *Krigeage* sont disponibles. Ces modèles sont fondés sur une approche purement mathématique des liens entre les entrées et sorties du problème, n'ayant pas de sens strictement physique, mais sont *non-intrusifs*.

Développement d'un modèle par Krigeage

Les travaux effectués dans le cadre de la thèse ont conduit à l'obtention d'un vaste ensemble de résultats expérimentaux, permettant de connaître la variabilité des propriétés mécaniques du matériau de base et de déterminer celle des propriétés des pièces. Cependant, cela est rarement le cas dans l'industrie. Cela a motivé l'adoption d'une approche purement numérique, mais fondée sur les résultats expérimentaux: le développement d'un modèle de type Krigeage. Cette méthode repose sur l'entrainement d'un modèle mathématique à partir d'un jeu de données d'entrée et de sortie. Ces valeurs réelles permettent à l'algorithme d'estimer les corrélations entre les variables et d'ajuster un modèle mathématique représentant leur distribution. Le modèle a été paramétré en considérant cinq variables d'entrée: le *temps d'exposition au vieillissement*, la *température d'exposition*, ainsi que *trois points de contrôle placés sur chaque loi de comportement mécanique de l'élastomère*. La variable de sortie est la *raideur macroscopique* de la pièce réelle, calculée avec des simulations éléments finis (EF) sous le logiciel MARC.

Le modèle EF a été mis à point pour reproduire un essai de caractérisation quasi-statique en compression verticale. Les simulations permettent d'obtenir les raideurs tangentes de la pièce (linéarisées autour d'un point) à trois niveaux d'efforts correspondant à autant d'états de chargement du véhicule ferroviaire. La géométrie de la pièce réelle a été récupérée et reproduite dans Hypermesh. En raison de la plus forte raideur des armatures métalliques, le modèle ne tient compte que de la partie élastomérique. Compte tenu des symétries de la pièce, la simulation d'un quart d'élément est suffisante pour décrire le comportement de l'organe. Afin de contrôler aisément le test de la pièce, le modèle a été piloté en déplacement avec un nœud de contrôle, lié rigidement à la face supérieure de la couche de caoutchouc. Le type d'éléments finis utilisés sont de 1^{er} ordre, intégration complète en déplacements (réduite en pression hydrostatique), avec une taille de 1 mm.

Résultats numériques: EF et Krigreage

Les simulations ont mis en évidence l'influence de l'évolution des paramètres identifiés à partir du vieillissement thermique. Pour une même température, plus le temps d'exposition est long, plus la pièce va se raidir. L'incrément de raideur le plus élevé a été de +27 % par rapport aux valeurs cibles imposées par Bombardier au prestataire.

Un tirage aléatoire de 20,000 configurations a été réalisé avec **le modèle de krigeage**. Il **a permis d'obtenir les enveloppes de raideur minimum et maximum de la pièce** en fonction de la configuration de vieillissement choisie. Ces résultats ont mis en évidence un résultat avec un fort intérêt: un maximum autour de certaines configurations est apparu, correspondant aux cas dont les caractéristiques mécaniques (courbes d'essais) constituent l'enveloppe supérieure du faisceau de courbes expérimentales. De ce fait, **il est possible d'estimer que le maximum des propriétés mécaniques du matériau cause un maximum de propriétés de la pièce**.

Il apparaît alors légitime de proposer une approche purement numérique, où une courbe base identifiée expérimentalement serait incrémentée par un facteur obtenu d'une notion de variabilité établie au préalable. Cette borne supérieure pourrait ainsi être fournie au modèle EF afin de calculer les niveaux de raideur associés, dans la configuration la plus contraignante. En appliquant cette technique, il a été déterminé que **la variabilité des raideurs de sortie est bornée à +35 %, pour des entrées variant jusqu'à +40 %**. Ces niveaux de variabilité justifieront les choix de variabilité à analyser sur les simulations de comportement dynamique du train.

Évolution des propriétés et comparaison avec cas réels

Nous avons pu comparer les résultats numériques à une courte série d'essais sur des pièces vieillies en service, ayant parcouru 981,000 km. Les résultats des essais montrent un faible (voire inexistant) changement des propriétés mécaniques de la pièce. Dans ce contexte, il est nécessaire de rappeler l'existence des mécanismes concurrentiels sur le matériau: *la fatigue* affaiblissant le matériau, *le vieillissement* le raidissant. Pour la durée de vie des pièces analysées, il est possible que les deux phénomènes aient agi simultanément sur la matière, donc se compensant mutuellement. De ce fait, il ne nous est pas possible d'établir un lien univoque entre les simulations fondées sur les essais de vieillissement thermique accéléré d'une part, et les propriétés observées sur les pièces réelles d'autre part. Néanmoins, des outils d'analyse alternatifs peuvent être mis en œuvre pour estimer le vieillissement de la matière, analysant l'état physico-chimique de la matière, notamment les essais de gonflement par immersion de prélèvements de caoutchouc dans un solvant approprié.

Dynamique: impact des variations de propriétés sur les les indices sécuritaires

Le **cinquième chapitre du manuscrit** s'intéresse au comportement dynamique des véhicules ferroviaires, dont le développement a été parallèle à l'évolution de ce moyen de transport. Le comportement oscillatoire (lacet cinématique) d'un essieu libre aux roue coniques a été décrit mathématiquement par Klingel au XIX^{ème} siècle, et les efforts entre roues et rails d'un assemblage rigide on été calculés par Boedecker [Iwnicki, 2006] [Garg and Dukkipati, 1984]. L'étude de la dynamique ferroviaire avec les formalismes mathématiques utilisés jusqu'aujourd'hui est dû à Carter [Carter, 1928], qui les appliqua dans les années 1920 au calcul de la stabilité dynamique de locomotives, y compris le contact roue-rail [Carter, 1926]. La prise en compte des non-linéarités des composants du véhicule [Wickens, 1965], ainsi que l'approfondissement de l'étude du contact entre les roues et les rails ouvrirent un nouveau champ d'études à partir des années 1950 [Kalker, 1968] [Kalker, 1991]. Des nombreux auteurs se sont intéressés à l'influence des propriétés mécaniques en utilisant des modèles formels du bogie [Garg and Dukkipati, 1984], notamment quant à la stabilité dynamique (cycles critiques [Ahmadian and Yang, 1998], comportement en courbe [Zboinski, 1997] [Dukkipati and Swamy, 2001] [Cheng et al., 2009]), mais aussi sur le déraillement [Brabie, 2007] [Andersson, 2012]. **L'impact de l'évolution des propriétés materielles des éléments élastomères sur les critères sécuritaires d'une rame est effectuée à l'aide d'un logiciel de calcul multicorps (MBS), SIMPACK**. Les modèles numériques ont été fournis par Bombardier et ont été validés préalablement par rapport aux essais effectués en ligne (demande explicite dans [UIC518, 2009]).

Évaluation de la sécurité d'un véhicule ferroviaire

Le standard international définissant les essais nécessaires à l'évaluation de l'aptitude sécuritaire des véhicules ferroviaires est l'UIC-518. Le matériel roulant a déjà passé une procédure d'homologation lui permettant de circuler sur le réseau. Le cas d'étude s'inscrit, donc, dans une procédure similaire à une extension d'homologation d'un véhicule préexistant. La norme autorise la réalisation d'une évaluation par simulation numérique de l'impact desdits changements, pourvu que le modèle numérique ait été comparé au cas réel et validé par les essais à l'échelle réelle lors de la première homologation. De ce fait, Bombardier a fourni plusieurs modèles numériques utilisés pour le calcul et l'étude d'un matériel roulant homologué en exploitation commerciale: un test numérique visant l'aptitude au déraillement du véhicule; une simulation de base pour évaluer le comportement en courbe en conditions quasi-statiques; enfin, un ensemble de modèles avec différents états de charge, voie et usure du train, permettant d'évaluer son comportement dynamique. **Plusieurs indices sécuritaires préconisés par la norme ont été évalués dans chacune des simulations**.

Dans le cadre d'une première phase, la sensibilité de ces modèles a été testée. Ces simulations ont permis de vérifier l'importance de la définition des paramètres de frottement lors de la définition du contact roue-rail, ainsi que la réactivité du modèle face à la défaillance des éléments structuraux et dissipatifs du bogie. La configuration des modèles a été vérifiée et validée sous la supervision et les conseils des ingénieurs en dynamique de Bombardier.

Plan d'expériences

Les tests préliminaires ont permis d'assurer la sensibilité du modèle face à des défaillances ponctuelles. Afin de simuler le vieillissement des composants, nous avons choisi de déployer une stratégie non-déterministe. Nous avons choisi deux niveaux de variation des propriétés: +15 et +30 % d'incrément, fondés sur les évaluations de variabilité pratiquées préalablement. Une dizaine d'ensembles de propriétés des éléments PSi et SSE a été générée. Les caractéristiques individuelles sont générées par tirage aléatoire dans l'intervalle de confiance de chaque variation de référence. Ces propriétés ont été propagées sur l'ensemble des modèles numériques, pour ensuite effectuer les calculs de chaque lot. Suite à des échanges avec des experts de Bombardier, une perte généralisée de 35 % des capacités dissipatives de *tous* les amortisseurs a été ajoutée pour simuler la dégradation de ces éléments (retour d'expériences interne). Les mises en données, simulations et post-traitements sont gérées de façon automatique par un script.

Résultats des simulations

Les *simulations de déraillement* de la rame ont montré une forte dépendance au raidissement de la chaîne cinématique de la suspension primaire et de la suspension secondaire. Un incrément excessif

de cette caractéristique pourrait entraîner des situations à risque sur cet aspect particulier.

Les modèles *d'évaluation du comportement en courbe* restent peu affectés par les variations appliquées. Les indices montrent un léger incrément du coefficient de déraillement, ainsi que des efforts latéraux sur les essieux, toujours dans les limites normatives.

Concernant les *simulations du comportement dynamique*, les variations de raideur ont des effets plus sensibles, bien qu'aucun indice sécuritaire ne dépasse les limites. Les simulations en *tracé droit avec perturbation latérale* montrent l'influence de la conicité équivalente appliquée aux roues: la dispersion des réponses du système sur l'indice mesurant le risque de déraillement est plus forte avec une moindre conicité, l'accélération latérale mesurée sur le châssis du bogie devient sensible aux variations de raideur, diminuant lorsque celle-ci augmente. L'état de chargement du véhicule est aussi un facteur d'influence, car il module la dispersion (moindre avec le véhicule sous charge exceptionnelle) et augmente les effets d'inertie: augmentation de l'accélération sur le châssis du bogie, moindre roulis si le véhicule est très chargé (pour des cas à même conicité de roue). Les simulations en *tracé courbe* mettent en évidence une dépendance de l'effort latéral sur l'essieu à la raideur, qui se manifeste plus clairement lorsque le véhicule s'engage sur des courbes à rayon large, haute vitesse et fortement chargé.

Bibliography

[Ahmadian and Yang, 1998] Ahmadian, M. and Yang, S. (1998). Effect of System Nonlinearities on Locomotive Bogie Hunting Stability. *Vehicle System Dynamics - VEH SYST DYN*, 29:365–384. (Cited on page ix.)

[Akiba and Hashim, 1997] Akiba, M. and Hashim, A. S. (1997). Vulcanization and crosslinking in elastomers. *Progress in Polymer Science*, 22(3):475 – 521. (Cited on pages iv, 55 and 56.)

[Andersson, 2012] Andersson, M. (2012). Derailment in track switches. Master's thesis, Chalmers University of Technology. (Cited on pages ix and 151.)

[ASTM-D6814-02, 2002] ASTM-D6814-02 (2002). *Standard Test Method for Determination of Percent Devulcanization of Crumb rubber Based on Crosslink Density*. ASTM. (Cited on pages v and 72.)

[Barbosa et al., 2017] Barbosa, R., Nunes, A. T., and Ambrosio, J. D. (2017). Devulcanization of Natural Rubber in Composites with Distinct Crosslink Densities by Twin-Screw Extruder. *Materials Research*, 20:77 – 83. (Cited on pages v and 72.)

[Bouchon-Meunier, 2007] Bouchon-Meunier, B. (2007). *La logique floue*. Presses Universitaires de France. (Cited on pages vi and 107.)

[Boukamel, 2006] Boukamel, A. (2006). Modélisations mécaniques et numériques des matériaux et structures en élastomères. Memoire d'habilitation à diriger des recherches, Université de la Méditerranée - Aix-Marseille II. (Cited on pages iv, v, 49, 55, 65, X and XI.)

[Brabie, 2007] Brabie, D. (2007). *On Derailment-Worthiness in Rail Vehicle Design Analysis of vehicle features influencing derailment processes and consequences*. PhD Thesis, Royal Institute of Technology Aeronautical and Vehicle Engineering Rail Vehicles, Royal Institute of Technology Aeronautical and Vehicle Engineering Rail Vehicles SE-100 44 Stockholm Sweden. (Cited on pages ix and 151.)

[Carter, 1926] Carter, F. (1926). On the action of a locomotive driving wheel. *Proceedings of the Royal Society of London A: Mathematical, Physical and Engineering Sciences*, 112(760):151–157. (Cited on pages ix, 143 and 144.)

[Carter, 1928] Carter, F. (1928). On the stability of running of locomotives. *Proceedings of the Royal Society of London A: Mathematical, Physical and Engineering Sciences*, 121(788):585–611. (Cited on pages ix and 140.)

[Chang Su and Hyun Sun, 2015] Chang Su, W. and Hyun Sun, P. (2015). Useful Lifetime Prediction of Chevron Rubber Spring for Railway Vehicle. *International Journal of Aerospace and Mechanical Engineering*, 9(8). (Cited on pages v, 49 and 69.)

[Cheng et al., 2009] Cheng, Y.-C., Lee, S.-Y., and Chen, H.-H. (2009). Modeling and nonlinear hunting stability analysis of high-speed railway vehicle moving on curved tracks. *Journal of Sound and Vibration*, 324(1):139 – 160. (Cited on page ix.)

[Chinesta et al., 2010] Chinesta, F., Amine, A., and Elías, C. (2010). Recent Advances and New Challenges in the Use of the Proper Generalized Decomposition for Solving Multidimensional Models. *Archives of Computational Methods in Engineering*, 17(4):327–350. (Cited on pages vii and 110.)

[David et al., 2012] David, A., J, Z. M., and Charbel, F. (2012). Nonlinear model order reduction based on local reduced-order bases. *International Journal for Numerical Methods in Engineering*, 92(10):891–916. (Cited on pages vii and 110.)

[Dukkipati and Swamy, 2001] Dukkipati, R. V. and Swamy, S. N. (2001). Non-linear steady-state curving analysis of some unconventional rail trucks. *Mechanism and Machine Theory*, 36(4):507 – 521. (Cited on page ix.)

[EN50126, 2010] EN50126 (2010). *Applications ferroviaires Spécification et démonstration de la fiabilité, de la disponibilité, de la maintenabilité et de la sécurité (FDMS)*. Association Française de Normalisation (AFNOR), 11, rue Francis de Pressensé – 93571 La Plaine Saint-Denis Cedex, 3 edition. (Cited on pages iii, 32 and 33.)

[EU, 2014] EU (2014). Fourth railway package still divides Member States. (Cited on pages i and 19.)

[Garg and Dukkipati, 1984] Garg, V. K. and Dukkipati, R. V. (1984). *Dynamics of Railway Vehicle Systems*. Academic Press, 55 Barber Greene Road, Don Mills, Ontario M3C 2A1. (Cited on pages ix, 24, 140 and 142.)

[Ghanem and Spanos, 1990] Ghanem, R. and Spanos, P. D. (1990). Polynomial Chaos in Stochastic Finite Elements. *Journal of Applied Mechanics*, 57(1):197–202. (Cited on pages vii and 109.)

[Gillen and Clough, 1997] Gillen, K. and Clough, R. (1997). Prediction of elastomer lifetimes from accelerated thermal-aging experiments. (Cited on pages v, 61, 69 and 79.)

[Gillen and Celina, 2000] Gillen, K. T. and Celina, M. (2000). The wear-out approach for predicting the remaining lifetime of materials. *Polymer Degradation and Stability*, 71(1):15 – 30. (Cited on pages v and 69.)

[Guth, 1945] Guth, E. (1945). Theory of Filler Reinforcement. *Journal of Applied Physics*, 16(1):20–25. (Cited on pages iv, 56 and 57.)

[Hanss, 2002] Hanss, M. (2002). The transformation method for the simulation and analysis of systems with uncertain parameters. *Fuzzy Sets and Systems*, 130(3):277 – 289. (Cited on pages vii and 109.)

[Holzapfel, 2000] Holzapfel, G. (2000). *Nonlinear Solid Mechanics : A Continuum Approach for Engineering / G.A. Holzapfel.* John Wiley & Sons, Chichester. (Cited on pages iv, 64 and VII.)

[ISO37, 2012] ISO37 (2012). *Caoutchouc vulcanisé ou thermoplastique - Détermination des caractéristiques de contrainte-déformation en traction.* Afnor. (Cited on pages v, 69 and 77.)

[Iwnicki, 2006] Iwnicki, S. (2006). *Handbook of Railway Vehicle Dynamics.* CRC Press Books. (Cited on pages ii and ix.)

[Jones, 2012] Jones, K. (2012). Rubber in Railways. (Cited on pages iv and 49.)

[Kalker, 1968] Kalker, J. (1968). The tangential force transmitted by two elastic bodies rolling over each other with pure creepage. *Wear*, (11). (Cited on pages ix and 144.)

[Kalker, 1991] Kalker, J. J. (1991). Wheel-rail rolling contact theory. *Wear*, 144(1):243 – 261. (Cited on pages ix and 144.)

[Kraus, 1965] Kraus, G. (1965). Interactions of Elastomers and Reinforcing Fillers. *Rubber Chemistry and Technology*, 38(5):1071–1114. (Cited on pages iv and 56.)

[Le Huy and Evrard, 2001] Le Huy, M. and Evrard, G. (2001). Methodologies for lifetime predictions of rubber using Arrhenius and WLF models. *Die Angewandte Makromolekulare Chemie*, 261-262(1):135–142. (Cited on pages v, 61 and 69.)

[Le Saux, 2010] Le Saux, V. (2010). *Fatigue et vieillissement des élastomères en environnements marin et thermique : de la caractérisation accélérée au calcul de structure.* PhD thesis, Université de Bretagne occidentale - Brest. (Cited on pages v and 69.)

[Lejeunes, 2006] Lejeunes, S. (2006). *Modélisation de structures lamifiées élastomère-métal à l'aide d'une méthode de réduction de modèles.* PhD thesis, Université de la Méditerranée - Aix-Marseille II. (Cited on pages iv, 49, 58, 64, 67, 85 and VII.)

[Loan, 1967] Loan, L. (1967). Mechanism of Peroxide Vulcanization of Elastomers. *Rubber Chemistry and Technology*, 40(1):149–176. (Cited on pages iv and 56.)

[Macbeth, 1939] Macbeth, C. (1939). *Rubber and Railways.* British Rubber Publicity Association, 2 edition. (Cited on pages iv and 49.)

[Massa et al., 2009] Massa, F., Lallemand, B., and Tison, T. (2009). Fuzzy multiobjective optimization of mechanical structures. *Computer Methods in Applied Mechanics and Engineering*, 198(5-8):631 – 643. (Cited on pages vii and 109.)

[McWilliam, 2001] McWilliam, S. (2001). Anti-optimisation of uncertain structures using interval analysis. *Computers & Structures*, 79(4):421 – 430. (Cited on pages vii and 109.)

[M.E.C, 1983] M.E.C (1983). A long life - and a 'care'-free one. *Rubber developments*, 36(1):2–3. (Cited on pages iv and 50.)

[Metropolis and Ulam, 1949] Metropolis, N. and Ulam, S. (1949). The Monte Carlo Method. *Journal of the American Statistical Association*, 44(247):335–341. (Cited on pages vii and 108.)

[Moens and Vandepitte, 2005] Moens, D. and Vandepitte, D. (2005). A survey of non-probabilistic uncertainty treatment in finite element analysis. *Computer Methods in Applied Mechanics and Engineering*, 194:1527–1555. (Cited on pages vi and 107.)

[Moore et al., 2009] Moore, R. E., Baker Kearfott, R., and Cloud, M. J. (2009). *Introduction to Interval Analysis*. Society for Industrial and Applied Mathematics, Philadelphia. (Cited on pages vii and 108.)

[Mott and Roland, 2001] Mott, P. H. and Roland, C. M. (2001). Aging of Natural Rubber in Air and Seawater. *Rubber Chemistry and Technology*, 74(1):79–88. (Cited on pages v and 69.)

[Rivlin and Saunders, 1951] Rivlin, R. S. and Saunders, D. W. (1951). Large elastic deformations of isotropic materials VII. Experiments on the deformation of rubber. *Philosophical Transactions of the Royal Society of London A: Mathematical, Physical and Engineering Sciences*, 243(865):251–288. (Cited on pages v and 67.)

[Rutzmoser and Rixen, 2017] Rutzmoser, J. B. and Rixen, D. J. (2017). A lean and efficient snapshot generation technique for the Hyper-Reduction of nonlinear structural dynamics. *Computer Methods in Applied Mechanics and Engineering*, 325:330 – 349. (Cited on pages vii and 110.)

[Ryckelynck, 2005] Ryckelynck, D. (2005). A priori hyperreduction method: an adaptive approach. *Journal of Computational Physics*, 202(1):346 – 366. (Cited on pages vii and 110.)

[Sidoroff, 1982] Sidoroff, F. (1982). Cours sur "Les Grandes Déformations". (Cited on pages iv, 64, 65, VII and XI.)

[Treloar, 1975] Treloar, L. (1975). *The Physics of Rubber Elasticity*. Oxford Classic Texts in the Physical Sciences. Clarendon Press - Oxford, 3 edition. (Cited on pages iv, 54, 56, 57, 65, 66 and 67.)

[UIC518, 2009] UIC518 (2009). *Testing and approval of railway vehicles from the point of view of their dynamic behaviour - Safety - Track fatigue - Runnign behaviour*. UIC, 4 edition. (Cited on pages ix, 35, 157 and 162.)

[Walker et al., 2003] Walker, W. E., Harremoës, P., Rotmans, J., Sluijs, J. P. v. d., Asselt, M. B. A. v., Janssen, P., and Krauss, M. P. K. v. (2003). Defining Uncertainty: A Conceptual Basis for Uncertainty Management in Model-Based Decision Support. *Integrated Assessment*, 4(1):5–17. (Cited on pages vi and 107.)

[Wickens, 1965] Wickens, A. (1965). The dynamic stability of railway vehicle wheelsets and bogies having profiled wheels. *International Journal of Solids and Structures*, 1:319–341. (Cited on pages ii, ix, 155 and 168.)

[Woo and Kim, 2006] Woo, C. S. and Kim, W. D. (2006). Heat-Aging Effects on the Material Properties and Fatigue Life Prediction of Vulcanized Natural Rubber. *e-Journal of Soft Materials*, 2:7–12. (Cited on pages v and 69.)

[Zadeh, 1965] Zadeh, L. A. (1965). Fuzzy sets. *Information and Control*, 8(3):338 – 353. (Cited on pages vii and 108.)

[Zadeh, 1975] Zadeh, L. A. (1975). The concept of a linguistic variable and its application to approximate reasoning-1. *Information Sciences*, 8(3):199–249. (Cited on pages vii and 109.)

[Zboinski, 1997] Zboinski, K. (1997). Dynamical investigation of railway vehicles on a curved track. *European Journal of Mechanics and Solids*, 17:1001–1020. (Cited on pages ix, 151, 155 and 160.)

Contents

List of figures

List of tables

Introduction

The operation of railway systems has always encompassed two complementary aspects: rolling stock and infrastructure. If one compares railways with other means of transport, parallelisms arise promptly: roads and tracks; stations and harbours or airports. From all four means of transport, the railways are the only one to have the sole right to use a reserved path exclusively, contrary to airlines, sealines, or road transport. This is a consequence of the nationalisation of railway systems, for rail networks were deemed strategical, thus becoming the states' property. The first example of a split between operations and infrastructure was performed in Sweden in the late 1980s, and became an example for other countries and the European Union, which issued a first directive to promote non-discriminatory track access (i.e. the right to run a train with equal rights of access to the network). Great Britain followed the trend, opening its railway system to public concurrence in 1994. The former monopole, British Railways, was split into an infrastructure managing company (Railtrack) and rolling stock and traffic routes were attributed to new private operators, which tendered for each of the service franchises in which operations had been split.

In an increasingly competitive ecosystem, rolling stock manufacturers have evolved and developed new solutions for railway operators. Customary rolling stock bids have evolved into large projects aiming to provide key-in-hand solutions jointly with the customers. Thus maintenance and life-cycle costs (LCC) are nowadays at the core of manufacture projects. This introduction will present some of the most relevant aspects on rolling stock bid process, as well as a brief insight on maintenance constraints and requirements. The project DYNABOG, which encompasses the thesis works, will be introduced along with the industrial and academic partners. The main aims of the project for the different participants will be subsequently addressed, developing the manuscript plan.

Rolling stock bids

The mechanism for railway operators to open a process to buy new trains is the call for bids, which is addressed to rolling stock manufacturers. This process encourages the competence between the attending companies, which will try to supply the most adequate offer to the customer. The

operator will issue a first document, stating the needs of the company and the requirements that must be fulfilled to be compliant with the call. Usual requirements in offers are the purpose of the train (high-speed, regional, commuter...), the expected capacity (number of passengers) or performances (top speeds and/or accelerations), technical requirements (kind of powering), environmental requirements (CO_2 emissions, green footprint, recyclability) and, more recently, maintenance aspects (costs, expected maintenance delays, etc.). For example, the last high-speed rolling stock bid issued by the Spanish public operator Renfe (November 2015) had the following technical and economic requirements.

1. Fifteen (15) high-speed passenger trains, with an option for 15 additional trains.
2. Standard UIC gauge.
3. Three-tension electric feed.
4. Maximal operational speed: 320 km/h.
5. Maintenance services to be included for a period of 30 years, with an optional extension for 10 years.
6. Reference cost for the bid: 2.642 B€ .

Rolling stock manufacturers can submit their offers to the company following the procedure which is established in the documentation issued with the public call. For a larger explanation on the stakes of a rolling stock bid, the reader is invited to refer to Appendix A. Once a manufacturer has been accepted as a potential bidder by the operator (public or private), the company's engineering teams begin the work to find the most suitable offer within the product portfolio. Up to the 1990s, rolling stock manufacturers used to work on a tailored fit solution approach for each customer. Although this method can give an precise solution to the railway operator's needs, it is expensive and might need extensive development or re-development of subsystems, sometimes starting from scratch. The search for economical efficiency has led to a new paradigm among manufacturers. Trains and rolling stock are classified within a series of families, named "platforms". For example, Bombardier Transportation has several families of products: Flexity (tramways), Talent and OMNEO (single/double-deck, for both commuter and regional services), TWINDEXX (double-deck intercity), ZEFIRO (high-speed trains) and TRAXX (locomotives). This principle can be transposed to a deeper level of development, creating families of subsystems, such as Bombardier's FLEXX bogie families.

As described before, each platform is designed to fit a "universe" of services or a certain kind of environment, thus standardizing the most expensive parts of the product's design, while being flexible enough to fit in the customer's needs. Furthermore, the standardization encompasses

several efforts, both in engineering and in economic domains, which seek to master all aspects regarding the platform. For example, "hollow" models of the platform are ready-to-use to test the main technical aspects of a potential bid, such as the train's general dynamic behaviour, supplying a quick answer to the customer's needs while ensuring a sound engineering basis. Respectively, economical assessment of production and supply chain costs are conducted during the platform design. This information is a strong asset for the manufacturer when tendering for a bid, as cost calculations will be more exact and eventual cuts to obtain best costs will be easier to evaluate.

A specific focus: maintenance operations

Current demands of railway operators focus more and more on maintenance, as it can be seen by the 30-year maintenance requirement from the Spanish high-speed described above. Maintenance and rolling stock availability (i.e. on the fleet's productivity) have an increasing importance, accounting up to 30% of a bid's global score. An unexpectedly disabled train or long, time-costly maintenance operations are undesired situations for a railway operator. Thus, rolling stock manufacturers pay special attention to these aspects and try to reduce as much as possible all aspects leading to immobilisation scenarios. There are two well-known principles regarding maintenance: correction and prevention. The former methodology consists in the mere replacement of worn or damaged components to ensure both the system's integrity and its performances. This means that the train will incur in an unsafe situation (the appear of a failure on one of its components), which will require palliative measures (roll at a reduced speed, immobilisation of the train, etc.). Preventive maintenance states that components must be replaced after a certain time in service, regardless of the part's state. This principle seeks the reduction of failing elements, ensuring a maximum operability. However, the replacement of components demands several workshop stops during the rolling stock's life-cycle, with the train being immobilised until the maintenance intervention is achieved. The optimum strategy is the balance between a certain amount of controlled, foreseen maintenance interventions, versus an uncontrolled amount of failure situations which can risk both the train and its payload's integrity. It is important to notice that, even under maintenance-controlled conditions, failure of elements might occur. It is the mission on the quality and RAMS engineering teams to prevent such events and reduce their periodicity. Furthermore, it is almost compulsory that most frequent failure modes do not engage the system's performances, preserving its integrity and allowing its operation until the end of that moment's mission.

The key element to the study of a system's maintenance is a deep knowledge of its components' properties. As previously explained, the design of railway rolling stock is a compromise between the customer's needs and the manufacturer's know-how and available platforms. Moreover, the design of the platforms is a compromise as well, this time between the manufacturer and its suppliers. Each of the components of the train or its subsystems is a careful balance between cost, life-cycle/durability, properties and performances, which must meet the manufacturer's needs. The

assembly of all maintenance needs leads to the forecast of a maintenance operations plan, which encompasses all the workshop interventions and stops for the vehicle and/or its subsystems. For example, a certain model of FLEXX Compact bogie from Bombardier Transportation is checked according to the following plan, every:

- 3,5 years - Wheel-set extraction for motor bogies. Axle's integrity check, wheel replacement.
- 5 years - Wheel-set extraction for trailer bogies. Axle's integrity check, wheel replacement.
- 6 years - Bearing dismounting for adjustment.
- 10 years - Bogie extraction for check. Replacement of: primary rubber spring's, secondary air-spring and auxiliary springs, bumpstops, hydraulic damper replacement. Check and repair some of the dampers.
- 15 years - Overhaul of the bogie. Check of the axle's integrity on all bogies. Replacement of all bearings. The bogie frames and the anti-roll organs are checked, sand-cleaned and repainted.

Since a train's design life-cycle is of around 30 to 40 years, one single vehicle will pass several times through maintenance facilities. Among all the operations, bogie maintenance is especially cumbersome. As listed before, operations around axles and primary suspension elements require the complete disposal of the wheel-sets and their associated suspension elements, thus immobilising the whole trainset to extract the bogie. The time length of some operations can be drastically cut off by stocking a small amount new bogies, which are fitted on the train immediately after extracting the bogies concerned by the maintenance operation. This reduces the immobilisation of the vehicle from several days up to 2 - 3 hours. The retrofitted bogies will be later installed under another vehicle, continuing the maintenance cycle for the whole series of rolling stock. The same principle can be translated to lower-scale subsystems, such as having wheel-sets with primary suspension elements already fitted.

DYNABOG Project - Global aims

In spite of the optimisation strategies explained previously, railway operators and rolling stock manufacturers would desire a further decrease of maintenance operations. A reduction on the interventions could be achieved by shifting some parts' replacement or check processes, so that their periodicity matches that of a thorough intervention where a long immobilisation is already foreseen. This increase of maintenance periods requires a high durability of the addressed parts. To warranty a higher life-cycle and endurance of the materials, it is necessary to either reformulate

the design principles of the addressed parts (new materials) or ensure that the current design is fit to serve for longer periods, based on current safety margins. The latter solution would be, from an economic point of view, less expensive than the former.

Participants on the project

The project DYNABOG was launched in October 2015 by three actors based in the region of Hauts-de-France ("Upper France"): Bombardier Transportation, the University of Valenciennes and Hainaut-Cambrésis through its laboratory LAMIH and the Institut de Recherche Technologique, IRT Railenium (IRT is the French abbreviation for Technological Research Institute). The region is one of the cradles of the French railway industry: apart from Bombardier's factory, the group Alstom has also a site in Valenciennes, producing tramways, subways, commuter and regional trains, plus a test ring. The freight wagon manufacturer Titagarh has a site at the near city of Douai as well.

Bombardier Transportation is the railway branch of the transnational group Bombardier, whose headquarters are based in Montreal (Canada), and which encompasses also an aerospace branch, Bombardier Aerospace. Due to the share of the European market in railway activities, the railway branch's headquarters are based in Berlin (Germany) since the merger with the former group ADTranz in 2001. The core of the tasks of this project is undertaken at Bombardier's facilities in Crespin (Nord, France. Former site of ANF), near Valenciennes. The supervision of the project is performed jointly by staff from Crespin, Siegen (Germany) and Zürich (Switzerland).

The research laboratory LAMIH (French abbreviation for "Laboratoire d'Automatique, Mécanique et Informatique Humaines") is a joint research unit of the French national centre for scientific research (UMR - CNRS # 8201). Its staff is administratively attached to the Université Polytechnique Hauts-de-France (UPHF), and has an extensive experience on railway research: aerodynamics, braking issues (squealing, surface interaction between brake pads and disks), overhead lines components, and many others.

The IRT Railenium was founded in 2013 by the French government as a part of a strategy called "Plan d'Investissements d'Avenir" ("Plan of investments for the future"). Railenium was created along eight other research centres, each of them related to a technological or scientific field in which French industry excels. It is the dedicated IRT for the railway industry, gathering both industrial and academical partners related to this precise ecosystem. Railenium's main purpose is the tightening of the bonds between the industry and the academical world, developing innovative projects that can foster economical growth and preserve the leading role of the French railway industry in the world. The ultimate aim being the spreading of the benefits of that leading position to the whole ecosystem of the IRT.

Main objectives

The scope of the project has been determined by Bombardier Transportation France, whose concern is to address the optimisation of the maintenance periodicity of a specific subsystem: the bogie. The object of this study will be a FLEXX Compact bogie, which has been fitted in trains all across the world, with more than 2,500 units produced. A specific model has been chosen to develop a general methodology, which would be subsequently tested and, if possible, exported to other cases or other kinds of equipment. In this case, the chosen bogie is equipped on Régio2N trainsets. A further application of the whole concept would be the offer of the optimisation study as a part of a services contract in the context of future bids.

To achieve this goal, Bombardier would like to develop a "standard methodology" which could address this issue even during the early stages of design phase. The industrial aims would be deployed in several stages, arranged as follows.

- The methodology would be based on the quality instruments which are currently in use within Bombardier, such as the FMECA of the bogie (Failure Modes and Effect Criticality Analysis). This tools would point the priority elements to be addressed, as well as the respective failure modes to be considered.
- The source of the failure mode (e.g. material properties, design flaws...) will be analysed and characterised thoroughly, especially time-dependent evolutions. This knowledge on the degradation phenomena of the components and the time scales involved in them is an strong asset. A proper mastering of the failure's sources is the basis for the development of preventive strategies, assessing the components' life-cycle and forecast the emergence of failure events.
- Safety is the main priority on the design and on the approval of a railway vehicle. Thus, failure modes evaluated previously will be converted into a mechanical, meaningful magnitude (e.g. a loss of damping/stiffness/mobility). The consequences of such failures modes, either isolated or combined, will be addressed through the safety norms' procedures, as well as the customer's operative constraints. Hence, it will be possible to establish a link between the components' properties and the safety indicators, which is directly related to the vehicle's compliance along its life-cycle.

The thesis aims to back Bombardier's aims and expectations through sound scientific knowledge, gathering the necessary information to proof the strategy's feasibility. The studies lead by the laboratory LAMIH and the IRT Railenium will address the points hereunder.

- A railway vehicle's structure is complex, especially the bogie. It withholds a multitude of suspension elements, which could fail simultaneously. The manuscript will evaluate the likeliness of a combination of failures occurring over a single specimen of rolling stock, causing a hazardous situation. This study will have its starting point on the existing tools within Bombardier's quality and maintenance practices, as well as on the failure's criticality and estimated appearance rates.

- The constituent material from the parts aimed by the first step of the analysis will be discussed in the manuscript. Time-dependent properties of materials are related to several phenomena: fatigue, ageing, creep, among others. The scientific goal for this part is to set up a description of the material's behaviour during its life-cycle based on the current literature, as well as to extend the description to the part's macroscopic properties. Experimental evidences will be collected to feed the necessary models of the materials and to provide empirical methods to perform this study on other rolling stock constituents. Finally, the variability observed on the material's properties will be evaluated, setting a thorough database of the element's possible evolution scenarios.

- Complex systems composed of many mechanical elements, such as the bogie, can be analysed through the *multi-body system* (MBS) formalism (i.e. the modelling of the system by a series of bodies with their mass and inertia, connected by idealized elements which contain the mechanical properties of the links). The scope of this part is to understand the system's behaviour under multiple failure scenarios. Such situations will be based on the assessment of the part's evolution over the life-cycle, thus providing a realistic basis for the analysis. The focus will be set on the system's safety limits and on their description, assessing the variability of the normative indicators due to the change on the system's properties.

Plan of the manuscript

The manuscript will address the different aspects required in the project, following the aforementioned stages.

- The **first chapter** will present a brief introduction on the railways, describing its historical development until the present day. The evolution of the railway operators and rolling stock manufacturers will set the industrial environment of the project and works.
- In the **second chapter** the bogie subsystem and its main features will be presented. The quality tools used on the railway industry will be discuss, along with the main safety principles and norms. These tools will be complemented by a methodology to choose certain suspension elements for the projects' purposes. Such methodology will be based on the quality tools and will yield several elements of interest, whose pertinence will be discussed. The possibility of using numerical simulations to assess rolling stock security will be presented as well. The issue of this first part is the choice of some rubber-to-metal parts to be studied.
- The **third chapter** will introduce the chosen suspension elements to the reader, explaining their main features and characteristics. The study of elastomeric materials will be discussed later, introducing the basis of the study of hyperelastic materials. Special attention will be paid to ageing phenomena of the rubber and how to model and test their effects. This will be followed by an explanation of the testing campaigns performed during the project. The determination of a hyperelastic strain energy function will be discussed, including the coupling between mechanical properties and thermal ageing. The outcome of the chapter will be the material variability and an ensemble of new and aged hyperelastic behaviour models.
- The **fourth chapter** is devoted to the quantification of the variability of the suspension elements. The principles and techniques to quantify and propagate uncertainties will be briefly discussed. A Kriging model will be presented, based on the experimental data obtained from the characterization tests and on a FE simulation campaign. The results from the FE simulations will be presented under two points of view: the prediction of the ageing of the suspension components, and the training of the Kriging model, as well as the most unfavourable behaviour predicted by the model. A discussion on the accuracy of the life-cycle predictions will ensue, with a comparison with test results on real components. The chapter will conclude on the variability levels of the macroscopic properties of the suspension elements.
- The **fifth chapter** addresses the assessment of the dynamic behaviour of a Bombardier rolling stock, the Régio2N. The first part of the chapter will introduce the reader to the main aspects of railway dynamics. The numerical models provided by Bombardier will be presented next, along with the preliminary tests which tested the sensibility of the system to failures in the

suspension. A design of experiment to integrate the variability of the suspension properties will ensue. The discussion on the simulation results for the cases with variability will close the chapter, concluding on the vehicle global behaviour under degraded mode.

- A **conclusion and perspectives** paragraph will summarize the results from the works, recalling the first objectives and the aims of each partner. A discussion of the results, its strong points and the weaker ones will outline the subjects which should be improved and/or would deserve further attention in future works.

Chapter 1

Historical context

> As regards railways, it is certain that nothing is so profitable, because nothing is so cheaply transported, as passenger traffic. Goods traffic, of whatsoever description, must be more or less costly. Every article conveyed by railway requires handling and conveyance beyond the limit of the railway stations; but passengers take care of themselves, and find their own way.
>
> George Stephenson

Contents

1.1 Railway technology: a brief introduction

Nowadays, railway systems are a fundamental part on the transportation scheme for many countries around the world. This long-date mean of transport has evolved from the primitive steam locomotives to modern high-speed trains connecting distant places in just a few hours. Railways have become a fast, environmentally-friendly, reliable system which contributes to the economic development of many countries, and is also the backbone of the mobility for several regions around the world. Railway technology has evolved over time accordingly, contributing to this success by supplying constant improvement and optimisation of each of the subsystems of the rail transport.

1.1.1 Historic examples of guided transport

The very basis of railway transport is the principle of a travelling element which carries goods and/or people by means of a guiding system, which ensures the safe motion of the vehicle over a dedicated path. The origin of this concept remains unclear, perhaps inspired by the parallel trails caused by horse-driven chariots. There is a well documented first example of a big-scale, railway-like mean of transport: the *Diolkos*. Archaeological remains on the Isthmus of Corinth (Greece) show the traces of which could have been a primitive railway-like transport, allowing a quick and advantageous transfer of boats or goods between the Ionian Sea and the Aegean Sea, instead of circumnavigating the Peloponnese peninsula. Cargo would have been loaded on some sort of wagons, which would have been hauled overland by man or horse power. This primitive "railway" was in operation from the 7th century BC up to the 1st century AD, when a first attempt on building Corinth channel split its western extremity [Werner, 1997]. Traces of other guided systems dating from Roman times have been found in Egypt as well, proving the interest of this principle well before automotive power had even been foreseen. In spite of their success, these primitive guided systems had little or no offspring after the fall of Rome, and the following examples of a transport by means of wagons following a guided path reappear well after Middle Ages, at the 16th century. Examples arise in gold mines in Transylvania, in the United Kingdom as well, or Salzburg castle (Hohensalzburg) [Tzanakakis, 2013], home to one of the first cable railways, the Reißzug. However, the guiding principle at that times relied more on the insertion of two matching geometries ("U-shaped" wheels over rails, wheels inserted into "U-shaped" rails, etc.), rather than the tapered wheels that are nowadays customary.

The development of an autonomous tractive device was a major challenge to achieve the basis of current railway technology. The possibility of using steam as a source of locomotive power was known since the Ancient times. It was again in Roman Egypt, at the 1st century AD, that Hero of Alexandria developed the "Aeolipile". It was a primitive steam turbine, able to spin around its axis thanks to two lateral steam outlets. The sphere was fed through the axis, which worked as the steam input as well. Although of no practical application, the device proved that steam

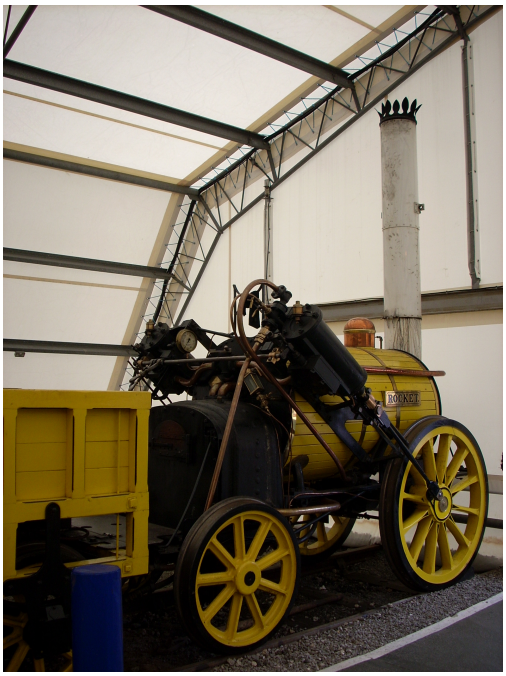

Figure 1.1: Full scale replica of George Stephenson's Rocket locomotive, standing at National Railway Museum in York, UK. *Self-owned picture.*

could be used so as to provide motion [Papadopoulos, 2007]. It was not until the 18th century that several inventors and researchers achieved the first practical and successful designs. It was in the United Kingdom in 1712, that Thomas Newcomen developed a pumping system to drain flooded mines, driven by an alternative-motion cylinder, based on steam condensation; James Watt designed the first steam machine able to convert a cylinder back-and-forth movement into rotative motion in 1781. These achievements paved the way for the development of smaller steam engines which could be mounted on vehicles, thus enabling autonomous motion. On the late 18th century, Richard Trevithick built several experimental machines like the renowned "Catch-me-who-can", which proved the feasibility of a steam-powered locomotive towing one or several wagons. It is at the beginning of the 19th century that we can find the first examples of a railway system as we understand it nowadays. The Stockton to Darlington railway saw George Stephenson's "Locomotion # 1" first runs, and the future opening of the Liverpool to Manchester railway led to the famous series of tests, known as Rainhill Trial, where Robert Stephenson's "Rocket" set a new era for locomotive technology (Figure 1.1). Many of its features became the chosen model to standardize several engineering principles for the railway technology, such as the tubular boiler.

Figure 1.2: Tile work representing the "Chemins de Fer du Midi" network at the beginning of the 20^{th} century. Bordeaux St. Jean station hall. *Self-owned picture.*

1.1.2 The railway development: 19th and 20th centuries

The development of railway technology on the 19th century was followed by a sheer enthusiasm. A run to gain access to a railway line ensued, and the development of the first railway lines was followed by a great number of extensions. The spreading network fostered economical growth and an increase on commercial exchanges, opening new trade routes. However, the thrill for this new technology was not always widely shared. Even George Stephenson, the so-dubbed "father of railways", expressed his concern as soon as 1824: "The rage for railroads is so great that many will be laid in parts where they will not pay.", well before the Railway Crash of the 1840s could be foreseen. The development of railway lines was usually granted by a government patent, which allowed an entrepreneur to undertake the necessary works to lay a railway from one place to another. The states would bestow a subvention covering a limited part of the costs per kilometre, plus the right to expropriate the land beneath the railway path, the rest of the costs being at the company's charge. Such conditions forced railway companies to search external investors to have the necessary founding to develop their activity [Millward, 2004]. Railways being a new-born technology, cost-assessment was uncertain and track-laying works were prone to excessive extra cost. Furthermore, excessively optimistic economic forecasts lead many companies to over-dimensioned infrastructure and means, contributing to the economical unbalance.

The enthusiasm around railways came to an end at the 1840s, when the speculative bubble involving railway companies exploded. First in the United Kingdom, and subsequently in France and continental Europe, railway companies were overwhelmed by financial trouble. The economical crisis led many companies to bankruptcy, forcing the governments intervention to find a solution,

granting aids or, as it happened in France, through the companies nationalisation. This was the opportunity for bank investors and better-financed railway companies to get newer opportunities, merging the bankrupt companies into their structures, as did the Great Western Railway in Britain or the Chemins de Fer du Nord (Northern railways) in France. At the outcome of the crisis, the development of railway companies shifted to a new paradigm, based on larger, more solid railway companies resulting from the merger of local lines. The new situation led to a more balanced development of the network, which was rather homogenised compared to the first stages of railway expansion. Instead of doubling existing routes and/or expanding on territories already "colonised" by another company, railway enterprises would remain on their specific geographical areas and would favour link or Joint Railways (UK) with other networks. For instance, by the end of the 19th century, most of France's railway network was held by six companies: "Chemins de Fer du Nord" (Nord), "Chemins de Fer de l'Est" (Est), "Compagnie des chemins de Fer à Lyon et à la Méditerranée" (PLM), "Compagnie du chemin de Fer de Paris à Orléans" (PO), "Chemins de Fer du Midi" (Midi) (Figure 1.2) and "Compagnie des chemins de fer de l'Ouest" (Ouest) [Papazian, 2000]. These companies would have little or no overlapping between their networks (see Figure 1.2), with strategic joint stations where they would exchange their traffics.

1.2 Railway transport and industry: the European context

The development of alternative means of transport at the beginning of the 20th century generated a new competitor for rail traffic. Buses, lorries of cars became useful for serving in short distances and local services. The era of the great railway companies was to last until the outbreak of World War I and the decade of the 1920s. Railway systems were one of the pillars of the military effort of each belligerent country, and were extensively damaged in war areas, due to their strategic value. Important works were needed to restore operations in some areas, and sometimes even rolling stock and network resources were subjected to the compensation policy enforced by the Versailles Treaty. The aftermath of the war was to be shocked again ten years later, this time by the economical crisis caused by Wall Street Crash in 1929. The contraction of the economy had a direct effect on railway traffic volumes, which were also being weakened by the incipient concurrence from road traffic.

1.2.1 National railway operations: merging and nationalisation

Railway companies began to suffer economical losses and financial difficulties. Although some countries had already conducted railway nationalisations (Switzerland, 1902)(Italy, 1905), the need for an optimisation of railway management and operation became more evident on the aftermath of the war. The United Kingdom enacted the Railways Act in 1921, which forced the merge of many of the pre-war 120 railway companies into the "Big Four" companies. The London and North Eastern Railway, the London, Midland and Scottish railway, the Great Western Railway and the Southern Railway were since then under the government control. Weimar Germany saw the merge of the public companies from Prussia, Bavaria and other German states into the Deutsche Reichsbahn, state-owned as well. The economic instability during the 1920s and 1930s led to the creation of SNCB in Belgium (1926), SNCF in France (1937) or NS in the Netherlands (1938). Later mergers appear in Spain (RENFE, 1941) of Portugal (CP, 1951). After World War II, the main core of the European network was publicly-run and state-owned.

1.2.2 Rolling stock manufacturers: from local market to global actors

Rolling stock manufacturers have followed railway history and endured an evolution throughout time which is parallel, in many aspects, to that of the railway companies. Early train builders were based, for obvious reasons, in Great Britain. Stephenson's company became one of the first suppliers of locomotives to continental Europe at the time: for instance, the first German train was pulled by a Stephenson's steam machine, "der Adler" (German for "eagle"). However, exporting full series of rolling stock from abroad was too expensive and strongly cumbersome. Thus, new workshops appeared in continental Europe, such as Börsig (1841, Germany) or Fives-Cail, later Fives-Lille (1850, France), among many others. Local manufacturers were granted exploitation

licenses of existing designs, which allowed a quicker development of the railway infrastructure and rolling stock, with reliable, near suppliers, able to comply with the local standards. Following railway development, local manufacturers grew skilful and developed their own designs. Their increasing activities made them grow in volume and explore new opportunities outside their usual markets. Countries with a later or slower development of railway industry were the ideal market to expand operations. As an example, one of Spain's foremost railway companies, the "Caminos de Hierro del Norte" ("Northern Railway"), were owned by two French bankers: the Pereire brothers. Thus, many standards or customs were set by French and Belgian engineers holding the leading roles, who usually ordered rolling stock to European builders from France (Creusot, Fives-Lille, Société Alsacienne...), Germany (Hartmann, Börsig, Maffei...) or other countries [Wais, 1976]. Local-licensed suppliers would eventually emerge and earn their share of the market, following the same principle that led to the birth of the earlier continental manufacturers.

Although some railway companies had strong technical offices which drafted the designs of trains, carriages and wagons - which was usual until the first half of the 20th century -, many others preferred to rely upon the capacity of manufacturing companies and their designs. This environment changed strongly after the nationalisation of Europe's railway systems, as each country became the home to a single company. Rolling stock manufacturers increased the export of their designs to assure their survival in the new context, while merging policies paved the way to first "champions" within each national market. French builder Alstom (then Alsthom) was born in 1928 in Alsace after a merger of two companies, and subsequently grew by absorbing other train producers during the second half of the 20th century. By the end of the 20th century, most of the local rolling stock manufacturers which were on a leading position started to expand on neighbouring countries. An example of this trend is Alstom, which entered the Spanish market in the early 1990s buying two sites (Barcelona and Valencia) and the German market with a site in Salzgitter. Other company which followed this trans-national policy was the former group ADTranz. Its origin starts with the Swiss builder Brown-Bovery, well-known by its electric rolling stock, which merged the Swedish ASEA in 1988 to form ABB. Their railway activities were grouped with the German builders Henschel and AEG in 1996 to form ADtranz.

The last stage of this merge-and-growth process appears on the brink of the 21st century, when companies seek a global role in railway market. The Canadian group Bombardier is a good example of this trend (Figure 1.3). It began its railway activities acquiring the former rolling stock builder MLW (Montreal Locomotive Works), and succeeded in entering the European market by buying two smaller manufacturers which had survived the merging tide of the late 20th century: Ateliers Nord de France (Crespin, France) in 1989, and BN Constructions Ferroviaires (Bruges, Belgium) in 1988. These sites granted Bombardier an access to the European railway market, as well as opening the possibilities to further acquisitions. This strategy was proved successful, as a final merger with ADtranz lead to the group Bombardier Transportation as it is known today,

with its headquarters based in Berlin.

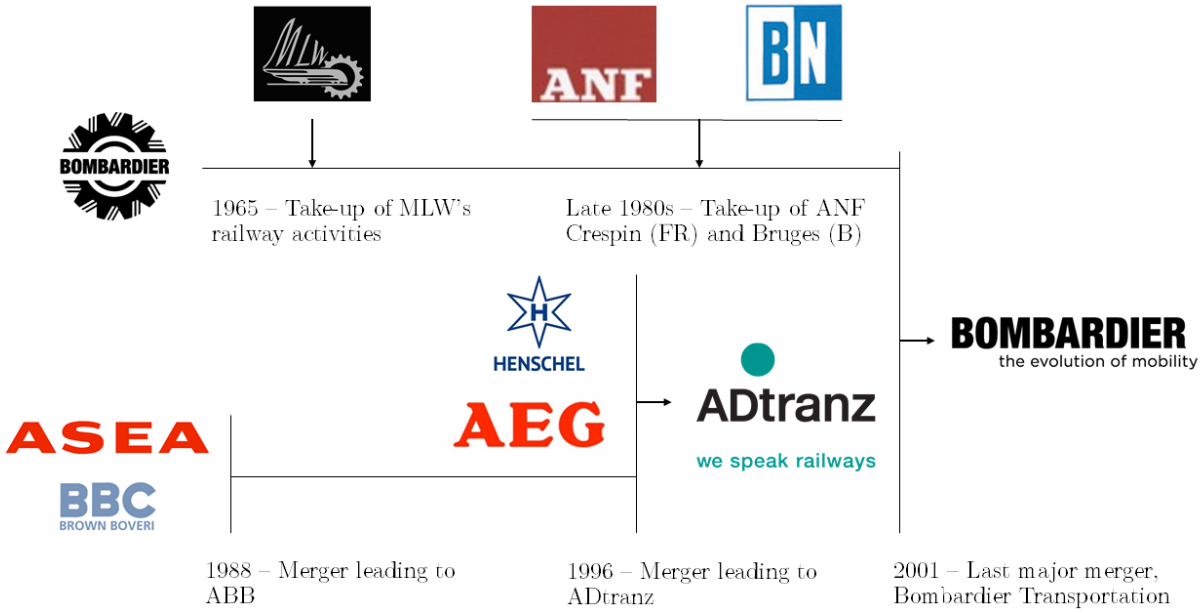

Figure 1.3: Historical development of Bombardier Transportation from its former constituents. *Self-designed, the trademarks remain the property of their respective owners.*

1.2.3 The EU context: infrastructure VS operations, railway liberalisation

Railway operations have always encompassed two complementary aspects: rolling stock and infrastructure. If one compares railways with other means of transport, parallelisms arise promptly: roads and tracks; stations and harbours or airports. From all four means of transport, the railways are the only one to have the sole right to use a reserved path exclusively, contrary to airlines, sealines, or road transport. This is a consequence of the nationalisation of railway systems, for networks were deemed strategical, thus becoming the state's property. The first example of a split between operations and infrastructure was performed in Sweden in the late 1980s, and became an example for other countries and the European Union, which issued a first directive to promote non-discriminatory track access (i.e. the right to run a train with equal rights of access to the network). Great Britain followed the trend, opening its railway system to public concurrence in 1994. The former monopole, British Railways, was split into an infrastructure managing company (Railtrack) and rolling stock and traffic routes were attributed to new private operators, which

tendered for each of the service franchises in which operations had been split.

The opening of railway systems to concurrence with public and private operators has been developed in several ways, depending on the subjected country and the respective context. With the European directive 2012/34/EU, other countries have opened their railways networks, having the Swedish and British experiences as reference examples. The opening for freight free competence was enacted in 2007, enabling transnational railway operators to run freight services across Europe. Long-distance passenger services must be opened to free concurrence after 2020 (regional and commuter services liberalisation is optional). In spite of this term, some countries have already allowed this possibility, even developed it extensively (Great Britain opened all services to concurrence from the first stage of liberalisation), or have chosen to allow specific domains of concurrence (high speed in Italy, among others) [EU, 2014].

This new context has lead to a change of paradigm on railway operators: ancient companies operated services, owned their rolling stock and maintenance facilities and performed their trains maintenance, which is still the case of the ancient monopoles. Alternatively, new railway operators seek to provide a transport service, but can have little to no experience regarding rolling stock maintenance, since their owners may come from domains other than railway industry. The need for a good maintenance service at a good cost has become an opportunity for rolling stock manufacturers, which have the appropriate know-how in this area. Thus, rolling stock manufacturers have developed a new role in this new environment, providing turnkey solutions for railway operators, old or new. An increasing number of bids include maintenance services, in which the manufacturer offers support, supplies and maintenance for a certain period of time, which can sometimes extend up to the trains complete life-cycle. Depending on the context, a manufacturer may offer different kinds of collaboration to each customer, from the joint operation of common workshops and shared staff, to dedicated facilities, completely separated from the operator itself. An example of the former is the Spanish operator Renfe, who has several common joint ventures with its trains' suppliers: BTREN (Bombardier Transportation), ACTREN (CAF), NERTUS (Siemens) or IRVIA (Alstom). If the point of view is that of the manufacturer, Bombardier Transportation is a suitable example: it has an implantation on the United Kingdom with several maintenance facilities. Staff on these sites works jointly with railway operators, such as Croydon's site (tramway maintenance for Transport for London, TfL) or East Ham (maintenance operations of the ELECTROSTAR fleet of c2c operator).

Bibliography

[EU, 2014] EU (2014). Fourth railway package still divides Member States. (Cited on pages i and 19.)

[Millward, 2004] Millward, R. (2004). European governments and the infrastructure industries, c.1840-1914. *European Review of Economic History*, 8(1):3–28. (Cited on page 14.)

[Papadopoulos, 2007] Papadopoulos, E. (2007). HERON OF ALEXANDRIA (c. 10–85 AD). In Ceccarelli, M., editor, *Distinguished Figures in Mechanism and Machine Science*, volume 1. Springer, Dordrecht. (Cited on page 13.)

[Papazian, 2000] Papazian, A. (2000). *Fabuleux trains du monde*. xxx, 1 edition. (Cited on page 15.)

[Tzanakakis, 2013] Tzanakakis, K. (2013). Earliest Traces In: The Railway Track and Its Long Term Behaviour. In *Springer Tracts on Transportation and Traffic*, volume 2, pages 3–6. Springer Verlag. (Cited on page 12.)

[Wais, 1976] Wais, F. (1976). *Historia de los Ferrocarriles Españoles*. Editorial Nacional, 2 edition. (Cited on page 17.)

[Werner, 1997] Werner, W. (1997). The largest ship trackway in ancient times: the Diolkos of the Isthmus of Corinth, Greece, and early attempts to build a canal. *J. R. Statistical Society*, 26(2):98–112. (Cited on page 12.)

Chapter 2

Railway rolling stock: safety and maintenance aspects

> People's lives are in the care of the railways when they get on a train. The railways should remember that.
>
> Nina Bawden

The second chapter of the manuscript addresses the industrial context and practices on safety and maintenance. The bogie subsystem, its suspension levels and some of the most relevant designs will be described, along with the specific structure of a FLEXX Compact bogie from Bombardier Transportation. A discussion on the quality methods and norms regarding the validation of rolling stock will ensue, underlining the definition of a risk, its criticality and acceptability. The analysis of the Failure Mode and Effects Criticality Analysis (FMECA) of the bogie will be presented and the possibility of multiple failure modes will be discussed. The safety practices regarding the dynamic behaviour of railway rolling stock (UIC-518) will be discussed, focusing on the use of virtual simulations for safety assessment and the suitability for the purposes of the works.

Contents

2.1 Technological aspects: the bogie

From its early stages of development, railway technology has required multiple innovations to meet the demands of railway operators. The bogie is one of the earliest evolutions of the architecture of the rolling stock and, more precisely, of the rolling gear in railway vehicles. Its origins are traced back to the first half of the 19th century, when early railway companies sought an increase of performances by transporting more passengers and goods, at higher speeds. First wagons and carriages where very much like chariots and had inherited many of their features, such as their short wheelbase. Engineers sought to enlarge wagons and carriages to increase the available space for payload, lengthening the vehicles wheelbase. This choice became cumbersome when it was coupled with the desired increase of operational speeds: the longer wheelbases were prone to hunt at the new speeds, leading to an excessive motion of the vehicles and an unstable behaviour [Wickens and Iwnicki, 2006], much to the passengers discomfort and the engineers concern for safety.

The bogie was the empirical solution to solve two different problems which had arisen with the lengthening of the vehicles wheelbase: hunting motion and unease curve negotiation of long vehicles on tight curves. A rigid frame holding two or more axles or wheel-sets, with a much shorter wheelbase, would be more stable at higher speeds, thus ensuring safe operation. Moreover, two arrangements of this system could be combined with a longer carbody. A link by means of a bolster and pivot link would hence result in a better ability of the vehicle to negotiate tight curves. Thus, the bogie became a commonplace solution to provide a smooth, stable ride. Although first applications were restricted to passenger carriages, mainly on luxurious trains, nowadays the bogie has been retained as the best arrangement of rolling gear on railway vehicles of any kind: powered units, passenger or freight vehicles.

2.1.1 Structure of a bogie

The formal structure of the bogie has remained stable since its conception in the 19th century. A rigid, metallic frame withholds two or more wheel-sets, as well as all suspension elements and other organs (braking systems, power chains or even tilting devices). Contrary to early railway vehicles, the suspension on bogies is split in two consecutive suspension stages, which provide a better performance in terms of both safety and comfort. The wheel-sets are attached to the bogie frame by means of the *primary suspension*, which ensures a correct transfer of the efforts coming from the carbody to the track, as the contact between wheels and rails and the guiding of the wheelsets is essential for the vehicle safety. The bogie frame is attached to the carbody by means of the *secondary suspension*. The complexity of this level depends on the kind of vehicle (Figure 2.1). In addition, secondary suspensions are responsible of ensuring gauge restrictions and/or passenger comfort.

Figure 2.1: TGV bogies (Alstom). The left image is a motor bogie, fitted with rubber-to-metal primary springs and secondary coil springs. On the right, a trailer Jakobs bogie between two cars, with rubber-to-metal primary springs and secondary air spring suspension. *Self-owned picture.*

From a formal point of view, one can split the bogie structure into several components represented by masses and a certain amount of mechanical properties, characterising the suspension (see Figure 2.2, right). Therefore, the primary suspension on a two-axle bogie could be represented by four ensembles of three couples of parallel stiffnesses and dampers, one per each spacial axis of the vehicle: longitudinal, transversal and vertical [Garg and Dukkipati, 1984]. The secondary suspension can be defined following the same principles. Additional stiffnesses can be added to represent the bogie frame inherent flexibility (e.g. torsional stiffnesses between two halves of the bogie).

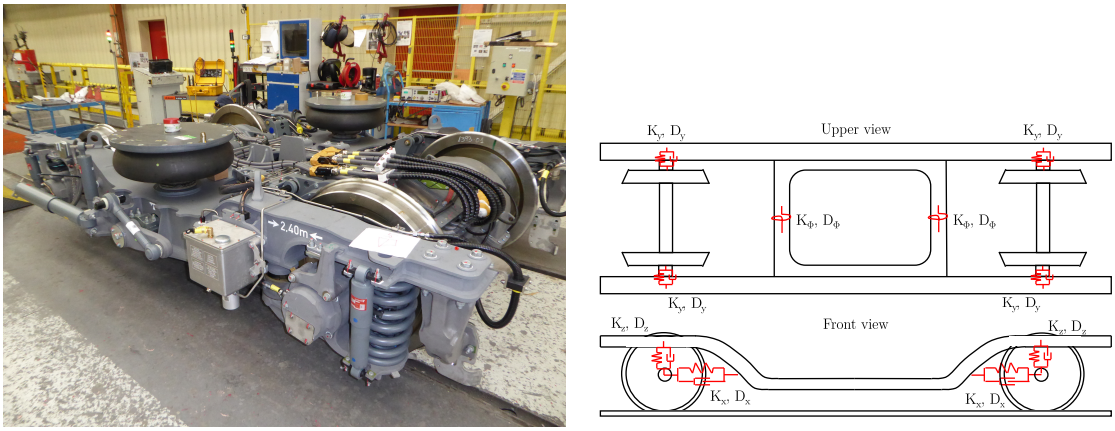

Figure 2.2: Left picture, FLEXX Compact extremity motor bogie to equip R2N trainsets. Right picture, formal scheme of a two-axle bogie. The primary suspension is composed of three couples of parallel springs and dampers, acting on the axleboxes. *Self-owned picture.*

Current bogie designs follow almost always the two-stage principle stated previously. There are multiple principles to address the specific design of each of the suspension stages, but there is a shared rule regarding their conception: the overall performance of the suspension stage is the result of several specific elements ensuring well-separated functions. For example, the primary suspension of a bogie can be split into several elements around the axlebox:

- There will be one or more elements bearing the vehicle vertical load, which has to be transmitted to the track. These efforts stick the train wheels to the rail and are crucial for some aspects on safety assessment, like the derailment aptitude of the vehicle or its curving behaviour.
- Each of the axleboxes has a structural element which ensures the guiding of the wheelsets and the transfer of the longitudinal efforts between the axles and the bogie frame. These suspension organs come in multiple forms, from lift arms to rubber-to-metal springs. Their role is foremost important for the study of dynamic phenomena like hunting motion.
- The dissipation or damping of the vibrations issued from the wheel-rail contact and the track irregularities is mainly ensured by several types of elements, such as hydraulic dampers or friction interfaces. Other structural elements (bushings, for instance) might provide additional complementary damping.

The sections hereafter will develop this principle in more detail, addressing each suspension level with examples of different architectures of bogies (either on freight and passenger trains), or tractive vehicles (locomotives, Electric Motor Units - EMUs, or Diesel Motor Units - DMUs).

2.1.1.1 Primary suspension

The primary suspension of a bogie connects the rolling parts (namely the wheelsets and the axle-boxes) to the bogie frame. The first elements used on the primary suspension were leaf springs, which were inherited from chariot technology. These elements are built as stack-layered, bow-like assemblies of metal sheets, clamped on their extremities with two metallic ties. The main handicap of leaf springs is their lack of damping properties, except for the friction between the metallic leaves. This dissipative effect is not sufficient to cope with higher energies. The evolution on primary suspension lead to the aforementioned split of functions between several elements and a wise layout arrangement of the suspension organs. Vertical efforts were granted a specific element, channelling them from the bogie frame to the axle box. The use of coil springs became commonplace, as they can provide an excellent vertical stiffness, K_z, although they have little to none damping capacities.

This lack of damping can be compensated by using other devices in parallel to the stiff suspension elements. For example, freight vehicles fitted with the UIC standard bogies Y25 and

Y26 bear two coil springs per axle-box in the primary suspension, plus a Lenoir link and friction plates (Figure 2.3). The axle-box has a plate surface which is greased and slides against a second surface, rigidly mounted on the bogie frame. The Lenoir link has the shape of a rounded square chain lock, linking the bogie frame and the axle box. When the axle box moves vertically, the link causes a relative rotative motion of one of the springs lower base. Such movement crushes the friction plates against each other, providing a damping D_z for the vertical motion. Damping on passenger trains is ensured by more refined organs, mainly hydraulic dampers filled with oil, which are fastened in parallel to stiffer, non-dissipative elements, linking the axlebox to the bogie frame.

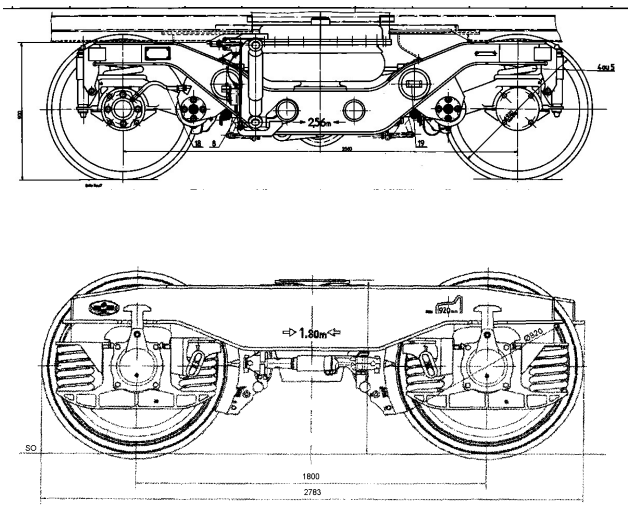

Figure 2.3: Passenger carriage bogie using an arm link (upper image), freight bogie fitted with coil-springs and axlebox guidings (lower image), damping is ensured by friction interfaces and a Lenoir link (Y25), or hydraulic dampers (Y32). *Images from: Y32 - http* : $//forum.e-train.fr/album_mod/upload/grandes/acd23064c8f4830e0f7e7db3fc1730ac.jpg$, *Y25 - http* : $//www.innobogies.de/en/ELH\%20Y25LsifC\%20en.html$.

The guiding efforts from the wheelsets are managed in several ways. In the case of passenger vehicles, early bogie frames were heavy, rigid structures, made of cast iron and holding the axle-boxes very tightly to ensure the guiding of the axles. Technology improvements have led to lighter structures and the design of the bogies has been reviewed extensively. The guiding of the axle-boxes and the wheelsets is performed nowadays by structural elements (Figure 2.3). Articulated links between the axle-box and the bogie frame are well spread among passenger vehicles, as well as elastic structural suspension elements, like rubber springs. These elements have strong longitudinal and lateral stiffnesses, K_x and K_y. The use of rubber-to-metal parts has become quite common from the 1970s until now, as their strong resistance is coupled with damping

Figure 2.4: Primary coil springs and secondary stack-layered rubber-metal spring on SNCF engine BB 7296. The axlebox traverse is linked to the bogie frame by a traction rod on its right side. *Self-owned picture.*

capacities, which are highly appreciated to filter vibrations at an early stage of the suspension.

Traction efforts in powered vehicles may need special arrangements to ensure their correct transmission through the bogie. Locomotives bear usually traction rods, which can link several axle boxes and be attached, either to the bogie frame or, sometimes, directly to the frame of the carbody (see Figure 2.4).

Other architectures for bogies combine all these functions through multi-purpose elements, rubber-to-metal chevrons for instance (Figure 2.5). In such cases, all functions are ensured by two twin elements acting as guiding elements and load conveyors, accounting for all the necessary stiffnesses for each role. The damping D_i on the primary suspension in this arrangement is restricted to vertical motion, damper systems acting in parallel to the suspension elements, directly over the axlebox.

2.1.1.2 Secondary suspension

The secondary suspension of the bogie links the carbody to the bogie frame, thus transmitting all the efforts from the body towards the primary suspension and, through it, to the track. Early examples of the secondary suspension came in the form of a bolster placed across the bogie frame, through two hollow spaces, bearing a center pivot link to the carbody. Sliding interfaces equipped with friction garments provided damping to this stage of the suspension. This principle has been

Figure 2.5: The axleboxes are framed by two stack-layered rubber-metal chevrons on each side. *Image by https* : $//www.feckin - mad.co.uk/forum/viewtopic.php?t = 2608$.

retained until today for freight vehicles, such as the mentioned Y25 and Y26 standard freight bogies, but is insufficient for the exigent performances required on passenger vehicles. The use of bigger, more resistant leaf springs, was a first attempt to improve slightly the performances of the secondary suspension.

Current solutions for passenger vehicles use a widespread principle: the use of air cushions (air springs) (Figure 2.8). This system consists on two bellows, inflated through a system of pressured air, which is regulated through a control loop. The cushions communicate through a pipe, complemented by a compensation reservoir attached. When the carbody rolls sideways, the cushions exchange the air and equilibrate the system. Air springs allow a regulation of the secondary suspension as well, ensuring the height of the train over a certain range of loads. The counterpart of this system is the air springs lack of a major transversal stiffness. The bogie is fitted with two systems which provide the necessary properties to counter longitudinal and lateral motion recovering the efforts from the carbody: the anti-roll bars and the pivot link placed on the bogie centre. The anti-roll bar system consists in two lateral levers, attached to the carbody and linked through a transversal torsion bar which crosses the inside of the bogie frame, placed on several bearings. Whenever the vehicle has a sideways roll motion, the levers translate the vertical movement of each side of the carbody into an asymmetrical torsion input, which is then transferred to each side of the anti-roll bar. The bar will then counter the displacement thanks to its torsional resistance. In case the lateral motion is strictly transversal (i.e. not caused by the carbody roll movement), the pivot is fitted with two sets of bump stops: lateral and longitudinal. The lateral bump stops prevent excessive lateral movements and act as a last system preventing gauge violations for extraordinary roll motion of the vehicle. Longitudinal bump stops are in charge of transmitting tractive and braking efforts to and from the bogies.

The damping of the different motions on the secondary suspension is clearly split in several

functions, each one with its own entitled dampers. Vertical movements between the bogie frame and the carbody are dissipated by vertical dampers. Their extremities are attached to each of the aforementioned structures, usually through spherical bushings. The lateral oscillations of the carbody are damped by a transversal damper, which can be placed beneath the bogie frame, connecting a bracket and the carbody pivot. Finally, some kinds of vehicles may bear yaw dampers, placed longitudinally along the bogie frame, linking it to the carbody. Yaw dampers have a major role, as they prevent the hunting motion of the bogie to spread across the vehicle and to excite any eigenmodes. They are customary when the vehicle top speeds overcome 160 km/h, but they can also be installed on lower speed trainsets, to provide enhanced comfort performances.

Pendular trains are fitted with much more complex secondary suspensions. The train roll motion is controlled by the tilting system, which increases the carbody roll motion in curves. The increased carbody roll compensates the stronger lateral acceleration, allowing higher speeds in curves. This arrangement makes anti-roll bars senseless, for the automatic loop which controls the tilting ensures the respect of gauge restrictions. The interface between the bogie frame and the secondary suspension is usually composed of a group of servo-motors and kinematic links acting over a "floating" bolster. Air-springs are placed over the bolster, thus providing the desired comfort for the vehicle. However, longitudinal efforts must still be transmitted to and from the bogie frame. The bolster is hence equipped with a centre pivot and a two-side bumpstop interface, which ensures this kinematic link.

2.1.2 Bogie components within a FLEXX Compact

In the context of our project, the trainset which will be studied is equipped with three kinds of FLEXX Compact bogies. Depending on their position and purpose, the bogies can be "extremity" (two per trainset, one on each end) or "Jakobs" (intermediate, one per inter-car space). According to their positions, the bogies have different layouts, so as to provide the required functionality on each position (Figure 2.2, left) In addition, bogies can be powered (motor bogies) or un-powered (trailer bogies). The trainsets which will be analysed comprise two Bogie Moteur d'Extrémité (BME, French abbreviation for extremity motor bogie), several "Bogie Trailer Jakobs" (BTJ, Jakobs trailer bogies) and one or two "Bogie Moteur Jakobs" (BMJ, Jakobs motor bogies). The main differences between the three versions of the FLEXX Compact arise from their respective roles within the trainset. Motor bogies are equipped with two motors with their gearboxes, one assembly per axle. Conversely, trailer bogies are not fitted with power systems.

A FLEXX Compact bogie has around 37 suspension elements of all kinds, distributed between the primary and the secondary suspension. The bogie elements can be classified in several general families, according to their base materials and their position within the structure:

Figure 2.6: Medium-length trainset of the OMNEO platform from Bombardier Transportation, supplied to SNCF in several configurations from 6 up to 10 cars. © *Bombardier*.

- Primary suspension components (Figure 2.7).
  - Metallic elements: four primary coil springs, four metallic bump stops, frames on other suspension organs.
  - Rubber-based elements: four primary rubber-springs, four rubber bump-stops, gaskets, etc.
  - Composed elements: four primary hydraulic dampers.

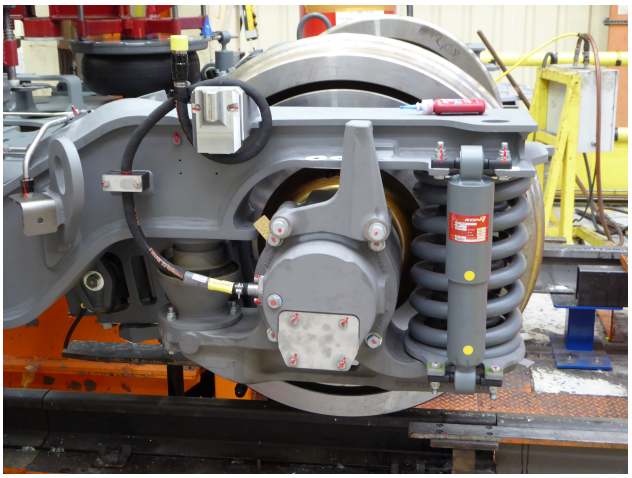

Figure 2.7: Primary suspension on a FLEXX Compact trailer Jakob bogie for a R2N trainset. The primary suspension consists in an outer coil spring on the right of the axlebox, an inner rubber spring on the left of the axlebox, a hydraulic damper parallel to the coil spring and a primary rubber bump stop on top of the axlebox (hidden from the view). *Self-owned picture.*

- Secondary suspension components.
  - Metallic elements: extremity motor bogies are fitted with two anti-roll bar levers and links, one anti-roll bar and four metallic bump stops. Jakobs bogies, powered or not, are fitted with four anti-roll bar levers and links, two anti-roll bars and four metallic bump stops (Figure 2.9).

  - Rubber-based elements: extremity motor bogies are fitted with four rubber bump-stops, several gaskets, two emergency springs and two bellows of the air springs. Jakobs bogies, powered or not, are fitted with four rubber bump-stops, several gaskets, four emergency springs and four bellows of the air springs (Figure 2.8).
  - Composed elements, such as the secondary hydraulic dampers. Except for the single lateral damper, common to all configurations, all the other dampers depend on the lay-out of the bogie: extremity motor bogies bear two yaw dampers, two vertical dampers and two air springs. Jakobs bogies have generally no yaw dampers, but are fitted with four vertical dampers and four air springs.
- Structural elements, such as the bogie frame, the bogie bolster, the carbody pivot, etc.

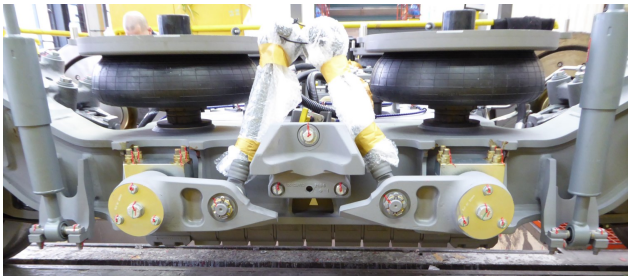

Figure 2.8: Secondary suspension on a FLEXX Compact inter-car Jakobs bogie for a R2N trainset. Higher speed vehicles also bear yaw dampers. Inter-car dampers can also be present, directly attached between the carbodies. *Self-owned picture.*

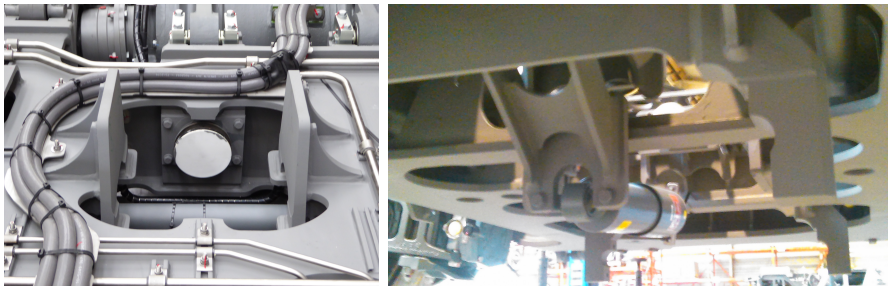

Figure 2.9: **Left picture**. Pivot hollow on a FLEXX Compact extremity motor bogie for a R2N trainset. The longitudinal bump stop is visible in the middle. Lateral bump stops are attached to the car pivot, which is inserted in the hollow space and links both of the abutting carbodies. **Right picture**. Lateral motion of the secondary suspension is damped by a dashpot placed under the bogie frame, attached to the carbody pivot. On the upper right corner, barely visible, one of the anti-roll bars. *Self-owned picture.*

2.2 Quality tools: norms and methods

The manufacture of railway rolling stock is subjected to strict controls, ensuring the quality of the products an their safe operation. The main standard superseding any local rule within the European Economic Space is the norm EN-50126. Derived in part from the electronics standard IEC-61508 (see [EN50126, 2010]), it encompasses its main principles, translating them to the railway industry. Its purpose is the specification and demonstration of Reliability, Availability, Maintainability and Safety of railway applications (RAMS for Railway). The rolling stock *reliability* relies on the study and knowledge of the system failure modes. It addresses the ratio of appearance of such failures - or at least, the estimated probability that such an event occurs - taking into account the impact over the vehicle systems. The *availability* of a railway vehicle would be the aptitude or readiness to give service, provided that it has been subjected to proper maintenance operations. *Maintainability* is defined as the aptitude of the system to be subjected to maintenance, hence the quantification of maintenance operations (time, planning, periodicity) in a manner that ensures the vehicle *safety* in operation.

The first stage of the method is the formal definition of a risk. The norm considers as a risk any event that may cause harm to the passenger, the environment or the railway system, being it isolated or combined to other failures. The risk source is the non-compliance of the system because of a hazardous event, or failure mode. These events can occur with different periodicities, from likely to incredibly rare. The consequences of a failure mode can rank from insignificant up to catastrophic. Thus, the norm sets a tool to assess each case to determine whether a risk would be tolerable or not. It is the risk matrix, which is set up by crossing the failure modes' outcome gravity with their occurrence rate (see Table 2.1). This matrices are modulated according to each countries own standards and customs. The EN-50126 lists several examples of risk acceptance principles for some countries:

- A risk can be deemed acceptable if it is *As Low As Reasonably Possible* (ALARP). It is a British standard which allows a risk to be undertaken if preventing the risk is impossible or if the costs of a preventive effort are too costly compared to the improvement. However, it is to be noted that the probability of occurrence of an ALARP risk must be reduced as much as possible.

- The concept of specific risk becomes more fuzzy within the French principle GAMAB, standing for "*globally at least as good*" (in French, Globalement Au Moins Aussi Bon). Here the norm grants much more freedom to the quality engineer, who is allowed to modulate individual risk rates, provided that the global outcome of his work is as good as the precedent system (for example, same or lower injury rate, passenger/km and train).

- The German principle of Minimum Endogenous Mortality (MEM) is set on a statistical basis. Human beings face injury or dead risks throughout their lives, among which one can count

technological hazards. The aim of this principle is to prevent the increase of the technological hazards associated to the analysed technology, in this case, railway applications. Thus, the norm states three rates (occurrences/Mkm and year) that must be respected: death rate, severe injuries rate and minor injuries rate.

	Insignificant	**Marginal**	**Critical**	**Catastrophic**
Frequent	Undesirable	Intolerable	Intolerable	Intolerable
Probable	Tolerable	Undesirable	Intolerable	Intolerable
Occasional	Tolerable	Undesirable	Undesirable	Intolerable
Remote	Negligible	Tolerable	Undesirable	Undesirable
Improbable	Negligible	Negligible	Tolerable	Tolerable
Incredible	Negligible	Negligible	Negligible	Negligible

Table 2.1: Risk assessment and acceptance criteria according to hazard (horizontal categories) and frequency (vertical categories) [EN50126, 2010].

Once the general risk assessment has been performed, its conclusions are translated to the system requirements and subsequently cascaded to the design of the vehicle, following the so-called "V-approach". The definition of the system design is followed by the draft of the Failure Mode Effects and Criticality Analysis (FMECA) of the vehicle and its subsystems, including the bogie. The FMECA lists *every* failure mode which can occur to each component of a subsystem, along with its causes, its consequences, the failure rate and the criticality rate which is associated to each case, according to the criticality matrix. The FMECA states the palliative measures that must be provided when a failure mode appears. Such dispositions might be a degraded operation mode, allowing the safe evacuation of both the vehicle and the payload, or might demand a strict stop of operations. This tool has, by its exhaustive draft, a specific interest for our works and constitutes the starting point to choose the suspension elements which will be studied further on.

2.3 FMECA study: a revision methodology

The main aim for Bombardier is to draft a methodology supplying some general rules, which would enable any quality engineer to determine several starting points to optimise the bogie maintenance cycles. Proceeding through the stages of the process, the engineer should be able to choose the elements which are most interesting for such purposes. The FMECA analysis of a FLEXX Compact bogie will be the basis of this methodology. The FMECA is divided into multiple subsections: bogie frame and structures, primary suspension elements, secondary suspension elements, wheel-sets, etc. Within this work, the focus will be placed on suspension elements, as they have a key role in defining the system behaviour.

FMECA analysis are drafted by the RAMS engineers attached to each project. In spite of sharing a common basis, FMECA analysis can appear in different arrangements or formalisms. An internal document from Bombardier has been used as an homogenization standard. Furthermore, there are families of elements which are distributed across the sections of FMECA, such as the dampers, which are distributed over the 1^{ary} and 2^{ary} suspension. In order to systematize the treatment of similar elements, their failure modes will be drafted or adapted to match certain standard cases. This preliminary check of the FMECA document of the bogie is customary before undertaking any review aiming optimisation.

2.3.1 Multiple-failure cases - FMECA Review

A railway vehicle has a considerably number of suspension elements within its rolling gear. It is reasonable to expect that some of such elements might incur in a failure mode simultaneously, thus leading to combined situations where their effects could have more serious effects to the vehicle integrity. The FMECA of the bogie has been used as the first stage of an assessment on multiple-failure events and their probability of appearance. Each element in FMECA is listed with all its failure modes. The feedback from previous projects and the discussions with suppliers allow the manufacturer to determine a failure rate for each component.

A component failure rate is usually expressed in *Failures Per Million Kilometres*, FPMK. That is, the amount of failures on such an element, over periods of one million kilometres. This is, however, the probability of encountering *one* of the element multiple failure modes, not a *precise* one. Hence, engineers attribute to each suspension organ internal share rates, which account for the probability of each failure mode occurring. Thus, the product of both rates yields the rate of each failure mode in FPMK. As the vehicle is expected to run a certain amount of kilometres throughout a year service, it is possible to calculate another safety rate, the *Failures Per Hour*, FPH, which is used extensively to define failure rate limits in criticality matrices. As one of the global aims of the project is to reduce the maintenance cycles and the

amount of interventions, the first step is the search for the most frequent failure mode combinations.

However, the FMECA supplies further information about each failure mode, most importantly, its criticality rate. The individual failure rates FPH and FPMK can be combined with this indicator, yielding the probability that an event of a certain criticality occurs. This criticality rate is directly linked to the safety matrix described previously, and to risk acceptance criteria. Thus, the subjective levels of the criticality matrix are translated into precise occurrence rates for each FMECA. These values set the safety aims that must be respected to ensure the vehicle compliance. Each level of criticality has its own limits: for example, extremely critical failure modes with an FPH higher than 10^{-9} occurrences per hour would be deemed unacceptable.

2.3.1.1 Failure rates and criticality: analysis on the bogie components

The FMECA analysis and its results have to be transposed to other engineering tools to test the conclusions. Safety assessment in rolling stock can be performed through numerical means (see conditions given by [UIC518, 2009]). Thus, it is of a great importance that the elements which are studied from FMECA are also represented on the modelling of the system. The suspension organs which will be subsequently analysed are listed below:

- The *primary coil spring* (named *Primary Outside Spring*, PSo, as well).
- The *primary rubber spring* (named *Primary Inside Spring*, PSi, as well).
- The *primary damper*, PD.
- The *secondary vertical damper*, SDz.
- The *secondary lateral damper*, SDy.
- The *yaw damper*, YD.
- The *secondary auxiliary spring* (named *Secondary Suspension Emergency spring*, SSE, as well).
- The *anti-roll bar* (named *Anti-Roll Torsion Lever*, ARLT, as well).

There are four criticality levels set up by the FMECA, which encompass all the possible failure modes within the suspension elements. They rank from A (topmost critical) to D (lowest criticality). Therefore, if one groups each element failure modes by their criticality rate, each suspension element can be described by four internal share rates, one per criticality level. For example, should a primary rubber spring, PSi, endure a failure, there is a 97,3 % of chances that the failure has the

lowest criticality level, "D"; no chances (0 %) to have a marginally critical level; 0,20 % chances to be a 2^{nd} criticality rate level, "B"; and 2,5 % chances that the level has the highest criticality, "A").

2.3.1.2 Frequency rates on failure mode combinations

The criticality levels can be paired to form failure rate matrices. The suspension elements listed above are set face-to-face, on each criticality level, with their own FPH/FPMK. Crossing the failure rates from both sides of the matrix yields the appearance rate for a combination of two failure modes over a trainset. Should the combination of the failure modes' rates fail to be lower than the fixed limits, the combination would be deemed critical. Therefore, the four criticality levels can be combined in ten couples of criticality levels: A - A, A - B, A - C, A - D, B - B, B - C, B - D, C - C, C - D, D - D. Each of this couples corresponds to a combination of two elements' failure modes of the criticality grades listed above, over a trainset, at any place of the train rolling gear (i.e. the failures can either be over the same bogie, or in opposite extremities of the train)(see Tables 2.2 and 2.3).

Each criticality level has an associated appearance rate beyond which a failure mode is deemed unacceptable. *Most critical* failures cannot have an FPH over 10^{-9} occurrences, *critical* failures are bounded to an FPH of 10^{-7} occurrences, *marginal* failures must not exceed an FPH of 10^{-5} occurrences, while *insignificant* failure modes are restricted to 10^{-3} occurrences per hour. Regarding the combinations of the criticality levels, it has been chosen that the most restrictive FPH of the two combined levels should be kept, to ensure the safety performance of the system.

			FPMK - A class failure mode							
			PSo	PSi	PD	SDz	SDy	YD	SSE	ARLT
			0,000E-00	1,845E-04	1,610E-04	0,000E-00	0,000E-00	0,000E-00	1,000E-03	0,000E-00
FPMK - A class failure mode	PSo	0,000E-00	0,000E-00	0,000E-00	0,000E-00	0,000E-00	0,000E-00	0,000E-00	0,000E-00	0,000E-00
	PSi	1,845E-04	0,000E-00	3,404E-08	2,970E-08	0,000E-00	0,000E-00	0,000E-00	1,845E-07	0,000E-00
	PD	1,610E-04	0,000E-00	2,970E-08	2,592E-08	0,000E-00	0,000E-00	0,000E-00	1,610E-07	0,000E-00
	SDz	0,000E-00	0,000E-00	0,000E-00	0,000E-00	0,000E-00	0,000E-00	0,000E-00	0,000E-00	0,000E-00
	SDy	0,000E-00	0,000E-00	0,000E-00	0,000E-00	0,000E-00	0,000E-00	0,000E-00	0,000E-00	0,000E-00
	YD	0,000E-00	0,000E-00	0,000E-00	0,000E-00	0,000E-00	0,000E-00	0,000E-00	0,000E-00	0,000E-00
	SSE	1,000E-03	0,000E-00	1,845E-07	1,610E-07	0,000E-00	0,000E-00	0,000E-00	1,000E-06	0,000E-00
	ARLT	0,000E-00	0,000E-00	0,000E-00	0,000E-00	0,000E-00	0,000E-00	0,000E-00	0,000E-00	0,000E-00

Table 2.2: Risk assessment and acceptance criteria according to hazard (horizontal categories) and frequency (vertical categories).

			FPMK - A class failure mode							
			PSo	PSi	PD	SDz	SDy	YD	SSE	ARLT
			0,000E-00	1,845E-04	1,610E-04	0,000E-00	0,000E-00	0,000E-00	1,000E-03	0,000E-00
FPMK - D class failure mode	PSo	1,020E-02	0,000E-00	1,882E-06	1,642E-06	0,000E-00	0,000E-00	0,000E-00	1,020E-05	0,000E-00
	PSi	7,181E-03	0,000E-00	1,325E-06	1,156E-06	0,000E-00	0,000E-00	0,000E-00	7,181E-06	0,000E-00
	PD	3,164E-02	0,000E-00	5,837E-06	5,093E-06	0,000E-00	0,000E-00	0,000E-00	3,164E-05	0,000E-00
	SDz	1,081E-02	0,000E-00	1,995E-06	1,741E-06	0,000E-00	0,000E-00	0,000E-00	1,081E-05	0,000E-00
	SDy	1,582E-02	0,000E-00	2,918E-06	2,547E-06	0,000E-00	0,000E-00	0,000E-00	1,582E-05	0,000E-00
	YD	9,820E-03	0,000E-00	1,812E-06	1,581E-06	0,000E-00	0,000E-00	0,000E-00	9,820E-06	0,000E-00
	SSE	4,000E-03	0,000E-00	7,380E-07	6,440E-07	0,000E-00	0,000E-00	0,000E-00	4,000E-06	0,000E-00
	ARLT	7,930E-03	0,000E-00	1,463E-06	1,277E-06	0,000E-00	0,000E-00	0,000E-00	7,930E-06	0,000E-00

Table 2.3: Risk assessment and acceptance criteria according to hazard (horizontal categories) and frequency (vertical categories).

The results of the crossed-failure modes have yielded a single combination which exceeds the FPH limit attributed for its criticality level. It is the combination of a critical failure on an emergency air-spring (SSE) plus a negligible failure on a primary damper (PD). Therefore, over one million kilometres, there might be $3{,}164 \cdot 10^{-5}$ occurrences of a coupling of one SSE from a trainset with a PD on the same EMU. Nevertheless, this index does not account for the fact that two simultaneous failure modes do not imply the cumulation of their effects. To expect a cumulative effect of such a kind, the failing elements should be placed on a neighbouring environment, such as the same bogie or the same train car. Thus, it is possible to calculate the amount of combinations of SSE + PD elements within a bogie or within a train car, then to translate them over the amount of combinations over the whole trainset, to yield a penalty factor which can be applied to the FPMK rates on the tables above.

Taking as an example the simplest version of a Régio 2N trainset with six cars, there are two extremity motor bogies plus five Jakobs bogies. Extremity bogies bear two SSE elements, whilst BTJ and BMJ bogies bear four SSE elements. Regardless of their type, all bogies are fitted with four PD elements. Therefore, there amount of combinations of SSE + PD failures can be calculated as:

$$N_{Total} = N_{BME} + N_{BXJ} \tag{2.1}$$

$$N_{BME} = 2bogies \times 2\frac{SSE}{bogie} \times 4\frac{PD}{bogie} \times 7bogies \tag{2.2}$$

$$N_{BXJ} = 5bogies \times 4\frac{SSE}{bogie} \times 4\frac{PD}{bogie} \times 7bogies \tag{2.3}$$

There are 672 combinations of SSE + PD elements over the simplest version of the Régio 2N trainset. From a close-neighbourhood point of view, an SSE element has four direct combinations with a PD element at a bogie scale. If the scale is each car of the train, each SSE can be related directly to eight primary dampers. Consequently, from all possible combinations of emergency springs and primary dampers, only 96 combinations would be critical on a bogie-scale basis (∼14 % of the combinations), for 256 combinations on a car-scale environment (∼38 % of the possibilities). Therefore, the expected FPMK of $3{,}164 \cdot 10^{-5}$ occurrences should be penalized by the factors to take into account the topological aspects on the coupling of failure modes. The final FPMK rate is, at the worst case, $1{,}2027 \cdot 10^{-5}$ combined failures of critical (A) rate on SSE plus negligible (D) rate on PD elements. This amount is lower than the limit for topmost critical failure modes on the FMECA, hence proving that the coupling of critical failure modes is an unlikely event within the context of the study.

2.3.2 Decision tree

The choice of the suspension elements which are most interesting for a possible optimisation of maintenance cycles requires a careful review. As it has been described, frequency rates of each failure mode do not justify the study of combinations of failure modes. Furthermore, the definition of some of the failure rates might be inaccurate when describing the phenomena involved in long-term ageing, beyond current life-cycles. Consequently, a different approach to analyse the FMECA has been drafted, aiming the choice of several suspension elements on a maintenance basis plus safety aspects. To do so, a sequence of questions has been developed. The questions are applied recursively to each suspension element (maintenance steps), then to each of its failure modes (safety steps), which will be then classified according to the outcome of the sequence. The decision process is set as follows:

- *"Are the bogie subsystem elements dismounted during overhaul operations?" (i.e. The subsystem is subjected to periodical replacements, not merely dismounted as part of another intervention on the bogie).* If it is not the case, like the *bogie frame and structural elements*, the subsystem or family will not be considered any further. The rest of the component families or subsystems will undergo further enquiry.

- *"Is the component relevant, in principle, for the analysis?"*. Should the answer be negative - like for bump stops or other metallic elements -, the suspension organs will be skipped for the rest of the analysis.

  Once the families of elements and subsystems of the bogie have been selected, the decision process addresses the elements individual failure modes, as they are stated on the bogie FMECA. The main concern for a RAMS engineer is that non-mastered phenomena might appear within the system behaviour. Random (stochastic) events are already taken into account within the design process. However, an unexpected drift on the component properties could be much more troublesome.

- *"Is the failure of the components of a stochastic nature?" (i.e. It has a random nature, thus not obeying any laws which could be quantified by means of mechanical analysis, but rather depending on manufacturing/process random changes).* If the failure has a *stochastic nature*, its detectability will be checked: *"can failure be detected by visual inspection?"*. If it can be easily detected, its control can be advised through maintenance guides and easily checked. If the failure mode cannot be detected visually or by field means, a detailed discussion is to be undertaken within the engineering team. If the failure mode *is not of stochastic nature*, it can be characterized by means of engineering science, thus mastering its sources and behaviour.

  For example, rubber parts may endure a change on their mechanical properties which is driven by the material. These failure modes (non-compliance with the specified properties) obey to mechanical and chemical laws, hence being quantifiable. The breakdown of a rubber part,

albeit obeying a degraded state within the material, has a stochastic nature, as the triggering phenomenon driving the breakdown is an internal flaw within the material, whose appearance is purely stochastic.

- *"Is the failure caused by ageing or wear?"*. Wear and ageing are quantifiable mechanisms, whose characterization is within the scope of this work. Thus, any failure mode suspected to be age or wear sourced will be subsequently analysed. Nevertheless, some failure modes are hard to classify, such as a hydraulic damper decrease of damping rate. This failure mode can be caused by a loss of properties of the oil or by the filling of the cylinder inlets between the damper chambers. Failure modes of such kind will be subjected to further discussion with the engineers in charge of their design and specification.

- *"Can failure be detected by visual inspection?"*. If so, there is no major concern for the safety engineer, as the failure mode would be easily detected, thus preventing any dramatic effects on the operation of the railway vehicle. However, should the failure mode come unnoticed, the RAMS engineer must provide further safety assessment.

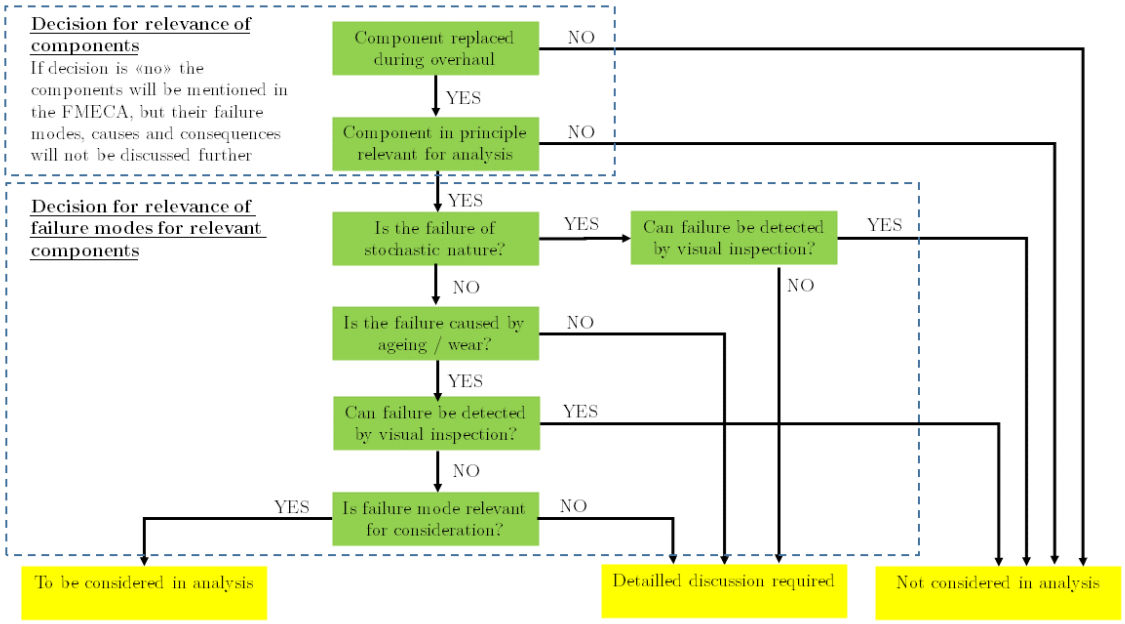

Figure 2.10: The element and failure mode analysis and the successive steps on the decision process are outlined within the diagram.

- *"Is the failure mode relevant for analysis?"*. This last question grants the engineer a great freedom of choice. Since the design of the subsystem foresees the introduction of countermeasures for certain failure modes, some of these can be left apart in the analysis. For example, the loss of integrity of a primary rubber spring will be countered by the inner center pin, which locks the spring and prevents it from disassembling. Furthermore, this failure would arise from a lack of cohesion between the rubber part and the metallic structures, thus being detectable by cracks or pitting. Therefore, the loss of stiffness in this part which could lead to its breakdown would not be as relevant as an uncontrolled increase of its stiffness, in the context of this process. This does not mean that such a failure mode is negligible, on the contrary, its relevance has already set design constraints on the parts design. At any case, failure modes considered as "non relevant" must be checked with each field experts, who would estimate the accurateness of the evaluation.

2.3.3 Review results

The former methodology has been applied to a FLEXX Compact FMECA provided by Bombardier. The outcome of this review has highlighted that rubber-based elements within the bogie account for most of the relevant, source-uncontrolled failure modes. Hydraulic dampers show some failure modes that could be interesting as well. The failure modes and elements which have been kept after the review are the following:

- Primary rubber springs, when suffering from an increase of stiffness.
- Auxiliary rubber springs of the secondary suspension, when suffering from an increase of stiffness.
- All kinds of dampers, when enduring a loss of damping ability, without oil leakage (which can be in turn easily detected).
- Damper bushings, when suffering from an increase of stiffness.

Some rubber-based elements have not been considered for analysis for different reasons, such as the bellows of the secondary air springs, or the bump stops of the bogie (both primary and secondary, around the bogie pivot). It can be argued that the bellows' volume and position are ensured by a control loop on the pneumatic system, which would force a stronger air input to cope with a higher stiffness on the bellows. The decision for the bump stops is based on their dimensioning. They are designed to be crushed under high efforts, with and underlying metallic frame providing a residual dry bump stop with ensures the system integrity. Thus, they will not being considered for this work purposes.

2.4 Safety risk assessment for rolling stock: UIC-518

The design of a railway vehicle requires thorough safety assessment to ensure its compliance with respect to the normative frame. The main text for safety assessment within the railway industry is the norm UIC-518, which supersedes any local norms - in fact, it inspires many countries' adaptations (such as the EN-14363 norm within the European Union). Its scope encompasses the vehicle safety assessment, as well as the train interaction with the infrastructure (track fatigue) and running behaviour.

The safety assessment on a vehicle can be undertaken at several situations: a design of a new vehicle requires several tests to assess its compliance according to UIC-518; safety assessment is compulsory as well for vehicles having endured thorough modifications which could have an impact on its dynamic behaviour, or if the operational conditions of the vehicle have been substantially changed. Since the aim of the DYNABOG project is to extend the maintenance periodicity of a vehicle, the safety assessment according to UIC-518 is hence mandatory. Moreover, it can be expected that the properties of some parts of the train may vary due to the lifecycle extensions, perhaps affecting the dynamic behaviour of the vehicle. Thus, both the second and third statements leading to safety assessment are fulfilled, and the tests indicated in the norm must be performed.

The UIC-518 provides the necessary indications to perform the safety assessment on both standard and special railway vehicles. Depending on the nature of the vehicle and whether it is a first approval or the re-issuing of an approval after substantial modifications, the norm grants some flexibility to engineers and manufacturers to adopt a certain test plan.

- Testing requires that the vehicle runs over all kinds of tracks that will be encountered under operation: straight tracks, curves of tight, medium or large radius, and special tracks such as switches or crossing points.

- For new rolling stock, it is compulsory that all conditions and situations are tested and/or simulated, which is called a *full testing*. *Partial* test procedures are applied when some of the conditions do not apply to the case (for example, a train does no longer run over a certain speed).

- The test methodology applied to the test procedure can be *normal* if it evaluates the vertical and lateral efforts on the vehicle wheelsets. It will be *simplified* if the train behaviour is assessed with shift effort measurements over the instrumented axles, as well as with lateral and vertical accelerations. *Numerical* methodology accounts for the same constraints of the normal case, implemented on an appropriate simulation software.

Another important point is the choice of the rail and wheel profiles, which should be a worn shape of a standard shape, such as the S1002 and UIC60 profiles. Moreover, the track profile and faults (alignment, levelling, etc.) must be representative of those of the routes served by the rolling stock. Faults in the rolling stock must be simulated as well, in order to ensure maximum safety. Weather conditions and changes on characteristics (such as several friction coefficients along different sections of the track) can also be taken into account.

According to the appendix B.2 of the norm, vehicles subjected to changes on their suspension characteristics must undertake tests under empty and loaded cases, and test runs over straight and curved tracks, with large and small radii.

In spite of having chosen an approved model of rolling stock to develop this procedure, from a formal point of view, the methodology could be applied to any kind of rolling stock produced by Bombardier: new-to-be-approved and already in service. According to the norm, numerical simulations fit best the needs of the project, as they can be used both for approving new vehicles and to extend pre-existing rolling stock approval, when it is derived from a "base" design in terms of the UIC-518.

2.5 Conclusion

The bogie FLEXX Compact from Bombardier belongs to one of the latest generations of bogie designs on the current state-of-art of the railway industry. Its conception mixes metallic, durable suspension elements, with rubber-to-metal parts, providing both structural and vibrational-damping properties, and composed elements like hydraulic dampers or air-springs. The studied model has been implemented on past projects from Bombardier, such as Talent trains in Germany, and in current deliveries in France, for the Francilien commuter EMUs for Paris and Île-de-France and the Régio 2N regional EMUs.

The development of a strategy to optimise maintenance cycles must start through soundly-based quality tools. The FMECA of the bogie provides the suspension component failure rates and criticality, allowing the engineer to choose the most critical events and to provide countermeasures. However, the analysis of the FMECA has proved the unlikeness of a combination of failure modes, for the most critical failures have been prevented via very low appearance rates. Furthermore, the use of a criticality approach on the search for a better maintenance periodicity does not appear as the optimal system, for some of the failure rates are based on current state-of-art knowledge and might not be accurate when used within an overhaul extension process. Therefore, a systematic approach through a decision tree has been drafted. It is based on maintenance observations (detectability of failures) and scientific knowledge (mastering of the phenomena involved on the failures, randomness of the mechanisms, etc.), rather than on criticality and failure rates alone. The developed approach has led to the choice of several suspension elements of the FLEXX Compact, which will be subsequently analysed throughout this document: the primary suspension *primary rubber spring* (PSi) and the secondary suspension *auxiliary rubber spring* (SSE).

The safety assessment for railway rolling stock must be set up accordingly with the normative frame. The demands enforced by the UIC-518 regarding the use of numerical simulations have been presented. Therefore, it will be necessary to assess the evolution on the properties of the suspension organs which have been extracted from the FMECA evaluation: the *primary rubber spring* (PSi) and the *secondary emergency spring* (SSE). The following chapter will set the basis of rubber study, addressing the main principles that are used to model such components. The phenomena linked to the ageing of the parts and the possible changes on the parts' properties will be explained as well.

Bibliography

[EN50126, 2010] EN50126 (2010). *Applications ferroviaires Spécification et démonstration de la fiabilité, de la disponibilité, de la maintenabilité et de la sécurité (FDMS)*. Association Française de Normalisation (AFNOR), 11, rue Francis de Pressensé – 93571 La Plaine Saint-Denis Cedex, 3 edition. (Cited on pages iii, 32 and 33.)

[Garg and Dukkipati, 1984] Garg, V. K. and Dukkipati, R. V. (1984). *Dynamics of Railway Vehicle Systems*. Academic Press, 55 Barber Greene Road, Don Mills, Ontario M3C 2A1. (Cited on pages ix, 24, 140 and 142.)

[UIC518, 2009] UIC518 (2009). *Testing and approval of railway vehicles from the point of view of their dynamic behaviour - Safety - Track fatigue - Runnign behaviour*. UIC, 4 edition. (Cited on pages ix, 35, 157 and 162.)

[Wickens and Iwnicki, 2006] Wickens, A. and Iwnicki, S. (2006). A History of Railway Dynamics. In *Handbook of Railway Dynamics*, pages 5–38. CRC Press Books, London. (Cited on pages 23, 139, 148, 154 and 155.)

Chapter 3

Rubber parts ageing: mechanical properties evolution

> While the inventor admits that these discoveries were not the result of scientific chemical investigations, he is not willing to admit that they were the result of what is commonly called accident; he claims them to be the result of the closest application and observation.
>
> Charles Goodyear

The third chapter of the manuscript is devoted to the study of the rubber reference which is the base constituent of one rubber-to-metal suspension element: the *primary rubber spring*. This component is the structural guiding device of the wheelsets on Bombardier's FLEXX Compact bogies. The first paragraph will introduce rubber materials and their associated phenomenology, as well as some wide-spread characterization techniques. Next, the chapter will address the context of the modelling of hyperelastic materials and the characterisation from tests. The experimental campaign of thermal ageing addressed during the PhD works will be described subsequently, along with the mechanical and chemical characterization results. The fit of a hyperelastic model will be presented after, discussing the influence of the thermal ageing over the parameters representing the rubber's behaviour. Several projections of the metrics evolution will be calculated by means of Arrhenius models throughout the chapter.

Contents

3.1 Technological aspects and fundamentals

The use of rubber as a base material for structural components in transport technology has been a wide-spread custom from the 1950s until now. Its mechanical resistance, coupled with the elastomer's' dissipative properties, have encouraged the use of composite rubber-to-metal parts in aeronautics, automotive design, as well as on railways or even in civil engineering applications (Table 3.1). The study of the properties of these components has been widely addressed on the scientific literature [Martinez, 2005] [Lejeunes, 2006] [Boukamel, 2006] (aeronautics) [Chang Su and Hyun Sun, 2015] (railways) [Kareaga-Laka, 2016] (automotive). It remains today a current research topic because of the wide range of phenomena involved: quasi-static properties, time-dependent metrics such as the dynamic characteristics, creep and ageing, wear and damage, among others. Beginning with natural rubber in the 19th century, the transport industry has benefited from the development of synthetic rubbers and the development of multiple additives like halogen compounds. These improvements have proved their utility in a wide range of applications, providing fire-proof properties, chemical resistance for aggressive environments and many more.

Field	Application	Year
Aeronautics	Trail damper (helicopter)	1970s
	Laminated bearings and articulations (helicopter)	1980s
Railways	Buffer dampers	1830s
	Suspension joints	1850s
	Stack-layered chevrons (1^{ary} suspension)	1950s
	Stack-layered blocs (2^{ary} suspension)	1970s
Automotive	Tires	1880s
	Rubber bushings	1930s
	Silent-blocks	-
Civil engineering	Seismic isolators	1980s
	Isolating joints	-

Table 3.1: Applications of rubber compounds to multiple engineering fields. Partially derived from [Thien An, 2014]

First examples of composite elements with a mixed structure of metal and rubber appear as early as the 19th century, with the development of railway technology. The rubber's ability to withstand large deformations and recover subsequently made it a good candidate for building vehicle buffers; the elastomer was concealed within a metallic frame, absorbing the shock's energy. Primary bushings on wheels suspension were also used in steam engines, as well as to isolate the footplate from the cabin platform [Macbeth, 1939]. These devices reduced vibrations and provided a smooth ride, enhancing the driving team's ride comfort [Jones, 2012]. The use of

rubber-to-metal elements systematically as part of the bogies design was embraced by London Transport Underground around 1957. Maintenance offices succeeded in replacing a wide variety of the bogies suspension elements, subjected to extensive wear on service, by rubber suspension elements [M.E.C, 1983]. The durability obtained with the new technique allowed a significant reduction on maintenance interventions. Regarding mainline rolling stock, the SNCF in France introduced stack-layered rubber-to-metal blocks as the secondary suspension for the BB-7200, BB-15000 and BB-22200 locomotive series on the early 1970s.

Since the middle of the 20th century, the use of these elements has become commonplace and they are part of the rolling gear design of rail vehicles of all kinds: tramway, subway and mainline rolling stock alike (Figure 3.1). Their role has become larger as well, rubber-to-metal parts are used on both primary (guiding elements, bell bushings, etc.) and secondary suspension elements (auxiliary springs, secondary elements in tramways, etc.), as well as on other functions such as the axleboxes' bumstops and the pivot trailing (longitudinal and transversal bumpstops).

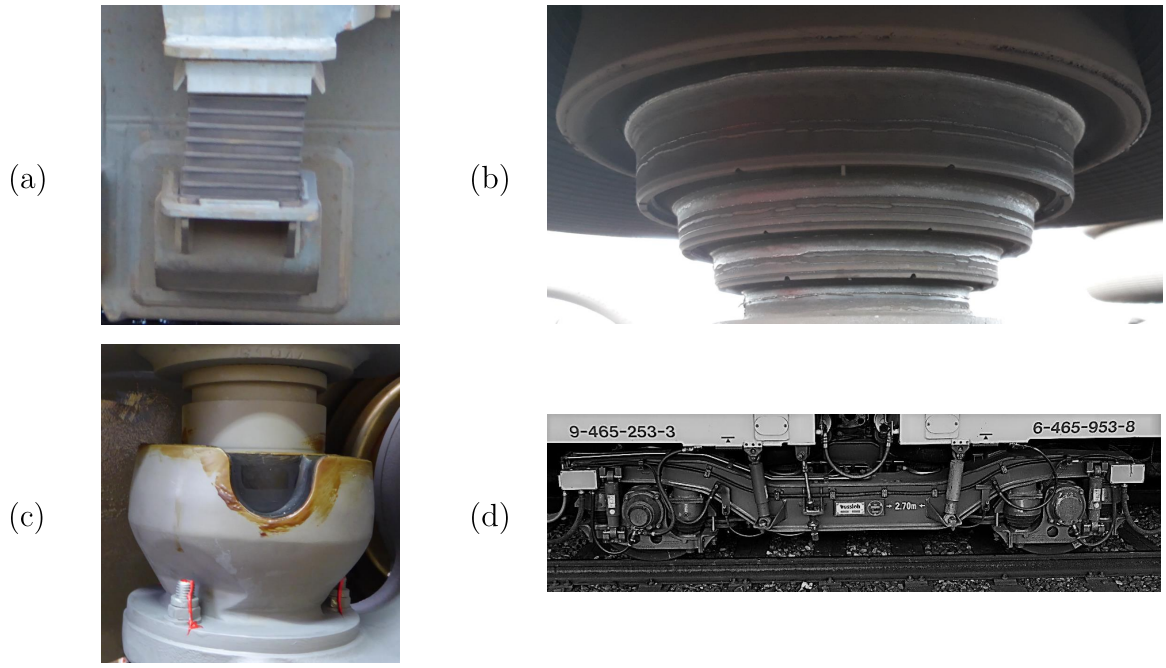

Figure 3.1: Stack-layered secondary suspension on a locomotive (a), concentric sandwich secondary auxiliary spring for an EMU's (b), conical primary rubber spring on an EMU (c), Jakobs bogie with fully rubber-based primary suspension (d).

The analysis strategy described in Chapter 2 has led to the choice of several suspension elements within a FLEXX Compact bogie. The first choice is the *primary rubber spring* (PSi), which acts as a guiding element on each axlebox, recovering longitudinal and lateral efforts from each wheelset of the bogie. The second choice is the *secondary auxiliary spring* (SSE), which is placed beneath the air cushions of the secondary suspension. Subjected to permanent load, it ensures a minimal stiffness if the secondary suspension were to be deflated (because of a failure or by preventive reasons). As regards of the phenomena undergone by the suspension elements, there are three main mechanisms which are outlined by our partner, and which are part of the approval procedure of the components. The testing procedure agreed between Bombardier and its manufacturers combines these phenomena in an experimental plan (see Table 3.2).

Test	**Type of test**
Vertical stiffness	*Quasi-static*
Transversal stiffness	*Quasi-static*
Longitudinal stiffness	*Quasi-static*
Radial stiffness	Quasi-static
Vertical stiffness	Dynamic
Creep test + Vertical stiffness	Quasi-static
Creep test + Vertical stiffness	Dynamic
Fatigue test + Vertical stiffness	Quasi-static
Fatigue test + Vertical stiffness	Dynamic

Table 3.2: Ensemble of test configurations conducted on the PSi suspension element for validation. Tests in italics will be addressed throughout this document.

- The elements are subjected to a permanent load, which is combined with cyclical loadings under service. Therefore, the material will endure *fatigue degradation*. A loss of mechanical properties towards the end of the life-cycle could be reasonably expected.

- The exposure of the parts to environmental agents can cause a drift on the properties of the parts due to natural ageing mechanisms. Oxidant elements, heat sources (powering systems, braking devices, etc.) can foster chemical reactions within the rubber of the elements, thus changing the mechanical properties. Rubber ageing tends to stiffen the material, although it becomes significantly more brittle, with a decrease of the ultimate strain and stress values.

- Since the suspension elements are always under permanent load (tare load at the least), time-dependent phenomena are likely to intervene during their life-cycle. *Creep* under the compression loads is foreseen in the technical requirements documents, which state the maximum allowable creep during the part's service.

From all those three mechanisms leading to a change of properties, fatigue and creep are already assessed through their specific tests during the design phase. Their evolution can be mastered via commonly used mechanics laws and maintenance practices, so that the effects can be foreseen and countered appropriately. For example, suspension elements which creep slightly under tolerance levels can be adjusted back to their position by adding steel shims under or above their functional interfaces. The ageing of the rubber, on the contrary, has not been extensively studied by the approval procedure. Mechanical testing is performed on some parts after being exposed to a thermal source. However, conducting a systematic review of the evolution of the parts' properties through ageing is not part of the testing procedures. The extent of the changes on the mechanical properties caused by the ageing remains relatively unexplored. Some feedback from suspension engineers within Bombardier has been gathered during the preliminary works. The specialists recall some cases in which the rubber-to-metal parts had seen their mechanical properties increased up to 30 % of the nominal values. Since both the PSi and SSE elements are at the core of the efforts distribution within the bogie structure, Bombardier has a strong interest on acquiring a deeper knowledge regarding the rubber ageing and the phenomena involved in it. Therefore, the aim of these works will be the **quantification of the changes of the properties** on the rubber-to-metal parts selected on Chapter 2.

Since the Régio2N rolling stock currently in service has not reached the earliest periods of overhaul intervention, it is not possible to obtain naturally aged and fatigued parts for comparison with laboratory tests. Therefore, to understand the behaviour of these parts throughout their respective life-cycles, an indirect approach will be necessary. The procedure will be schematically set as follows:

- Accelerated tests will be necessary, so as to attain the degradation state which would be expectable on aged parts. Samples of the base rubber used on the PSi and SSE elements will undergo accelerated ageing experiments, following a suitable experimental plan.
- As the accelerated tests are expected to change the material's properties, the samples will be characterised by means of mechanical testing. Chemical experiments will also be undertaken, for the molecular structure of the material will be affected by the accelerated ageing and the in-vitro testing could be compared later with real samples.
- The approval procedures set by the manufacturers offer an ensemble of aged/degraded properties of the real parts. The mechanical characterization of the rubber constituents will feed FE models of the suspension parts. The evolution of the properties will be assessed virtually, then compared with the results from the approval reports.
- In spite of the lack of spare parts from Régio2N trainsets, Bombardier has recovered similar pieces from the same bogie model - the FLEXX Compact -, which had run under a Talent 2 trainset in Germany, for the Deutsche Bahn (DB). These parts can be used as a reference for

environmentally aged parts. Their characteristics and material samples will be most useful to set an additional reference on the ageing process.

- A description of the ageing evolution of the rubber parts, specially with respect to their mechanical properties and variability, is the aim of this chapter. The combination of FE simulations plus the analysis of the recovered parts and approval reports will be the basis for the conclusions.

Each kind of suspension element is currently supplied by two different manufacturers, one for the PSi (Figure 3.2a), the other for the SSE (Figure 3.2b). Upon request, both manufacturers were eager to participate in the project, yet solely the PSi supplier sought a tighter collaboration and complied with the time exigences of the project. The manufacturer's support supplying samples, data and advise on their parts is a strong asset on the project. The description of the works and results that will ensue *concerns only the analysis performed on PSi suspension elements*. The SSE elements could not be analysed, thus not being part of this report.

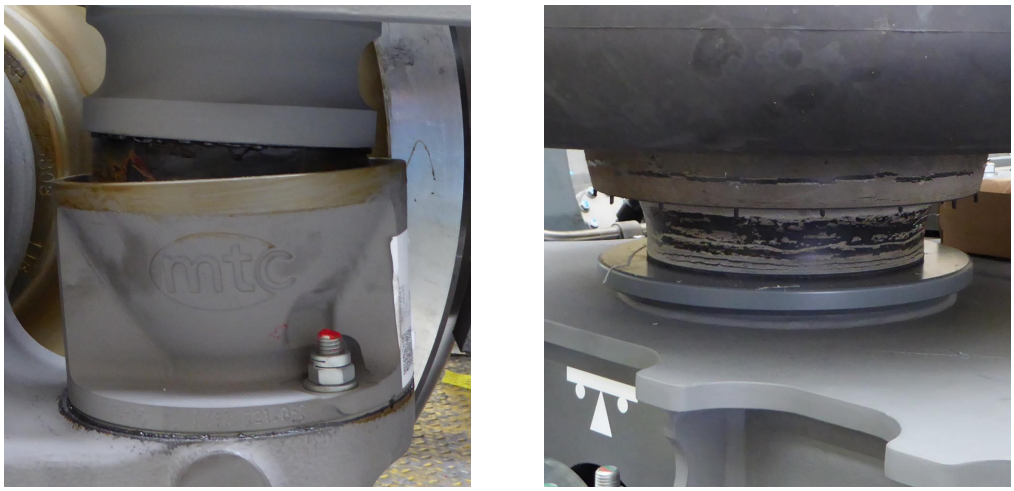

Figure 3.2: Left, primary rubber spring PSi, *aim of the current works*. Right, secondary auxiliary spring SSE.

3.1.1 Rubber chemistry and general properties

Pre-Columbian civilizations in Central and South America knew of rubber well before the arrival of Spanish colonizers, which discovered with awe the Mayan ritual ball game practised

by the natives. Natural rubber is extracted from the tree *Hevea brasiliensis* by practising an incision on the tree's trunk, recovering the sap in an attached recipient. This practise is at the origin of the Mayan word for the rubber: "crying tree", which yields "caoutchouc" or "caucho" in several languages [Treloar, 1975]. Its chemical characterisation is due to Faraday, who proposed for the first time the formulation $[C_5H_8]_n$, and Williams, who isolated and named the rubber's constituent monomer, the *isoprene*. Appreciated by its waterproofing properties and its malleability, the rubber had little uses other than tissue coatings. It was soon after that Charles Goodyear (United States) and Thomas Hancock (United Kingdom) were bestowed two individual patents on the vulcanization process of the rubber, which paved the way to the use of rubber compounds in a wide range of - until then - unexplored applications [Loadman, 2003b].

The chemical description of natural rubber was determined early during the 19th century and has subsequently expanded with the notion of polymers. Natural rubber is composed by a complex network of long, interlocked molecular chains. These macromolecules of natural rubber consist on thousands of simple units of the substance Williams had isolated, hence the name "polyisoprene". The isoprene monomer is composed of a main chain of four carbon atoms, the central bond being a double carbon link, with a methyl group clinging to one of the central carbon atoms. Since the double carbon link prevents the molecule to rotate about the bond's axis and the functional extremities for the polymerization are placed on the same side, the natural rubber's polymer is known as well as "cis-1,4-polyisoprene" (see Figure 3.4a). In its extraction form, natural rubber has a viscous, liquid consistence, which coagulates naturally into a rigid paste, not suitable for immediate use. This states are mutually reversible and linked to the temperature of the material: *viscous liquid at high temperatures* versus *crystallised solid at low temperatures*. To recover a workable form, early industrial processes "masticated" the coagulated raw rubber by mechanical means, thus producing a mass which could be worked into the desired applications [Loadman, 2003a]. The discovery of vulcanization strongly improved the fabrication of rubber, allowing a finer control of the curing processes.

The molecular structure of the rubber is intimately related with the rubber's properties, specially to the characteristic "S-shaped" stress-strain curve associated to their rubbery state (Figure 3.3b). When the stretch increases, the molecules start de-entangling, aligning themselves on the direction of the effort, until the bonds between the chains lock the extension and the chains start being stretched along their axis. However, in the raw state, the macromolecules within the rubber could be compared to a mass of boiled noodles. The polyisoprene chains stick one to each other by means of weak inter-molecular interactions, typically Van-der-Waals dipoles, but can mutually slip within the matrix. Some chains may be bonded at some points with carbon links, as well as by the chains' spacial distribution. The absence of a high density of entangled points and the weakness of the molecular interactions yield the malleable properties of the rubber. The vulcanization process creates new links between the existing chains, either by adding new chemical species and bonds

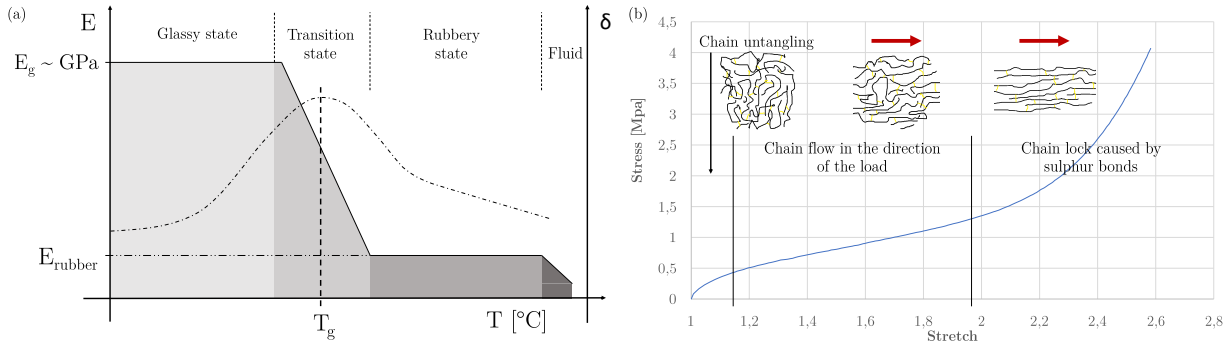

Figure 3.3: (a) From left to right, crystalline state, transition phase, amorphous state and rheological state (extracted from [Boukamel, 2006]). (b) Experimental traction curve for natural rubber, with the *molecular associated state* to each part of the curve.

or by operating new locks on the polyisoprene molecules. The two major families of vulcanizing methods which are extensively used nowadays are the following:

- *Sulphur-based vulcanization* is based on the interaction of sulphur atoms within the polyisoprene chains, clinging to the carbon atoms by substitution of a former carbon-hydrogen bond or the breakdown of the double carbon link [Akiba and Hashim, 1997] [El Labban, 2008]. The catalysts of the reaction are two activators: zinc oxyde (ZnO) and stearic acid ($C_{17}H_{35}COOH$) forming a stearate, mixed with an accelerator, usually CBS ($C_{13}H_{16}N_2O_2S_2$). Zinc atoms react with the CBS to form active groups, which in turn split the cyclic sulphur molecules, enabling the reaction of the clinging sulphur atoms with the polyisoprene chains [Dimier, 2003].

  Depending on the processing conditions, the sulphur links can be more or less complex: mono- and bi-sulphur bonds for the tightest links, poly-sulphur links for the loosest bonds (see Figure 3.4b) [Akiba and Hashim, 1997]. Some sulphur structures lead to uneffective bonds such as rings or clinging sulphur-reactive radicals. Hence, there is a rate between the needed sulphur to obtain an amount of effective sulphur bonds, which leads to the definition of *conventional, half-efficient and efficient vulcanizations* [Thien An, 2014]. As a consequence, the mastering of the chemical reaction's catalysis is the key to enhance its efficiency (i.e. the amount of sulphur atoms reacting to form interlocking chains) and to reduce the duration of the process.

- *Peroxide vulcanization* allows a neater reticulation of the polyisoprene, as the locking occur directly between the existing chains. During the reaction, the oxygen link within the peroxyde molecule is broken, generating a strong, unpaired available bond on the oxygen atoms. Since oxygen is strongly electronegative, it fetches hydrogen atoms from the elastomeric chains and creates free links on chordal carbon atoms, thus enabling cross-linking with other chains. As

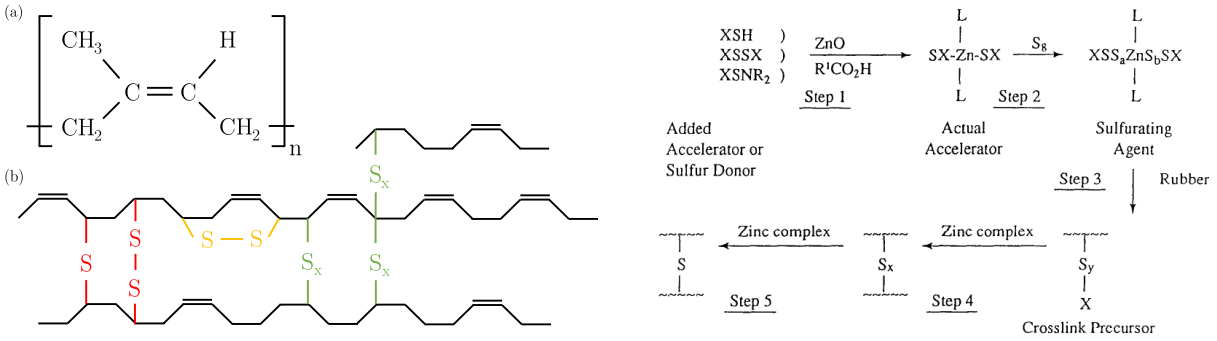

Figure 3.4: Isoprene monomer (a), simplified representation (b) and polyisoprene chains linked by mono-, disulphide links (red), sulphur rings (yellow) or poly-sulphide links (green). (d) Generic steps on a vulcanization reaction, Yamada and Okumoto (1991) [Akiba and Hashim, 1997].

the reaction is thermally activated and there are no foreign substances added to the material to constitute the cross-links, the regulation of the process and the accuracy of the results are easier to master than for sulphur vulcanization [Loan, 1967].

Apart from its chemical structure and conformation, natural rubber shows a wide range of properties and states depending on the temperature, just as many other polymers [Moore, 1950]. Polymers at a low temperatures adopt a *crystallised state*, where the molecules ply and stack themselves into an ordered structure. Therefore, the crystallised polymer shows a stiff tensile modulus and a higher hardness, yet becoming significantly brittle. A *transition state* appears around the so-called *glass transition temperature*, where the material has mixed properties between the crystallised state and the rubbery state. A fraction of the molecules remain organised in crystals, linked to a messy dough of molecular chains. The elastomers at the *rubbery state* have a strong strain capacity and a viscous behaviour, their molecules being intertwined in an amorphous state. Higher temperatures melt the material, yielding a *flow state* were the polymer acts as a viscous fluid (see Figure 3.3a). The properties of the rubber can be further modified by the addition of fillers, which reinforce the material, as well as reducing the mass of raw rubber required on the mixture. Carbon black or silica particles (among others) have been extensively used as additives for natural rubber, the fillers being mixed with the polyisoprene matrix, forming aggregates or clusters within the molecules which can be dissolved in a reversible process by stirring or masticating the mixture. Carbon black particles interact with the isoprene, which forms an adsorbed coating over the clusters. Polyisoprene molecular structures are then attached to this surface coating [Treloar, 1975]. The inclusion of additives on the mixture has an influence on the rubber mechanical properties, such as a stiffening of the mechanical response of the material with an increasing rate of fillers [Guth, 1945] [Kraus, 1965] (Figure 3.5).

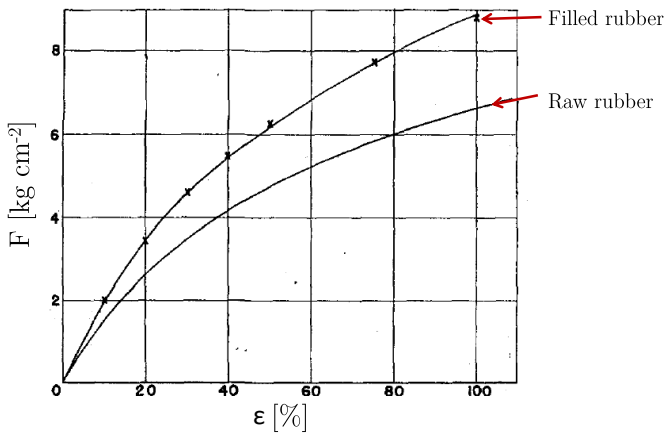

Figure 3.5: Evolution of the rubber stress-strain response depending on the rubber's filler rate [Guth, 1945].

3.1.2 Rubber phenomenology and characterization

The determination of the characteristics of an elastomer encompasses a wide range of tests, each of them aiming to determine the properties related to a specific aspect of the rubber behaviour. Experimental testing can address the material *mechanical properties* solely, it can address the *dependence with time* (frequency, creep, fatigue) and/or the *dependence with temperature* of the rubber mechanical properties, as well as the *physico-chemical properties* of the rubber, which are intimately related with the material microstructure. The paragraphs hereafter will address briefly some of the phenomena involved on the study of a natural rubber properties, as well as the most frequent experimental settings.

From a broad point of view, the different phenomena involved in the characterization of the behaviour of rubber compounds can be classified in *hyperelastic behaviour* (entropic elasticity), *viscoelasticity* and *viscoplasticity*, depending on the temperature and frequency range of the phenomena.

Quasi-static mechanical tests

The mechanical response of rubber (and other elastomers) to an uniaxial effort is a characteristic "S-shaped" curve, relating stress and strain within the material (Figure 3.3b). Owing to its strong non-linearity and high strain levels, elastomers required new mechanical theories to describe their behaviour. The analytic frame was developed from the 1940s [Treloar, 1975], giving birth to the hyperelasticity. The study of the rubber's mechanical characteristics is customarily performed

through a series of families of standardised tests, whose configuration is directly related to several cases of idealised solicitations [Jones and Treloar, 1975] [Lejeunes, 2006]. The *homogeneous strains tests* family groups four experimental procedures which are set up so as to ease the interpretation of the results, enabling a quicker calculation of the constitutive relationship between the applied efforts and the stretches measured on the material.

- *Uniaxial stress tests* are undertaken with long, thin material samples, which are stretched along their main axis. Owing to the sample's little thickness and to the practised loading, it is possible to assume that the useful portion of the sample is under pure axial stress.

- *Bi-axial or equiaxial tests* are performed on this material samples which are stretched symmetrically over several coplanar directions. Therefore, the assumption that the material is under plane-stress solicitation is reasonable, which facilitates the description of the material behaviour.

- *Simple shear tests* require a composite structure with three metallic plates, framing two thin, rectangular layers of elastomer. The outside frames are pulled opposite from the central plate, which induces a simple shear load on the material.

- *Pure shear tests* are performed on wide, rectangular pads of elastomer. The upper and lower sides of the sheet are pulled away, thus stretching the pad's thickness, which sets the metrics for the characterization of the shear stress on the sample.

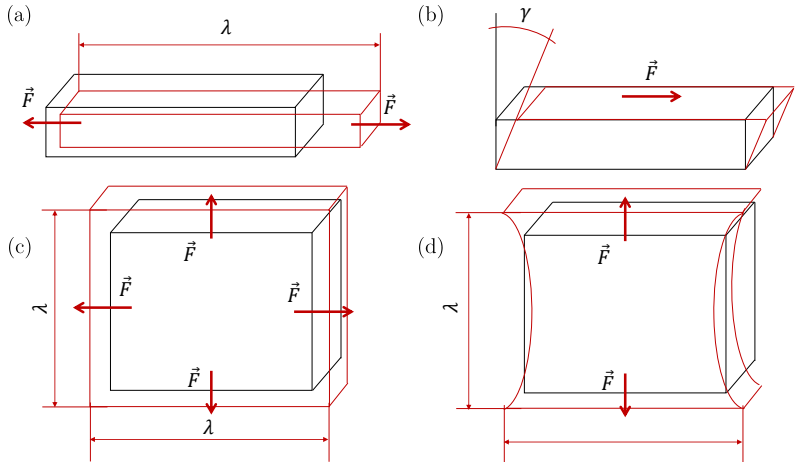

Figure 3.6: Homogeneous strain tests. (a) Simple extension. (b) Simple shear. (c) Biaxial extension. (d) Pure shear. Based on [Lejeunes, 2006].

The mechanical characterization of an elastomer can be achieved by other experimental sets. Depending on the assumptions taken on the material nature, additional experiments can be carried out to determine specific metrics, such as the *isostatic pressure tests*. This specific tests consists on the compression of a cubic or rectangular sample of rubber, which is placed at the bottom of a square pit carved in a metallic die. The rubber sample is subsequently compressed by means of a metallic die. The compression efforts, as well as the material sinking are measured. Both magnitudes are used to calculate the material *bulk modulus*, a metric of the rubber's compressibility.

Performing quasi-static tests demands, for a matter of coherence, that no time-dependent effects appear on the material during the experiments. Transient phenomena such as the Mullins Effect can affect the measurements and bias the results of the tests. Therefore, the stabilization of the rubber's characteristics during the set up of the experiment is a part of the procedure. For instance, tensile stress tests are set up with a maximum fixed strain, ensuring that the desired strain levels lay below the applied limit. Several cyclical loadings are practised up to the maximum strain level, until the transient phase associated to the Mullins Effect becomes negligible 3.16. Hence, only the stabilized curves are used to characterise the material behaviour. Nevertheless, since the tests are performed at a certain range of speeds, the results will remain partially time-dependent of this parameter.

The *Mullins Effect*, also known as *softening under cyclical strain*, is a time-dependent phenomenon which causes a decrease on a material's maximum stress under repeated loading, for a given strain level. In the case of overpassing the maximum strain level applied, the material's characteristics regain the virgin state characteristics. Moreover, if the material is subjected to cyclical loading at a higher strain level, the repeated softening of the Mullins Effect will occur again [Mullins, 1969]. The application of heat restores the material's state back to its initial properties [Diani et al., 2009], in a similar way as annealing works for metals and alloys, thus "erasing" the softening caused by the Mullins Effect.

Thermo-viscoelastic tests

One of the key characteristics of elastomeric materials is their dissipative properties, which place them under the mechanics formalism of the *viscous materials* (which is be combined, in the rubbers' case, with their hyperelastic behaviour). These properties depend on the amplitude of the solicitation (be it stress or strain) and its frequency, as well as on the temperature of the material itself. When an polymer undergoes a dynamic loading, its response shows a phase lag between stresses and strains. This mechanical behaviour is piloted by the *dynamic or complex modulus*, a composed magnitude encompassing the *storage modulus* (G'), which accounts for the elastic recoverable energy stored within the material, and the *loss modulus* (G''), which describes the viscous dissipation within the material, in the form of self-heating. The dynamic modulus can

be expressed as a complex number with an imaginary part, as described in Equation 3.1, such as in other engineering fields (e.g. electric impedance on AC current systems). Both magnitudes can be related via the *loss angle*, whose tangent ($\tan\delta$) equals the ratio between the loss and the storage moduli (Equation 3.2). Several time-dependent phenomena have been extensively studied and described in the literature and are customarily considered on the rubber's characterisation.

$$G = G' + iG'' \tag{3.1}$$

$$\tan\delta = \frac{G''}{G'} \tag{3.2}$$

- The *Payne Effect* is associated with filled elastomers and it is described as an amplitude-dependent decrease of the storage modulus of the rubber. This change has an impact as well on the material's loss angle, which increases with the filler rate and amplitude [Payne, 1969].
- The *Fletcher-Gent Effect* is observed in filled elastomers as well, and its manifestation is a frequency-dependent increase of the stiffness [Fletcher and Gent, 1953].

The relation between the frequency of the loading and the mechanical response of the rubber has a strong link with the microscopical properties and state of the material (namely, the molecular structure and crystalline state). Since the material state is tightly related with temperature, these factors are extensively used to perform characterization tests on the rubber dynamic behaviour. The DMA (*Dynamic Modulus Analysis*) experiments are performed over a standard sample, set on an homogeneous strain test configuration, then subjected to cyclical loading. Displacements and efforts are measured on the same time basis, allowing the comparison of both metrics and the calculation of the complex modulus of the material. Furthermore, the dependence of the material's characteristics to the temperature is particularly useful to determine the rubber's temperature of glassy transition, T_g, which is marked by a singular peak on the loss angle ($\tan\delta$) (see the dotted plot on Figure 3.3). However, the strong link between temperature and mechanical characteristics, added to the material's self-heating derived from its dissipative properties, complicates the set up of experiments to determine the evolution of properties through polycyclic tests. Rubber self-heating can cause temperature to rise up to levels affecting the microstructural state of the material itself, which in turn will not reflect the rubber's true response under polycyclic loading.

When dealing to a characterization of a frequency-dependent behaviour on rubber materials, the evolution of a material's mechanic characteristics may follow a certain pattern, which is dubbed as a "master curve". Performing the same tests at different temperatures causes a time shift of the evolution curve. For instance, applying higher temperatures makes the material's long-term cyclical behaviour reachable at a lower amount of cycles. Therefore, it is possible to gather several partial portions of the polymer's behaviour curve at different test temperatures and to re-build

the master curve. The relation between the applied temperatures and the induced time shift with respect to the reference temperature can be described by means of an empirical equation: the Williams-Landel-Ferry (WLF) law [Le Huy and Evrard, 2001] [Gillen and Clough, 1997], with a decade-logarithm dependence of the shift factor and two factors, A_1 and A_2, that can be experimentally determined. However, the WLF law is not of general application, being restricted to the temperature range above the glassy transition temperature, T_g, up to $T_g + 100$ degrees (Celsius or Kelvin). Its application is usually associated with the characterisation of a polymer's viscoelastic properties [Le Huy and Evrard, 2001].

$$log(a_T) = \frac{A_1(T - T_{ref})}{A_2 + (T - T_{ref})} \tag{3.3}$$

The curves "assembled" through this method describing the evolution of the material properties along the time are plotted at a reference temperature. To exploit the curves, it is customary to shift them back to the operational temperature of the material. To do so, the extrapolation of WLF equations allow the calculation of the necessary shift factor to reach the material's working temperature. The a_T thus obtained can then be inserted into the function describing the properties evolution.

Physic-chemical properties tests

The mechanical properties of elastomeric materials are deeply intertwined with their chemistry. Therefore, the analysis of their chemical composition, structure and behaviour is a sound source of information, in particular regarding the degree of vulcanization and its derived properties. Most of the techniques applied to polymer analysis look for the chemical of thermochemical markers left by the vulcanization. Several experiments are commonly applied within the rubber industry, yet we will focus only on some of the most widespread techniques, as well as on other tests which can be of interest for the present works.

The *Thermo-Gravimetric Analysis (TGA)* is one of the customary analysis performed by rubber manufacturers. This test is performed to obtain the mass percentage composition of the rubber. The experimental procedure starts by placing sample of the material over a weighing plate, which is installed within an isolated capsule. The cell can be filled with a specific atmosphere (nitrogen, argon) if required through an inlet valve, and it recovers the volatile substances during the process via an outlet pipe. Next, the sample is heated continuously, which causes several reactions among the compounds of the rubber, each of them marked by a decrease on the weighed mass. Such variations are connected to the rubber composition and are representative of its material state. Therefore, the continuous plot of mass variations versus the temperature rise is the result of the TGA (see Figure 3.7). For example, natural rubber (NR) shows typically a slight loss of volatile

elements until 200-300 degrees Celsius, followed by a dramatic loss of weight associated to the polymer itself, around 400-500 °C. A plateau ensues until 600 °C, followed by a stabilization phase with a decrease of temperature to 400 degrees and a subsequent heating. Temperatures during last phase can rise up to 700-800 °C, the heat volatilising the charges of the polymer. The remaining ashes are the residual constituents of the polymer. While having a certain interest regarding the rubber's mass composition, the TGA technique alone does not yield any specific results on the chemical composition. Coupled with complementary devices, it supplies much richer results. For example, the analysis of the fumes exhaust from the TGA by means of a *gas spectroscopy* can add complementary information.

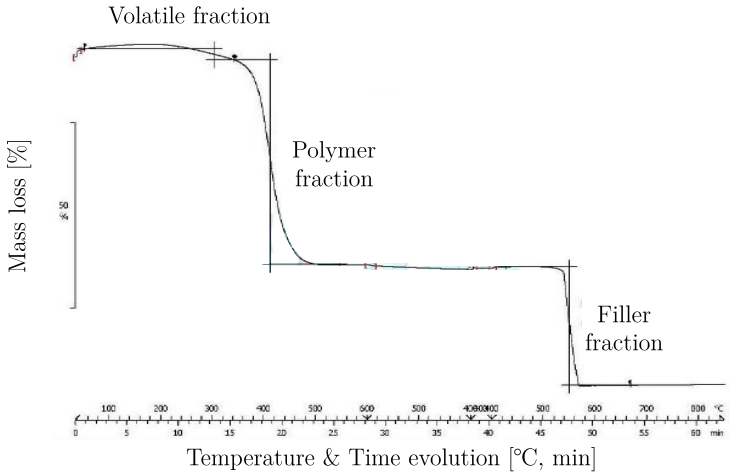

Figure 3.7: Thermogravimetric analysis of a rubber reference. The three steps associated with polymers are clearly visible: volatile compound evaporation, polymer degradation and inert fillers at the highest temperatures.

The *Differential Scanning Calorimetry (DSC)* has, by its resolution, a strong interest in polymer analysis. Contrary to the TGA, DSC is performed with two samples: a reference material with a stable, well-defined thermal capacity, and the sample to be analysed. Both samples are heated simultaneously and the thermal flux absorbed by each sample is measured. Should the polymer undergo any phase transition or change of state, its thermal capacity would increase significantly, thus causing a rise on the absorption curve. Therefore, the observed peaks through a DSC analysis would match the reactive steps through a vulcanization process or the degradation mechanisms on an ageing test. DSC curves can be integrated so as to obtain several "process enthalpies" associated with each of the observed phenomena.

The analysis of the reticulation degree of a vulcanised rubber can be inferred indirectly through thermal analysis, yet the results would be somewhat approximative. An approach using chemical analysis permits a better study of the rubber's vulcanised state: the *swelling tests*. These experiments are based on Flory's theories on the swelling of a polymer on an adequate solvent [Flory and Rehner, 1943b]. Mullins and Moore used them to compare chemically- and mechanically-obtained reticulation rates [Treloar, 1943] [Mullins, 1956] [Moore and Watson, 1956]. In a general way, a polymer sunk in an affine solvent would have its molecular structure progressively untangled, its molecules becoming part of the solution. However, a sufficiently cross-linked polymer will not become a part of the solution, but will swell in turn. The extent of the sample's swelling is determined by the polymer molecules' aptitude to stretch, so as to withhold the solvent molecules within their three-dimensional structure (in a process resembling the swelling of a dipped pastry in a tea cup). The calculation of the reticulation is obtained through a two-step process: the increase of mass (m_s) due to the absorption of solvent is measured by hydrostatic weighing. Combined with the initial mass (m_0) and the densities of both the sample and the solvent (ρ_0 and ρ_s), one can retrieve the reticulation volume (V_r) with the Equation 3.4. The reticulation volume is used to calculate the *density of reticulation*, v_e, measured in moles of cross-links by cm^3, using the Flory-Rehner Equation (Equation 3.5). The Flory-Huggins interaction parameter, χ, has a specific value for each couple polymer-solvent [Barton, 1990], whereas V_l is the molar volume of the solvent.

$$V_r = \frac{\frac{m_0}{\rho_0}}{\frac{m_0}{\rho_0} + \frac{m_s}{\rho_s}} \tag{3.4}$$

$$v_e = -\frac{ln(1 - V_r) + V_r + \chi V_r^2}{V_l(V_r^{1/3} - V_r)/2} \tag{3.5}$$

However, the application of the Flory-Rehner equation becomes more complex for filled polymers [da Costa et al., 2001], as the fillers interact with the molecular chains and alter the swelling behaviour. A corrected expression was given by Lorentz et al. [Lorenz and Parks, 1961] (Equation 3.6), were "a" and "b" are material-dependent coefficients and "z" is the fillers to rubber mass ratio. To determine the set of constants, tests must be conducted on both filled and raw rubber to obtain the relation between the parameters [Cunneen and Russell, 1970].

$$\frac{v_{r0}}{v_r} = a \exp^{-z} + b \tag{3.6}$$

3.2 Hyperelastic models

The study of the mechanical behaviour of rubbery compounds had a strong complexity from its very beginnings. The strongly non-linear material behaviour plus the high-strain levels under loading demanded a combination of existing formalisms (*mechanics formalisms* and *thermodynamical approach*) plus a series of new theories to describe the material's constitutive laws (the *hyperelastic models*). Thorough descriptions of the *mechanics formalisms* regarding with great deformations by Sidoroff [Sidoroff, 1982] and Holzapfel [Holzapfel, 2000] provide a deeper insight on the issue to the reader. The academic works from Méo [Méo, 2000] or Lejeunes [Lejeunes, 2006] have addressed these aspects extensively. The reader is invited to refer to the Appendix B for a detailed explanation. The following paragraphs intend to present the main aspects regarding the study of hyperelasticity on the various aspects cited above.

The mechanical description of a large strain problem is addressed as part of the description of the solids mechanics, which can be related to several configurations. These can be regarded from three reference frames: the original, undeformed configuration (*Lagrangian description*), the modified configuration (*Eulerian description*), plus an *intermediate configuration*. The definition of a constitutive relation between the deformations observed on the material and the applied efforts can be done, consequently, under three different reference frames. However, it appears necessary that such a relation should be independent of the observer's point of view, i.e. *objective*. Therefore, the law's constituent metrics will necessarily be objective as well. Hence, the *tensors* measuring the material's metrics will be objective too. The objective tensors measuring the deformations on a material are $\bar{\bar{C}}$ and $\bar{\bar{B}}$ (Appendix B). A further step into determining a set of objective metrics to describe the rubber behaviour involves the mathematical *invariants of the deformation tensors*. Two-dimensional tensors have three associated metrics, whose expressions are given by Equations B.21 and which remain unchanged regardless of the chosen reference. This specific property makes them interesting to study the material's behaviour.

$$I_1(\bar{\bar{X}}) = tr(\bar{\bar{X}}) \tag{3.7}$$

$$I_2(\bar{\bar{X}}) = \frac{1}{2}(tr(\bar{\bar{X}})^2 - tr(\bar{\bar{X}}^2)) \;\; were \; \bar{\bar{X}} = \bar{\bar{B}} \; or \; \bar{\bar{C}} \tag{3.8}$$

$$I_3(\bar{\bar{X}}) = \det \bar{\bar{X}} \tag{3.9}$$

The formal frame for the analysis of a hyperelastic material involves the thermodynamics of continuum solids. Within its postulates, it defines the *first and second* principles of thermodynamics. The addition of Helmholtz's Free Energy function combined with both principles yields the *Clausius-Duhem inequality*, which states the nullity or positivity of the dissipation of energy within the material. The inequality relates the mechanical work within the material with the

dissipative and thermal effects and can be written for each of the reference frames discussed previously [Boukamel, 2006].

Hyperelastic environments are a specific case of non-linear elasticity which are characterised by the material having a reference configuration which is free of stress, an absence of energy dissipation and the material's behaviour being described by a specific free energy density function which is dependent on the material's strains and temperatures [Boukamel, 2006]. Under such conditions, the inequality of Clausius-Duhem (Equations B.24) can be rewritten without its dissipative terms; if one takes the *energy's density function* $\mathcal{W} = \rho_0\psi$, the expressions of the constitutive relation between the metrics for deformations and stresses can be written in a generalized form, given on Equation 3.10 for an *intermediate configuration*. Nevertheless, the formulation of the hyperelastic behaviour law is not yet complete, as further considerations must be taken into account. Rubbery materials are generally considered as *incompressible* (i.e. the efforts engaged to changes their volume are tremendous compared to any other deformation modes [Sidoroff, 1982]). On the current configuration, the latter condition adds a *spheric part* to the stress tensor, which is modulated by an arbitrary parameter "p", associated to the *hydrostatic pressure*. The condition is transportable to the intermediate configuration, yielding the equality in Equation 3.11. The *deviatoric part* of the stress tensor is thus defined by the material properties, while the *spheric part* with the hydrostatic pressure is obtained from the particular boundary conditions on each configuration.

$$\bar{\bar{\Pi}} = \frac{\partial \mathcal{W}}{\partial \bar{\bar{F}}} \tag{3.10}$$

$$\bar{\bar{\Pi}} = \frac{\partial \mathcal{W}}{\partial \bar{\bar{F}}} - pCof\bar{\bar{F}} \tag{3.11}$$

Therefore, it appears that the definition of a hyperelastic behaviour law requires the definition of a suitable energy's density function $\mathcal{W}$, so that the constitutive law represents the stress-strain relationship observable experimentally. The determination of hyperelastic strain energy functions has been at the core of the study of rubber-like materials during the 20^{th} until today. First attempts to explain the origins of the elastomers' elastic properties focused on the fact that, unlike metals or ceramic materials, whose properties are determined by the storage of elastic energy within their structure, rubber-like materials get their extreme strain and recovery aptitude from their molecular structure. More precisely, the changes on the macromolecules' arrangement through an *entropic mechanism* yields the elastomers' specific properties. Works on the 1940s by Anthony et al. [Treloar, 1975] determined the fraction of elastic and entropic energy within a rubber sample (Figure 3.8). Consequently, the study of the molecular structure and its three-dimensional distribution were at the core of the early attempts to characterize the hyperelastic behaviour.

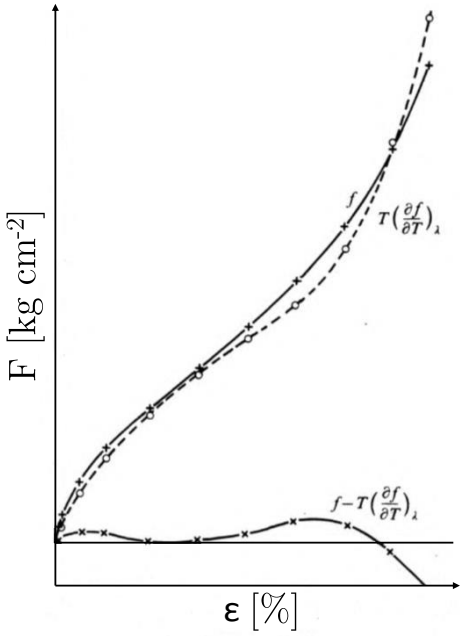

Figure 3.8: Entropy's contribution to the internal energy on an extension test, traced by Anthony et al. (1940) via [Treloar, 1975].

Two approaches on the hyperelastic problem have been addressed by researchers, depending on the underlying postulates which are considered. Therefore, the models belong to two wide families: the *physically-based models* and the *phenomenological models*, which will be addressed separately in the following paragraphs. The accuracy of both models depends on the deformation frame and the strain levels: sometimes both families yield suitable results, whereas sometimes one or none of the families are able to provide an accurate approach of experimental results.

3.2.1 Phenomenological models

Mooney's works produced a model based on the three main stretches on a material, using a mathematical procedure to obtain the stress-strain relation [Mooney, 1940] (Equation 3.12). Taking a general form, successive applications of constraints to the material (isotropy, etc.) lead to the hypothesis that the chosen energy function would depend on the material's main stretches (λ_i) [Treloar, 1975], thus being related to the strain invariants. Since the material is incompressible for most cases, $I_3 = 1$, the strain energy function can depend solely on the two first invariants, I_1 and I_2. The stress-strain function suggested by Mooney took the form in Equation 3.12. The -3 term ensures that the energy remain zero on an unstrained state.

$$\mathcal{W} = C_1(I_1 - 3) + C_2(I_2 - 3) \tag{3.12}$$

Furthermore, Mooney related the above formula with an homogeneous strain test: the simple shear. In this case, the energy function yields a form in the shape of Hooke's law, where the shear modulus is $G = 2(C_1 + C_2)$ [Lejeunes, 2006]. On its side, the C_1 term could be related, by means of the $(I_1 - 3)$ term to the molecular theories which arose later (explained in the following paragraphs, see Equation 3.21). However, the attempts to give a physical sense to C_2 failed to give a reasonable explanation. Rivlin pursued Mooney's works jointly with Saunders [Rivlin and Saunders, 1951], generalizing the strain energy expression (Equation 3.13). Each term on $(I_1 - 3)^i(I_2 - 3)^j$ has a preceding C_{ij} coefficient, which needs to be determined from experimental results, while $C_{00} = 0$ to ensure the nullity of the expression at the unstrained configuration.

$$\mathcal{W} = \sum_{0 \leq i,j}^{\infty} C_{ij}(I_1 - 3)^i(I_2 - 3)^j \tag{3.13}$$

Subsequent works by Gent and Thomas proposed a hyperelastic strain function with a logarithmic term for I_2 [Gent and Thomas, 1958], while other researchers like Isihara, Tschoegl, Yeoh or James (among others) sought specific forms on the generalized expression of Mooney-Rivlin, to fit particular deformation ranges in which the previous models had proven to be unsuccessful to provide an accurate fit of the experimentally observed behaviour (Equations 3.14 to 3.18)

$$\mathcal{W} = C_{10}(I_1 - 3) + C_{01}(I_2 - 3) + C_{20}(I_1 - 3)^2 \tag{3.14}$$

$$\mathcal{W} = C_{10}(I_1 - 3) + C_{01}(I_2 - 3) + C_{22}(I_1 - 3)^2(I_2 - 3)^2 \tag{3.15}$$

$$\mathcal{W} = C_{10}(I_1 - 3) + C_{20}(I_1 - 3)^2 + C_{30}(I_1 - 3)^3 \tag{3.16}$$

$$\mathcal{W} = C_{10}(I_1 - 3) + C_{01}(I_2 - 3) + C_{11}(I_1 - 3)(I_2 - 3) + C_{20}(I_1 - 3)^2 + C_{30}(I_1 - 3)^3 \tag{3.17}$$

$$\mathcal{W} = C_1(I_1 - 3) + \ln(I_2/3) \tag{3.18}$$

3.2.2 Physically-based models

The main drawback of phenomenological models is that their formulation does not rely on physically meaningful metrics [Treloar, 1975] [Arruda and Boyce, 1993]. From all three strain invariants, solely I_3 has a physical meaning: the REV's *volume*. The other two invariants have not a direct, meaningful interpretation, which combined with the C_{ij} coefficients makes those models appear as "artificial", a rather mathematical approach lacking a direct link with the material's chemistry and physics. Therefore, several researchers have worked to provide hyperelastic energy functions which can be related with the rubber's physical properties. First researches took an interest on the topology of the molecules amidst the elastomer structure and their elasticity

[Flory and Rehner, 1943a]. A molecule spanning freely, taking the carbon links' valence angles to orientate the monomers, would spread up to a certain length, which is lower than the length of a fully stretched molecule. The RMS value of the radius r withholding a whole random chain is proportional to the square root of the chain's amount of carbon bonds (Equation 3.19), and the distribution of lengths within the material can be described by means of a Gaussian distribution. Thus, it is possible to calculate the entropy change on a molecule from its unstrained configuration to a fully stretched situation (Equation 3.20), where "N" is the number of molecules and "k" Boltzmann's constant. This expression can be expanded ultimately to obtain the network's strain energy (Equation 3.21), at a temperature "T".

$$\bar{r^2}^{\frac{1}{2}} = ln^{\frac{1}{2}} \frac{1+\cos\theta}{1-\cos\theta} \tag{3.19}$$

$$\Delta S = -\frac{1}{2} Nk(\lambda_1^2 + \lambda_2^2 + \lambda_3^2 - 3) \tag{3.20}$$

$$W = \frac{1}{2} NkT(\lambda_1^2 + \lambda_2^2 + \lambda_3^2 - 3) \tag{3.21}$$

However, Gaussian statistics may not fully represent the network's properties. Therefore, the use of a different kind of probability distribution describing the molecules' length, Langevin statistics [Kuhn and Grün, 1946]. Here, the entropy depends on Langevin's inverse function (Equation 3.22), "k" is again Boltzmann's constant, "N" the amount of chains, "l" the limiting extension of a chain, with "r_{chain}" the chain actual span. Arruda and Boyce used this formulation to suggest their strain energy function (Equation 3.23) [Arruda and Boyce, 1993], with "n" the amount of chains in moles, at a given temperature "T".

$$s = k[c - N(\frac{r_{chain}}{Nl}\mathcal{L}^{-1}(\frac{r_{chain}}{Nl}) + \ln\frac{\mathcal{L}^{-1}(\frac{r_{chain}}{Nl})}{\sinh\mathcal{L}^{-1}(\frac{r_{chain}}{Nl})})] \tag{3.22}$$

$$W = nkT(\frac{1}{2}(I_1 - 3) + \frac{1}{20N}(I_1^2 - 3^2) + \frac{11}{1050N^2}(I_1^3 - 3^3) + \frac{19}{7000N^3}(I_1^4 - 3^4) + \frac{519}{673750N^4}(I_1^5 - 3^5)) \tag{3.23}$$

3.3 Experimental campaign

The design of experiences for the study of the ageing of the rubber reference has been deployed in three stages. A *thermal ageing campaign* to accelerate the rubber ageing, a *physic-chemical characterization* and the *mechanical characterization* of both new and aged samples. The following sections hereunder will describe each part of the experimental campaign.

3.3.1 Accelerated ageing tests

Dealing with long-term time scales hinders the set up of experimental procedures to understand the behaviour of the materials during a several-year life-cycle. The chemical state of an elastomer evolves during the lifecycle of a compound, hence the interest to perform characterization tests under conditions equivalent to a naturally aged chemical state. This well-spread practise is coupled with the use of Arrhenius' law [Le Huy and Evrard, 2001]. For instance, elastomers withstanding aggressive environments are usually subjected to this kind of tests: Mott studied natural rubber ageing on air and marine environment [Mott and Roland, 2001], while Le Saux addressed the ageing of SBR elastomers under marine environment (salty immersion conditions) [Le Saux, 2010]. The ability to extrapolate the results Arrhenius law has a key interest to predict a component's expectable lifespan [Gillen and Clough, 1997] [Gillen and Celina, 2000]. Moreover, the degradation induced on a material can ease the study of long-term fatigue behaviour of some compounds [Woo and Kim, 2006] [Chang Su and Hyun Sun, 2015]. These works have been a useful source to prepare the experimental plan for thermal ageing. The following paragraphs will describe the set-up of the experiences, as well as the equipments used to perform the tests.

A substantial amount of standard samples of the element's rubber mixture were delivered for characterisation. The samples are ISO-37 H1 dumbbell-shaped specimens for standard tensile stress, as shown in Figure 3.9 [ISO37, 2012]. The accelerated thermal ageing of a polymer is a well-established practice to study the degradation of the material's properties [ASTM-D3045-92, 2003] [ISO2578, 1994]. Nevertheless, some conditions regarding temperature and time of exposure must be met, depending on the material's operational temperature range [ASTM-D3045-92, 2003]. The PSi parts operate between -20 and +50 degrees Celsius. Therefore, according to the norm, their ageing can be induced at standard temperatures of 70 °C or 90 °C, for periods extending from 3 to 1 week, respectively of the temperature levels. Hence, a choice of temperature levels from ambient to 90 °C has been established, jointly with several times of exposure, ranking from 1 to 30 days depending on the applied temperature, so as to obtain different aged states on each batch. The configurations are shown in Table 3.3. Each configuration is identified by a double index: the *temperature* of the oven and the *time* of exposure. To ensure the statistical soundness of the study, five samples per configuration have been aged.

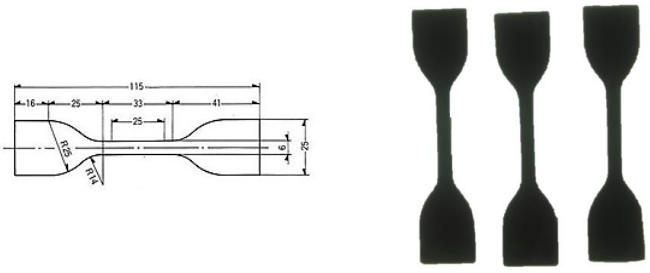

(a) (b)

Figure 3.9: Tensile stress test standard ISO 37 - H1 samples.

The ensembles of specimens have been weighed and measured prior to exposure to thermal ageing. The weighing was carried out with a precision scales and the measuring with an electronic calliper. Measures were taken at room temperature and concerned the axial length of the samples, three thickness measurements (top, middle and bottom of the useful area) and three width measurements (top, middle and bottom of the useful area). A Thermo-scientific Heraeus 6060 oven with back venting and temperature thermostat control was used for the tests. The oven was switched on two hours before the beginning of the tests, ensuring the stabilization of the temperature by the time the samples were introduced. The standards ask for the samples to be pending inside the oven during thermal ageing [ASTM-D573-99, 1999]. To ease manipulation and extractions on intermediate periods during each temperature, the samples were placed on stainless steel trays. The extractions were practised at the periods mentioned in Table 3.3, leaving a stabilization time immediately after extraction. The samples were subsequently weighed and their dimensions measured, by means of the same precision scales and calliper used prior to thermal ageing. The specimens were numbered and stored away from light and heat sources to preserve the material's stability until mechanical characterization.

From a strictly chronological point of view, ageing tests were conducted in four phases: a *feasibility* stage, a *global campaign* phase, plus a *complementary* test campaign and a *punctual* detail campaign. The temperatures aimed for the global experimental set were ambient (reference) temperature, plus 50, 70 and 90 °C. The interpretation of the results required further experimentation to enlighten some dubious observations, hence the addition of an 80 °C campaign. Last, two sets of temperatures were added at 60 and 75 °C, to provide additional data. Unfortunately, these two ageing temperatures lacked of enough samples to perform a thorough analysis. To optimise the amount of configurations, two samples per configurations were aged and tested, versus five samples in the previous configurations.

Temperature levels						
Amb	50 °C	60 °C	70 °C	75 °C	80 °C	90 °C
∞	-	-	-	-	1 day	1 day
-	-	*2 days*	2 days	*2 days*	2 days	2 days
-	-	-	5 days	-	5 days	5 days
-	-	*10 days*	10 days	*10 days*	10 days	10 days
-	15 days	*15 days*	15 days	*15 days*	15 days	-
-	30 days	-	30 days	-	-	-
-	45 days	-	-	-	-	-

Table 3.3: Red-coloured configurations resulted in an extremely weakened material, failing to withstand mechanical testing for a substantial number of samples. Configurations in italics were conducted with a lower amount of available specimens (< 3), thus being less representative.

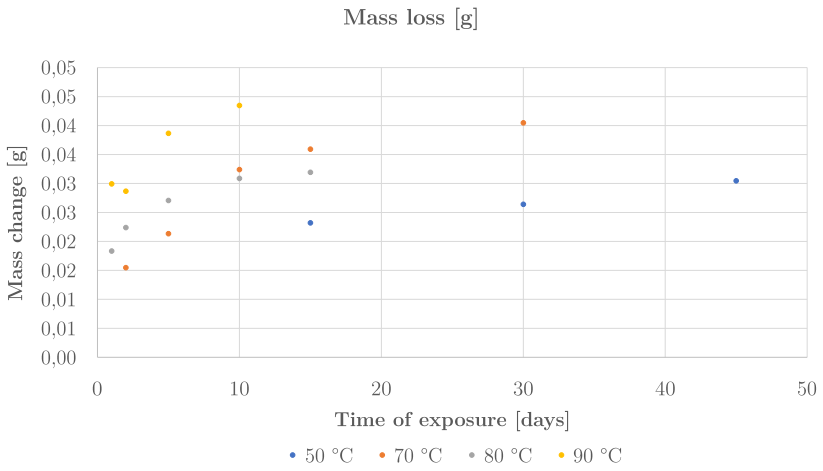

Figure 3.10: Average mass loss on the standard rubber samples after thermal ageing.

3.3.2 Physical-chemical characterization

Dimensional analysis

The specimens' macroscopic metrics have been modified during the thermal ageing tests. There is a direct relation between the temperature and time of exposure and the *mass of the samples*. The specimens undergo a loss of mass throughout the ageing tests (see Figure 3.10), which tends to stabilize at longer exposure periods. The weight loss is evident with time exposure at a

constant temperature, as well as with increasing temperature for the same isochrone. As regards of the samples' dimensions, the specimens have shrunk slightly during ageing, although measuring uncertainties have arisen due to the use of a calliper. Among all the specimens' measurements, thickness records show that there is a decrease on the part's volume, although not all measurements reflect it. The samples' axial length records can sometimes show a slight longitudinal shrinkage as well.

Spectroscopy tests: EDX, FTIR

The observations carried on the specimens after ageing showed the release of some yellowish emanations. Stains were found on the back of the venting outlet of the oven and on the stainless steel trays carrying the specimens. Long-lasting specimens showed slight iridescent traces on the upper surface as well. Reasonable concerns about the release of sulphur components (yellow) or possible changes on the molecular structure arose at the issue of the tests. The laboratory LAMIH has a correspondent research structure at the University of Valenciennes, the LMCPA, which works on material science and has chemical analysis facilities. Samples from the aged rubber were transferred to the LMCPA to perform deeper analysis on the composition of the rubber. Spectroscopy results by EDS-EDX detailed in Table 3.4 revealed that there were little to no losses on sulphur tenure on the aged samples, which had been a primary source of concern. Further spectroscopy analysis with infra-red FTIR tests showed that the spectroscopic signature of the samples was significantly similar on all stages, as appears on Figure 3.11. Moreover, sulphur bond signatures lay beyond the resolution of FTIR: peaks appear around and below 500 cm^{-1} [Trofimov et al., 2009] and can easily be mistaken with background noise. We believe that the evaporation traces observed do not correspond to sulphur compounds, but might be related to plastifying additives withholding amine radicals. Some nitrile organic compounds are known to have a yellowish colour, which may have caused the tainting mentioned above.

Swelling tests

The assessment of the chemical characteristics of the aged samples has been resumed after the mechanical test campaign. The scrap remainders of the tested specimens have been recovered for further analysis by means of *swelling tests*. As discussed in Section 3.1, sunk samples of a polymer within an appropriate solvent will swell in a manner which is proportional to the cross-link rate of the polymer. The design of our experiment has been based on an experimental set up used by [Barbosa et al., 2017], aiming the assessment of the devulcanization of crumb rubber, using a protocole based on the standard test drafted by the ASTM [ASTM-D6814-02, 2002].

Scrap remainders of the ISO-37 specimens were collected during mechanical characterisation

Ageing configuration	Oxygen [%]	Sulphur [%]	Zinc [%]
Non-aged	47,59	17,51	34,90
	35,52	21,87	42,61
	40,73	20,11	39,16
2 days, 70 °C	32,49	23,40	44,11
	24,18	24,77	51,05
	34,57	25,11	40,31
5 days, 70 °C	32,28	25,14	42,59
	29,85	25,14	45,01
	35,41	22,70	41,88
2 days, 90 °C	30,19	24,24	45,58
	31,32	23,87	45,58
	29,40	24,13	46,47
5 days, 90 °C	27,24	25,54	47,23
	28,70	25,93	45,37
	26,90	26,91	46,20

Table 3.4: EDS mass tenure of Oxygen, Sulphur and Zinc on the samples. Mass measurements by EDX do not allow an accurate detection of elements lighter than nitrogen (carbon is detected as a strong peak, yet its magnitude is not quantifiable). Therefore, the results are given in % of mass relative to non-carbon/hydrogen measurable elements, with an accuracy of $\pm 3 - 5\%$.

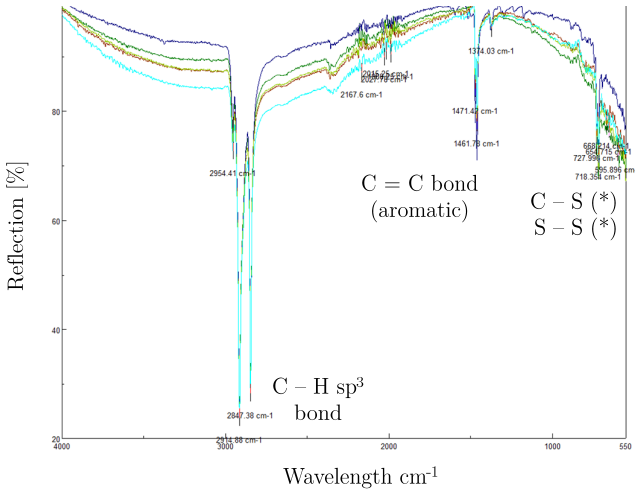

Figure 3.11: Rubber FTIR spectre for five ageing configurations. In spite of the absorption differences between the curves, peak values are strongly intertwined, hindering a neat interpretation of the ageing effects. Peaks marked with (*) correspond to possible sulphur signatures (not confirmed).

and classed according to the ageing conditions to which they had been subjected. The configurations of thermal ageing which were chosen are listed in Table 3.5. The remainders were supplied to the laboratory LMCPA to perform swelling tests according to the following protocol.

- The remainders are cut to obtain a piece of rubber with an approximate mass of 2 grams.
- Rubber samples are weighed so as to obtain their dry mass.
- The samples are sunk into a xylene solution during 24 hours.
- The stabilized, swollen samples are dried, then weighed to obtain their swollen mass. The difference with the dry mass is due to the solvent absorbed during the sunk phase.
- The *reticulation volume*, V_r, is calculated by means of the Equation 3.4.
- The *density of reticulation* [mol/cm^3] is calculated using Flory-Rehner Equation (Equation 3.5). The Flory-Huggins interaction parameter, χ, equals 0,34 for the couple natural rubber - xylene [Barton, 1990]. Since no pure rubber was available, the Lorentz-Park correction [Lorenz and Parks, 1961] [Cunneen and Russell, 1970] could not be applied to the material. Consequently, the obtained results have a lesser accuracy.

Thermal ageing configuration	**Samples**
50 °C - 45 days	1 sample
70 °C - 2 days	2 samples
70 °C - 5 days	2 samples
70 °C - 30 days	1 samples
80 °C - 2 days	1 sample
80 °C - 5 days	2 samples
90 °C - 2 days	2 samples
90 °C - 5 days	3 samples

Table 3.5: Thermal ageing configurations and amount of samples having undergone swelling tests.

The reticulation densities obtained from swelling tests show that there is a dependence between the cross-linking within the rubber and the ageing temperature and periods of exposure. In a general way, the increase of both parameters fosters a growth of the reticulation density in the rubber. Further analysis of the experimental data have been undertaken, shifting each temperature series so as to build a master curve with 50 °C as the base point temperature. The corridor suits fairly well an exponential pattern ($R^2 \simeq 0,81$); however, such a description would imply an infinite reticulation with increasing time. Sigmoid functions offer an alternative form which reaches a

saturation barrier after a certain time (Figure 3.12), thus being consistent with the stabilization of the reaction rate and termination of the chemical process [Blake, 1930] [Nordlander, 1929]. The mean standard deviation of the experimental data with respect to the analytic curve is of 4,75 %.

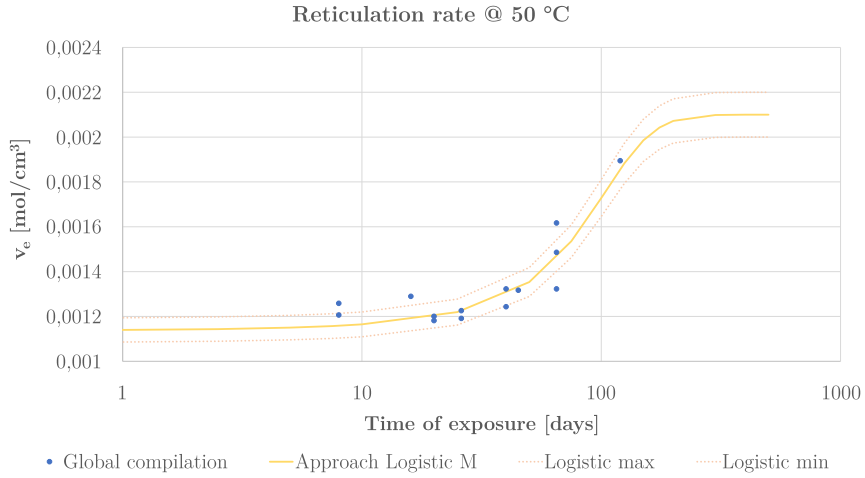

Figure 3.12: Composed master curve at a reference temperature of 50 °C (blue, dotted points), approached by a fitted sigmoid curve (yellow curve, analytical). The corridor width between the orange curves is twice the averaged standard deviation between experimental and analytical data.

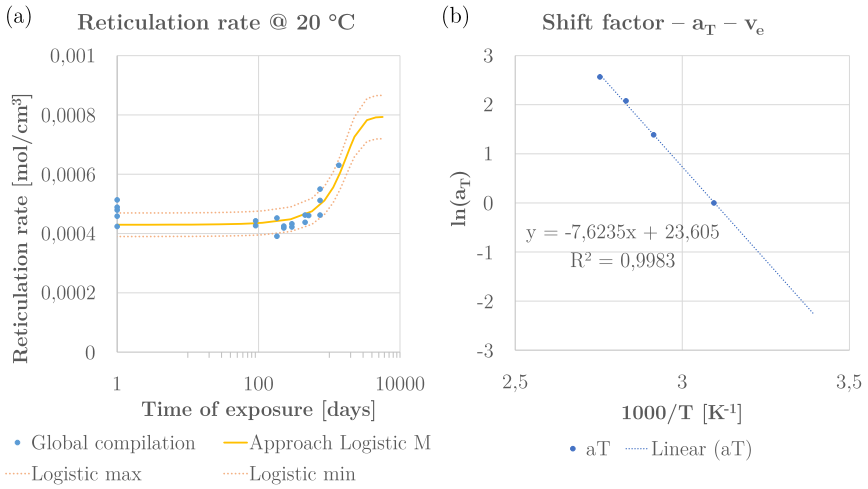

Figure 3.13: (a) Master curve experimental data at 20 °C (dotted blue series), approached by a fitted sigmoid curve (yellow curve, analytical). The corridor width between the orange curves is twice the averaged standard deviation between experimental and analytical data.

The shift factors composing the master curve have been plotted against the reciprocate of the temperature to form an Arrhenius plot. The resulting regression has shown a very good agreement between the linear interpolation and the shift factors ($R^2 \simeq 0,99$) (Figure 3.14a). The extrapolation of the regression to an ambient temperature of 20 °C yields a shift factor $a_t = 0,0879$. Therefore, the master curve at 50 °C can be shifted back to the reference temperature and therefore obtain the evolution of the reticulation density under such premises (Figure 3.14b). However, on can discuss the accuracy of the saturation curve, which will not be realistic for very long exposure times or high temperatures. The supplied heat will begin to degrade the material by causing the sulphur bonds to break. Thus, the model should be further completed by experimental research and tests on longer times of exposure to thermal ageing, in order to add a degradation term with a later activation.

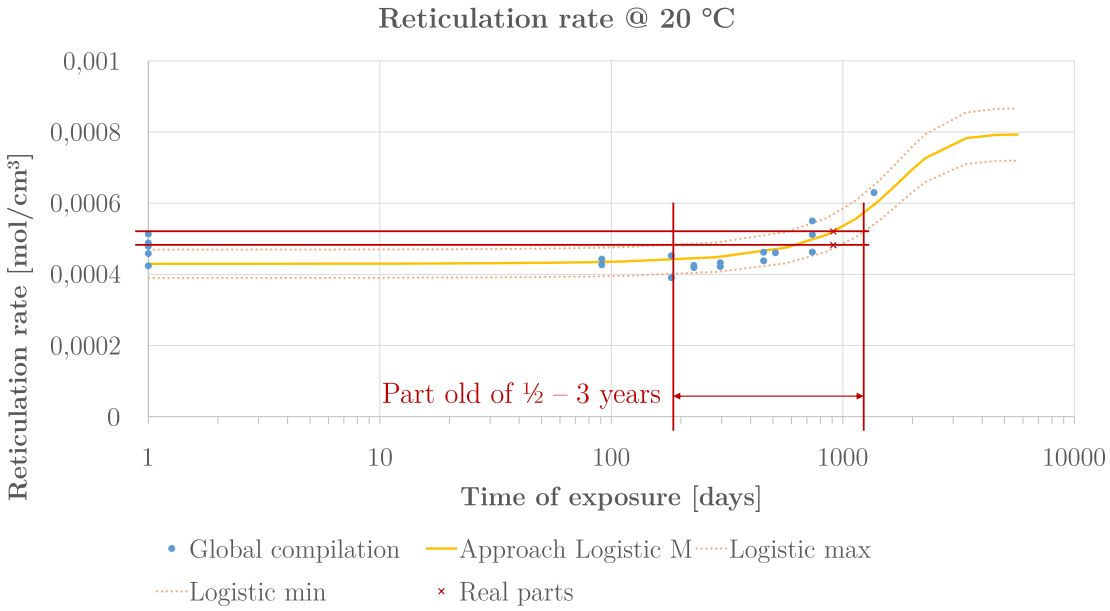

Figure 3.14: Master curve experimental data at 20 °C (dotted blue series), approached by a fitted sigmoid curve (yellow curve, analytical). The red cross points are the results for two real samples recovered from Germany.

Ageing identification: inverse analysis with reticulation curves

Several parts having served on Talent 2 trainsets in Germany (Deutsche Bahn) were recovered. Samples of rubber were extracted out from a sectioned suspension element. Their reticulation rates were of $5{,}2038 \cdot 10^{-4}$ and $4{,}8221 \cdot 10^{-4}$ mol/cm^3. According to the corridors obtained from the swelling tests, the part's age would be somewhere from 6 months to 3 years. However, the

parts have served for around 6 years, implying that the ageing of the real part did not cause a reticulation equivalent to that of the aged specimens in the laboratory.

3.3.3 Mechanical characterization

The characterization of the mechanical behaviour of the rubber reference used on PSi elements has been performed via standard tensile stress tests. The aged samples supplied by the part's manufacturer were ISO37-H1 dumbbell samples [ISO37, 2012], which is the standard procedure for rubber characterization. All tests were performed on the same machine with an identical test set-up. All samples from each ageing batch were tested consecutively at the same date, although the test campaigns were undertaken progressively at the pace set by the ageing tests.

3.3.3.1 Experimental set-up

Mechanical characterization tests were performed at the facilities of the *CERMEL* laboratory in Tours (Centre-Val-de-Loire region, France). The test devices consisted on a Zwick-Roell Z010 test machine, coupled with the acquisition software "testXpert II". The machine was equipped with an integrated extensometre measuring the displacements across the useful section of the samples and a USB connected micrometer for section measurements. The experimental protocol set to prepare each test session is developed as follows.

- The machine grips have been placed at a distance of 60 mm, set by a standard patron shim of the same size.
- A specimen is placed between the machine grips clamped, the extensometer tweezers closed as well to set their position over the sample's usable area.
- The test protocol is uploaded to the acquisition software and prepared for the test campaign.

As regards of the test procedure, it is deployed in several stages. The introduction of the *test parameters* on the control and acquisition software, the *set-up of the sample itself*, the *test execution* plus the *post-processing* of the tests. The steps are listed below.

- The test steps applied to each of the samples are the following.

- A light pre-load over the specimen before the beginning of the test (around 2 N).
- 10 complete cycle loads on the sample, to soften the material and stabilize the Mullins effect. The tests rise to a strain of 200 % for a crossbeam speed of 500 mm/min.
- 1 complete cycle load, up to a strain of 200 % at a crossbeam speed of 50 mm/min.
- Finally, a final loading stage up to the specimen's breakdown, with a crossbeam travelling speed of 50 mm/min.

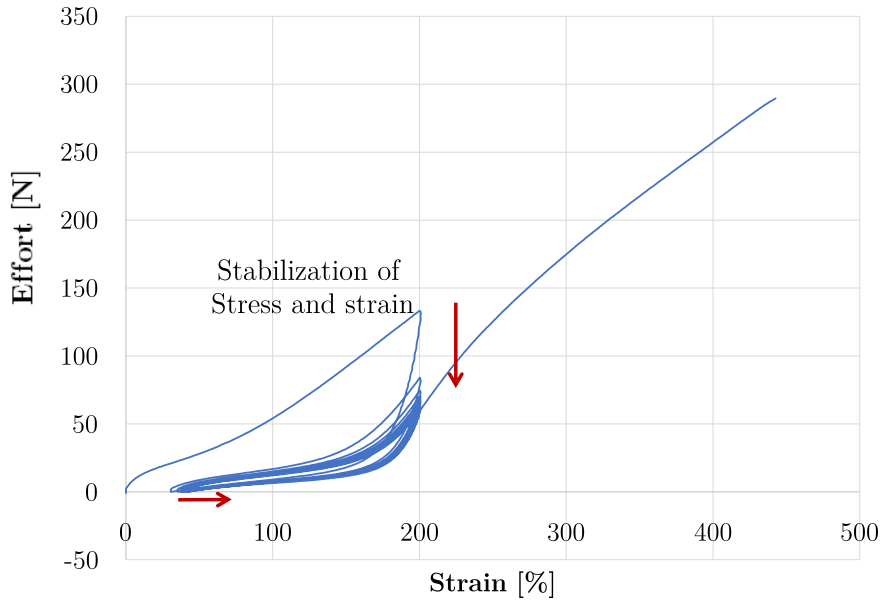

Figure 3.15: Effort-strain curve from the characterization tests.

- The testing practise is undertaken following the steps below.
  - Measurement of the central section of the specimen with the micrometer which is connected to the machine's control software.
  - The sample is placed on the test bench. The following checks are customary: the centring of the sample, aligned with the references on the grips; the correct alignment along the longitudinal axis, to avoid parasitic shear loads. These aspects are verified with both grips clamping the specimen.
  - Release of the upper grip and calibration of the offset efforts, due to the specimen's weight and the clamping effort on the sample.
  - Clamping of the upper grip and launch of the test until the end of the test program (sample breakdown).

  - When the specimen breaks down, the upper crossbeam is stopped, the results checked and recorded. The remainders of the specimen are recovered and a new sample can be prepared for further testing if necessary.

- Once all results have been gathered, the post-processing of the experimental data takes place.
  - The raw data is analysed to extract the last recorded curve, up to the specimen's breakdown. The curve under the maximum strain level applied to stabilize the Mullins effect is the material's characteristic response.
  - Since the recorded data are given as stress-strain curves, the post-processing of the information includes the calculation of the stretch levels of the curve, as well as the effort levels.
  - The following metrics have been extracted: the *maximum strain level at breakdown*, the *maximum stress level at breakdown*, the *secant stiffness at 200 % strain levels*, as well as the evolution during the cycles of the *minimum residual strain level* and the *maximum stress level* at the maximum applied strain.

3.3.3.2 Experimental results - Ageing effects

The characterization of the mechanical properties from the aged specimens have yielded some interesting results, which match the observations from the scientific literature [Gillen and Clough, 1997]. We have observed a systematic loss of mechanical resistance on the rubber. As shown in Figure 3.17a, the samples' *ultimate strain* decreases with the time exposure for a fixed temperature. The strain falls as well for same-time exposures with increasing temperature. The *ultimate stress* withstood by the rubber decreases as well with both temperature and time of exposure (Figure 3.17b). On the contrary, the rubber's *secant stiffness at 200 % strain* increases with the time of exposure for an isotherm configuration (Figure 3.17c). This effect can also be observed with the increase of temperature for isochronal configurations. This trend cannot, however, be generalized upon the whole range of temperatures. An excess exposure at very high temperatures has a negative effect on the material, strongly degrading its properties. In spite of being in accordance with the material's loss of ultimate strain and stress, it has also a counter-effect on the rubber's stiffening. Temperature series at 80 °C and 90 °C reach a critical state beyond 10 and 5 days of exposure respectively (red-coloured series on Table 3.3). Over the five specimens on each series, only one sample from 80 °C - 15 days withstood the testing process, two for the 90 °C - 10 days configuration. The rejected samples broke down at the first load, well before any softening of the Mullins effect could have occurred.

As regards of the Mullins effect, the *residual strain* and the *maximum strains' stresses* have been plotted versus the number of load cycles for new, 50 °C, 70 °C and 90 °C configurations. The stabilization of the Mullins effect can be inferred after the ten cycles. The residual strains

on Figure 3.16a sensibly follow a logarithmic law ($R^2 \geq 0,95$). There are five exposure couples whose averaged residual strain is higher than that of the new samples: 70 °C at 10, 15 and 30 days, plus 90 °C at 2 and 5 days, while the other curves lay about or below the new samples' averaged curve. A clearly defined hierarchy can be observed for 50 and 90 °C strain curves: for 50 °C, the higher the time of exposure, the lower the strains; the trend is reversed for 90 °C, with higher strains for higher exposure times. Interestingly, the evolution of the maximal strains' stress plotted in Figure 3.16b has shown the same internal dependence on the time exposure for isothermal configurations: higher times of exposure yield higher recorded stresses for 70 and 90 °C, while yielding lower stresses for 50 °C. The behaviours can be reasonably approached either by a logarithmic law ($R^2 \simeq 0,80$) or by negative-exponent potential law ($R^2 \simeq 0,86 - 0,87$). The overall results show that a change in the material's behaviour occurs during the ageing, with a yielding point placed somewhere around 70 °C.

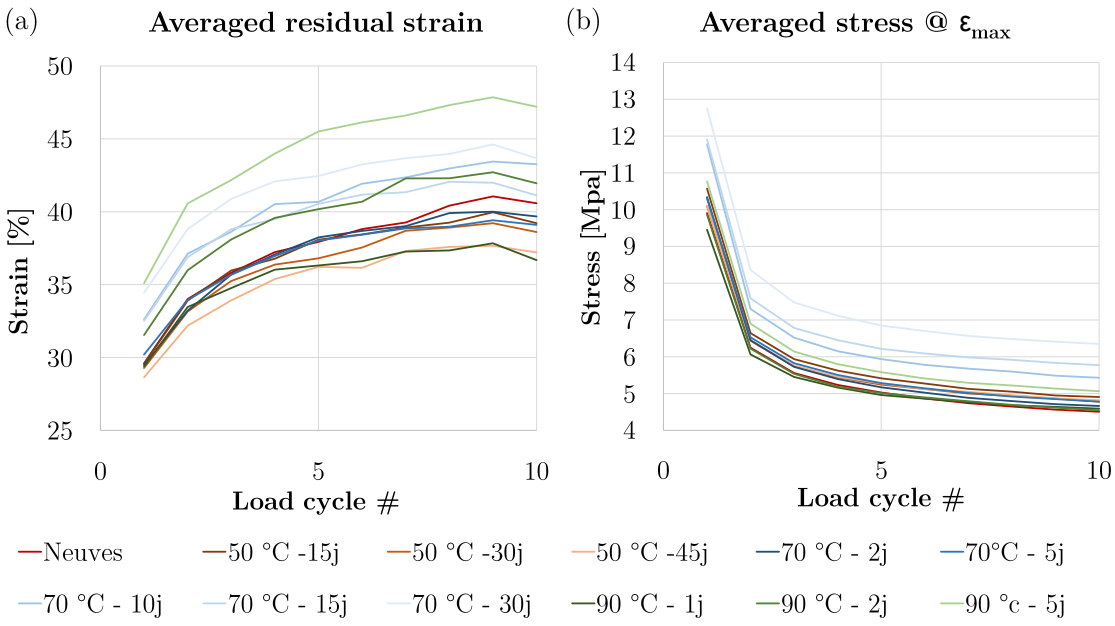

Figure 3.16: Tensile stress test standard ISO 37 - H1 samples.

The compilation of the aforementioned metrics according to the times of exposure, by isothermal series, is the starting point to perform a correlation analysis with an Arrhenius' law. Mixed curves on Figure 3.17 can be displaced via a set of appropriate shift factors, so as to build the "master curve" of the metric (Figure 3.18). Each set of couples temperature-shift factor can be plotted to find a linear adjustment which hence demonstrates the dependence of the metric to an Arrhenius law, should it exist. We have found a very good agreement between the linear regressions and

the shift factors, with R^2 indexes above 0,95 which consolidate the approach. Analytic fits of the ultimate strain and the ultimate stress show that an *exponential function* would explain up to 70 % of the variability within experimental results (Figures 3.19a and 3.19b). As regards of the samples' secant stiffness at a deformation of 200 %, the master curve is modelled by a logistic function with an offset set at the average value of the new-state stiffnesses (Figure 3.19c). It has an averaged standard deviation of 7,6 %, although some experimental data show deviations up to 24 - 25 % of the predicted values.

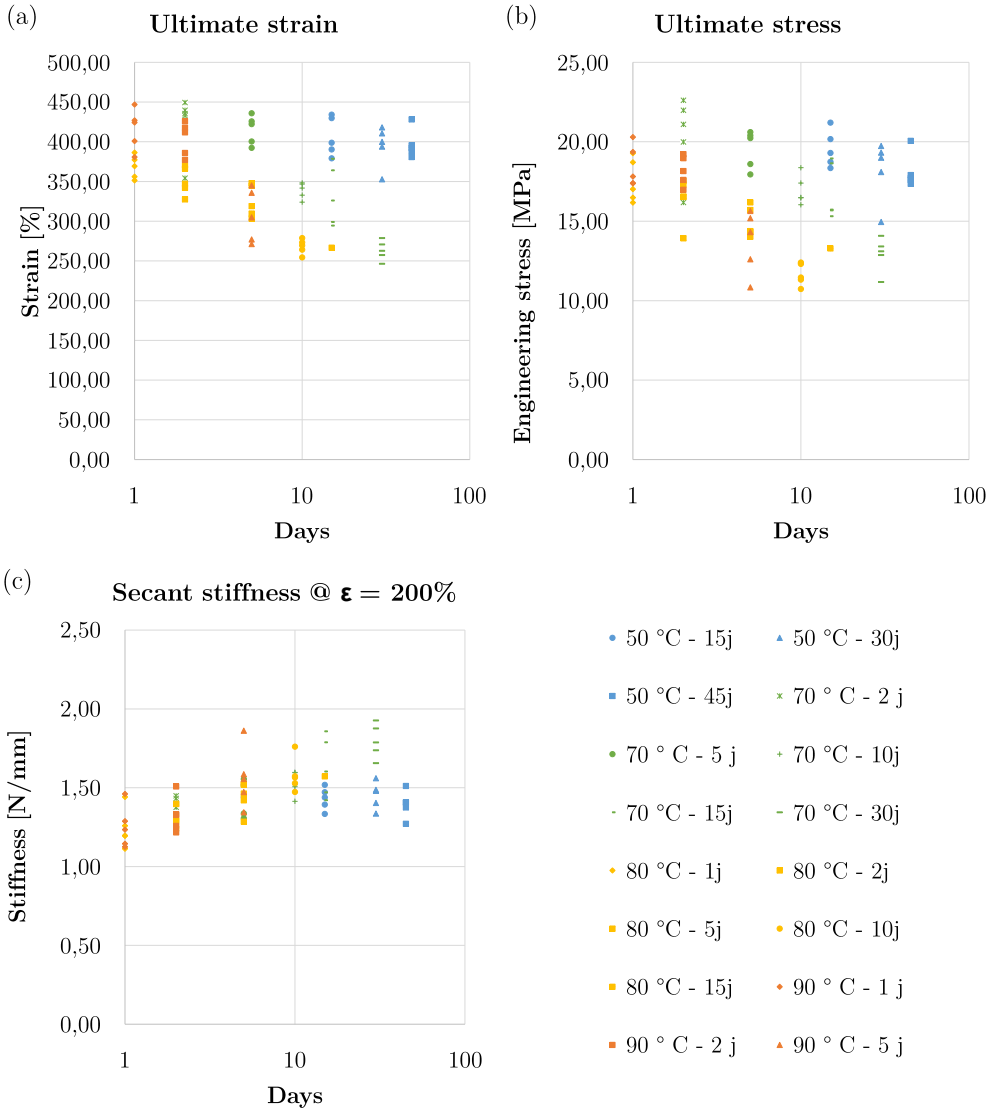

Figure 3.17: Results from the standard characterization tests, performed on thermally aged samples.

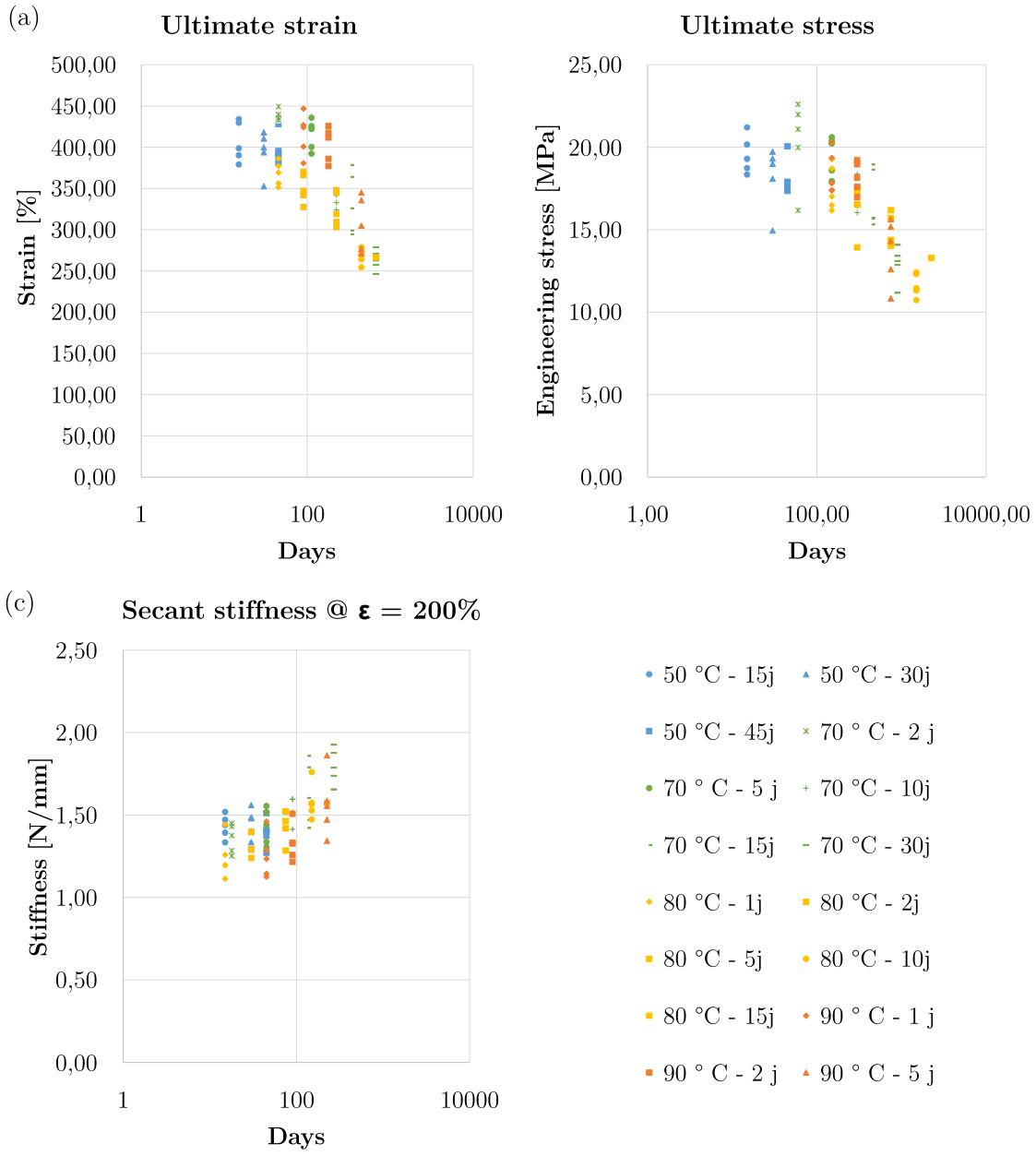

Figure 3.18: Master curves obtained from the standard test results performed on the thermally aged samples. The Arrhenius plots of strain (a), stress (b) and stiffness (c) show a very good agreement between the shift factors and the reciprocate of temperature (right side graphics).

(a)

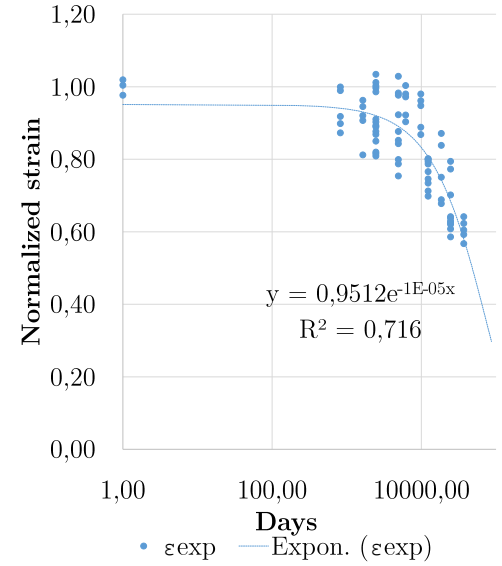
Ultimate strain
Normalized strain
1,20
1,00
0,80
0,60
0,40
0,20
0,00
y = 0,9512e-1E-05x
R² = 0,716
1,00
100,00
10000,00
Days
εexp
Expon. (εexp)

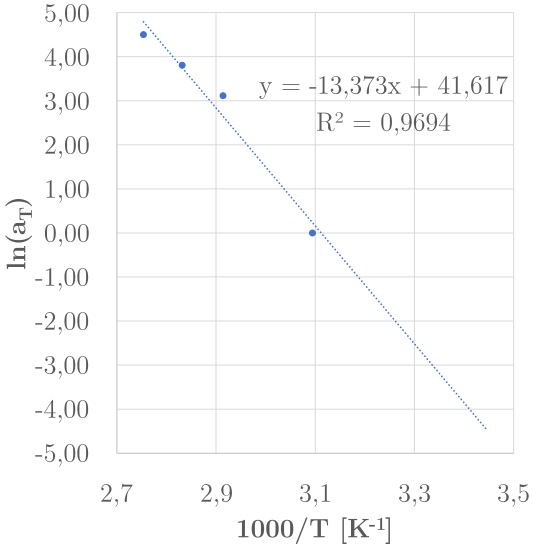
Shift factor – aT – ε
ln(aT)
5,00
4,00
3,00
2,00
1,00
0,00
-1,00
-2,00
-3,00
-4,00
-5,00
y = -13,373x + 41,617
R² = 0,9694
2,7
2,9
3,1
3,3
3,5
1000/T [K-1]

(b)

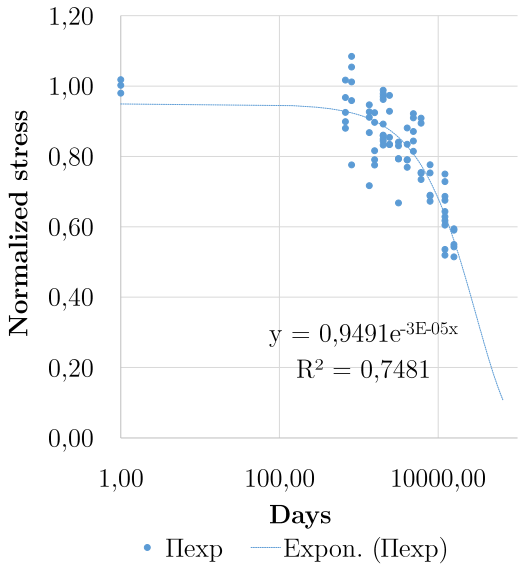
Ultimate engineering stress
Normalized stress
1,20
1,00
0,80
0,60
0,40
0,20
0,00
y = 0,9491e-3E-05x
R² = 0,7481
1,00
100,00
10000,00
Days
Пexp
Expon. (Пexp)

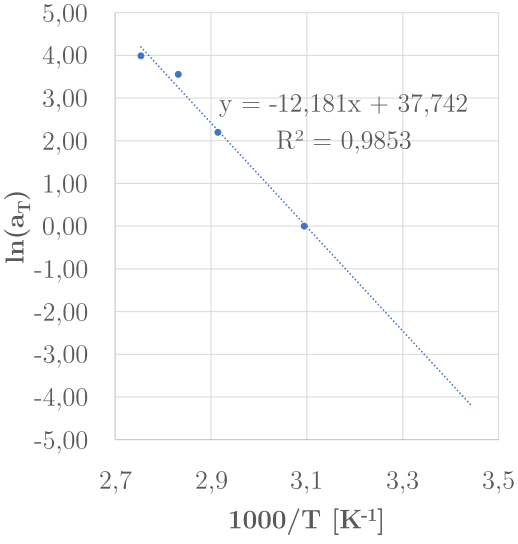
Shift factor – aT – Π
ln(aT)
5,00
4,00
3,00
2,00
1,00
0,00
-1,00
-2,00
-3,00
-4,00
-5,00
y = -12,181x + 37,742
R² = 0,9853
2,7
2,9
3,1
3,3
3,5
1000/T [K-1]

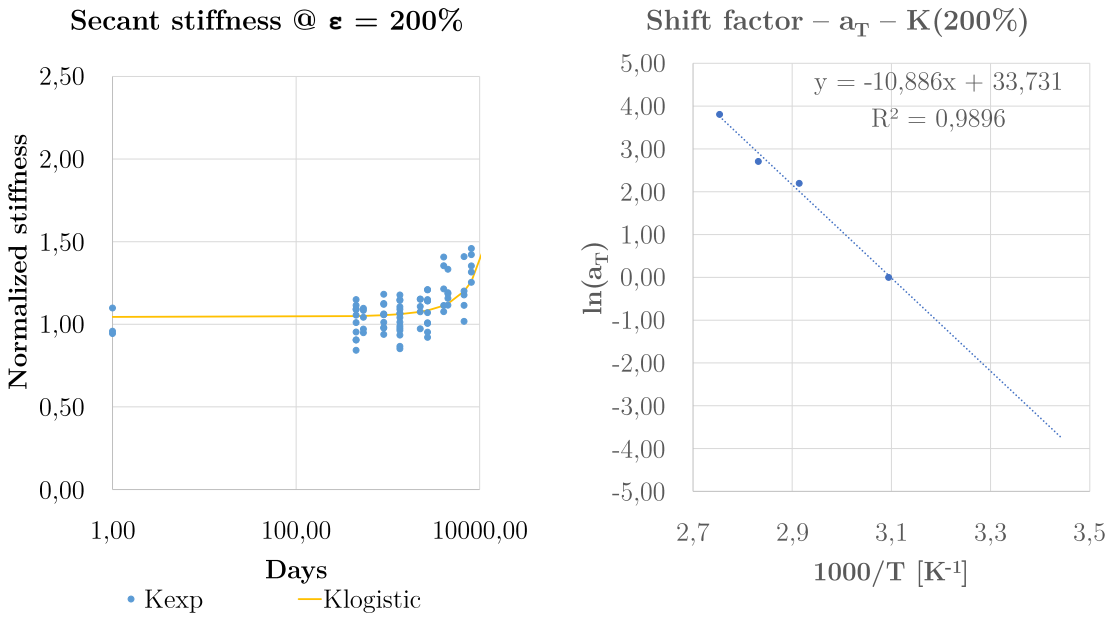

Figure 3.19: Linear regression of the stiffness shif factors. The Arrhenius plot shows a linear dependence of the factors with the reciprocate of temperature.

Interestingly, experimental data conforming the master curves spread well beyond 10 years (approximately, 3650 days). Dramatic drops on the material's characteristics occur after this period, with no major changes at 15 years (5480 days). Therefore, we can make the guess that *the particular action of natural ageing* of the rubber up to these periods does not cause a potential loss of its mechanical properties. However, other concurring phenomena such as fatigue under cyclic loading might cause further losses of mechanical resistance, which are not reflected on the figures above. Moreover, a stiffening on the rubber can embrittle the material, thus being more easily crackable and damageable. Thus, the study of the combination of all effects is strongly recommended before concluding on a hypothetical resilience of the material against ageing.

3.4 Identification of an hyperelastic energy strain function

By applying the expressions discussed in Section 3.2 (see [Lejeunes, 2006] for a detailed development), it is possible to calculate the analytical expression of the stress-strain hyperelastic law for a material for a given configuration. For instance, the base Mooney model yields Equation 3.24 for uniaxial stress tests on an intermediate configuration. Therefore, the determination of the C_{ij} coefficients on the strain energy function can be determined by a least-square fit analysis, comparing an experimental curve with the analytic results corresponding to the same experimental configuration. In order to obtain sound results on the identification of the strain energy function, it is customary to perform multiple tests in different homogeneous strain configurations. Since the potential $\mathcal{W}(I_1, I_2)$ has a unique form for the material, the fits on the experimental curves will provide different sets of C_{ij} coefficients, establishing the ranges in which their values would lay.

$$\Pi_{11} = \frac{\partial \mathcal{W}}{\partial I_1}(\lambda - \frac{1}{\lambda^2}) + \frac{\partial \mathcal{W}}{\partial I_2}(1 - \frac{1}{\lambda^3}) \quad \textit{for an incompressible material.} \tag{3.24}$$

According to the wide variety of formalisms available within the scientific literature, a preliminary work has been addressed to determine the most suitable form for the strain energy function. The choice of a certain model has been based on the accuracy of the approach with respect to the experimental data, plus the compatibility of the model with commercial FE software which could be used or provided within the project. Furthermore, one must bear in mind that the strain energy functions must respect some requirements regarding the material stability, be it mathematically or from a thermodynamic point of view [Lejeunes, 2006]. Among the latter we can find Hill's Criterion, which can ultimately be translated as the positivy of the Hessian of the strain energy function. A simplified application of Hill's Criterion can be found for phenomenological hyperelastic models [Kumar and Venkateswara, 2016], with several forms depending on the model order (see Table 3.6).

The experimental results from the uniaxial traction tests on the new, non-aged samples have been used to test the models' aptitude to approach our rubber's behaviour accurately. By means of the analytic calculation software Mathematica ©, we have calculated the analytic expression of the stress-strain function for each chosen energy function. A fit has been performed with the software, so as to find the suitable C_{ij} coefficients and to compare the experimental and analytic results (Figure 3.20). The best candidates for our works were four *phenomenological models*: *Biderman's model* $(C_{10}, C_{01}, C_{20}, C_{30})$, *Tschoegl's model* (C_{10}, C_{01}, C_{22}), *Yeoh's model* (C_{10}, C_{20}, C_{30}), and *James' model* $(C_{10}, C_{01}, C_{11}, C_{20}, C_{30})$. The soundness of the fit was evaluated by an averaged error measurement between the experimental result and the analytic stress calculated at the measured strain points. James' energy function yields the best results, with an averaged error lesser than 5 % (Figure 3.21). The local error falls below 5 % at low strain levels (around 10 - 20 % strain), which we consider as a fairly good approach. Moreover, the C_{ij} coefficients respect the material stability constraints and the model is usually implemented in commercial FE software (Nastran,

Marc, Abaqus...), allowing further simulation works.

Model	Conditions on C_{ij}
2 parameters	$C_{10} + C_{01} \geq 0$ $C_{01} \geq 0$
3 parameters	$C_{10} + C_{01} \geq 0$ $C_{11} \geq 0$
5 parameters	$C_{10} + C_{01} \geq 0$ $C_{20} \geq 0$ $C_{02} < 0$ $C_{20} + C_{02} + C_{11} \geq 0$
9 parameters	$C_{10} + C_{01} \geq 0$ $C_{30} \geq 0$ $C_{03} < 0$ $C_{20} + C_{02} + C_{11} \geq 0$ $C_{30} + C_{03} + C_{12} + C_{21} \geq 0$

Table 3.6: Stability conditions for phenomenological models of the generalized Mooney-Rivlin form, according to the number of C_{ij} coefficients required to define the model [Kumar and Venkateswara, 2016].

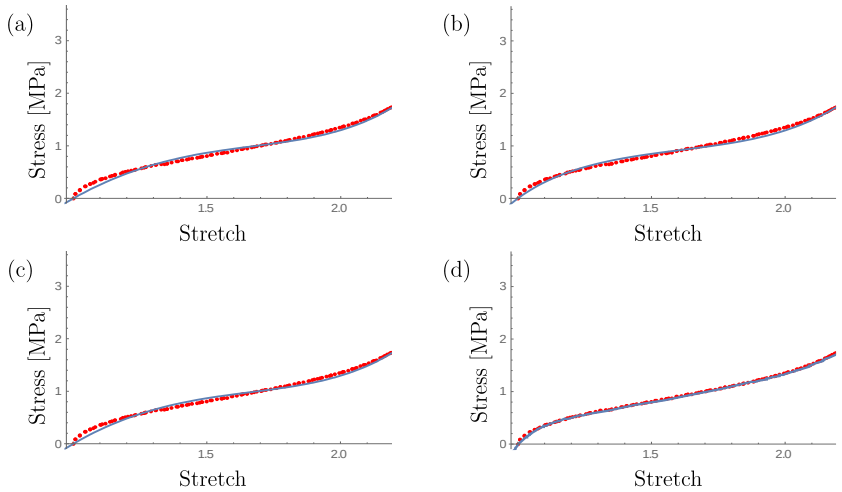

Figure 3.20: Analytic models fitting experimental curves: Biderman (a), Tschoegl (b), Yeoh (c) and James (d) models.

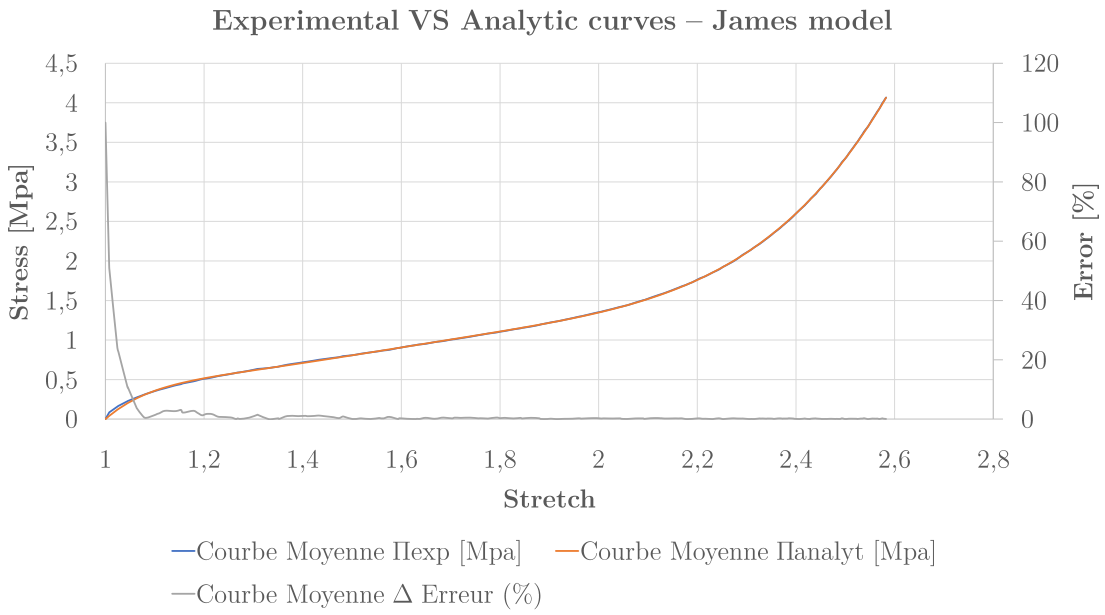

Figure 3.21: Comparison between the experimental stress-stretch curve and the analytic curve from a James model fit. Error drops dramatically at a low strain level, with an excellent accuracy over a wide deformation range.

3.4.1 Adjusted Hyperelastic model

The five-parameter James' model has been confronted systematically to the experimental results obtained from the test campaign. From each ageing configuration, five curves have been obtained. Three curves from each configuration have been subjected to an analytical fit to obtain their strain energy function: the *middle/average curve*, the *upper/maximum curve* and the *lower/minimum curve*. Thus, we have gathered all the C_{ij} coefficients corresponding to each of the ageing configurations in the tables below, classed by temperature of ageing and increasing time of exposure.

Reference		C_{ij} **coefficients - New samples**				
Days	Sample	C_{10}	C_{01}	C_{11}	C_{20}	C_{30}
∞	Avg	-2,64049	3,56444	2,244533333	-1,0894425	0,045907667
∞	Max	-2,47896	3,33498	2,253216667	-1,12165	0,051435
∞	Min	-2,6011	3,50824	2,245616667	-1,09788	0,047431333

Table 3.7: James' strain function coefficients for **new samples**.

Reference		C_{ij} **coefficients - 50 °C samples**				
Days	Sample	C_{10}	C_{01}	C_{11}	C_{20}	C_{30}
15	Avg	-2,78549	3,75563	2,406716667	-1,1724925	0,0489295
15	Max	-3,10458	4,17072	2,631333333	-1,2750275	0,0531485
15	Min	-2,87975	3,88642	2,421666667	-1,16996	0,048584333
30	Avg	-2,96938	4,00862	2,472416667	-1,1873975	0,048082333
30	Max	-2,98439	4,03068	2,5264	-1,2211725	0,050372667
30	Min	-2,56551	3,49659	2,177833333	-1,051035	0,043120833
45	Avg	-3,03497	4,14884	2,387616667	-1,1219	0,042931333
45	Max	-3,21127	4,35781	2,552366667	-1,2042925	0,046313
45	Min	-2,85261	3,85303	2,395566667	-1,15418	0,047205

Table 3.8: James' strain function coefficients for **50 °C samples**.

Reference		C_{ij} **coefficients - 70 °C samples**				
Days	Sample	C_{10}	C_{01}	C_{11}	C_{20}	C_{30}
2	Avg	-2,88239	3,87824	2,4174	-1,167205	0,048278333
2	Max	-2,98417	4,00368	2,563066667	-1,2483625	0,0530585
2	Min	-2,64369	3,58608	2,206233333	-1,0637075	0,0443255
5	Avg	-3,12813	4,17542	2,5546	-1,22386	0,049689
5	Max	-3,0314	4,06399	2,560166667	-1,23918	0,0515665
5	Min	-2,94151	3,95332	2,4365	-1,1699825	0,047551333
10	Avg	-3,11391	4,16143	2,76765	-1,36139	0,058601667
10	Max	-3,19855	4,24578	2,92225	-1,451315	0,063420333
10	Min	-2,84352	3,80083	2,647566667	-1,3235675	0,059915333
15	Avg	-3,25065	4,31608	2,954883333	-1,4628975	0,0634165
15	Max	-3,63418	4,85675	3,120533333	-1,515575	0,062679667
15	Min	-3,26156	4,35759	2,778966667	-1,346065	0,055071833
30	Avg	-3,41379	4,52614	3,191866667	-1,5902975	0,069778667
30	Max	-3,63816	4,84059	3,345166667	-1,6575	0,072164667
30	Min	-3,49624	4,65114	3,200883333	-1,5879525	0,070080167

Table 3.9: James' strain function coefficients for **70 °C samples**.

Reference		C_{ij} **coefficients - 80 °C samples**				
Days	Sample	C_{10}	C_{01}	C_{11}	C_{20}	C_{30}
1	Avg	-3,45878	4,59371	2,932166667	-1,426105	0,060533
1	Max	-3,45878	4,59371	2,932166667	-1,426105	0,060533
1	Min	-2,91478	3,89273	2,484966667	-1,206775	0,050374
2	Avg	-2,90321	3,85453	2,5919	-1,2752575	0,054088667
2	Max	-3,13375	4,20234	2,721733333	-1,3261925	0,055804333
2	Min	-2,77167	3,68174	2,4878	-1,227265	0,053052667
5	Avg	-3,5189	4,61343	3,029	-1,47878	0,062469833
5	Max	-3,24446	4,31347	2,908916667	-1,4381575	0,063113333
5	Min	-2,887	3,84217	2,682333333	-1,339435	0,059841833
10	Avg	-3,22075	4,28203	2,9349	-1,451045	0,062792667
10	Max	-3,2256	4,29689	2,9486	-1,4589625	0,063755167
10	Min	-3,26233	4,33162	2,965083333	-1,467065	0,064062

Table 3.10: James' strain function coefficients for **80 °C samples**.

Reference		C_{ij} **coefficients - 90 °C samples**				
Days	Sample	C_{10}	C_{01}	C_{11}	C_{20}	C_{30}
1	Avg	-2,75727	3,71746	2,309983333	-1,10574	0,043382
1	Max	-2,96075	4,0125	2,478516667	-1,184915	0,046760333
1	Min	-2,57094	3,51242	2,106283333	-0,999885	0,038794667
2	Avg	-2,84676	3,81795	2,4699	-1,20191	0,050272667
2	Max	-2,83078	3,77058	2,50685	-1,2260425	0,051332167
2	Min	-2,66893	3,56606	2,352966667	-1,1483725	0,0476955
5	Avg	-3,5191	4,59782	3,2577	-1,6243725	0,072266
5	Max	-2,87446	3,8042	2,708133333	-1,3514725	0,060067667
5	Min	-2,81453	3,75317	2,7087	-1,3576325	0,060967833

Table 3.11: James' strain function coefficients for **90 °C samples**.

3.4.2 Ageing effect on a hyperelastic model

The effects of the thermal ageing do not only affect the metrics measurable directly by means of standard tests. Indeed, the exposure to higher temperatures during sustained periods has an effect on the characteristic curves recovered from the samples. The five curves obtained on each ageing configuration have been averaged in a single curve, thus easing the observation of the effects of temperature and time of exposure on the curves most significant features. A hyperelastic curve has a characteristic "S-shape" which is directly related to the molecular structure of the

rubber. A stiff beginning which is related to the irreversible breakdown of some intermolecular bonds, as well as with the de-entanglement of the molecules. The curve softens immediately after, with a quasi-linear mid-part, usually translated as a regime of molecular sliding, the polymer chains slipping along the loading direction. The final stiffening starts at the locking of the molecules because of the cross-linking, increasing as the molecule's elasticity becomes dominant.

Therefore, the averaged curves have been plotted on multiple contexts to observe the changes on the three areas discussed previously. If one's point of view is the *isothermal* evolution, the initial gradient on the curve appears to increase with the time of exposure (Figure 3.22). Its is particularly evident for the ageing at 50 °C and 70 °samples, although the pattern is more subtle at 80 °C and 90 °C, more clearly on the latter. As regards of the high strain stiffening, it tends to increase globally, although some particularities have arisen from the tests: while the curves at 70 °C and 80 °C show a sustained stiffening with the time of exposure, the longest exposed curve at 50 °C appears to be slightly less stiff than the preceding configuration. Moreover, the samples aged at 90 °C seem to soften at first, recovering their stiffness with increasing exposure.

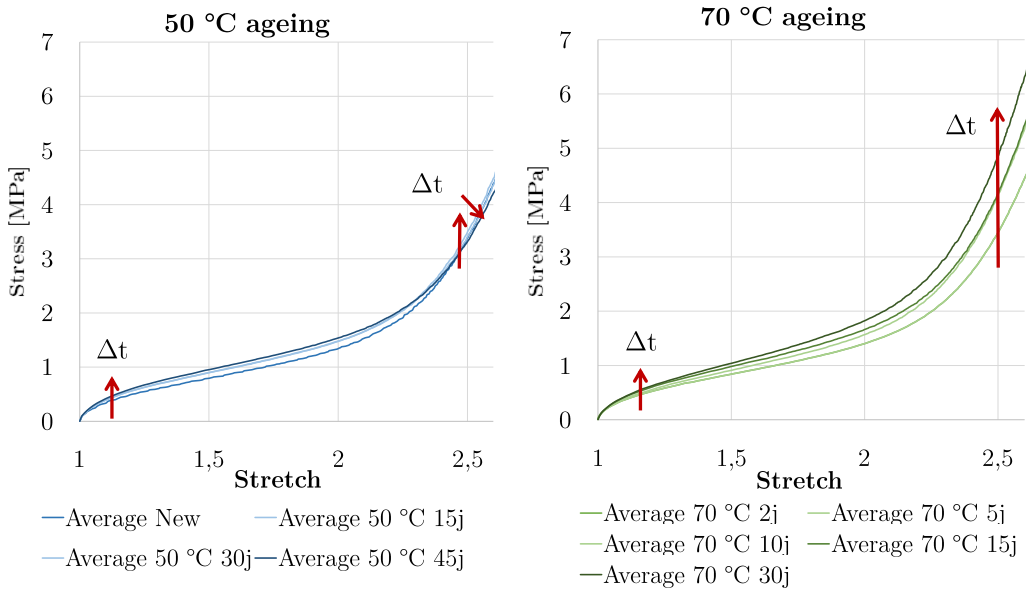

Figure 3.22: Average curves on isothermal plots. The effect of the time of exposure is represented by the red arrows.

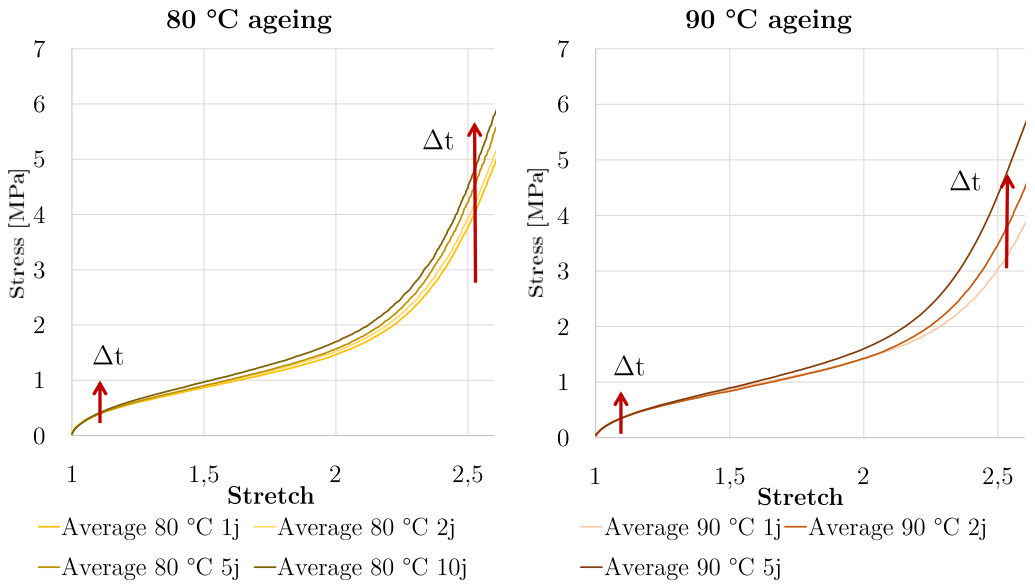

Figure 3.23: Average curves on isothermal plots. The effect of the time of exposure is represented by the red arrows.

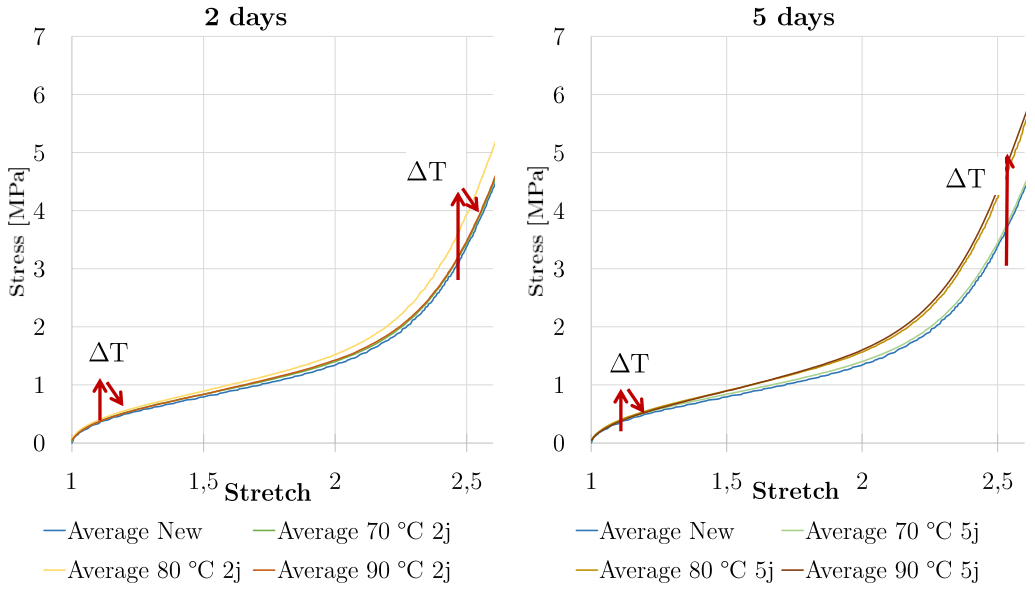

Figure 3.24: Average curves on isochronal plots. The effect of the temperature of exposure is represented by the red arrows.

From an *isochronal* point of view, two configurations with sufficient tested samples are available: 2 days and 5 days of exposure. The evolution of the initial gradient shows an initial increase, which is replaced by a decrease at 90 °C. This behaviour was observed on both configurations (see Figure 3.24). As for the high strain stiffening, it definitely increases with the temperature of exposure, although a decrease on the 90 °C curve at two days has been observed.

The results shown in Figures 3.22, 3.23 and 3.24 seem to point out the activation of a chemical transformation. The thermal ageing may have activated a mechanism which fosters a higher resistance at early strain levels. As discussed earlier, the behaviour of the material at this stage depends on the molecule's entanglement and on the low-energy, irreversible links. The links which act within the rubber are, in this case, the sulphur cross-links between the molecules. As exposed earlier, these come in multiple lengths and cling more or less effectively between the poly-isoprene chains. Sulphur bonds have a lower energy than carbon-carbon or carbon-hydrogen bonds, thus being less stable and prone to scission. One could argue that the exposure to thermal ageing destabilizes the longest poly-sulphide chains, breaking them in two branches with different lengths. The free radicals would generate newer bonds. Since the new cross-links would be a mixture of short-medium-length chains, they would display different resistances to breakdown. This variety of cross-links would explain the rise on the first-stretch resistance, sustained by less stronger chains, as well as the increased resistance obtained from new, mono- or bi-sulphide cross-links, at higher strain levels.

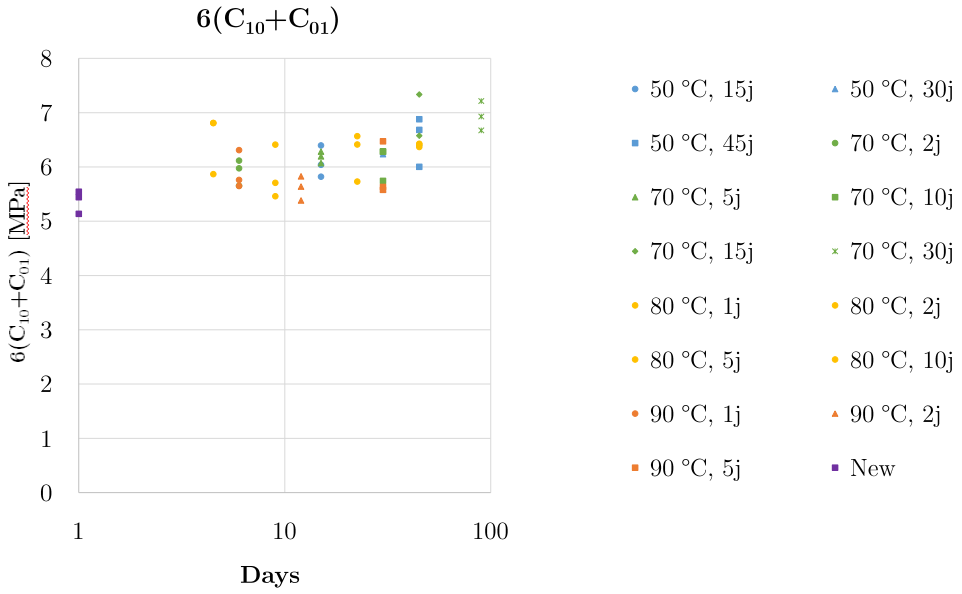

Figure 3.25: Values of the 1^{st} derivative of the stress curve at the origin.

The qualitative observations obtained from the average curves have been confirmed by an analytical result. The analytical expression of the stress for a five-parameter hyperelastic model (coefficients C_{10}, C_{01}, C_{11}, C_{20}, C_{30}) can be derived with respect to the stretch λ. Substituting the stretch by its value at the origin ($\lambda = 1$), one can obtain the analytical expression of the gradient of the curve at the beginning of the traction test: $6(C_{10} + C_{01})$. The values of the gradient at the origin have been obtained for all the identified models, then plotted with respect to the ageing time. The results have shown that the gradient increases with both time and temperature for 50 and 70 °C, stabilizing and/or slightly decreasing at 80 °C and 90 °C (Figure 3.25). The change on the evolution of the properties had already been guessed in some of the presented metrics. The analytical results regarding the evolution of the term $6(C_{10} + C_{01})$ seem to comfort the idea of two different ageing regimes, below and over 70 °C.

Regarding the relation between adjusted C_{ij} coefficients from the hyperelastic model and the time of exposure to thermal ageing, some interesting results arise from their plots. The graphics on Figures 3.26 to 3.28 plot the coefficients of the identified energy strain functions. The plot of the energy function's coefficients at 70 °C show an evolution of these with the exposition periods, suggesting a trend or dependence which has also been remarked for other samples at different ageing temperatures. In spite of the non-physical significance of the coefficients, it can be argued that their values are somehow related to the underlying characteristics of the material. The internal trend observed within the plots at 70 °C are reproduced slightly on the coefficients from 80 °C tests and more accurately on 90 °C.

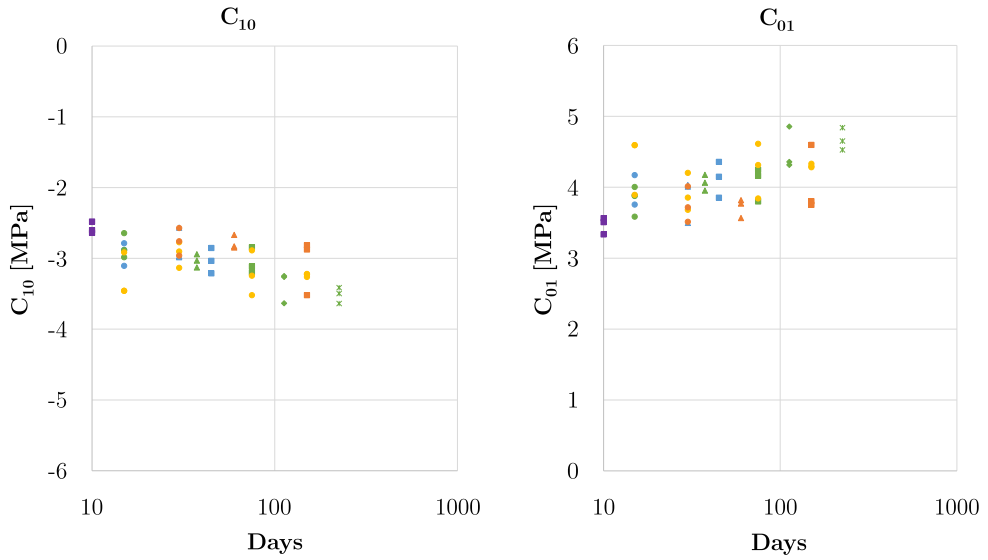

Figure 3.26: Evolution corridors for each C_{ij} coefficient identified following James' model, based on the mechanical characterization tests performed on the thermally aged samples.

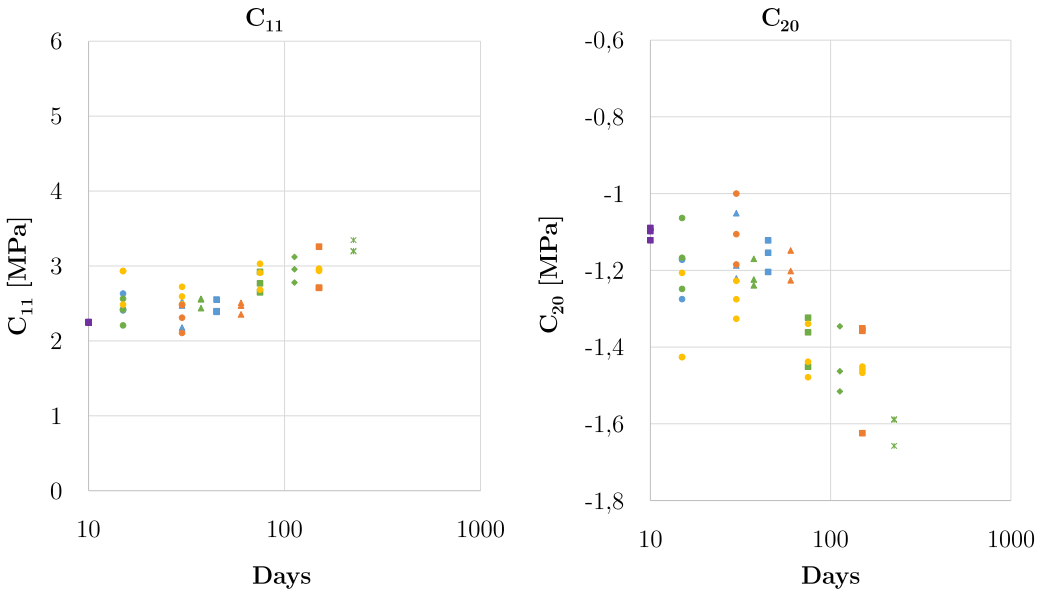

Figure 3.27: Evolution corridors for each C_{ij} coefficient identified following James' model, based on the mechanical characterization tests performed on the thermally aged samples.

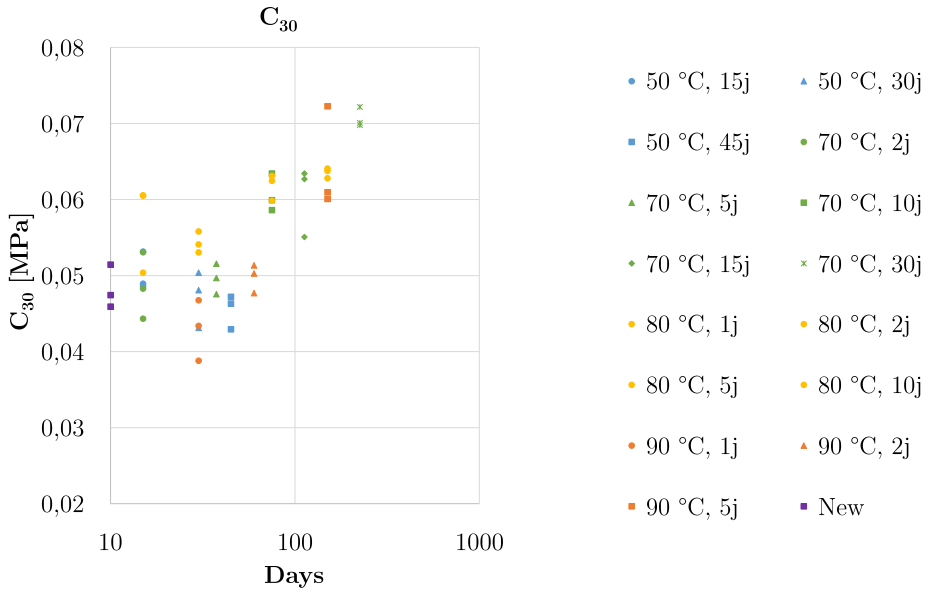

Figure 3.28: Evolution corridors for each C_{ij} coefficient identified following James' model, based on the mechanical characterization tests performed on the thermally aged samples.

If one observes the global evolution of the C_{ij} coefficients, they can be gathered on a pseudo-corridor by means of a set of shift factors. A fairly acceptable Arrhenius plot was found to gather the five ensembles of James' model coefficients into five master corridors, rather than curves. In spite of the good agreement on the regression, the description of the global trend of the C_{ij} coefficients with shifting is far from being immediate. Indeed, the results for the fitting functions rank from a R^2 index of barely 0,31 up to 0,63 at the best, which is not conclusive at all. Since the material model is directly dependent of ageing, other physical parameters among our test results have been confronted with the coefficients, in an attempt to obtain a link with ageing conditions. Indeed, there have been researches to find a physical sense to Mooney's first model [Mooney, 1940], successfully linking its first parameter C_{10} (C_1 in early papers) to the reticulation rate of swollen rubber (Equation 3.21) [Moore and Watson, 1956]. In our case, the C_{ij} coefficients have been plotted against the reticulation rate of their samples, showing a much better agreement than for ageing exposure (Figure 3.29) (the averaged plots yielded R^2 indexes between 0,65 and 0,75). The lack of sounder data makes difficult to enunciate a clear conclusion on the effects of the ageing over the families of adjusted energy functions, although it appears that the reticulation is, in some way, slightly linearly related with the strain energy function and its coefficients.

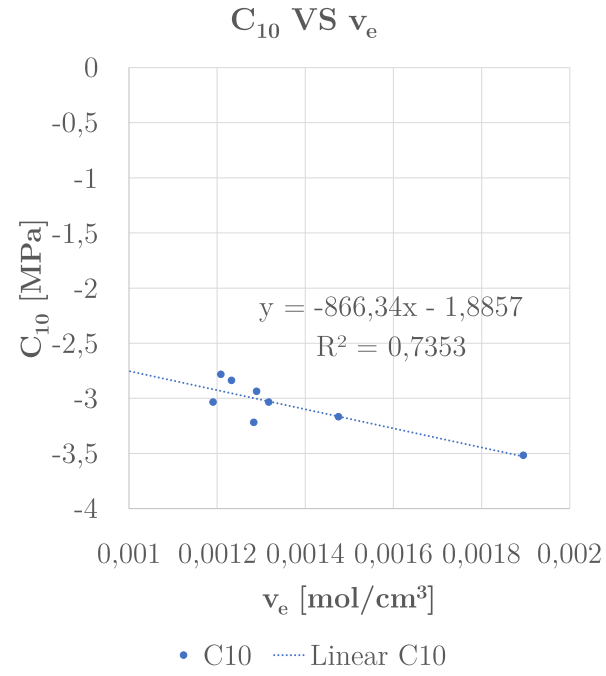
C10 VS ve
0
-0,5
-1
-1,5
-2
-2,5
-3
-3,5
-4
C10 [MPa]
y = -866,34x - 1,8857
R² = 0,7353
0,001 0,0012 0,0014 0,0016 0,0018 0,002
ve [mol/cm³]
C10
Linear C10

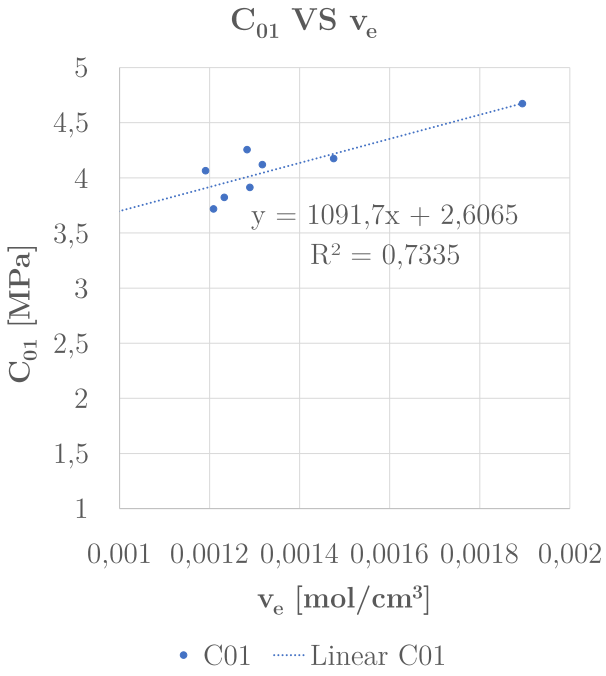
C01 VS ve
5
4,5
4
3,5
3
2,5
2
1,5
1
C01 [MPa]
y = 1091,7x + 2,6065
R² = 0,7335
0,001 0,0012 0,0014 0,0016 0,0018 0,002
ve [mol/cm³]
C01
Linear C01

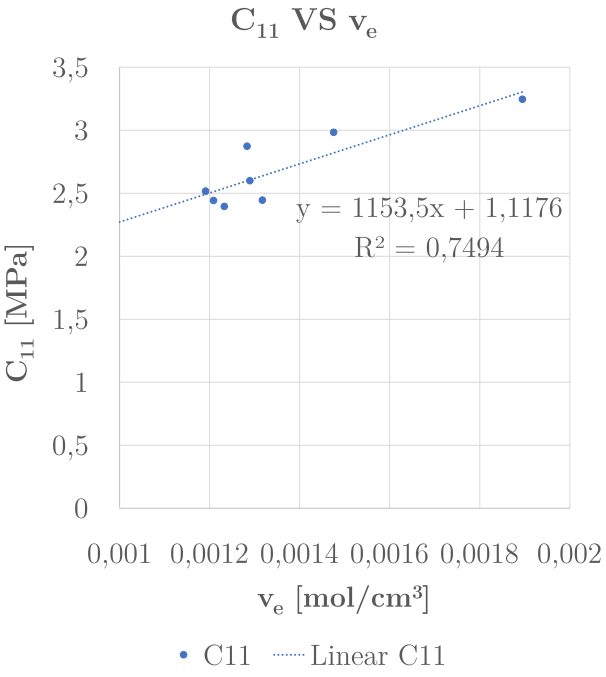
C11 VS ve
3,5
3
2,5
2
1,5
1
0,5
0
C11 [MPa]
y = 1153,5x + 1,1176
R² = 0,7494
0,001 0,0012 0,0014 0,0016 0,0018 0,002
ve [mol/cm³]
C11
Linear C11

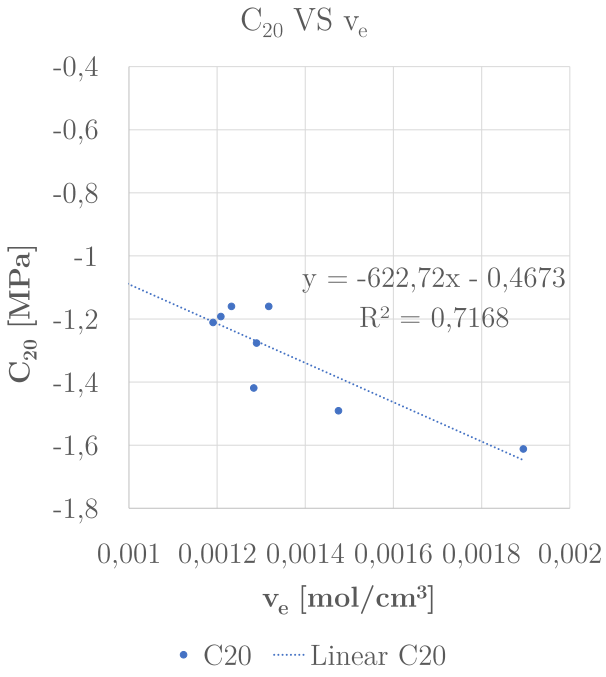
C20 VS ve
-0,4
-0,6
-0,8
-1
-1,2
-1,4
-1,6
-1,8
C20 [MPa]
y = -622,72x - 0,4673
R² = 0,7168
0,001 0,0012 0,0014 0,0016 0,0018 0,002
ve [mol/cm³]
C20
Linear C20

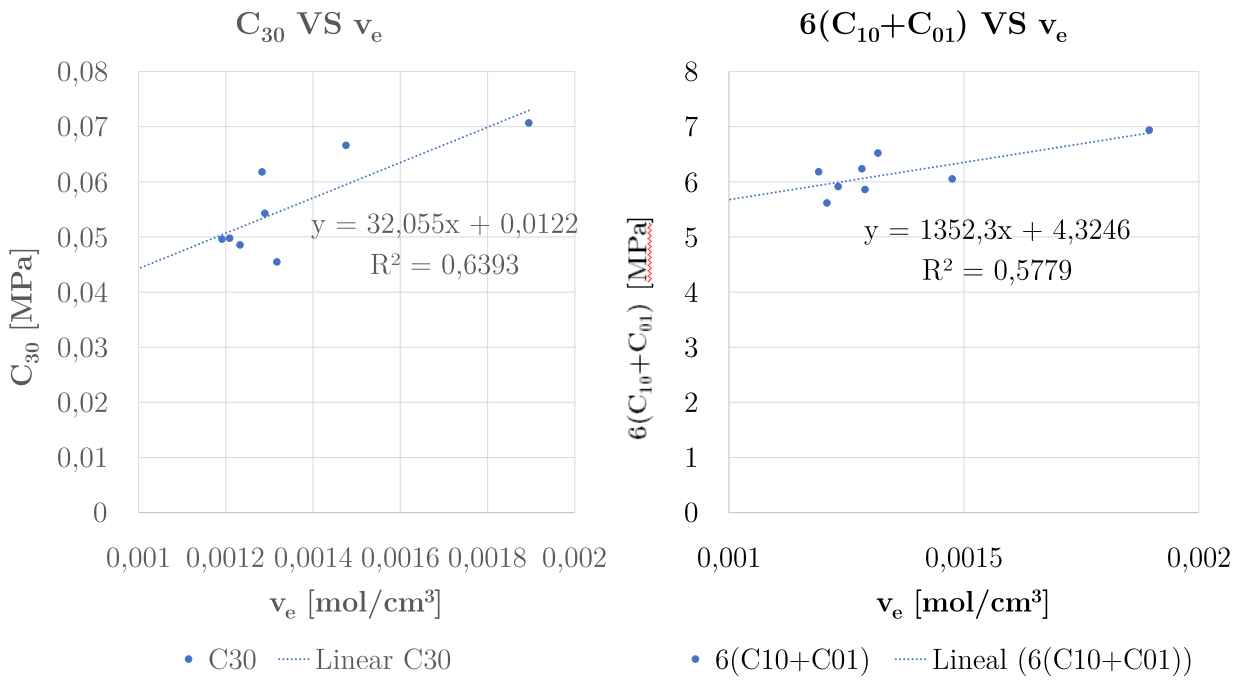

Figure 3.29: Plot of the averaged C_{ij} coefficients VS the reticulation rate associated to each thermal ageing configuration.

3.5 Conclusion

The contents of this chapter have addressed the industrial context of rubber-to-metal parts within the transport industry and their well-spread use. A special focus has been made on railway applications of such elements, with a historic perspective of their evolution from auxiliary functions to suspension roles during the 20th century. A description to the rubber's historic background and general aspects, leading to its chemistry and fabrication techniques, has served as an introduction for the mechanics-related aspects of the rubber. The rubbers' main mechanic, thermal and chemical properties have been discussed, with an specific stress on quasi-static testing and swelling test aspects, as well as a focus on accelerated thermal ageing and the empirical laws allowing the exploitation of the experimental results.

The set up of a thermal ageing campaign has been addressed, explaining the test protocols, the type of samples which have been used, as well as describing the experiments' conditions and laboratory equipment. The results from the campaign have shown that the thermal ageing of rubber has a direct impact on the material's properties. Heating during sustained periods causes the samples to shrink slightly, as well as to lose a part of its volatile compounds, with a stabilization towards 10 to 30 days of exposure. Despite volatile loses, chemical analysis by FTIR and EDX have shown that the material's composition remains essentially stable throughout thermal ageing. Should the mechanical properties of the rubber change, the source would be intrinsic to the material's chemical structure. However, practising thermal ageing at high temperatures or extreme periods of exposure can be counter-effective. It might cause a degradation on the material's properties and extreme fragility, as it was proved by the configurations with premature breakdowns (80 °C, 15 days and 90 °C, 10 days).

Several swelling tests were successfully conducted, showing that there is a direct link between thermal ageing and the increase of the reticulation rate v_e within the rubber. An analytic sigmoid-like curve has been proposed to describe the evolution of the reticulation rate along thermal ageing, respecting the idea of a saturation threshold limiting the extent of such an increase. There are certainly competing mechanisms which may act beyond the periods tested in these works, and which would complete the proposed approach with a term decreasing the properties. The determination of a sample's ageing through the reticulation rate remains still uncertain. The reticulation rates obtained from samples of a naturally aged component show a mismatch between the age of the samples and their placement along the forecast curve.

A series of mechanical characterization tests have been undertaken with the thermally aged rubber specimens. The experiments showed the loss of mechanical resistance of the rubber throughout thermal ageing. The material's ultimate strain and stress decrease with increasing temperature and time of exposure. Conversely, the rubber's secant stiffness (at 200 % strain) increases proportionally with ageing conditions. The three metrics have undergone an Arrhenius

analysis, which has permitted to adjust three master curves describing the metrics' variations during thermal ageing and, more interestingly, at ambient temperature. Moreover, the three curves span over a time period which is equivalent to more than two times the suspension elements life-cycle, which could be useful to discuss hypothetical expansions of a parts' life-cycle. Last, the secant stiffness results have been compared with the reticulation rate of the respective samples. The agreement between both metrics is fairly good, showing that there is some relationship between the material's chemical state and its macroscopic properties.

The rubbers' characterization has been achieved with the adjustment of a hyperelastic energy function to the experimental curves. A phenomenological, five-parameter, generalized Mooney-Rivlin model was used to fit the stress-strain characteristics of the thermally aged samples. James' model has shown a very good agreement with the experimental data, providing an wide set of models which have fed a large campaign of FE simulations, addressed on Chapter 4. The plots of the curves show that the ageing has an effect on the different characteristics of the curve: initial stiffening, mid-strain linear zone and the high-strain stiffening. The analytical expression of the derivative of the stress-stretch curve at the origin has shown that the ageing has a stiffening effect up to a threshold, becoming constant or slightly decreasing over 80 °C.

Bibliography

[Akiba and Hashim, 1997] Akiba, M. and Hashim, A. S. (1997). Vulcanization and crosslinking in elastomers. *Progress in Polymer Science*, 22(3):475 – 521. (Cited on pages iv, 55 and 56.)

[Arruda and Boyce, 1993] Arruda, E. M. and Boyce, r. C. (1993). A three-dimensional constitutive model for the large stretch behavior of rubber elastic materials. *Journal of Mechanics and Physics of Solids*, 41(2):389–412. (Cited on pages 67 and 68.)

[ASTM-D3045-92, 2003] ASTM-D3045-92 (2003). *Standard Practice for Heat Aging of Plastics Without Load*. ASTM. (Cited on page 69.)

[ASTM-D573-99, 1999] ASTM-D573-99 (1999). *Standard Test Method for Rubber — Deterioration in an Air Oven*. (Cited on page 70.)

[ASTM-D6814-02, 2002] ASTM-D6814-02 (2002). *Standard Test Method for Determination of Percent Devulcanization of Crumb rubber Based on Crosslink Density*. ASTM. (Cited on pages v and 72.)

[Barbosa et al., 2017] Barbosa, R., Nunes, A. T., and Ambrosio, J. D. (2017). Devulcanization of Natural Rubber in Composites with Distinct Crosslink Densities by Twin-Screw Extruder. *Materials Research*, 20:77 – 83. (Cited on pages v and 72.)

[Barton, 1990] Barton, A. (1990). *Handbook of Polymer-Liquid Interaction Parameters and Solubility Parameters*. Taylor & Francis. (Cited on pages 63 and 74.)

[Blake, 1930] Blake, J. T. (1930). III—Kinetics of Vulcanization of Rubber with Sulphur and Selenium. *Industrial & Engineering Chemistry*, 22(7):744–747. (Cited on page 75.)

[Boukamel, 2006] Boukamel, A. (2006). Modélisations mécaniques et numériques des matériaux et structures en élastomères. Memoire d'habilitation à diriger des recherches, Université de la Méditerranée - Aix-Marseille II. (Cited on pages iv, v, 49, 55, 65, X and XI.)

[Chang Su and Hyun Sun, 2015] Chang Su, W. and Hyun Sun, P. (2015). Useful Lifetime Prediction of Chevron Rubber Spring for Railway Vehicle. *International Journal of Aerospace and Mechanical Engineering*, 9(8). (Cited on pages v, 49 and 69.)

[Cunneen and Russell, 1970] Cunneen, J. I. and Russell, R. M. (1970). Occurrence and Prevention of Changes in the Chemical Structure of Natural Rubber Tire Tread Vulcanizates during Service. *Rubber Chemistry and Technology*, 43(5):1215–1224. (Cited on pages 63 and 74.)

[da Costa et al., 2001] da Costa, H. M., Nunes, R., Visconte, L. L. Y., and Furtado, C. R. G. (2001). Physical Properties and Swelling on Natural Rubber Compounds containing Rice Husk Ash. *Kautschuk Gummi Kunststoff*, 54(5):242–249. (Cited on page 63.)

[Diani et al., 2009] Diani, J., Fayolle, B., and Gilormini, P. (2009). A review on the Mullins effect. *European Polymer Journal*, pages 601–612. (Cited on page 59.)

[Dimier, 2003] Dimier, F. (2003). *Reactive systems injection: kinetic and rheological laws determination and modelisation.* Theses, École Nationale Supérieure des Mines de Paris. (Cited on page 55.)

[El Labban, 2008] El Labban, A. (2008). *Optimisation du cycle de cuisson d'une pièce moulée en élastomère.* PhD thesis, Université de Nantes. (Cited on page 55.)

[Fletcher and Gent, 1953] Fletcher, W. P. and Gent, A. N. (1953). Nonlinearity in the Dynamic Properties of Vulcanized Rubber Compounds. *Rubber Chemistry and Technology*, 27:209–222. (Cited on page 60.)

[Flory and Rehner, 1943a] Flory, P. J. and Rehner, J. (1943a). Statistical Mechanics of Cross-Linked Polymer Networks I. Rubberlike Elasticity. *The Journal of Chemical Physics*, 11(11):512–520. (Cited on page 68.)

[Flory and Rehner, 1943b] Flory, P. J. and Rehner, J. (1943b). Statistical Mechanics of Cross-Linked Polymer Networks II. Swelling. *The Journal of Chemical Physics*, 11(11):521–526. (Cited on page 63.)

[Gent and Thomas, 1958] Gent, A. N. and Thomas, A. G. (1958). Forms for the stored (strain) energy function for vulcanized rubber. *Journal of Polymer Science*, 28(118):625–628. (Cited on page 67.)

[Gillen and Clough, 1997] Gillen, K. and Clough, R. (1997). Prediction of elastomer lifetimes from accelerated thermal-aging experiments. (Cited on pages v, 61, 69 and 79.)

[Gillen and Celina, 2000] Gillen, K. T. and Celina, M. (2000). The wear-out approach for predicting the remaining lifetime of materials. *Polymer Degradation and Stability*, 71(1):15 – 30. (Cited on pages v and 69.)

[Guth, 1945] Guth, E. (1945). Theory of Filler Reinforcement. *Journal of Applied Physics*, 16(1):20–25. (Cited on pages iv, 56 and 57.)

[Holzapfel, 2000] Holzapfel, G. (2000). *Nonlinear Solid Mechanics : A Continuum Approach for Engineering / G.A. Holzapfel.* John Wiley & Sons, Chichester. (Cited on pages iv, 64 and VII.)

[ISO2578, 1994] ISO2578 (1994). *Plastics – Determination of time-temperature limits after prolonged exposure to heat.* DIN. (Cited on page 69.)

[ISO37, 2012] ISO37 (2012). *Caoutchouc vulcanisé ou thermoplastique - Détermination des caractéristiques de contrainte-déformation en traction.* Afnor. (Cited on pages v, 69 and 77.)

[Jones and Treloar, 1975] Jones, D. F. and Treloar, L. (1975). The Properties of Rubber in Pure Homogeneous Strain. *Journal of Physics D: Applied Physics*, 8:1285. (Cited on page 58.)

[Jones, 2012] Jones, K. (2012). Rubber in Railways. (Cited on pages iv and 49.)

[Kareaga-Laka, 2016] Kareaga-Laka, Z. (2016). *Dynamic Stiffness and Damping Prediction on Rubber Material Parts, FEA and Experimental Correlation.* PhD Thesis, Lea Artibai Ikastetxea S. Coop. and London Metropolitan University. (Cited on page 49.)

[Kraus, 1965] Kraus, G. (1965). Interactions of Elastomers and Reinforcing Fillers. *Rubber Chemistry and Technology*, 38(5):1071–1114. (Cited on pages iv and 56.)

[Kuhn and Grün, 1946] Kuhn, W. and Grün, F. (1946). Statistical behavior of the single chain molecule and its relation to the statistical behavior of assemblies consisting of many chain molecules. *Journal of Polymer Science*, 1(3):183–199. (Cited on page 68.)

[Kumar and Venkateswara, 2016] Kumar, N. and Venkateswara, R. V. (2016). Hyperelastic Mooney-Rivlin Model: Determination and Physical Interpretation of Material Constants. *MIT International Journal of Mechanical Engineering*, 6(1):43–46. (Cited on pages 85 and 86.)

[Le Huy and Evrard, 2001] Le Huy, M. and Evrard, G. (2001). Methodologies for lifetime predictions of rubber using Arrhenius and WLF models. *Die Angewandte Makromolekulare Chemie*, 261-262(1):135–142. (Cited on pages v, 61 and 69.)

[Le Saux, 2010] Le Saux, V. (2010). *Fatigue et vieillissement des élastomères en environnements marin et thermique : de la caractérisation accélérée au calcul de structure.* PhD thesis, Université de Bretagne occidentale - Brest. (Cited on pages v and 69.)

[Lejeunes, 2006] Lejeunes, S. (2006). *Modélisation de structures lamifiées élastomère-métal à l'aide d'une méthode de réduction de modèles.* PhD thesis, Université de la Méditerranée - Aix-Marseille II. (Cited on pages iv, 49, 58, 64, 67, 85 and VII.)

[Loadman, 2003a] Loadman, J. (2003a). Dry rubber processing. (Cited on page 54.)

[Loadman, 2003b] Loadman, J. (2003b). Vulcanization. (Cited on page 54.)

[Loan, 1967] Loan, L. (1967). Mechanism of Peroxide Vulcanization of Elastomers. *Rubber Chemistry and Technology*, 40(1):149–176. (Cited on pages iv and 56.)

[Lorenz and Parks, 1961] Lorenz, O. and Parks, C. R. (1961). The crosslinking efficiency of some vulcanizing agents in natural rubber. *Journal of Polymer Science*, 50(154):299–312. (Cited on pages 63 and 74.)

[Macbeth, 1939] Macbeth, C. (1939). *Rubber and Railways.* British Rubber Publicity Association, 2 edition. (Cited on pages iv and 49.)

[Martinez, 2005] Martinez, J.-M. (2005). *Modelization and characterization of the hyper-visco-plastic behavior of an elastomer under multi-harmonic loadings at differents temperatures*. Theses, Université de la Méditerranée - Aix-Marseille II. (Cited on page 49.)

[M.E.C, 1983] M.E.C (1983). A long life - and a 'care'-free one. *Rubber developments*, 36(1):2–3. (Cited on pages iv and 50.)

[Méo, 2000] Méo, S. (2000). *Modélisation numérique du comportement mécanique de structures en élastomère : de l'élasticité à la thermo-visco-hyperélasticité*. PhD thesis, Université de la Méditerranée - Aix-Marseille II. (Cited on pages 64 and VII.)

[Mooney, 1940] Mooney, M. (1940). A Theory of Large Elastic Deformation. *Journal of Applied Physics*, 11(9):582–592. (Cited on pages 66 and 95.)

[Moore and Watson, 1956] Moore, C. G. and Watson, W. F. (1956). Determination of degree of crosslinking in natural rubber vulcanizates. Part II. *Journal of Polymer Science*, 19(92):237–254. (Cited on pages 63 and 95.)

[Moore, 1950] Moore, J. (1950). Some Chemical and Physical Properties of Rubber. *British Journal of Applied Physics*, 1(1):6. (Cited on page 56.)

[Mott and Roland, 2001] Mott, P. H. and Roland, C. M. (2001). Aging of Natural Rubber in Air and Seawater. *Rubber Chemistry and Technology*, 74(1):79–88. (Cited on pages v and 69.)

[Mullins, 1956] Mullins, L. (1956). Determination of degree of crosslinking in natural rubber vulcanizates. Part I. *Journal of Polymer Science*, 19(92):225–236. (Cited on page 63.)

[Mullins, 1969] Mullins, L. (1969). Softening of Rubber by Deformation. *Rubber Chemistry and Technology*, 42(1):339–362. (Cited on page 59.)

[Nordlander, 1929] Nordlander, B. W. (1929). The Kinetics of the Vulcanization of Rubber. *The Journal of Physical Chemistry*, 34(9):1873–1902. (Cited on page 75.)

[Payne, 1969] Payne, A. R. (1969). The dynamic properties of carbon black-loaded natural rubber vulcanizates. Part I. *Journal of Applied Polymer Science*, 6(19):57–63. (Cited on page 60.)

[Rivlin and Saunders, 1951] Rivlin, R. S. and Saunders, D. W. (1951). Large elastic deformations of isotropic materials VII. Experiments on the deformation of rubber. *Philosophical Transactions of the Royal Society of London A: Mathematical, Physical and Engineering Sciences*, 243(865):251–288. (Cited on pages v and 67.)

[Sidoroff, 1982] Sidoroff, F. (1982). Cours sur "Les Grandes Déformations". (Cited on pages iv, 64, 65, VII and XI.)

[Thien An, 2014] Thien An, N. V. (2014). *Sur la modélisation et la simulation du couplage thermo-chimio-mécanique au sein des élastoméres chargés*. PhD thesis, Aix-Marseille Université. (Cited on pages 49 and 55.)

[Treloar, 1975] Treloar, L. (1975). *The Physics of Rubber Elasticity*. Oxford Classic Texts in the Physical Sciences. Clarendon Press - Oxford, 3 edition. (Cited on pages iv, 54, 56, 57, 65, 66 and 67.)

[Treloar, 1943] Treloar, L. R. G. (1943). Theory of Large Elastic Deformations. *Nature*, 151. (Cited on page 63.)

[Trofimov et al., 2009] Trofimov, B. A., Sinegovskaya, L. M., and Gusarova, N. K. (2009). Vibrations of the S–S bond in elemental sulfur and organic polysulfides: a structural guide. *Journal of Sulfur Chemistry*, 30(5):518–554. (Cited on page 72.)

[Woo and Kim, 2006] Woo, C. S. and Kim, W. D. (2006). Heat-Aging Effects on the Material Properties and Fatigue Life Prediction of Vulcanized Natural Rubber. *e-Journal of Soft Materials*, 2:7–12. (Cited on pages v and 69.)

Chapter 4

Rubber-to-metal parts: properties variability assessment

> Exploring the unknown requires tolerating uncertainty.
> Information is the resolution of uncertainty.
>
> Brian Greene - Claude Shannon

The fourth chapter of the manuscript will address the study of the variability of the mechanical properties of the rubber-to-metal parts. A brief introduction will address the methods to quantify and propagate variability, as well as its management in an engineering context. The choice of a surrogate model approach will be reasoned, discussing the input variables. The results from a simulation campaign by means of FE models will be presented in this context. The exploitation of the Kriging model and the analysis of the output variability will be subsequently addressed. The results will be confronted to the experimental results from real parts and discussed in the context of the life-cycle of suspension elements. A conclusion about the variability levels of the properties of the suspension elements will close the chapter.

Contents

4.1 Study of variability: theory and fundamentals

The study and quantification of the variability of metrics is a well-spread practise in multiple disciplines. It is part of the statistical analysis of many processes, thus allowing a more accurate comprehension of a system's behaviour and its properties. A process can be considered as the relationship between a series of input parameters and the output variables. These can be sorted out to extract the *Quantities of Interest* (QoIs), which can describe the problem on a certain context. In some cases, both sets of variables can be related by a series of known laws, usually in the form of equations, thus allowing the resolution of the problem in a rather straightforward way. Other processes may have a complex form (large number of variables, complex relationship between the parameters and the QoIs) and have no evident relation. However, "available knowledge on a specific situation is, in general, imperfect; either because of the doubts one may have about such knowledge, which is then *uncertain*, or because one encounters difficulties to express it precisely, thus being *imprecise*" [Bouchon-Meunier, 2007].

Characterising the variability on a system's behaviour can be a vast undertaking, since by its definition it affects *all the metrics* which master a process: inputs, outputs and the properties intervening on the relationship. A key concept to understand variability is the notion of *uncertainty*, which can be defined as "any departure from the unachievable ideal of complete determinism" [Walker et al., 2003]. Walker et al. further precise this concept stressing the difference between *epistemic uncertainty* and *variability uncertainty*. The former is related to the lack of knowledge inherent to the current state-of-art of methods and technology (i.e. something which is unknown or which cannot be detected remains therefore unknown). The latter relates to a wide range of uncertainties: human, social, environmental... Our focus will be set on the category of *natural variability*. The determination of the sources of uncertainty within a process is a key step on the variability analysis. Some of them might be *reducible uncertainties*, which can be minimised through rigorous practises and methodologies, or with better equipment, whilst *irreducible uncertainties* may have complex sources or be directly impossible to tackle, needing to be assumed and quantified for the analysis purposes [Moens and Vandepitte, 2005].

Since the variability of a component's properties has consequences on the behaviour of the system to which it belongs, a mastered response is crucial in spite of the drift on the components properties. The *quantification of the uncertainties* (UQ) appears the first step to describe variability, which can affect a system. The study of how such uncertainty can impact the outcomes of a process falls within the *propagation of uncertainties* (UP). In a general way, both stages contribute to the global vision of the variability intrinsic to a process and contribute to the *uncertainty management* (UM).

4.1.1 Non-deterministic methods and anti-optimisation

The quantification of the uncertainties on a system depends strongly on the information which is available and on its quality. Should a consistent set of data be available, the description of the variability can be addressed under a *probabilistic approach* by using the classic, commonplace statistic moments (mean, standard deviation, variance, etc.), as well as random variables or by random fields if spatial variation of the model properties is concerned. The construction of probability distributions (normal/Gaussian, Fisher, Weibull, etc.) requires a statistical study of measured data from specific tests to introduce realistic variations. When few experimental data are available from some observations of the system, an optimal prior stochastic model of uncertainties can be built using the maximum likelihood method or an *ensemblist approach* can be used to quantify the variability. *Interval methods* set the boundaries of variation for a metric with a maximum and minimum [Moore et al., 2009], all values being equi-confident. *Fuzzy approaches* [Zadeh, 1965] expand the concept of the interval or set, whose elements have a degree of membership given by a function valued between zero (no membership at all) and one (full membership).

When the relation between a system's input and outputs is known, it is possible to characterize the variability of output solutions after an uncertainty propagation step, which relies on either sampling, specific series and Taylor developments, ad-hoc projections or optimization strategy. Numerous non deterministic methods are available within the literature. Considering a probabilistic formalism, Monte Carlo Simulations (MCS) or Polynomial Chaos Expansion (PCE) are generally used, whereas Zadeh's Extension or optimization techniques are favoured in the context of the ensemblist formalism. These methods are briefly described below:

- The first *Monte-Carlo simulations* (MCS) were created in the late 1940s as a statistic tool in the context of nuclear research [Metropolis and Ulam, 1949]. There is not a single "Monte-Carlo simulation", but an ensemble of models with diverse probability density functions (PDF) fitting an ensemble of *previously obtained data*, which is used to generate a set of random inputs (thus consistent with the existing input samples, real or forecast). These results are subsequently fed to the transfer function representing the process in a *deterministic calculation*, obtaining a set of associated results for each set of values on the MC random set. Sometimes despised against other statistical methods by its extensive need of calculations, Monte-Carlo methods are reputed for ensuring the finding of a solution, if the calculation time is affordable [Bigoni and Engsig-Karup, 2015].

  Monte-Carlo methods have already been used widely in risk engineering assessment. Within the railway industry and research, several cases are found: the calculation the overturning risk of a high speed trainset under transverse wind gush [Quost, 2005]; the influence on the dynamic behaviour of the uncertainty in the suspension characteristics

[Mazzola and Bruni, 2011].

- *Polynomial Chaos methods* (PCE) are based on Wiener expansion, developed on the late 1930s [Wiener, 1938] and brought back on the 1990s by Ghanem et al. [Ghanem and Spanos, 1990]. Wiener methods are based on the representation of the random variables which are to study (Z) by an ensemble of *orthogonal polynomials* (Ψ_j) (Legendre, Hermite, etc.) expressed as function of a series of *normal random variables* (ξ_n). The actual random variables are then transposed to the set of normal variables ξ_n by the isoprobabilistic transform [Sudret, 2008]. The transposition enables the calculation of the statistic moments of the QoIs with respect to the input variables, based on the polynomial expansion.

  The application of the PCE methods in railways has proven its usefulness regarding the modelling of track irregularities [Perrin et al., 2013]. Its use is wide-spread as well regarding the analysis of stability problems related to friction phenomena [Nechak et al., 2011].

- The reference method used to solve problems described by the *fuzzy formalism* is based on Zadeh's Extension Principle (ZEP) [Zadeh, 1975a] [Zadeh, 1975b] [Zadeh, 1975c], which extends general operations for real numbers to the corresponding operations for fuzzy numbers. In practice, fuzzy numbers are discretized according to the membership degree and the uncertainty propagation step leads to a combinatorial process based on different Designs Of Experiments (DOE) or specific samplings [Hanss, 2002] [Hanss, 2003] [Donders et al., 2005] [Hanss and Turrin, 2010] [Haag et al., 2010]. The membership functions of output solutions are built considering the membership degrees of input data as for ZEP.

- The best alternatives to ZEP have been obtained using either sensibility analyses or optimization algorithms. The first works were initiated by McWilliam [McWilliam, 2001] and relied on monotonic evolutions of response surfaces. The boundaries of the solutions are determined with the boundaries of the intervals associated to each parameter. Several authors have proposed to transform the original interval problem as a min-max optimization problem to limit computational time of the uncertainty propagation step, thus rendering the method compatible with an industrial context [Massa et al., 2009]. Indeed, this approach relies on iterative search for global optima in a search space, the size of which is gradually increasing when the degree of membership is decreasing [Massa et al., 2006] [Massa et al., 2008] [Degrauwe et al., 2009].

When all the non-deterministic information is not necessary, anti-optimization approaches [McWilliam, 2001] can be performed. The idea is to choose/optimize the design variables to obtain the best design and, at the same time, antioptimize the uncertainty, seeking the worst condition for a given design. The anti-optimization technique of uncertainty produces the maximum or least

favorable response of the structure, and the minimum or a best favorable response.

All these non-deterministic techniques significantly increase the CPU time in comparison to classical deterministic ones due to a time consuming multiparametric or optimization step. Thus, the integration of an approximation is mandatory by using Reduced Order Models (ROM) or surrogate models, described in the following section.

4.1.2 Surrogate models and Reduced Order Models

The modelling of complex systems encompassing large ensembles of variables cannot be tackled directly, as the amount of calculations required by MCS or PCE methods can be extremely cost-expensive. Therefore, a lighter version of the problem representing the bulk of the system's response can become a useful strategy to address the issue. Two main families arise on this context: *Reduced Order Models* (ROM), and *surrogate models*.

- The general idea of *Reduced Order Models* (ROM) is to approximate a higher dimension system by another one of much lower dimension, such as Proper Orthogonal Decomposition (POD) [Ryckelynck, 2005] [Yvonnet et al., 2007] [David et al., 2012], Proper Generalized Decomposition (PGD) [Chinesta et al., 2010] [Nouy, 2010] [Ladevèze and Chamoin, 2011] or [David et al., 2012], more recently Hyperreduction methods [Rutzmoser and Rixen, 2017] or [Ryckelynck, 2005], and homotopy projection techniques [Massa et al., 2017]. However, to be highly efficient, these techniques imply a manipulation of equations of the problem, thus being *intrusive* and generally complex to integrate for engineering problems, whose calculations are performed by industrial software.

- As regards of *surrogate models*, the original problem is replaced by an approximation based on regression and/or correlations models, such as polynomial approximations or Response Surface Methods (RSM) [Myers et al., 2009], Radial Basis Functions (RBF) [Baxter, 1992] or Kriging [Sakata et al., 2003] [Wei et al., 2004] [Kaymaz, 2005][Wang et al., 2013]. The functions are an alternative to classical numerical simulations, and are built only with a set of specific samples (the *training set*) obtained from a DOE.

  Contrary to ROM, surrogate models are a series of mathematical tools which permit the construction of a "black box" relationship between the chosen inputs and the QoIs. Albeit lacking a physical sense, these methods can provide a statistically sound model which can relate effectively the inputs and QoIs on the process. Surrogate models work without modifying the nature of the real system, thus being *non-intrusive*.

In the case of the present works, a wide database of experimental tests and experimentally determined behaviour laws has been gathered. The multiple ageing tests at different times and temperatures of exposure have been extensively discussed in Chapter 3, aiming to characterize the macroscopic properties of a specific suspension element. The characterization of the variability of the mechanical stiffness is one of the objectives of the process, as well as the determination of the *most constraining* cases for the design of a railway vehicle. Thus, the proposed study falls within the domains of the *anti-optimisation*. A Kriging model based on a set of the experimental data can be used to determine the upper and lower boundaries on the variation of the mechanical stiffness, obtaining both the variability on the properties and the extreme cases which could be foreseen. The main steps of the study are described on the flowchart in Figure 4.1.

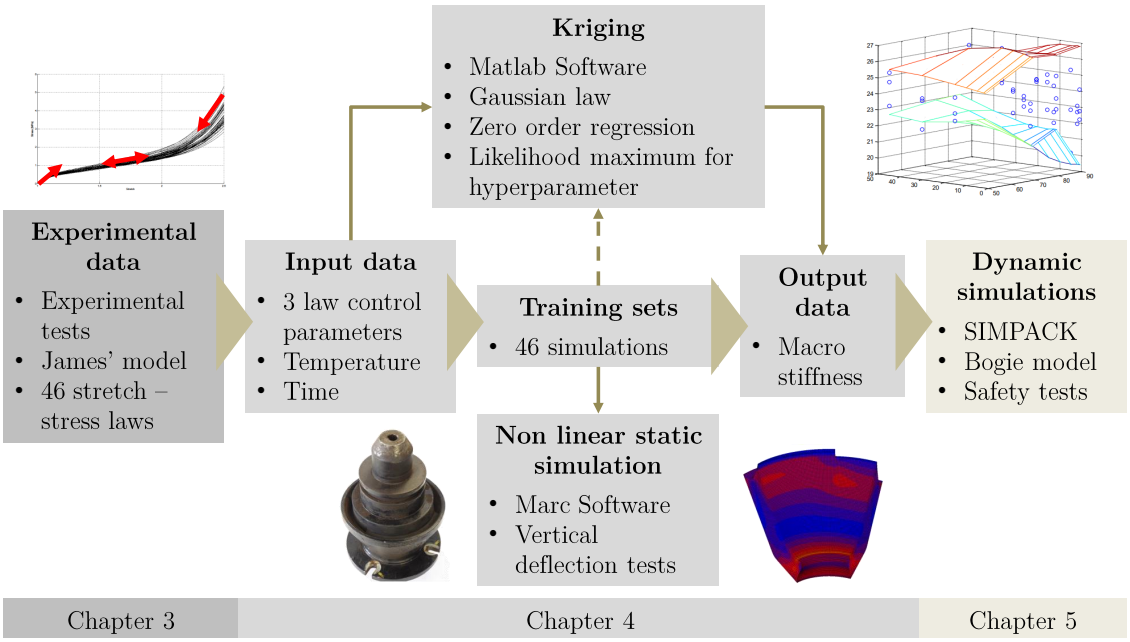

Figure 4.1: Flowchart of the data treatment within Chapter 4, from the inputs obtained in Chapter 3 to the outputs to feed Chapter 5.

4.2 Kriging model

One family of surrogate models is the *Kriging methods*, which began their development from the late 1960s and during the 1970s. They take their name from the South African mines engineer Krige, who worked on gold extraction mining and whose work inspired the method [Cressie, 1990]. Kriging algorithms have proven extremely useful on analysing and predicting data by linear extrapolation, based on the covariance of a set of previously determined data. A strong tool in geostatistics [Oliver and Webster, 1990], its applications have expanded to robustness analysis on mechanical systems.

The strength of Kriging algorithms relies on their ability to bridge the gap between inputs and outputs when no knowledge of their link is available, but outputs can be repeatedly obtained from a series of chosen inputs. When sufficient data have been gathered, the algorithm can build a prediction based on a weighed interpolation of the original data set. Moreover, the simplification of the relationship between both sides of the system makes Kriging models especially useful when coupled with methods requiring vast ensembles of runs (Monte-Carlo, optimization methods, etc.).

Kriging methods have been used extensively on mechanical engineering. As regards of the railway industry, Kriging has been applied to optimisation strategies for welding on bogie frames [Gao and Zhao, 2014] or suspension parameters [Yang et al., 2016], to calculate wear rates on the infrastructure [Cremona et al., 2016], as well as to optimize the reduction of braking loads in freight rolling stock [Arcidiacono et al., 2018]. Other applications of Kriging include the modelling of short reinforcement fiber in composites [Sakata et al., 2008] or adjusting FE models for bone simulations [Guan et al., 2011].

4.2.1 Set up of a Kriging model

The Kriging model is built as a predictive or extrapolation function based on a set of existing values of a certain process. Its precise formulation is given on Equation 4.1, where $y_j(\mathbf{z})$ is the estimate function, β_i and $f_i(\mathbf{z})$ are the weighing parameters and the basis functions used on the model, which conform the *regression model* and $W(\mathbf{z})$ a *random term* accounting for the distribution of the samples z_i.

$$y_j(\mathbf{z}) = \sum_{1 \leq i}^{N} (\beta_i f_i(\mathbf{z})) + W(\mathbf{z}) = \mathbf{f}(\mathbf{z})^T \boldsymbol{\beta} + W(\mathbf{z}) \tag{4.1}$$

The distribution $W(z)$ is chosen so as to have a zero mean value (thus adding no bias), and having a covariance given by Equation 4.2, with σ the *process variance* and R the correlation

function relating two samples of the process, z_1, z_2, and θ a scaling factor.

$$E(W(z_1), W(z_2)) = \sigma^2 R(\theta, z_1, z_2) \tag{4.2}$$

$$R(\theta, z_1, z_2) = \prod_{i=1}^{n_p} R(\theta_i, \mathbf{p}_{1,i} - \mathbf{p}_{2,i}) \tag{4.3}$$

The correlation function $\mathrm{R}(\theta, z_1, z_2)$ can have multiple forms (exponential, Gaussian, etc.), which are modulated by the parameter θ. This parameter accounts for the accuracy of the chosen function to fit the set of data which is the base of the Kriging model. It is calculated as an optimisation problem within the model, following Equation 4.4, were $\mathbf{R}$ is the *correlation matrix* (Equation 4.5), with $R_{ij} = R(\theta, z_i, z_j)$.

$$\boldsymbol{\theta}^\star = arg\min_{\boldsymbol{\theta}}(det(\mathbf{R})^{\frac{1}{n_s}}\sigma^2) \tag{4.4}$$

$$\mathbf{R} = \begin{bmatrix} R_{11} & R_{12} & \cdots & R_{1n_s} \\ R_{21} & R_{22} & \cdots & R_{2n_s} \\ \vdots & \vdots & \ddots & \vdots \\ R_{n_s1} & R_{n_s2} & \cdots & R_{n_sn_s} \end{bmatrix} \tag{4.5}$$

The problem in Equation 4.1 can be therefore reformulated to the expression in Equation 4.6. Then $\hat{\beta}$ and $\hat{\gamma}$ can be calculated as $\hat{\boldsymbol{\beta}} = (\mathbf{F}^T\mathbf{R}^{-1}\mathbf{F})^{-1}\mathbf{F}^T\mathbf{R}^{-1}\mathbf{Y}$ the least square estimate of $\boldsymbol{\beta}$ and $\hat{\boldsymbol{\gamma}} = \mathbf{R}^{-1}(\mathbf{Y} - \mathbf{F}\hat{\boldsymbol{\beta}})$.

$$y_j(\mathbf{z}) = \mathbf{f}(\mathbf{z})^T\hat{\boldsymbol{\beta}} + \mathbf{r}(\mathbf{z})^T\hat{\gamma} \tag{4.6}$$

The first step in the Kriging process is to evaluate the vector of regression functions $\mathbf{f}(\mathbf{z})$ and the correlations $\mathbf{r}(\mathbf{z})$ with a set of initial data.

$$\mathbf{f}(\mathbf{z}) = \begin{bmatrix} f_1(\mathbf{z}) \\ \vdots \\ f_{n_f}(\mathbf{z}) \end{bmatrix} \tag{4.7}$$

$$\mathbf{r}(\mathbf{z}) = \begin{bmatrix} R(\boldsymbol{\theta}, \mathbf{z}_1, \mathbf{z}) \\ \vdots \\ R(\boldsymbol{\theta}, \mathbf{z}_{n_s}, \mathbf{z}) \end{bmatrix} \tag{4.8}$$

As regards of $\mathbf{F}$, it is the regression matrix evaluated on the different shots $\mathbf{p}_i, i = 1...n_s$ (Equation 4.9).

$$\mathbf{F} = \begin{bmatrix} f_1(\mathbf{z}_1) & f_2(\mathbf{z}_1) & \cdots & f_{n_f}(\mathbf{z}_1) \\ f_1(\mathbf{z}_2) & f_2(\mathbf{z}_2) & \cdots & f_{n_f}(\mathbf{z}_2) \\ \vdots & \vdots & \ddots & \vdots \\ f_1(\mathbf{z}_{n_s}) & f_2(\mathbf{z}_{n_s}) & \cdots & f_{n_f}(\mathbf{z}_{n_s}) \end{bmatrix} \tag{4.9}$$

A MATLAB routine implementing a Kriging model (DACE) was used to generate a surrogate model, based on the forty-six configurations recovered from the thermal ageing tests. For a thorough explanation on the implementation of the Kriging model within the MATLAB tool DACE, the reader is invited to refer to [Lophaven et al., 2002].

4.2.2 Input and output variables of the model

The input variables involved in the Kriging model are a mixture of experimentally set parameters and numerical results. The thermal ageing configurations have provided the *experimental parameters*:

- A series of *times of exposure*, t: one, two, five, ten, fifteen and thirty days.
- Several *temperatures of exposure*, T: 50 °C, 70 °C, 80 °C, 90 °C.
- Three *control points* extracted from the analytically fitted curved, in the form of stress-stretch couples. These couples describe the characteristic features of a hyperelastic curve: the *low strain stiffness*, the *molecular slip plateau at mid-strains* and the *stiffening at high strains*.

The metrics mentioned above have permitted to study the variability of the input for the Kriging model. All thermal ageing configurations have been characterised by an average curve, which showed the range of variability of the experimental sets. The array of curves plotted in Figure 4.2 increases up to +40 % of the new properties of the samples (lowest curve) up to the highest values of the control points. Therefore, an envelope driven by such an increase encompasses all the variabilities observed through thermal ageing.

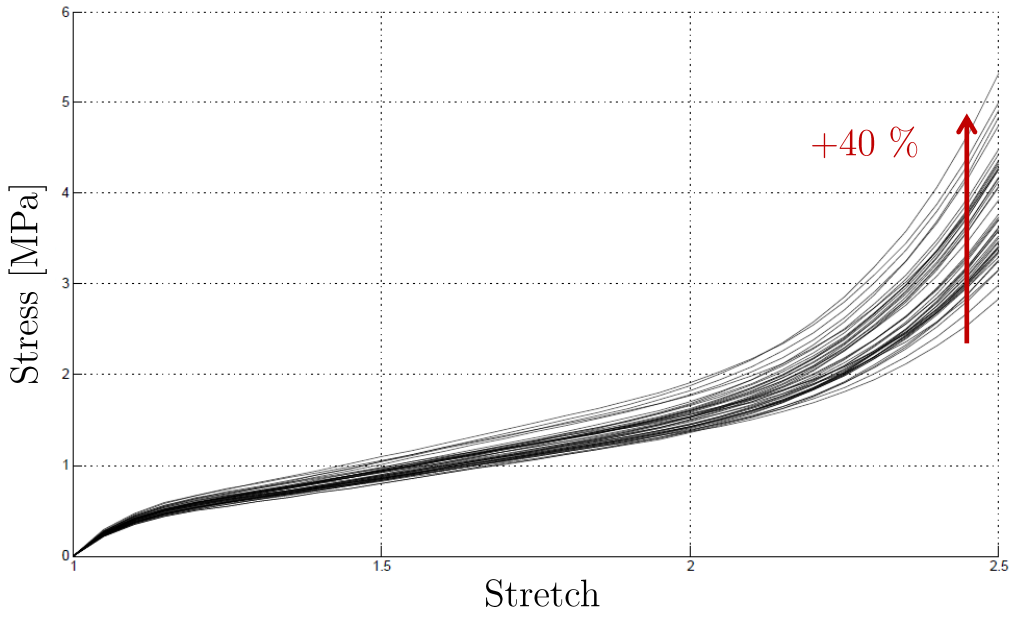

Figure 4.2: Array of experimental laws. The variability on the control points reaches +40 % between the base curve and the highest values.

These results have been completed by the *numerical results* obtained from the simulations by FE of the primary rubber spring. The mechanical stiffnesses recovered from FE simulations for each experimental set of input parameters yield an experimental set of outputs for the Kriging model. The FE calculations will be presented in the following section.

4.2.3 Training of the Kriging model - FE simulations

Kriging models use, as described earlier, an ensemble of experimental data to set up the regression parameters and weights of the algorithm. In the present case, the input parameters *time, temperature and control points* have been recovered from the characterisation in Chapter 3. Assembled appropriately in a matrix, they are fed to the Kriging script for its training. As for the outputs related to the experimental data, they are calculated by means of forty-six FE simulations with the software MARC - Mentat.

Non-linear, quasi-static, FE simulations

The aim of the experimental campaigns carried out in Chapter 3 was the characterization of the rubber reference. As stated at the introduction of the present chapter, these characteristics are

the necessary inputs for the study of the macroscopic properties of some suspension elements. The rubber-to-metal primary rubber spring PSi has been chosen at the core of the study: its rubber constituent was tested extensively through thermal ageing, mechanical characterization and chemical characterization. The hyperelastic models thus identified set the starting basis to widen the analysis scale and address the changes in the properties of the complete parts. Primary rubber springs are manufactured on the shape of two co-axial, conical, metallic frames: a lower, hollow frame and a massive upper pivot, with an interstice between their nominal positions. The space between both metallic parts is filled with rubber, which adheres to both frames, providing the physical link between them. A safety spigot arises from the lower frame and is inserted into a hollow space within the upper frame, ensuring the assembly's integrity in case of an extreme structural failure on the rubber layer (Figure 4.3). The rubber has two nicks on each side, which ease the expansion of the rubber under loaded conditions.

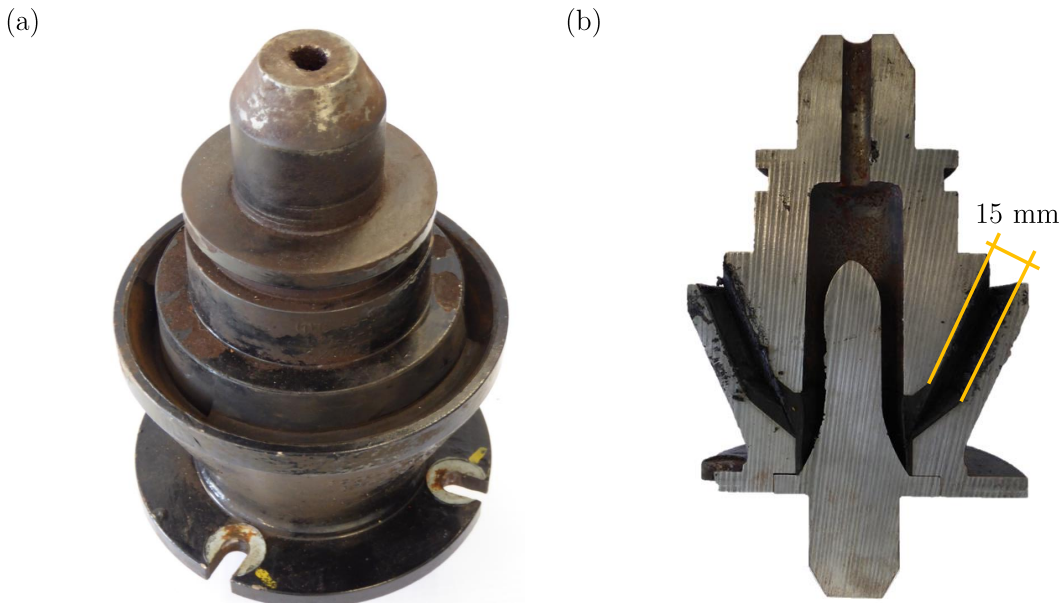

Figure 4.3: Service-worn PSi elements recovered from a German Talent 2 EMU from DB - (a) (complete) and (b) sectioned.

The customary characterization of the part's behaviour encompasses a wide range of characteristics. Both the *static* and *dynamic* stiffnesses are measured along the three spacial axis, *longitudinal*, *transversal*, *vertical*, plus the conical stiffness. Furthermore, the measurements are repeated for several configurations with a relative angle between the part's functional surfaces. Concerning the present works, *the sole characterization case which was available corresponds to*

the vertical compression test with parallel functional surfaces. The modelling of the PSi element has been undertaken based on the following hypothesis and assumptions:

- Since steel has a higher stiffness compared to rubber, it appears suitable to state that the part's mechanical properties arise from its rubber layer. Therefore, the numerical simulations which will be addressed subsequently will encompass solely the rubber part.
- The steel frames will be modelled as two different boundary conditions. The upper frame will be substituted by a control node on the axis of the PSi element, piloting the nodes placed on the surfaces between rubber and steel. The lower frame will be represented by means of a constraint of the displacement degrees of freedom.
- Two symmetry planes have been considered: XZ and YZ. The vertical stiffness model represents a quarter of the suspension element.
- The material is modelled as a generalized Mooney-Rivlin polymer with five parameters $(C_{10}, C_{01}, C_{11}, C_{20}, C_{30})$, with a small compressibility.
- The variational formulation within MARC models the volumetric FE elements with a central node with a single degree of freedom: the *hydrostatic pressure* [MARC, 2016]. For Mooney-Rivlin polymers, it is defined by a *penalty method* with a constant parameter, depending of the *bulk modulus*, K. In the present works, the Bulk modulus is approximately defined as $K = 100(C_{10} + C_{01})$.
- The part mesh is composed of hexahedral, 1st-order (displacement, 0-order for pressure), Hermann integration finite elements (type 84 on Marc - Mentat) [MARC, 2016], whose characteristic size is of 1 mm. The geometry is discretized by 112,051 elements (123,362 nodes).
- The model is piloted through a displacement input over the axial master node, rigidly tied to the upper frame surface.

Calculation of the PSi stiffness

On real-scale parts, the *static stiffnesses* are measured after two cyclic loadings, during the third increasing cycle, at three predefined loads (30 kN, 32 kN, 40 kN). The cycle loadings soften the material and stabilize its response, as discussed previously for the rubber characterization. Nevertheless, such a softening is not necessary when performing numerical simulations. The simulations calculate directly the compression of the primary rubber spring, taking 7 increments to achieve the calculation (12-13 minutes). The stiffnesses are calculated as a local linearisation at $\pm$ 5 kN around each reference load from the effort-deflection curve (see for example Figure 4.4). The stiffness is hence calculated with Equation 4.10, where "X" is the predefined load in kN. The characteristic which will be studied on these works is the *static vertical stiffness* of the primary

rubber springs.

$$K_{static}(X)[kN] = \frac{(X+5)-(X-5)}{\Delta L(X+5)-\Delta L(X-5)} \tag{4.10}$$

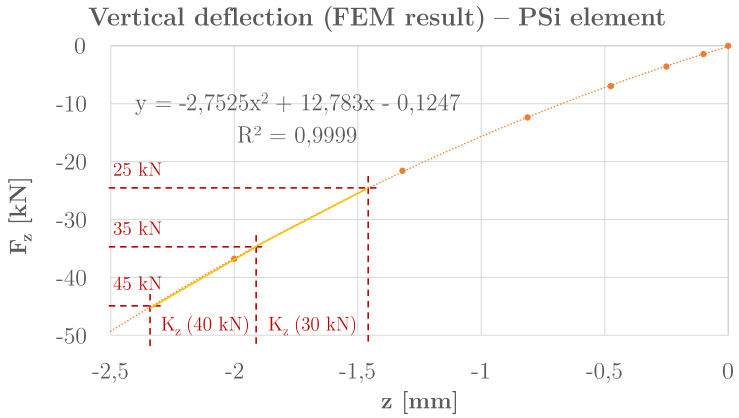

Figure 4.4: Numeric results from a FE simulation under Marc. Effort-displacement curve for the vertical compression test with brand-new rubber characteristics.

Simulation results

Prior to the tests with the bulk parts, four validation simulations were launched to reproduce a characterisation test in MARC. All the tests conducted showed that the sofware reproduced accurately the behaviour of the standard specimens, retrieving the experimental curves with the simulations. The software showed equivalent results regardless of the integration order of the elements (1^{st} or 2^{nd}) and of the piloting mode (imposed displacements or efforts) (Figure 4.5).

Regarding the results on the primary rubber spring, the maximum strain and stress were checked to ensure that the material behaves within the strain range stabilized on the characterization. The levels retrieved on the simulations remain lower than 100 % (i.e. $\varepsilon \leq 1$) with the highest Von Mises stresses around 20-30 MPa (Figures 4.6a and 4.6b). Therefore, the stabilized curved for a maximum strain of 200 % from the experimental tests is valid to undertake the study. The control node has been used on each calculation to obtain seven outputs of the vertical reaction effort (F_z), plotted against the vertical displacement to obtain the vertical stiffness characteristic of the PSi element. The vertical behaviour of the primary rubber spring follows a parabolic curve, which can be obtained from the numerical tests (Figure 4.4). Therefore, one can easily calculate the efforts at the measuring points at 25, 27, 35, 37 and 45 kN. The extraction of the linearised stiffnesses is immediate using Equation 4.10. For a matter

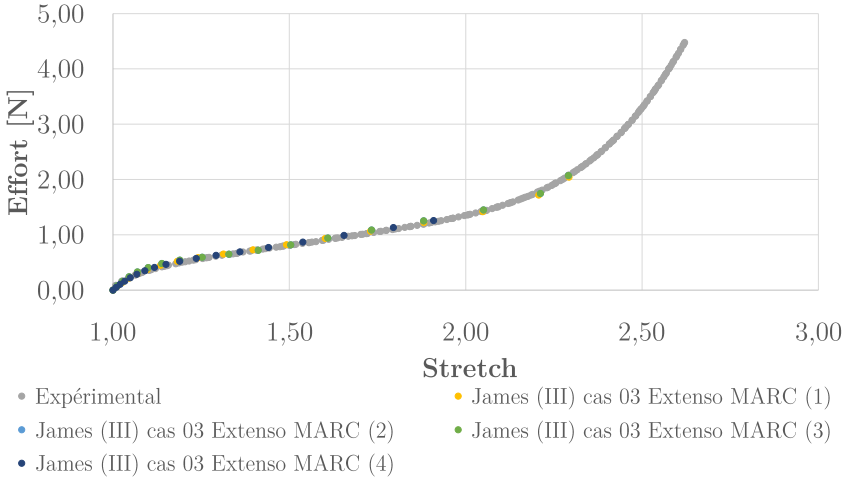

Figure 4.5: Numeric results from FE simulations under Marc. Comparison of numerical results for a standard traction test with experimental data.

of representativeness, three different curves at each ageing configuration were chosen, so as to obtain slightly different hyperelastic models. Therefore, the results account for the intrinsic variability of the material itself, producing an ensemble of different stiffnesses through the FE simulations.

As shown in Table 4.1, the stiffnesses retrieved numerically for a brand-new material fit well the nominal values imposed by Bombardier's specifications. These stiffnesses are defined as 22 kN/mm for a 30 kN load, 23 kN/mm for 32 kN and 27 kN/mm for 40 kN. The three results are respectively +0,6 % higher, -1,5 % lower and -9,1 % lower than the imposed stiffnesses. The stiffness at the lower loads are more accurate, but the part appears to be slightly softer at high loads. Nevertheless, the results of the validation tests practised by the supplier show also a lower stiffness at high loads on the real components.

The results from the simulations with MARC - Mentat show that there is an evolution of the part's vertical stiffness with the thermal ageing. Higher temperatures result in more evident increases, as well as for higher ageing periods. In absolute terms, the changes on the stiffness do not overpass the tolerances agreed between Bombardier and the supplier except for three ageing configurations: one at 50 °C and 45 days and two at 70 °C, 15 and 30 days (marked in red on Table 4.1). The three cases consist in several non-compliances at low load levels (30 and 32 kN), the models being compliant for the highest test load. In relative terms, the highest increase of stiffness is of about 22 - 23 % of the nominal stiffness.

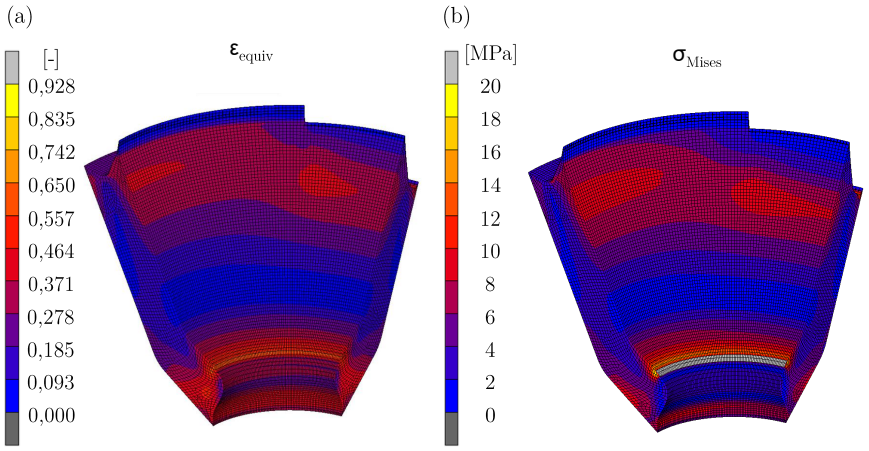

Figure 4.6: Numeric results from FE simulations under Marc. Equivalent strain plot (a) and Von Mises equivalent stress plot (b) over a quarter of the element.

Ageing configurations	**Vertical stiffnesses K_z**		
	K_z @ 30 kN	K_z @ 32 kN	K_z @ 40 kN
New samples	22,15	22,65	24,52
50 °C - 15 days	22,95	23,45	25,37
	24,42	24,94	26,92
	23,42	23,93	25,85
50 °C - 30 days	23,94	24,45	26,39
	24,06	24,57	26,52
	22,15	22,64	24,50
50 °C - 45 days	24,83	25,34	27,26
	25,41	25,93	27,89
	23,32	23,82	25,74

Table 4.1: Vertical stiffnesses of the primary rubber spring.

Ageing configurations	Vertical stiffnesses K_z		
	K_z @ 30 kN	K_z @ 32 kN	K_z @ 40 kN
70 °C - 2 days	23,30	23,81	25,73
	23,74	24,26	26,21
	22,33	22,82	24,68
70 °C - 5 days	24,13	24,64	26,61
	23,91	24,43	26,39
	23,51	24,02	25,95
70 °C - 10 days	24,35	24,87	26,88
	24,47	25,01	27,05
	23,01	23,53	25,50
70 °C - 15 days	24,77	25,31	27,36
	26,94	27,49	29,58
	24,97	25,50	27,52
70 °C - 30 days	25,61	26,16	28,27
	26,88	27,44	29,58
	26,13	26,68	28,79
80 °C - 1 day	25,21	25,72	27,67
	23,79	24,31	26,29
	23,12	23,63	25,57
80 °C - 2 days	22,92	23,44	25,40
	24,56	25,08	27,08
	22,25	22,75	24,68
80 °C - 5 days	25,23	25,77	27,84
	24,74	25,27	27,31
	23,03	23,55	25,53
80 °C - 10 days	24,70	25,24	27,29
	24,82	25,36	27,41
	24,81	25,35	27,40
80 °C - 15 days	26,34	26,89	29,00
90 °C - 1 day	22,74	23,24	25,14
	24,10	24,61	26,55
	22,22	22,71	24,55
90 °C - 2 days	23,05	23,56	25,49
	22,67	23,18	25,12
	21,94	22,44	24,34
90 °C - 5 days	25,24	25,80	27,92
	22,75	23,28	25,26

Table 4.2: Vertical stiffnesses of the primary rubber spring.

4.3 Ageing effect on PSi properties

4.3.1 Most unfavourable behaviour - Experimental data

The stiffness results recovered from the FE simulations have contributed to the set up of a Kriging model, fed by a random process has generated 20,000 different shots of the input variables (time, temperature, control points). The model predicted the boundaries of the stiffness values which could be expected from the FE simulations and from the experimental characterisations.

The two main variables driving the evolution of the mechanical properties are the *time and temperature of ageing*. Consequently, the results will be plotted as a function of these parameters. The results from the Kriging model show that the best fit to calculate the *maximum and minimum envelopes* of the experimental results was obtained when the regression functions $f_i(z)$ were zero-order polynomials (i.e. constant values). Otherwise, the model would fail to find a reasonable approach to the set of data, as the response of the stiffness shows a highly non-linear pattern. The maximum envelope shows a topmost area around 70 °C (15, 30 days), as recovered from the approach experimental tests plus FE simulations. Moreover, the area of maximum values spreads slightly towards 80 °C, 15 days, which would indicate that there is a set of ageing configurations which can cause a maximum stiffness increase on the component (see Figure 4.7).

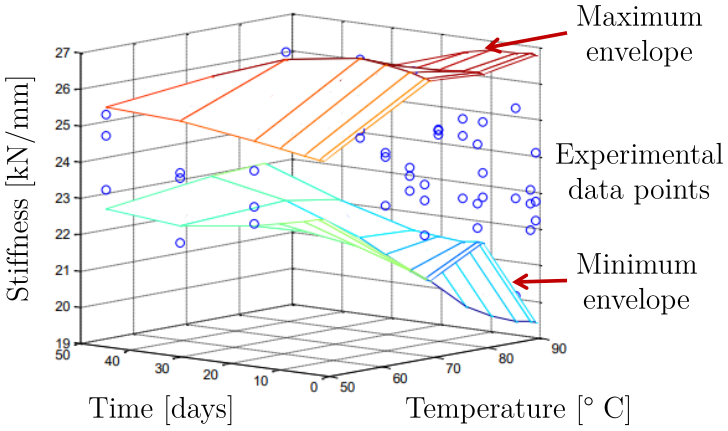

Figure 4.7: Maximum and minimum envelopes obtained by a Kriging model. The blue points are the FE stiffnesses recovered from the FE simulations.

Interestingly, the most pessimistic thermal ageing configurations pointed out by the Kriging model show a particular feature when plotted within an array of averaged curves. As discussed earlier on the text, hyperelastic curves exhibit a characteristic "S-shape", corresponding to three

different molecular behaviours within the structure, thus determining three strain/stretch areas. The averaged curves at 70 °C for 15 and 30 days, plus 90 °C for 5 days, cross each other and overfly the rest of the curves, constituting an upper boundary for the variability of the properties of the rubber. As shown in the details from Figure 4.8, the curve 70 °C - 15 days effectively encloses the rest of the curves at *low strains*, being overtaken by 70 °C - 30 days around the *mid-strain range*. The *final stiffening* marks the rise of the curve 90 °- 5 days, which closes the graphic.

Albeit lacking a physical sense, since none of the specimens exhibited such a behaviour, the combination of the portions of the three curves has a certain interest as *upper limit* of the expectable variability on the rubber. Moreover, it can be eventually fitted with an analytical model, obtaining the limiting parameters of the rubber characteristics. The fitted hyperelastic model, fed to a FE model, could be used to obtain a *corresponding stiffness* associated to the maximum envelope of the properties. This kind of numerical approach to the anti-optimization problem will be discussed in the following section.

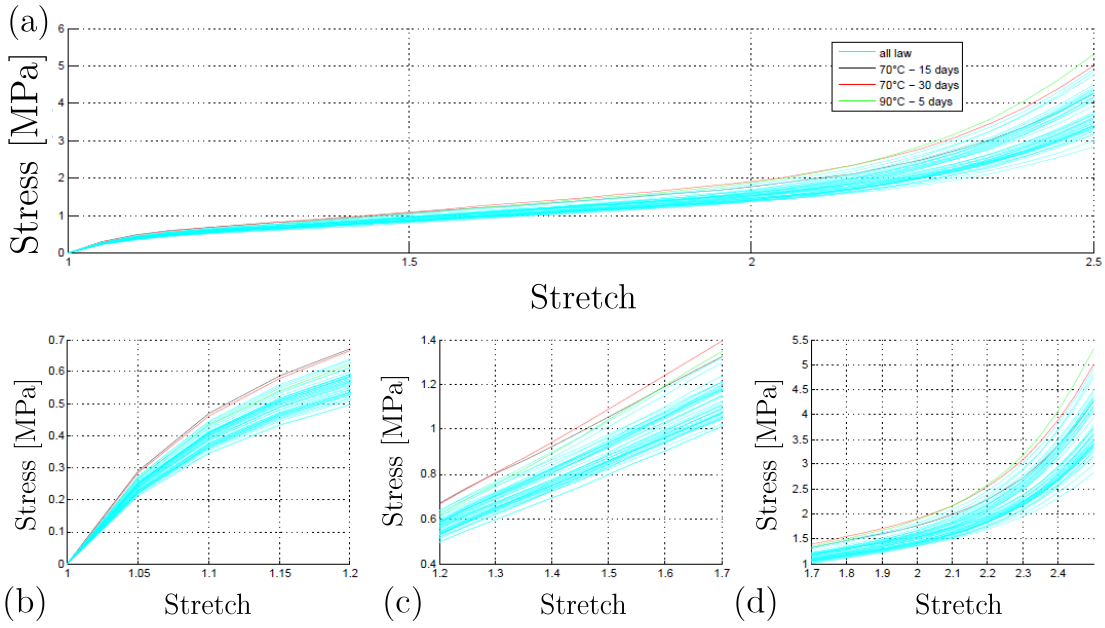

Figure 4.8: (a) Maximum envelope of the array of average curves. The curves of 70 °C at 15 (b), 30 days (c) and 90 °C 5 days (d) compose the upper boundary of the array.

4.3.2 Most unfavourable behaviour - Numerical stiffness

The results of the Kriging model have shown as well the most constraining configurations for thermal ageing. However, the use of accelerated ageing tests is a time-expensive technique,

requiring long test campaigns and equipments which are not always available. Furthermore, undertaking vast experiments at design stages is not an option in most of the cases, when quick results establishing the necessary boundaries to the problem are required. Hence the usefulness of a purely numerical approach based on a surrogate model, whose input base is made of previously recovered data from real cases. The Kriging model that has been presented accounts for the system's extreme boundaries, matching the maximum and minimum data recovered from the real scale tests. Moreover, it has comforted the observed relation between the maximum properties (upper envelope curves) and the maximum measured stiffnesses, for a quasi-static, non-linear problem.

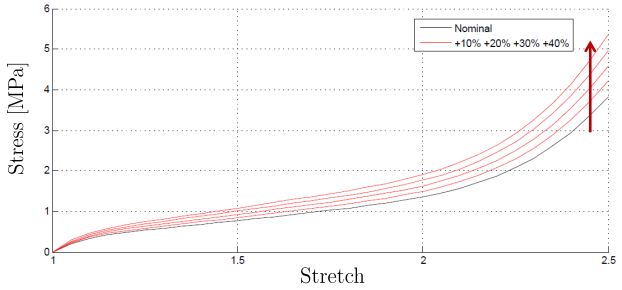

Figure 4.9: Array of artificially generated curves (red, +10, +20, +30, +40 % increases) from an original hyperelastic curve (black)

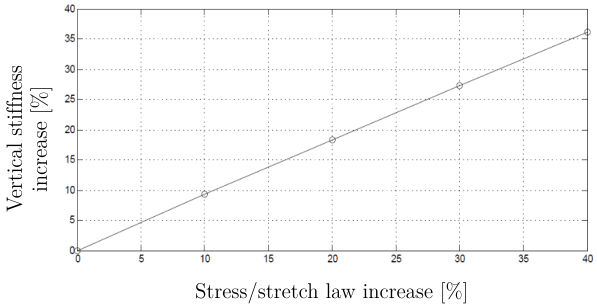

Figure 4.10: Associated increase on the part vertical stiffness for each law issued from a set of increases applied to an experimental curve.

The variability observed on the curves shows an increase of stress levels with ageing. The variation from brand-new samples up to the strongest ageing was imposed up to a maximum stress

value of +40 %. However, the results gathered from the FE simulations show that the increase of stiffness remained under +35 % of the nominal values for most of the configurations. Moreover, the FE results from the simulations comfort the approach, since the experimental variability is effectively about +40 % of the new properties (Figure 4.2) while the variability of the numerical stiffness is of +27 %. Therefore, one can conclude that the process describing the behaviour of the component *slightly reduces the dispersion*, decreasing the variability of the final metrics, the *mechanical stiffnesses* of the suspension element.

These results open the path to evaluate the most constraining cases by a perturbation of a selected representative material curve. Base material behaviour curves can be obtained from relatively quick test campaigns. The curves can be shifted up with an increasing factor so as to generate an upper envelope, recalling a maximum frontier of the material behaviour, thus obtaining a maximum possible stiffness, which can be treated as the topmost variability expected for the mechanical characteristics. The *stiffness* and its associated *variability* can be therefore fed to a dynamics MBS software to determine the effects on the dynamic behaviour of a whole railway vehicle. Moreover, they can be confronted to the curves describing the evolution of the properties throughout the parts life-cycle, in order to determine the periods when the stiffness can take the most critical values.

4.4 Experimental confrontation - Stiffness prediction

4.4.1 Evolution curves of the PSi vertical stiffness

The calculated stiffness from the numerical simulations which have fed the Kriging model have been used as well to develop an ageing model, describing the evolution of the vertical stiffness during the primary rubber spring life-cycle. The numerical stiffnesses recovered from MARC - Mentat have undergone an Arrhenius method in a process which follows the same principles stated for the mechanical properties and the hyperelastic coefficients in Chapter 3. For a matter of coherence, we have considered that the ageing mechanisms must have affected the three stiffness values alike. Therefore, the shift factors a_T which have been used to build the master curves of the three calculated stiffnesses are the same. The quality of the regression is very good, with an R^2 value of 0,961 (Figure 4.12).

The master curves show an increasing stiffness pattern along time, which show an exponential-like dependence with time. However, the fitness of the exponential curve is low. Therefore, an approach based on a sigmoid-like function of the logistic family has been proposed (Equation 4.11) (yellow-dotted curve on Figure 4.12). The logistic curves fit the experimental data with an averaged standard deviation of less than 4,5 % for the three levels of stiffness, being a suitable approach to describe the evolution of the stiffness throughout ageing time.

$$K(t) = K_0(1 + \frac{1}{1 + e^{t-t_0}}) \tag{4.11}$$

4.4.2 Naturally aged samples: characterization test campaign

In order to contrast the results from the experiments with real results, four spare PSi parts have been recovered from Deutche Bahn. They belonged to a Jakobs bogie from a Talent 2 EMU, having run for approximately 981,000 km. The suspension elements were recovered by Bombardier's teams from Siegen (Germany), for testing and characterization. The parts were recovered in a very good state: no rust was visible on the metallic parts and the rubber outer surfaces did not exhibit any cracks or pitting. The characterization tests for the *vertical stiffness* were conducted by Bombardier at its laboratory facilities in Siegen (Germany)

Vertical stiffness assessment tests were conducted by means of a Zwick-Roell test machine, coupled with the acquisition software "testXpert II". Each of the four PSi elements was tested twice. The parts were subjected to a two cycle loading up to 50 kN with the upper jig travelling at a speed of 8 mm/min. The calculation of the stiffness is conducted over the ascending curve of each cycle (Figure 4.13).

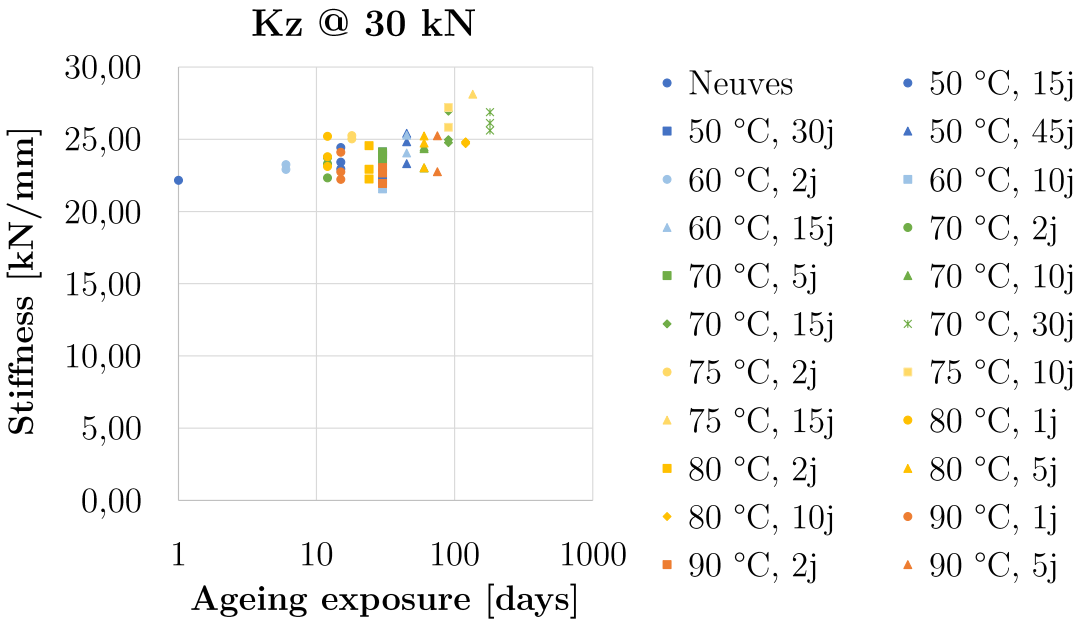

Figure 4.11: Master curve for K_z under 30 kN vertical load, at 50 °C.

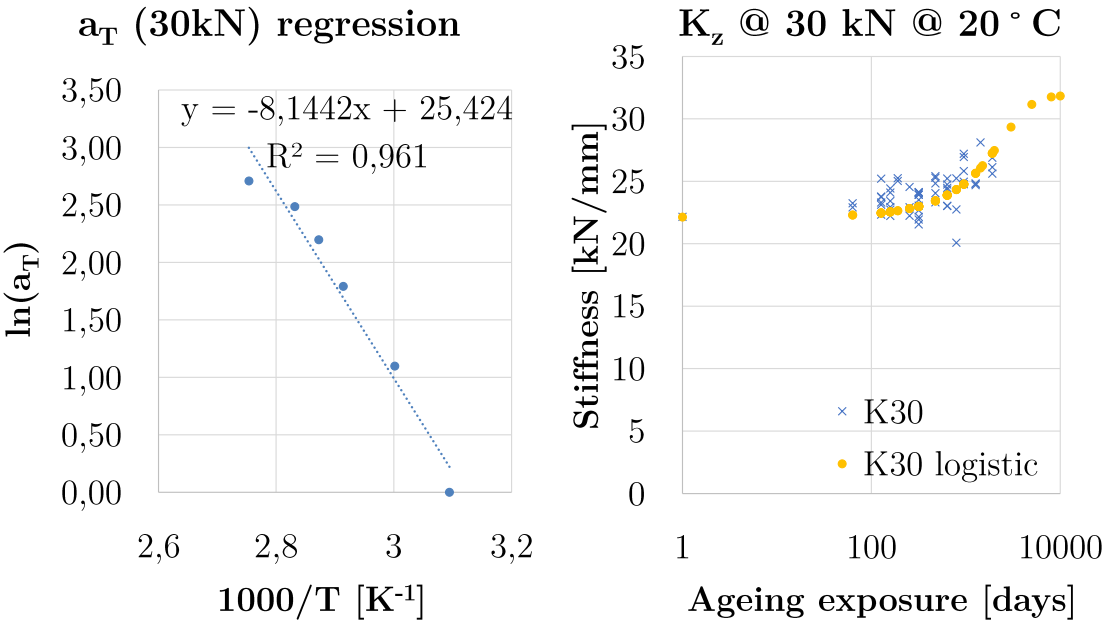

Figure 4.12: Arrhenius plot of the shift factors and ambient temperature stiffness curve.

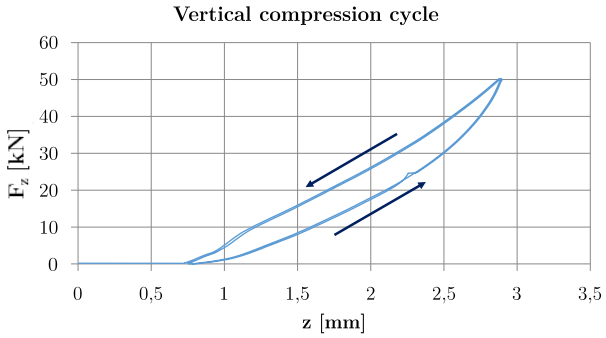

Figure 4.13: (Left) Experimental results obtained by Bombardier at its test facilities in Siegen (Germany) on a service-worn PSi element which belonged to a Talent 2 EMU from DB. (Right) Compression test on a PSi element.

The test results show a load curve which is neatly parabolic, as the results obtained from the numerical simulations. The closest experimental points to 25, 27, 35, 37 and 45 kN have been retrieved, allowing the calculation of the linearised stiffnesses at 30, 32 and 40 kN (Table 4.3). The stiffnesses from the characterized PSi elements are, after 981,000 km in service, still within the tolerance values of ±15% agreed with the supplier. Average results are within tolerances as well, although the stiffnesses at 30 and 32 kN show a slight drift to the upper part of the tolerance interval. The stiffness at 40 kN is very close to the nominal stiffness of 27 kN/mm.

# of sample	**Vertical stiffnesses K_z**		
	K_z @ 30 kN	K_z @ 32 kN	K_z @ 40 kN
1	23,26	24,35	28,86
2	24,03	24,52	27,74
3	25,30	25,69	28,94
4	21,23	21,81	24,96
5	25,06	25,45	28,37
6	22,40	22,81	25,51
7	23,63	23,99	26,64
8	20,18	20,72	23,62

Table 4.3: Vertical stiffnesses of several PSi elements from a Talent 2 EMU run by DB.

4.4.3 Results assessment

Both study campaigns, experimental testing and FE simulations, have yielded valuable results on the part's mechanic characteristics and their evolution. The numerical simulations have aimed to reproduce virtually the supplier's tests, introducing the mechanic characteristics recovered from characterisation tests of thermally aged rubber. Each characteristic stiffness has been evaluated separately according to the supplier's test procedure. Real-scale tests were performed by Bombardier on some spare parts to determine the vertical stiffness after several years in service.

As regards of the *vertical stiffness* of the PSi element, a vertical deflection curve has been recovered via a FE simulation with the brand-new state of the material. The three numerical stiffnesses extracted from the curve lay within the tolerance intervals set by Bombardier, thus being consistent with the technical requirements. The difference between the numerical reference stiffnesses and the validation tests is of less than 6 %.

The change on the vertical stiffness induced by the thermal ageing has been estimated by means of a series of characterization tests on aged samples, whose properties were subsequently fed to multiple FE simulations of the primary rubber spring. Three curves describing the evolution of the vertical stiffness of the PSi element, at three reference loads (30, 32 and 40 kN) have been drafted, successfully fitting the points recovered from the numerical simulations. However, the comparison with the experimental data from the supplier's validation report and from Bombardier's tests shows a major discrepancy: the test results on the components having been in service for 6 years show that their approximate ageing life spans from new to 2,5 years, according to the analytic curves (Figure 4.14).

The "analytic" times matching the stiffness data from experimental sources fail to match the times scales of the tests. We believe that the source for this mismatch would be the difference between the thermal ageing of a massive component and dumbbell samples. Since the structure of primary rubber spring effectively protects the bulk of the rubber layer from the atmosphere, the extent of the effects of the heat transfer and the ageing reactions on it could be lesser than predicted by the model. Therefore, the material displays an heterogeneous state, the core of the rubber being preserved and its properties spared, resulting in a "younger" result, compared to core-aged rubber specimens.

Interestingly, the results obtained from the FE simulations show a correspondence between the maximum stiffness increases, obtained for 70 °C (15 and 30 days of ageing) and 90 °C (5 days of ageing), and the respective averaged curves. The plot of averaged curves is enveloped by a combination of the averaged curves of these three ageing configurations: 70 °- 15 days sets the maximum function for low stretch values, 70 °- 30 days spans across the mid-stretch, being overtaken by 90 °- 5 days in higher strains. The calculation of the stiffness, made under the

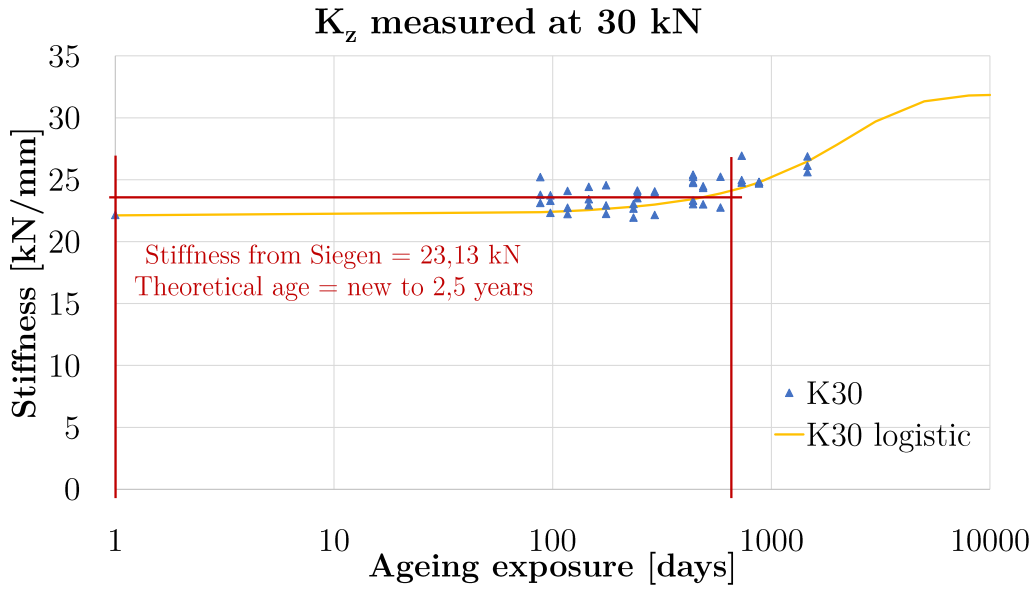

Figure 4.14: Comparison of the stiffness result from the real PSi component from DB versus the evolution curve extrapolated with ageing tests.

conditions of a *quasi-static, non linear analysis*, shows that the maximum envelope curves yield the maximum stiffness increases by FE simulations.

4.5 Conclusion

The present chapter has addressed some of the techniques used to quantify and propagate variability, pointing out the interest of such practices within the field of railway engineering. The set up of a Kriging model has been described, as well as the variables which feed the model. The results from the FE simulation campaign have proved that the thermal ageing has an effect on the mechanical properties of the primary rubber spring. Long periods of heat exposure can cause an increase on the parts' stiffness, causing it to overpass the tolerance margins set by Bombardier and it suppliers.

The results have fed two tools: the Kriging model and a series of Arrhenius plots describing the evolution of the three reference stiffnesses.

- The Kriging model has provided interesting data about the variability of the primary rubber spring stiffness. Moreover, the maximum envelope has pointed out the link between the higher stiffnesses and the maximum experimental curves, which set an upper boundary for the variability on the rubber properties. The variability of the curves does not fully translate through the part behaviour: the subsequent stiffness variability is lesser than for the rubber.

  The variability observed on the stiffness results and from the Kriging model will be most useful, as it will set appropriate variation levels on MBS simulations. The effect of the variability on the vehicle's dynamic behaviour will be addressed in Chapter 5.

- However, the predictive ability of the curves is limited, as they forecast a strong increase of the stiffness which, after contrast with the available data, appears to be excessive. Real scale tests with naturally aged data showed in turn a rather limited increase of stiffness. Differences between the extent of thermal ageing within a bulk part such as the primary rubber spring are surely at the core of these differences. The simulation assumption that the part is globally aged, rather than a more realistic gradient of properties across the piece, is an aspect which deserves further improvement.

Bibliography

[Arcidiacono et al., 2018] Arcidiacono, G., Berni, R., Cantone, L., Nikiforova, N. D., and Placidoli, P. (2018). A Kriging modeling approach applied to the railways case. *Procedia Structural Integrity*, 8:163 – 167. (Cited on page 112.)

[Baxter, 1992] Baxter, B. J. C. (1992). *The interpolation theory of radial basis functions.* PhD Thesis, Cambridge University. (Cited on page 110.)

[Bigoni and Engsig-Karup, 2015] Bigoni, D. and Engsig-Karup, A. (2015). *Uncertainty Quantification with Applications to Engineering Problems.* PhD thesis, Kgs. Lyngby: Technical University of Denmark (DTU). (Cited on page 108.)

[Bouchon-Meunier, 2007] Bouchon-Meunier, B. (2007). *La logique floue.* Presses Universitaires de France. (Cited on pages vi and 107.)

[Chinesta et al., 2010] Chinesta, F., Amine, A., and Elías, C. (2010). Recent Advances and New Challenges in the Use of the Proper Generalized Decomposition for Solving Multidimensional Models. *Archives of Computational Methods in Engineering*, 17(4):327–350. (Cited on pages vii and 110.)

[Cremona et al., 2016] Cremona, M. A., Liu, B., Hu, Y., Bruni, S., and Lewis, R. (2016). Predicting railway wheel wear under uncertainty of wear coefficient, using universal kriging. *Reliability Engineering & System Safety*, 154:49 – 59. (Cited on page 112.)

[Cressie, 1990] Cressie, N. (1990). The origins of kriging. *Mathematical Geology*, 22(3):239–252. (Cited on page 112.)

[David et al., 2012] David, A., J, Z. M., and Charbel, F. (2012). Nonlinear model order reduction based on local reduced-order bases. *International Journal for Numerical Methods in Engineering*, 92(10):891–916. (Cited on pages vii and 110.)

[Degrauwe et al., 2009] Degrauwe, D., Roeck, G. D., and Lombaert, G. (2009). Uncertainty quantification in the damage assessment of a cable-stayed bridge by means of fuzzy numbers. *Computers & Structures*, 87(17-18):1077 – 1084. (Cited on page 109.)

[Donders et al., 2005] Donders, S., Vandepitte, D., Peer, J. V. d., and Desmet, W. (2005). Assessment of uncertainty on structural dynamic responses with the short transformation method. *Journal of Sound and Vibration*, 288(3):523 – 549. (Cited on page 109.)

[Gao and Zhao, 2014] Gao, Y. and Zhao, W. (2014). Adaptive Optimization with Weld Fatigue Constraints Based on Surrogate Model for Railway Vehicles. *Mechanics Based Design of Structures and Machines*, 42(2):244–254. (Cited on page 112.)

[Ghanem and Spanos, 1990] Ghanem, R. and Spanos, P. D. (1990). Polynomial Chaos in Stochastic Finite Elements. *Journal of Applied Mechanics*, 57(1):197–202. (Cited on pages vii and 109.)

[Guan et al., 2011] Guan, F., Han, X., and Mao, H. (2011). Application of Optimization Methodology and Specimen-Specific Finite Element Models for Investigating Material Properties of Rat Skull. *Annals of Biomedical Engineering*, 39(1):85–95. (Cited on page 112.)

[Haag et al., 2010] Haag, T., Herrmann, J., and Hanss, M. (2010). Identification procedure for epistemic uncertainties using inverse fuzzy arithmetic. *Mechanical Systems and Signal Processing*, 24(7):2021 – 2034. (Cited on page 109.)

[Hanss, 2002] Hanss, M. (2002). The transformation method for the simulation and analysis of systems with uncertain parameters. *Fuzzy Sets and Systems*, 130(3):277 – 289. (Cited on pages vii and 109.)

[Hanss, 2003] Hanss, M. (2003). Simulation and analysis of fuzzy-parameterized models with the extended transformation method. *JProceedings of the 22th International Conference of the North American Fuzzy Information Processing Society, NAFIPS, Chicago, USA*. (Cited on page 109.)

[Hanss and Turrin, 2010] Hanss, M. and Turrin, S. (2010). A fuzzy-based approach to comprehensive modeling and analysis of systems with epistemic uncertainties. *Structural Safety*, 32(6):433 – 441. (Cited on page 109.)

[Kaymaz, 2005] Kaymaz, I. (2005). Application of kriging method to structural reliability problems. *Structural Safety*, 27(2):133 – 151. (Cited on page 110.)

[Ladevèze and Chamoin, 2011] Ladevèze, P. and Chamoin, L. (2011). On the verification of model reduction methods based on the proper generalized decomposition. *Computer Methods in Applied Mechanics and Engineering*, 200(23-24):2032 – 2047. (Cited on page 110.)

[Lophaven et al., 2002] Lophaven, S. N., Nielsen, H. B., and Sondergaard, J. (2002). DACE - A MATLAB Kriging Tool. Technical report, Technical University of Denmark, Kongens Lyngby. (Cited on page 114.)

[MARC, 2016] MARC (2016). *Volume B: Element Library*. (Cited on page 117.)

[Massa et al., 2009] Massa, F., Lallemand, B., and Tison, T. (2009). Fuzzy multiobjective optimization of mechanical structures. *Computer Methods in Applied Mechanics and Engineering*, 198(5-8):631 – 643. (Cited on pages vii and 109.)

[Massa et al., 2008] Massa, F., Ruffin, K., Tison, T., and Lallemand, B. (2008). A complete method for efficient fuzzy modal analysis. *Journal of Sound and Vibration*, 309(1-2):63 – 85. (Cited on page 109.)

[Massa et al., 2006] Massa, F., Tison, T., and Lallemand, B. (2006). A fuzzy procedure for the static design of imprecise structures. *Computer Methods in Applied Mechanics and Engineering*, 195(9 -12):925 – 941. (Cited on page 109.)

[Massa et al., 2017] Massa, F., Turpin, I., and Tison, T. (2017). From homotopy perturbation technique to reduced order model for multiparametric modal analysis of large finite element models. *Mechanical Systems and Signal Processing*, 96(Supplement C):291 – 302. (Cited on page 110.)

[Mazzola and Bruni, 2011] Mazzola, L. and Bruni, S. (2011). Effect of Suspension Parameter Uncertainty on the Dynamic Behaviour of Railway Vehicles. *Applied Mechanics and Materials*, 104. (Cited on page 109.)

[McWilliam, 2001] McWilliam, S. (2001). Anti-optimisation of uncertain structures using interval analysis. *Computers & Structures*, 79(4):421 – 430. (Cited on pages vii and 109.)

[Metropolis and Ulam, 1949] Metropolis, N. and Ulam, S. (1949). The Monte Carlo Method. *Journal of the American Statistical Association*, 44(247):335–341. (Cited on pages vii and 108.)

[Moens and Vandepitte, 2005] Moens, D. and Vandepitte, D. (2005). A survey of non-probabilistic uncertainty treatment in finite element analysis. *Computer Methods in Applied Mechanics and Engineering*, 194:1527–1555. (Cited on pages vi and 107.)

[Moore et al., 2009] Moore, R. E., Baker Kearfott, R., and Cloud, M. J. (2009). *Introduction to Interval Analysis*. Society for Industrial and Applied Mathematics, Philadelphia. (Cited on pages vii and 108.)

[Myers et al., 2009] Myers, R., Montgomery, D., and Anderson-Cook, C. (2009). *Response Surface Methodology: Process and Product Optimization Using Designed Experiments*. Wiley Series in Probability and Statistics. Wiley. (Cited on page 110.)

[Nechak et al., 2011] Nechak, L., Berger, S., and Aubry, E. (2011). A Polynomial Chaos Approach to the Robust Analysis of the Dynamic Behaviour of Friction Systems. *European Journal of Mechanics - A/Solids*. (Cited on page 109.)

[Nouy, 2010] Nouy, A. (2010). A priori model reduction through Proper Generalized Decomposition for solving time-dependent partial differential equations. *Computer Methods in Applied Mechanics and Engineering*, 199(23-24):1603 – 1626. (Cited on page 110.)

[Oliver and Webster, 1990] Oliver, M. A. and Webster, R. (1990). Kriging: a method of interpolation for geographical information systems. *International Journal of Geographical Information Systems*, 4(3):313–332. (Cited on page 112.)

[Perrin et al., 2013] Perrin, G., Soize, C., Duhamel, D., and Funfschilling, C. (2013). Track irregularities stochastic modeling. *Probabilistic Engineering Mechanics*, 34:123 – 130. (Cited on page 109.)

[Quost, 2005] Quost, X. (2005). *Modélisation de l'effet du vent sur les trains à grande vitesse. : Une étude dynamique et stochastiqe appliquée au risque de renversement.* PhD Thesis. (Cited on page 108.)

[Rutzmoser and Rixen, 2017] Rutzmoser, J. B. and Rixen, D. J. (2017). A lean and efficient snapshot generation technique for the Hyper-Reduction of nonlinear structural dynamics. *Computer Methods in Applied Mechanics and Engineering*, 325:330 – 349. (Cited on pages vii and 110.)

[Ryckelynck, 2005] Ryckelynck, D. (2005). A priori hyperreduction method: an adaptive approach. *Journal of Computational Physics*, 202(1):346 – 366. (Cited on pages vii and 110.)

[Sakata et al., 2003] Sakata, S., Ashida, F., and Zako, M. (2003). Structural optimization using Kriging approximation. *Computer Methods in Applied Mechanics and Engineering*, 192(7-8):923 – 939. (Cited on page 110.)

[Sakata et al., 2008] Sakata, S., Ashida, F., and Zako, M. (2008). Kriging-based approximate stochastic homogenization analysis for composite materials. *Computer Methods in Applied Mechanics and Engineering*, 197(21):1953 – 1964. (Cited on page 112.)

[Sudret, 2008] Sudret, B. (2008). Global sensitivity analysis using polynomial chaos expansions. *Reliability Engineering & System Safety*, 93(7):964 – 979. (Cited on page 109.)

[Walker et al., 2003] Walker, W. E., Harremoës, P., Rotmans, J., Sluijs, J. P. v. d., Asselt, M. B. A. v., Janssen, P., and Krauss, M. P. K. v. (2003). Defining Uncertainty: A Conceptual Basis for Uncertainty Management in Model-Based Decision Support. *Integrated Assessment*, 4(1):5–17. (Cited on pages vi and 107.)

[Wang et al., 2013] Wang, P., Lu, Z., and Tang, Z. (2013). An application of the Kriging method in global sensitivity analysis with parameter uncertainty. *Applied Mathematical Modelling*, 37(9):6543 – 6555. (Cited on page 110.)

[Wei et al., 2004] Wei, C., Ruichen, J., and Agus, S. (2004). Analytical Variance-Based Global Sensitivity Analysis in Simulation-Based Design Under Uncertainty. *Journal of Mechanical Design*, 127(5):875 – 886. (Cited on page 110.)

[Wiener, 1938] Wiener, N. (1938). The Homogeneous Chaos. *American Journal of Mathematics*, 60(4):897–936. (Cited on page 109.)

[Yang et al., 2016] Yang, Y., Zeng, W., Qiu, W.-s., and Wang, T. (2016). Optimization of the suspension parameters of a rail vehicle based on a virtual prototype Kriging surrogate model.

Proceedings of the Institution of Mechanical Engineers, Part F: Journal of Rail and Rapid Transit, 230(8):1890–1898. (Cited on page 112.)

[Yvonnet et al., 2007] Yvonnet, J., Zahrouni, H., and Potier-Ferry, M. (2007). A model reduction method for the post-buckling analysis of cellular microstructures. *Computer Methods in Applied Mechanics and Engineering*, 197(1-4):265 – 280. (Cited on page 110.)

[Zadeh, 1965] Zadeh, L. A. (1965). Fuzzy sets. *Information and Control*, 8(3):338 – 353. (Cited on pages vii and 108.)

[Zadeh, 1975a] Zadeh, L. A. (1975a). The concept of a linguistic variable and its application to approximate reasoning-1. *Information Sciences*, 8(3):199–249. (Cited on pages vii and 109.)

[Zadeh, 1975b] Zadeh, L. A. (1975b). The concept of a linguistic variable and its application to approximate reasoning-2. *Information Sciences*, 8(4):301–357. (Cited on page 109.)

[Zadeh, 1975c] Zadeh, L. A. (1975c). The concept of a linguistic variable and its application to approximate reasoning-3. *Information Sciences*, 9(1):43–80. (Cited on page 109.)

Chapter 5

Railway dynamics: suspension variability and safety assessment

> The form of the railway wheels are conical (...). Then from a small irregularity of the railway the wheels may be thrown a little to the right or a little to the left (...) which will cause the wheels to proceed in an oscillatory but easy motion on the rails.
>
> George Stephenson

The fifth chapter of the manuscript is devoted to the study of the dynamic behaviour of the Régio2N rolling stock under varying suspension properties. An introduction on the dynamic behaviour of railway vehicles and to the relevant phenomena influencing it will be addressed in the first paragraph. Next, a description the numerical models for safety assessment on railway rolling stock will be done. The main safety indicators and practises enforced by the safety norm UIC-518 will be described as well. The design of experiment to introduce the variability on the mechanical properties from Chapter 4 will be discussed and its results will be presented. The most critical cases will be pointed out, underlining the exploitation limits of the system and the recommendations for further works and developments on this subject.

Contents

5.1 Technological aspects and fundamentals

From its early beginnings, the study of the dynamic behaviour of the rolling stock has been a constitutive part of railway engineering. The introduction of tapered, inner-flanged wheels rose the first of many phenomena which would be studied subsequently: the oscillation of a free wheelset. Tapered wheels with an inside flange have many practical advantages, such as the wheelsets intrinsic capacity of self-centring its position while running along a straight track, or the flange safety role to prevent the wheels from jumping out of the track path. George Stephenson's observations as soon as 1821 show the early conscience of this phenomenon, whose first explanation is due to Klingel (1883) [Wickens and Iwnicki, 2006].

The hunting in wheelsets is not an isolated case of oscillations on railway rolling stock. Early examples of rolling stock preserved in conservation institutions show that the carriages and wagons were much like their road counterparts: relatively short, with a rigid wheelbase. Rigid-wheelbased vehicles withholding two hunting wheelsets were a most suitable arrangement to give rise to a wide range of oscillatory phenomena at increasingly higher frequencies. In addition, railway companies were confronted to the need to transport more goods and passengers. The solution of lengthening the rolling stock was of little help to deal with the dynamic behaviour issues. However, the uneasy ride of longer, rigidly wheel-based wagons and carriages led to an empirical solution - the bogie -, which would ultimately lead to the solution of both problems: to provide a smooth ride while ensuring a good curving ability.

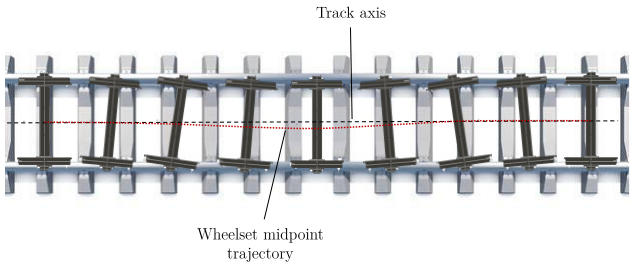

Figure 5.1: Kinematic oscillation of a free wheelset about the track central axis.

5.1.1 Railway dynamics: theory and key aspects

The first mathematical description of the behaviour of a free wheelset was set by Klingel, as discussed earlier, on the basis of pure kinematic considerations. Redtenbacher suggested an explanation on the same basis to the curving behaviour of a free wheelset as well. Yet none of the

methods would explain the actual *dynamic behaviour* as it is understood today. Carter derived the first explanation to the dynamic behaviour of a wheelset, a bogie and the full vehicle by applying the equation of motion [Carter, 1922]. The development of electric locomotives, with stability problems derived from their symmetric layout, motivated Carters' research on stability. These works were the first use of the equation of dynamics and eigenvalue analysis in a manner which has become customary ever since [Carter, 1928].

For a formal explanation, the monograph from Garg and Dukkipati offers a thorough discussion on the basis of dynamics [Garg and Dukkipati, 1984]. The study of railway vehicle dynamics is addressed today via the *Multibody System Dynamics* (MBS), which relies on an multi-dimensional form of the equation of motion (Equation 5.1). The manipulation of this equation allows the description of a system's response under free or forced oscillation, as well as its *modal analysis*, obtaining the system eigenvalues or modal frequencies and eigenmodes. MBS simulations allow the analysis of several bodies (most of the cases rigid), linked by *kinematic constraints* or by *mechanical elements* which introduce the necessary properties to the study of the system's behaviour.

$$[m]\{\ddot{x}(t)\} + [c]\{\dot{x}(t)\} + [k]\{x(t)\} = \{F(t)\} \tag{5.1}$$

Depending on the system properties, the terms on the *mass*, *damping* and *stiffness matrices* in Equation 5.1 can be either constant - which is the case of *linear* systems -, or might be variable, which is the case of *non-linear* systems. Non-linearities can arise from several sources: the mechanical characteristics of suspension elements (for instance, rubber compounds, dashpots, air cushions, etc.), or the boundary conditions of the dynamic problem. The early works from Carter made evident that the analysis of the rolling stock dynamic behaviour encompassed several non-linear aspects which demanded further research. The contact between the wheel tread and the rail, with a point-wise definition of both profiles, is not solvable by a linear scheme, especially when it comes to multiple-contact situations. Besides the vehicle interaction with the rails, the track geometrical characteristics and its associated signals are a source of non-linear inputs for the system as well. The following paragraphs will address with more detail this three aspects.

5.1.1.1 Track geometry

The key element on the railway infrastructure is the track, since it is the pathway along which the rolling stock circulates. Its characteristics are determinant for the smooth ride of the vehicle and depend on the different constituents of its structure. The track base structure is composed of several stacked layers (Figure 5.2). A platform of consolidated ground or *subgrade*, which serves as the primary substrate for the railway platform. The *sub-ballast* is an intermediate layer made of fine gravel, offering an interface between the subgrade and the ballast layer and allowing a correct draining of rain water. The topmost substrate of the track substructure is the *ballast*, a gravel layer

of tough rock (sometimes granite), coarser than the sub-ballast, with irregular edges and shapes, so as to grip tightly the track sleepers. The *sleepers* are a series of evenly spaced, transversal profiles which bear the rails and link them to the underlying ballast. Made of tarred wood to prevent rotting by humidity or eating by xilophagous insects, railway ties are currently made in the shape of one steel-reinforced concrete block (Figure 5.2). The sleepers have two side bearings for the rails, which are placed over a rubber pad. This layer has an isolating purpose, separating the rail from the ground so that both the track circuits and the return currents travel through the rails rather than the track platform. The fastening of the rails depends on the underlying sleepers: spikes might be used on wooden tracks, although most frequently rails are attached by means of a chair screw and a fastener, the assembly effectively clamping the rail foot against the rubber pad.

The track quality can be defined by several metrics related to its geometry and the arrangement of its components. Observing the track from above, the track axis sets the rails direction and serves as central reference for *gauge* measurements. *Alignment* flaws, which are directly related to the gauge, arise when the rails do not respect the distance between themselves and with the track axis. Similarly, the track platform (ballast or concrete slab) can be compared to an ideal datum plane. The unevenness of the track basis can cause *profile* issues on each individual rail, which can be measured by means of the *cross-level* (the average of both vertical profiles of the rails). The rate of change of the cross level along the track axis is the *twist* of the track.

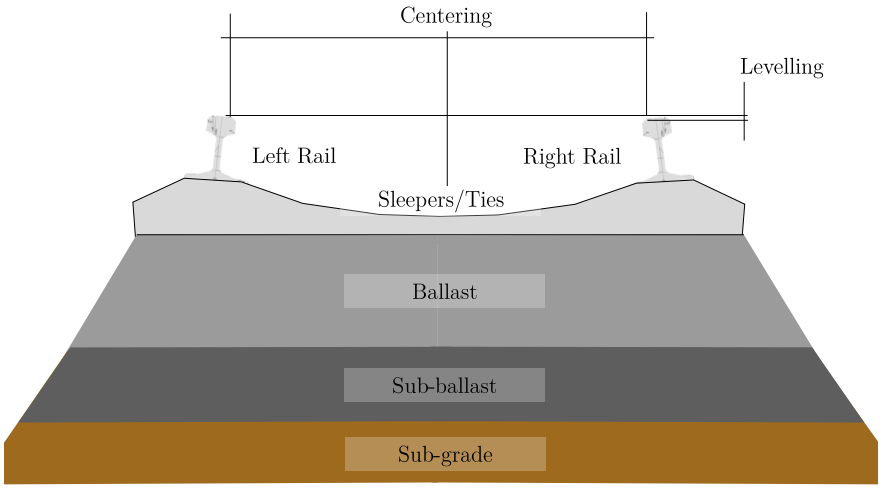

Figure 5.2: Structure of a railway track.

These metrics can be measured by specific rolling stock, thus characterizing a track signature. Moreover, most of the times these metrics appear in the form of periodic flaws, thus being interpretable as a series of harmonic functions describing the shift from the ideal geometry. Power

spectral density (PSD) measurements from the track are especially useful to test the rolling stock response when travelling stationary over a certain type of infrastructure. Alternatively, some specific track devices or configurations can be represented by a specific analytic signal [Garg and Dukkipati, 1984].

The integration of such characteristics under the formalism of Multibody Simulations (MBS) depends on the degree of detail desired for the analysis. Some models consider the track as a rigid assembly of rails and sleepers, which is attached to the ballast surrounding the ties by two sets of spring and dashpot in parallel. The mechanical parameters of these elements give the track resistance in the vertical and lateral direction. The MBS software SIMPACK uses this principle to model railway tracks. More refined models take the rails as flexible beams (for example, Euler-Bernoulli beams), and their links with sleepers via the rail pads are modelled as parallel sets of springs and dashpots representing the rail pads' behaviour (Figure 5.3). Moreover, the sleepers lay as well as several spring-dashpot assemblies, which describe the ballast's consistency and behaviour. To model realistically the track's behaviour, the description of the track can be further enriched by adding mechanic elements between a sleeper and its neighbours, which would represent the longitudinal behaviour of the track. The purpose of these refined models is to account for the various phenomena arising from the track response: train dynamics and instability, infrastructure wear and noise emissions [Chamorro and Escalona, 2012]. A discretized description of the track does not imply the incompatibility with a continuous description by means of, for example, a real track signature derived from a PSD spectrum. Both aspects can be superposed so as to provide an accurate model of the track's geometric and mechanic state.

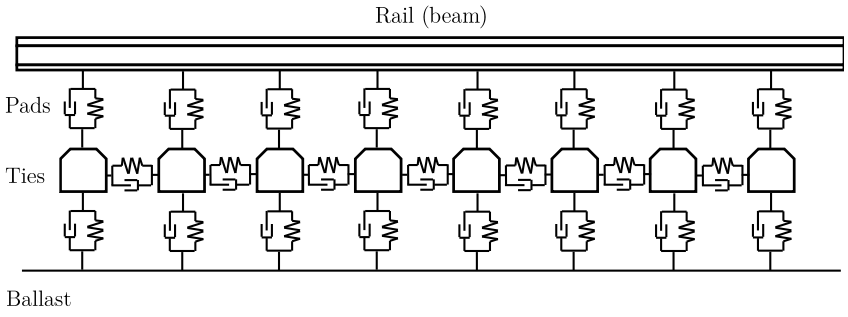

Figure 5.3: Multi-body model of track discretizing the interfaces between rails and sleepers, and sleepers and ballast.

5.1.1.2 Wheel-rail interfaces

Carter's first inclusion of contact phenomena in the modelling of wheel to rail contact opened a new research field on the study of railway dynamics. The contact surface between a railway wheel and the rail takes the form of a small ellipse, barely the size of a fingertip. It is over this small interface that the rolling stock's grip is conveyed to the rail and which ensures the tractive effort and the braking aptitude of the vehicle. The assessment of contact conditions is customarily performed with a two-step approach: the *normal problem* and the *tangential problem* [Ayasse et al., 2006]. The solution of a normal contact point could be described by Hertz's contact theory, thus being the starting point for the theories aiming to solve the tangential problem. Carter is credited for finding the first solution to the latter, his model imagining the contact as if two cylinders were in contact edge-to-edge. The theory proceeds to the definition of a pressure profile along the contact area (Figure 5.4). One of the main difficulties to characterize this interface arises from the "stick-and-slip" behaviour over the contact patch. As the wheel moves forward, the wheel's tread comes into contact against the rail. A primary front is established, where the contact forces stick both surfaces, which undergo a mutual creepage, ensuring the vehicle's grip on the track. When friction forces are overpassed, the contact switches to a slip phase on a second area of the contact patch, before the surface lifts up, resuming its circular motion around the wheels' tread.

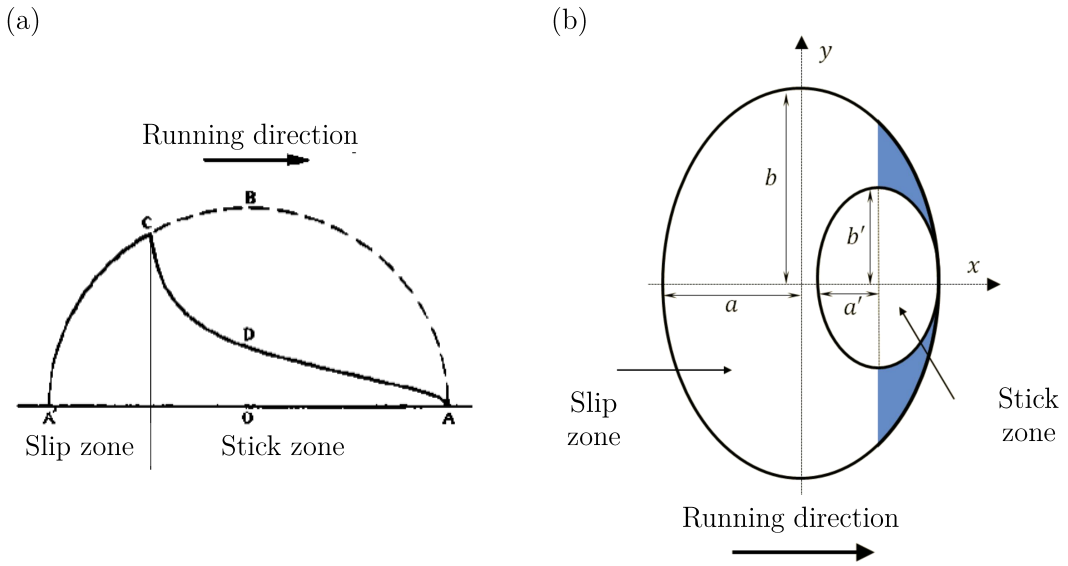

Figure 5.4: (a) Tractive effort (purely longitudinal) along the contact patch [Carter, 1926]. (b) Johnson and Vermuelen contact theory [TOUMI, 2016].

Hence the contact patch is divided in two areas: a frontal *stick zone* where efforts are transmitted effectively, plus a rear *slip area* where the contact pressure is no longer enough to ensure the wheels' grip [Carter, 1926]. Carter succeeded in providing an expression relating tractive effort to the wheel's radius and contact pressure. The sole drawback of this model was the lack of assessment of the transversal efforts over the contact patch, which prevented its use in the perspective of a full dynamics analysis. Nevertheless, Carter's model was successfully used until the late 1960s, when Kalker's theory gave a complete explanation to the contact problem.

The introduction of the Hertzian contact theory to calculate the shape of the contact patch by Johnson and De Pater paved the way for more complex theories. A complete theory by Johnson and Vermuelen and a linearized form of the problem by De Pater and, ultimately, by Kalker [Kalker, 1991] were developed in parallel on the 1960s. These theories focused on the problem globally, accounting not only for the longitudinal creepage of the wheel-rail contact, but explaining the lateral and spin creepages as well. The methods were successfully validated by comparison to the results from a British Rail software, DUVOROL, which calculated a wide ensemble of tables regarding the properties of Hertzian contact [Kalker, 1991]. Nevertheless, the application of both theories remained computationally ineffective, leading to further research to find computationally-efficient algorithms allowing the calculation of the contact's properties and metrics in an exploitable way. The Shen-Hedrick-Elkins (SHE) model and Kalker's algorithm FASTSIM coped with the needs of the railway research, as both systems provided a computational-compatible solution for the study of a railway vehicle's dynamic behaviour. The reader is invited to refer to the articles by Kalker for further detail on his theory [Kalker, 1968].

5.1.1.3 Rolling stock suspension properties

The properties of the suspension elements play a key role on the dynamic response of the rolling stock. As a general principle, one can consider that suspension elements provide two main properties: first, the *mechanical stiffness* necessary to ensure the resistance and stability of the system; second, the *damping* or *dissipation* capacity to blur the vibrations and parasitic motion endured by the rolling stock. Early rail vehicles wore suspension elements which supplied both characteristics, such as leaf springs, but their magnitudes were far from being optimal. The need of stabler, smoother riding qualities and the introduction of the bogie lead to a new paradigm on the suspension design. The suspension was subsequently split on two stages and its constituents would adopt a specific role within the subsystem. Consequently, some elements would provide the necessary stiffness at certain points of the structure, while a series of dissipative devices would damp the motion of the structural elements acting complementarily to them. For an extensive description on the modelling of suspension elements, the reader is invited to refer to a thorough article by Stefano Bruni and co-workers [Bruni et al., 2011].

The following paragraphs will address briefly some wide families of suspension elements, as well as their specific translation to the virtual MBS model which has been used on the thesis works. The MBS software which has been used for simulation purposes within this works has been provided by Bombardier: SIMPACK 8.9, which is one of the commercial codes for multi-body simulations available in the market (other examples are ADAMS, MEDYNA or VOCO).

Current bogie designs include varied examples of *metallic elements* which usually have a structural role. They provide the necessary link between the different stages of the suspension, having an adequate balance between structural resistance and flexibility. As discussed in Chapter 2 for the *primary suspension*, the physical connection between the axleboxes and the bogie frame relies quite often on these suspension devices. When the design is that of leaf or coil springs, a particularity arises: these elements have their structural resistance in one or two directions (usually the vertical and one transversal stiffness). Therefore, the suspension design around the axlebox must be done in such a manner that the remaining stiffnesses can be ensured. Freight bogies couple coils springs in pairs over the axlebox's frame, or include sliding horns framing the axlebox in the case of leaf springs (Figure 5.5a and 5.5b), thus providing the necessary resistance in the longitudinal and transversal directions, ensuring the wheelsets' guidance. Similarly, some passenger vehicles bear trail arms which contribute to the guiding of the wheelset, in parallel to a coil spring topping the axlebox (Figure 5.5c).

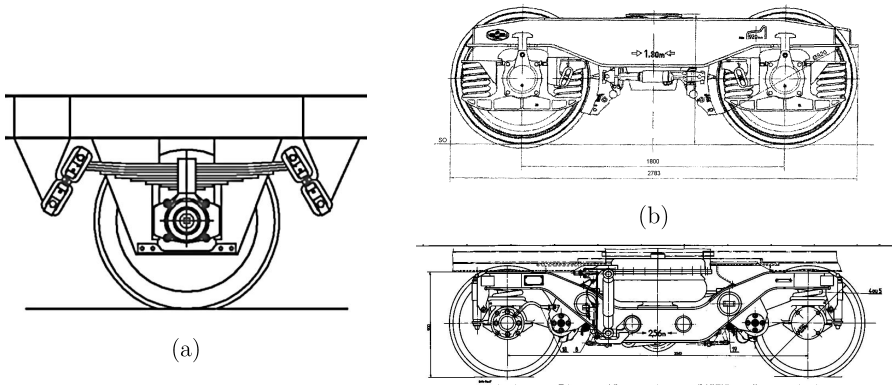

(a) (b) (c)

Figure 5.5: (a) Leaf-spring, horn-guide axlebox arrangement [Jönsson, 2004]. (b) Freight bogie Y-25 bearing a suspension composed of coil springs, Lenoir links and friction interfaces. (c) Passenger bogie Y-32, with arm links and air cushions secondary suspension.

Regarding *the secondary suspension*, freight vehicles bear friction interfaces between the bogie's bolster and the bogie frame, with no proper secondary suspension elements. Nevertheless, the relative sliding of the bolster over the bearings provides some dissipative behaviour. On the contrary, the secondary suspension on passenger vehicles has a more complex structure, since stricter comfort requirements are to be met. These are ensured by a combination of several parallel mechanisms, among which one can find the anti-roll bars. In the shape of a torsion bar connected to two lateral assemblies of a lever plus a connecting rod, they counter the roll motion of the carbody.

Metallic elements have a specific particularity related to their constituent materials: they have almost no damping abilities. Therefore, they are usually modelled as one or several stiffnesses acting in the direction of their real-scale counterpart, sometimes adding a small amount of damping in the form of a parallel dashpot. For example, coil springs can be represented by a strong vertical stiffness and a lower radial stiffness. Torsion bars take the form of a torsional stiffness about their longitudinal axis. Finer representations are possible for bilinear springs as well (i.e. springs with variable winding or concentric coil springs) (Figure 5.6a). The case of leaf springs is more complex, since it requires the addition of a *slider* to represent the inter-leaf friction (Figure 5.6b). The friction element allows the characteristic hysteresis of the leaf spring behaviour and accounts for its intrinsic dissipative behaviour.

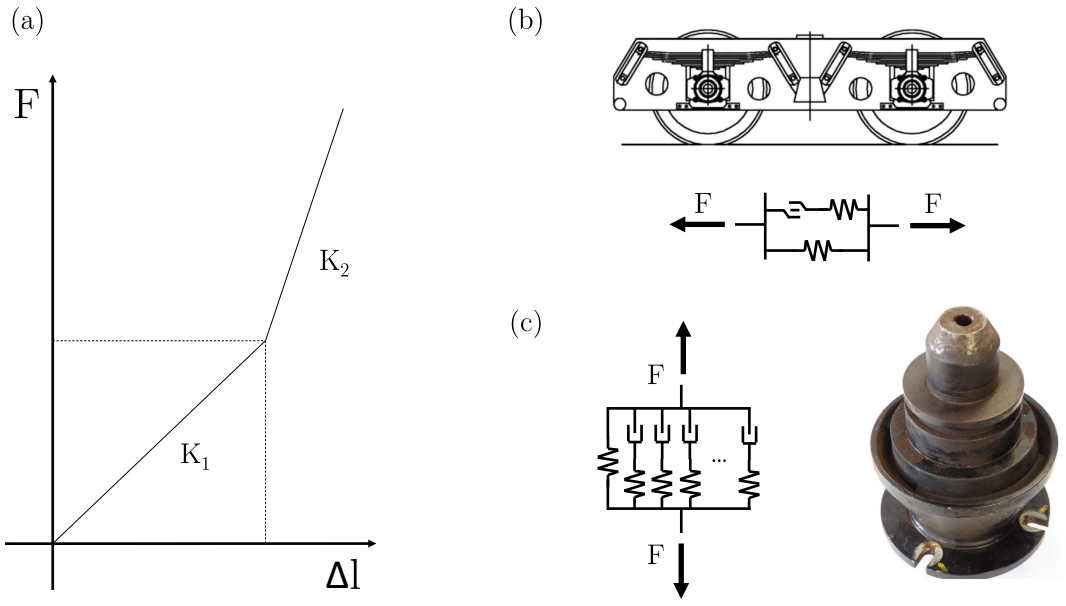

Figure 5.6: (a) Bilinear stiffness characteristic. (b) Leaf-spring modelling proposed by [Stichel, 1999]. (c) Multi-branch rubber bushing modelling.

The historic context on Chapter 3 details the introduction of the rubber as base constituent of suspension elements at the 1950s, thanks to the development of increasingly resistant rubber compounds and the better comprehension of its hyperelastic behaviour. From a formal point of view, the behaviour of *rubber-based suspension elements* is a hyper-viscoelastic behaviour, that is, highly non-linear and dissipative. The modelling of these elements is usually made by combinations of the classic spring-dashpot systems of Maxwell, Kelvin-Voigt or Zener arrangements (Figure 5.6c). The spring accounts for the elements' static or quasi-static stiffness, whereas the dashpots add the velocity dependence associated the viscous dissipation [Berg, 2016]. Complex behaviours requiring variable dissipative capacities at different frequency ranges can be represented by multiple Maxwell branches on the same model, each one accounting for an identified frequency range of operation of the element.

Purely dissipative elements such as the hydraulic dampers are very usually described as a single direction actuators modelled by a Maxwell element (series spring-dashpot). When a more detailed description of the dampers is required, for example to include the effect of the damper's extremity bushings, two identical Maxwell elements might be added to represent the behaviour of the rubber garments (Figure 5.7). In spite of its simplicity, this dissipative models can represent the non-linear behaviour of a damper by means of an input function relating the elementary dashpot effort versus the relative speed of its extremities.

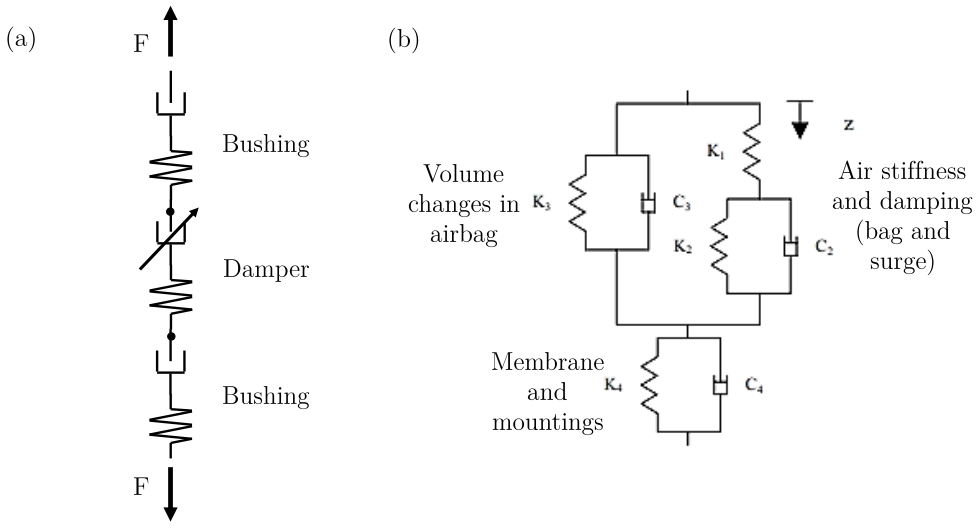

Figure 5.7: (a) Damper and extremity bushings modelling. (b) SIMPACK air spring modelling [Presthus, 2002].

Complex suspension elements such as the air springs have challenged the researchers to find a proper representation. Composed by a solid emergency spring at its base, topped or surrounded by the inflated bellow, the mechanical stiffness of the spring depends strongly on the properties of it bellow membrane and of the air pressure (Figure 5.7). Moreover, the compensation reservoirs and the air's fluid inertia add a damping behaviour and a fluid stiffness which is represented by a polytropic equation [Presthus, 2002].

5.1.2 Rolling stock running behaviour

The dynamic behaviour of railway rolling stock is a complex discipline, declined in multiple subjects. From the beginning of railway technology, dynamic phenomena have driven the research of safer designs which could prevent any undesirable behaviour on the vehicles, such as the hunting motion or the self-induced derailment. As regards of the safety assessment, norms such as the UIC-518 tend to group the safety issues in some broad families: derailment, curving and vehicle dynamics. Each of these aspects will be developed in detail on the following paragraphs.

5.1.2.1 Derailment

The derailment of a railway vehicle occurs when one or several of its wheels is no longer over the rails. Such a situation may occur when a wheel succeeds in jumping over the rail to the outside of the track or if it falls in the space between both rails. One can distinguish three main sources of derailment: the derailment *caused by an obstacle* on the tracks, which can be partially prevented by rail-guards preceding the rolling gear as long as the obstacle's size remains relatively small [Brabie, 2005]. The second source is the *failure of the infrastructure* sur as the overturning of a rail, causing the fall of the wheel within the track [Morales-Ivorra et al., 2016]. The third source is *self-induced derailment*, which means that the contact conditions between the train and the rails, combined with the rolling stock's dynamic state, can trigger under certain circumstances the jump of a wheel flange over the rail head, thus leading to a derailment. As regards of the present works, the latter form of derailment is the only having an interest, especially regarding safety assessment in validation procedures.

Wheelsets rolling normally over a track should have two single contact points, one per wheel. However, the slightly asymmetric position of the wheelset within the track, combined with the tapered wheels, is the source of the *kinematic oscillation* remarked by Stephenson and explained by Klingel and Redtenbacher on straight and curved tracks [Wickens and Iwnicki, 2006]. Moreover, when the vehicle engages in a tightly curved section, the leading wheelsets do not easily follow the track alignment, thus finding themselves in an *underradial position*. Wheelsets undergoing this situation have their axis slightly lagged behind the curve radius, which causes the outer wheel

flange to approach the rail head and come eventually into contact with it. This sliding contact causes an increased, undesirable wear on both the rail head and the wheel flange, being a source of screeching as well [Ayasse et al., 2006]. To reduce the effects of such friction, flange greasers are fitted on the attack wheels of some rail vehicles (almost customarily on tramways and light rail vehicles negotiating very tight curves).

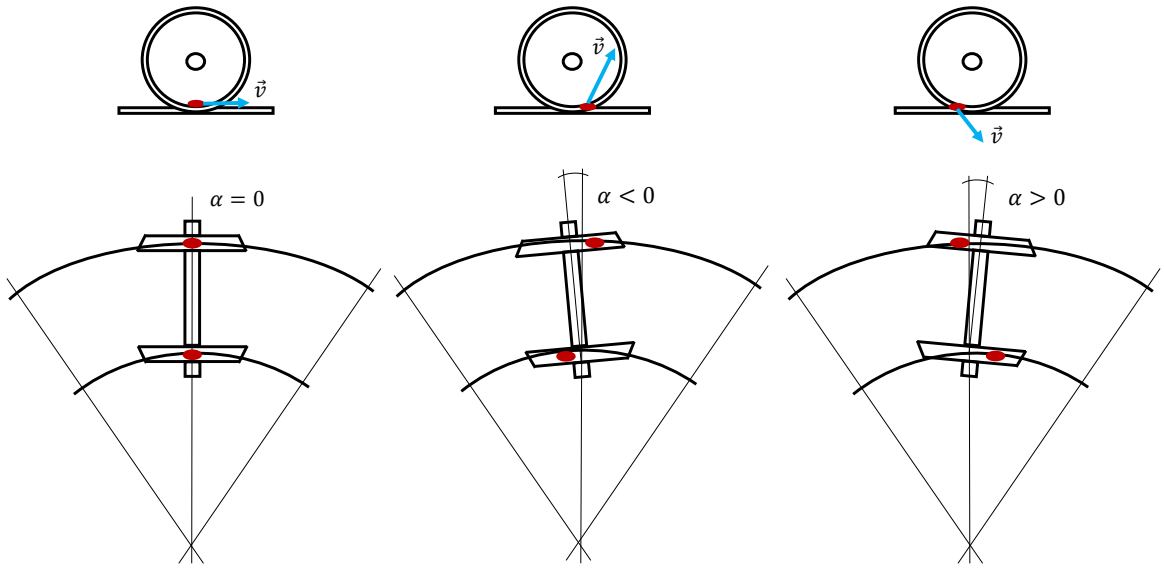

Figure 5.8: Wheelset can adopt several positions with respect to the radius of a curved track. Depending on the positions, two-point contacts may arise, leading to situations where the effort balance over the wheelset is disturbed. Under-radial position may trigger derailment-risk situations.

The interface at the wheel and the rail in Figure (Figure 5.9) shows the typical efforts over the contact patch of a centred wheelset: the *normal effort*, Q, from the vehicle's weight and the *lateral effort*, Y, arising from the rolling stock dynamic behaviour. The addition of the two lateral efforts over the wheelset yield the *shift effort*, ΣY or S. However, the contact points adopt a very different position when the wheelset sways sideways: the contact patch moves from its position right on the tread, approaching the wheel flange. Since both surfaces are strongly non-linear and do not match perfectly, there is a band of relative positions where the wheel and the rail can be in contact on two points, one on the inner side of the tread band, another on the wheel flange. At such a state, the efforts between wheel and rail are transmitted via both surfaces. Moreover,

the flange's pressure against the rail surface generates a vertical effort which, depending on the wheelset's radial position, would be able to trigger a derailment situation.

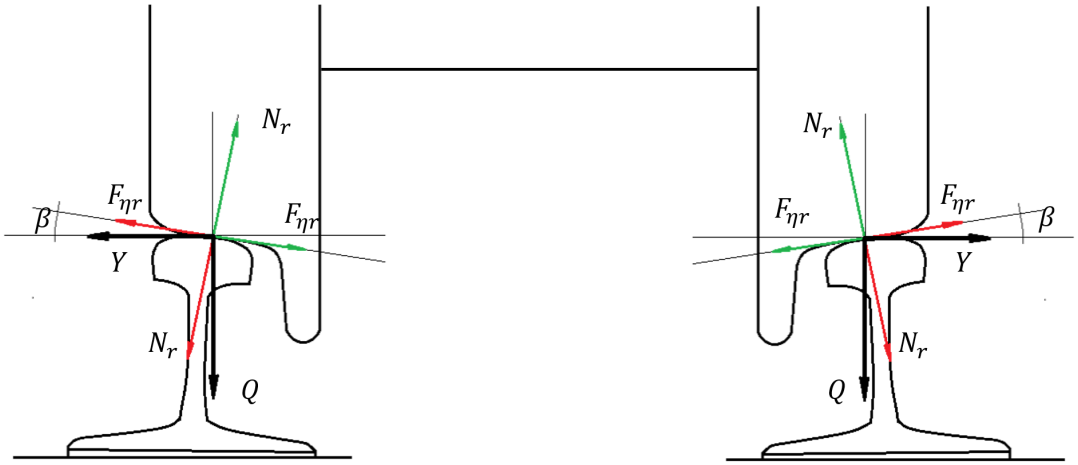

Figure 5.9: Efforts given in the intrinsic reference of the contact point (subscript "r" and "η" efforts). Y and Q are the lateral and vertical effective efforts over the rail, with respect to a general reference frame.

$$Y = F_{\eta r}\cos(\beta) - N_r \sin(\beta) \tag{5.2}$$

$$Q = -F_{\eta r}\sin(\beta) + N_r \cos(\beta) \tag{5.3}$$

From a strictly kinematic point of view, the arising of a two point contact generates an instantaneous rotation center relative to both points. Depending on the wheelset position (*overradial*, *radial* or *underradial*), it allows a downwards, neutral or uplift motion of the axle. The underradial situation is utmost critical, as a vertical load combined with the instantaneous centre of rotation would act upwards. Should the vertical friction load generated on the flange contact reach a critical threshold, countering the vehicle's actual vertical load, the wheel could be lifted upwards. Such uplifting would result in the wheel flange climbing over the rail head and, depending on the context, falling outside the rail, thus effectively leading the vehicle into a derailment situation [Ayasse et al., 2006]. The derailment risk was first assessed by Nadal, who developed his empiric limit (Equation 5.4). The limit was further completed by Weinstock, with

an enriched expression referring to the whole wheelset rather than to each wheel individually (Equation 5.5) [Andersson et al.,].

$$\frac{Y}{Q} \leq \frac{\tan(\beta) - \mu}{1 + \mu \tan(\beta)} \tag{5.4}$$

$$\sum \frac{Y}{Q} \leq \frac{\tan(\beta) - \mu}{1 + \mu \tan(\beta)} + \mu \tag{5.5}$$

A series of surveys and researches conducted by a task group from the UIC, the Office for Research and Experiments (ORE), concluded that self-induced derailment situations shared a common basis: vehicles derailed under empty or small payload conditions, while rolling at low speeds through sections mixing a tight alignment and abrupt changes on the track cant or level between the rails, such as in switch points [Andersson, 2012]. The outcome of these surveys was a derailment test which could be implemented by all the UIC members. First as a real track portion where new rolling stock could be tested and, subsequently, as a virtual test of this track that can be modelled with the appropriate software.

The study of derailment phenomena is still addressed to define better safety indicators and to understand the triggering phenomena [Andersson, 2012] [Cherniak, 2013]. Usually less studied, the derailment behaviour of rolling stock once the vehicle has abandoned its position between the rails has drawn a little less attention. The works by Dan Brabie offer the reader some insight on the situations leading to a derailment and the consequences for the rolling stock. [Brabie, 2005] [Brabie, 2007]. Jha [Jha and Gokhale, 2017] worked as well on the parameters fostering the derailment of express trains.

5.1.2.2 Vehicle dynamics: curving behaviour and instabilities

The assessment of the dynamic behaviour of railway rolling stock via numerical simulations is performed under several premises: some tests are performed under *quasi-static* conditions; that is, the vehicle rolls over an idealized track which induces no transient inputs to the system, excepted the cant transitions at the beginning of the curved sections [Zboinski, 1997]. Therefore, the behaviour shown by the vehicle is its base response, depending on its sole characteristics, which is especially useful to estimate the curving response of the rolling gear and the carbody. Complementary tests with the signature of a real track section permit to assess the behaviour of the train under *dynamic simulations*, corresponding to all the types of alignment which are expected on the vehicle's everyday life.

Kinematic-static curving

Regarding the *quasi-static* behaviour of the rolling stock when negotiating curved track sections, one can distinguish two main aspects of interest: the *behaviour of the rolling gear* under an increased lateral acceleration due to the curving, and the *behaviour of the carbody* in terms of the accelerations perceived at different points of the structure (especially when dealing with passenger vehicles), as well as *gauging constraints*.

The behaviour of the rolling gear is assessed by two parameters related to the wheelsets: the *derailment ratio* (Y/Q) of the outer wheels, which could trigger a derailment situation, plus the *shift effort* (ΣY), whose excess can cause an increased wear of the infrastructure and rolling gear, as well as deformations on the track alignment. The limiting expression for both phenomena are Nadal's limit for the derailment ratio (Equation 5.4) and the Prud'homme formula for the shift efforts (Equation 5.6). α is a train-dependent coefficient which equals 1 for passenger vehicles.

$$\Sigma Y \leq \alpha(10 + \frac{P_0}{3}) \tag{5.6}$$

As for other terrestrial means of transports, railway infrastructure is designed to provide some compensation to lateral accelerations on curved sections. Thus, tracks are built with a cant, according to the curve radius on each section and the desired running speeds (Figure 5.10). Taking the equations from kinematics, and for a given speed, v_{MAX}, it is possible to calculate the lateral acceleration for a given radius, R.

$$\ddot{y} = \frac{v^2}{R} \tag{5.7}$$

If the curve has a certain cant, defined by an angle φ_{tr}, the lateral acceleration can be decomposed in two components according to the track inertial frame: a normal acceleration pointing towards the track plane, plus a lateral acceleration parallel to the rolling plane, which is expected to be compensated by the gravity contribution.

$$\ddot{y} = \frac{v^2}{R}\cos(\varphi_{tr}) = g\sin(\varphi_{tr}) \tag{5.8}$$

In spite of this simple definition, the attribution of a specific cant to a track is far from being immediate. Since the infrastructure is used by multiple kinds of trains, each of them rolling at different speeds, it is not possible to choose a maximum allowed speed to set the track cant. Therefore, the norms allow the trains to roll with a certain amount of uncompensated acceleration. Hence, quicker trains will be authorised to run through the curves at speeds higher than that of the equilibrium, and some excess lateral acceleration (this situation is called *cant deficiency*). Conversely, slower trains will roll at speeds lower than equilibrium, thus being slightly inclined to

the inside of the curve (this situation is called *cant excess*). Infrastructure is made so that trains rolling through it meet all constraints at any situations: both in terms of gauge and acceleration limits (see Figure 5.11).

Cant deficiency is especially important for passenger trains, as lateral acceleration is a source of discomfort for passengers. The design of the trains suspension has also an influence on this phenomenon, as the carbody roll will be fostered or countered, depending on the elements stiffness. Thus, the lateral quasi-static acceleration is the indicator of the rolling stock aptitude on this particular aspect for curving. The limit for safety and comfort is 1,5 m/s^2.

This limit is directly related to another design constraint: the gauge restrictions imposed by the network and the vehicle characteristics (overhead lines feeding a pantograph, for example), which are expressed through the roll coefficient. The roll coefficient, s_R, is defined as the ratio of the vehicle roll angle φ_{cb}, with respect to the track rolling plane, over the track cant angle φ_{tr}.

$$s_R = \frac{\varphi_{cb}}{\varphi_{tr}} \tag{5.9}$$

This coefficient applies only in static conditions. When the vehicle is negotiating a curve, its roll motion is composed of two factors: the vehicle suspension intrinsic flexibility causes a slight sway movement of the carbody over the bogie base, plus the kinematic roll derived from the lateral acceleration. Therefore, the definition of the flexibility coefficient can be derived from the expression of the uncompensated lateral acceleration (a_{ycb}), measured wih respect to the carbody local inertial frame (which is slightly turned due to the carbody roll) and the lateral acceleration (a_y) in the track inertial frame.

$$s_R = \frac{a_{ycb}}{a_y} - 1 \tag{5.10}$$

Hence, since the rolling stock can roll with cant excess or cant deficiency, the vehicle carbody will be subjected to a slight roll motion to the inside and the outside of the curve. This specific motion is countered by the anti-roll bars, which ensure the respect of all constraints. Depending on the vehicles, the gauge constraints are tighter or looser. As an example, some restrictions for passenger vehicles are set as follows: electrically-powered units: $0{,}15 \leq s_R \leq 0{,}25$; passenger diesel-powered units or non-powered passenger vehicles: $0{,}2 \leq s_R \leq 0{,}4$.

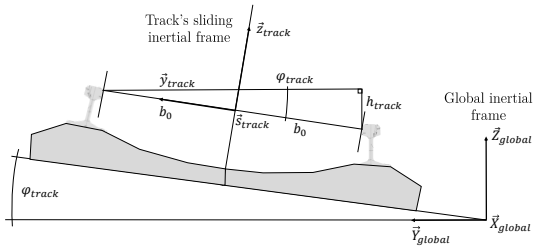

Figure 5.10: Section view of a curved track. φ_{tr} is the track cant angle, h_t is the track cant, and b_0 is the track semi-width.

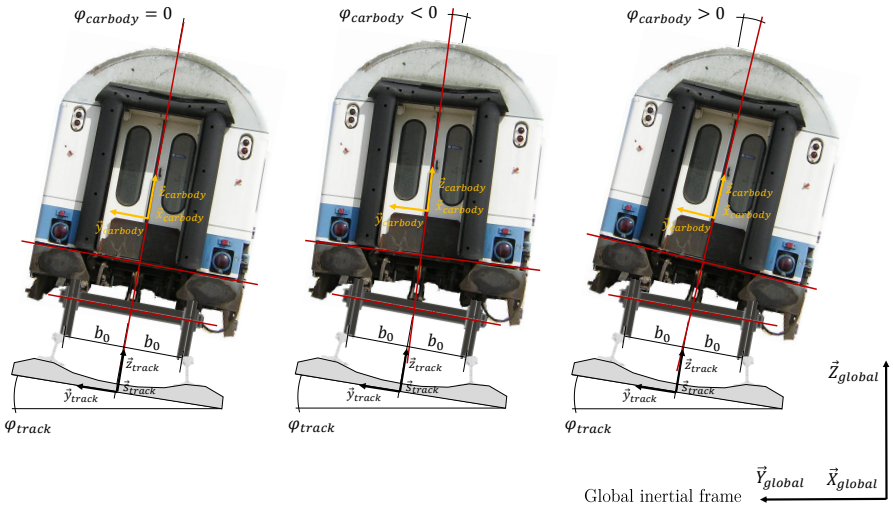

Figure 5.11: Section view of a vehicle rolling a canted, curve track. From left to right, the train is rolling with fully compensated lateral acceleration, cant deficiency and cant excess. *Image by Hanspore, https : //es.wikipedia.org/wiki/Material_remolcado#/media/File : Coche9k.JPG, cut to the section.*

Dynamic behaviour and instabilities

The central interest of the simulations of the *dynamic behaviour* of the rolling stock is to assess the absence of dynamic instabilities on the vehicle at operational speeds. As discussed earlier on the historic perspective, the motivation of the bogie was the unfitness of the rolling stock to cope with the hunting motion of the wheelsets at high speeds [Wickens and Iwnicki, 2006]. Similarly, bogie-fitted vehicles reproduce the hunting instability at the bogie level over a certain

speed threshold [Wickens, 1965]. The triggering phenomena is usually a *lateral impulsion*, be it due to an irregularity, a track apparatus (such as switch blades) or the increasing lateral effort when negotiating a curve. Consequently, the safety indexes which are evaluated rely on the following metrics:

- The *lateral displacement* on wheelsets, bogie frame of carbody.
- The *shift efforts* over the wheelsets via an adapted form of Prud'homme formula ($s\Sigma Y = \Sigma Y/2$).
- The *lateral acceleration on the bogie frame* over the axleboxes, limited empirically by the following equation: $\ddot{y}^{+} \leq 12 + \frac{m_b}{5}$, with m_b the mass of the bogie with all its features, in tonnes (Tn).
- The *accelerations* over the carbody at several points of the structure.

The instabilities are considered to appear at a *critical speed*, where the system is no longer able to dissipate the oscillations, thus showing a *limit cycle* behaviour with constant amplitude oscillations [Zboinski, 1997]. A railway vehicle's *critical speed* depends, virtually, on all the parameters defining the system: the state of the rolling gear, for instance the geometry of the wheel treads (*conicity*), the *loads on the train*, since they define the masses acting on the vehicle; the *characteristics of the suspension elements* of the train; the *track geometry itself*. The literature on railway dynamics has widely addressed these subjects, as described on the points below.

- The *wheel profile conicity* has an effect on the hunting behaviour and on the stability of the wheelset. Klingel's expression shows already the dependence of the wavelength of the *kinematic oscillation* with the *equivalent conicity* as well as the *wheel radius*. Natural wear in service increases this parameter, which causes in turn a lowering of the critical speed [Wickens, 1965].
- The *loading* of the railway vehicle affects the dynamic behaviour as well. The inertial effects differs from an empty vehicle to that of a trainset under crush load. The simplest relation between the frequency of oscillation for a mass-spring system is given for the conservative oscillator ($f = \frac{1}{2\pi}\sqrt{K/m}$), which shows that a higher mass would cause the decrease of the frequency value. Of course, the translation to a railway vehicle cannot be done in such a straightforward manner. However, in a general way, a heavily loaded vehicle would be less sensitive to high frequency vibration, whereas low-frequency perturbations might cause stronger oscillations.
- As regards of the *properties of the suspension elements*, their effect has been widely discussed since Carter's pioneering works. Matsuidara's works in the 1950s first included the effects of non-linearities in the suspension [Wickens and Iwnicki, 2006]. The different elements and

stages of the suspension have separate influences on the vehicle and can depend strongly on its specific characteristics.

- The *primary suspension* characteristics have proved to have an influence on safety parameters [Park et al., 2009] [Xie et al., 2016]. The longitudinal and lateral guiding stiffnesses affect safety indexes, while the vertical influence can affect significantly the *comfort parameters* [Suarez et al., 2013] [Zhou et al., 2014]. Limit cycle oscillations can be triggered while negotiating curves for some variations of the primary suspension, especially for the lateral stiffness [Zboinski and Golofit-Stawinska, 2018].
- Regarding the *secondary suspension*, its characteristics have a recognised influence on the *comfort levels* on the vehicle, which depend of the accelerations over the carbody [UIC513, 1994]. Safety indexes can be affected by damping [Suarez et al., 2013], causing an increase on lateral efforts; strong changes in the anti-roll devices can alter significantly both the safety indexes and the comfort levels [Park et al., 2018].

5.2 Numerical models for rolling stock safety assessment

An introduction to safety assessment on railway vehicles was addressed in Chapter 2, discussing the safety context and the appropriate means to evaluate the aptitudes of a vehicle for validation. Numerical models cannot substitute real-scale tests with the vehicle, although they can be used under certain circumstances. When the numerical model has been compared with real tests and adjusted so as to respond like the real vehicle, it can be fit to assess validation extensions. Consequently, the use of numerical simulations is appropriate for the assessment of the rolling stock behaviour within the frame of these works.

The assessment of the dynamic behaviour of railway rolling stock is enforced by several norms, addressing different aspects related to the vehicle. The *safety evaluation* and the *wear and fatigue* interaction with the infrastructure are addressed by the UIC-518 and the EN-14363 [UIC518, 2009] [EN14363, 2005]. The *comfort aspects* are dealt within the UIC-513 [UIC513, 1994]. Complementary aspects such as the *dynamic gauge envelopes* are dealt in other norms ([UIC505, 2006]). In the present works, the main interest is set on the safety aspects. Therefore, the evaluation of the fatigue indexes and comfort will not be assessed.

The safety indexes which are customary on the evaluation of the safety performances of railway rolling stock are the following:

- Each guiding wheelset ratio of vertical and lateral efforts, $\frac{Y}{Q}$, also known as Nadal's ratio.
- Each wheelset shift effort or sum of guiding efforts ΣY.
- Lateral accelerations over the bogie frame ($\ddot{y}^{+}$).
- Lateral and vertical accelerations over the carbody ($\ddot{y}^{*}$) and ($\ddot{z}^{*}$).
- Lateral quasi-static acceleration over the carbody ($\ddot{y}^{*}_{qst}$).

A complementary index regarding the *gauge restrictions* has been added to the panel of indicators: the *flexibility coefficient*, s_R. It can be defined by two different expressions, depending on its definitions: Equation 5.9 allows the calculation from the carbody roll angle, while Equation 5.10 expresses it as a metric derived from the lateral accelerations over the carbody.

The limiting values for the safety indexes within these works are given in Table 5.1. Some of the indexes may adopt a different value depending on the track alignment or the simulation characteristics and its values are specified accordingly.

The simulation works within this study have been performed with the multi-body simulation code SIMPACK 8.9. The set of models was delivered by Bombardier, and is based on the three

Safety index limits		
Index	**Straight track**	**Curved track**
Y/Q	0,8	1,2
ΣY	68 kN	
sΣY	34 kN	
$\ddot{y}^+$	10,3 m/s^2	
s$\ddot{y}^+$	5,3 m/s^2	
$\ddot{y}^*$	3 m/s^2	3 m/s^2 2,8 m/s^2 (R = 600 m) 2,6 m/s^2 (R = 300 m)
$\ddot{z}^*$	3 m/s^2 or 5 m/s^2 (fault mode)	
s_R	0,21 (pantograph car) or 0,225	

Table 5.1: Safety limits calculated for the specific rolling stock evaluated within this work.

aspects described previously: derailment risk, curving behaviour and dynamic behaviour. There is not a single model, but several cases adapted to fit the needs of safety assessment according to the norm UIC-518. They will be detailed in the following sections.

5.2.1 Derailment

Derailment risk assessment is performed with a single test or simulation. The track is composed of two straight sections of sufficient length, so as to fit a complete trainset within them. Both straight racks are connected trough a curve section of 150 metres of radius, with a 45 mm cant. Its particularity arises from the track layout: the cant of the track is twisted halfway through the curve (-45 mm), from the inside to the outside. This abrupt change should foster an imbalance on the bogie loads, unloading the wheels rolling on the outer rail. A flaw of -55,43 mm on the outer rail level is added immediately after the cant twist. The combination of both effects is expected to cause a lift of the attack wheel and to maximise the risk of derailment (Figure 5.12).

The train is set up to roll under *tare load*, at a *low speed* (no more than 15 km/h), with its secondary suspension deflated. On the one hand, the low speed allows the rolling gear to embrace the flaws on the track, rather than "jumping" over them due to a higher speed and the relatively slow response of the bogie to adapt itself to the track geometry. On the other hand, the low loads reduce the resistance of the rolling gear against lifting, and the deflated secondary suspension provides a stiffer overall suspension, thus fostering derailment phenomena. The train configuration is an eight-car trainset of the Régio 2N model.

The safety indexes which are evaluated under this simulation are the wheels vertical and lateral loads (Q and Y), the derailment coefficient or Nadal's coefficient (Y/Q) and the wheels upward lift (Δz), whose limits are given on Table 5.2.

Derailment - Safety index limits	
Y/Q	1,2
Δz	5 mm

Table 5.2: Safety limits applied on simulations of derailment aptitude.

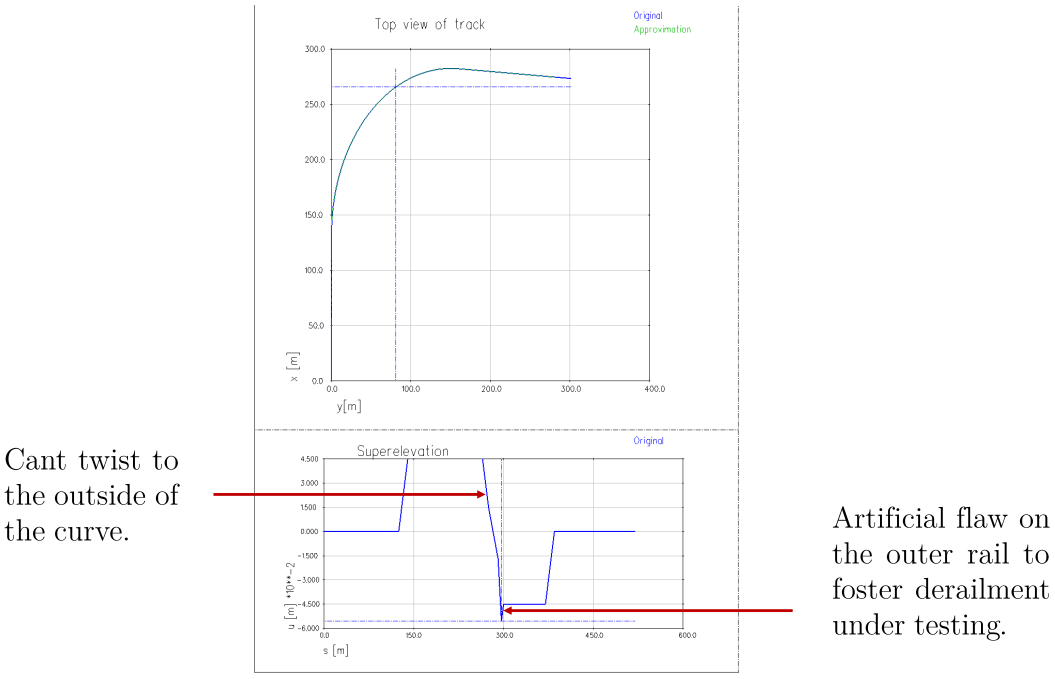

Figure 5.12: The derailment track stretches through a right-hand curve with a twisted cant (as seen on the superelevation graphic).

5.2.2 Curving performance

The trainset curving behaviour is characterised through a series of tests performed over a base model. The vehicle rolls through an "S-shaped" track section: two straight tracks long enough to host the whole trainset are linked by a curve/counter-curve alignment with a common radius of 300 metres. Each curved section is preceded and followed by a clothoid transition zone, and both curved sections are separated by a small straight section (see Figure 5.13). The total length of

the track is of 2000 metres. The track has no real irregularities. The conditions for this tests are dubbed "*quasi-static*", because the train runs at a constant speed, the track does not generate any transient inputs other than the transition curves. This situation is dubbed as well "kinetically static" [Zboinski, 1997]. Therefore, the observed behaviour will be a result of the rolling stock properties (mechanical properties of its components, etc.) and will not be influenced by random parameters such as, for example, track irregularities.

Trains negotiating curved track sections must comply to two core aspects: safe rolling and gauge restrictions. Since the rolling stock can run through a curve at a wide range of speeds, there is a special interest on assessing the train behaviour at different speeds, namely in terms of the lateral uncompensated acceleration. The limit for lateral acceleration is 1,5 m/s^2. Since the curve radius "R" is known, as well as the track cant "h", one can calculate the theoretical speeds at several fixed acceleration levels. Using the formulation 5.11, where "g" is the gravity constant and "b_0" the track half-width, several speeds have been obtained as an input on this curving behaviour model. The acceleration levels were set at even intervals of 0,25 m/s^2 (see Table 5.3).

$$v_{comp}^2 = R(a_y + \frac{hg}{2b_0}) \tag{5.11}$$

Acceleration level [m/s^2]	**Speed [km/h]**
0	50,43
0,25	59,29
0,5	66,98
0,75	73,88
1	80,19
1,25	86,04
1,5	91,51

Table 5.3: Analytically calculated speeds for curving behaviour assessment.

Curving - Safety index limits	
Y/Q	1,2
ΣY	68 kN
$\ddot{y}^{+}$	10,3 m/s^2
$\ddot{y}^{*}_{qst}$	1,5 m/s^2
$\ddot{y}^{*}$	2,6 m/s^2
$\ddot{z}^{*}$	5 m/s^2
s_R	0,21 - 0,225

Table 5.4: Safety limits applied on simulations of kinetically static curving behaviour.

Railway norms define some orientations for curve design, regarding the possible combinations of speed, cant and curve radius [UIC703, 1989]. These rules allow a quick verification yielding the maximum top speed for the set of data. On this present case it was set at approximately 80 km/hour. Therefore, some of the runs which are simulated fall beyond operational limits. Nevertheless, the cases above 80 km/h remain useful, for they provide an insight on the train behaviour over its usual operation limits. Regarding the acceleration levels, maximum theoretical lateral accelerations might not be reached under normal service conditions because of the speed restriction. However, the acceleration levels endured by the passengers will not match exactly the values used to set the test speeds. As the train suspension is composed of two levels, it has an intrinsic flexibility which makes it sway laterally in curves. Since the kinematic calculation of the acceleration does not take this phenomenon into account, the values will be slightly under the predicted behaviour. Furthermore, it is possible to perform a linear regression between the measured roll coefficients and the acceleration levels on fully stabilized curve rolling, obtaining the vehicle sway coefficient (i.e. the suspension intrinsic flexibility coefficient).

The train configuration is a six-car trainset of the Régio 2N model, with its secondary suspension inflated, running under an extraordinary load. This loadcase maximises the inertial effects over the trainset carbodies, thus fostering roll motion when engaged in curves. Its is expected that these conditions constitute the most exigent loadcase in terms of lateral accelerations and risk of non-respect of gauge restrictions.

The safety indexes which are evaluated under this simulation are the wheels' vertical and lateral loads (Q and Y), the derailment coefficient or Nadal's coefficient (Y/Q), the shift effort over the axles (ΣY), the lateral accelerations over the bogie frame ($\ddot{y}^{+}$) and carbody ($\ddot{y}^{*}$) and the gauge restrictions through the flexibility coefficient (s_R). Within the DYNABOG project, the trainset which has been chosen has powered units with pantographs and passenger coaches. The roll coefficients for each kind of carriage are 0,21 for power units and 0,225 for non-powered cars. The limits for the indexes in this particular simulations are detailed in Table 5.4.

5.2.3 Dynamic behaviour

The characterisation of the vehicle dynamic behaviour demands a thorough analysis of all the possible situations that the rolling stock might encounter during its life-cycle [UIC518, 2009]. Both the evolution of the train characteristics and the infrastructure are taken into account: the train wheels bear two different conicities "λ" (new wheel treads and worn wheel treads), plus several track alignments, all of them with a real track input signal. Moreover, the trainset behaviour will be assessed under different payload conditions. The different models that are used are condensed in the Table 5.5.

Track layout		**Load cases**	
Straight track, v = 176 km/h	$\lambda = 0{,}05$	VOM	CE8
	$\lambda = 0{,}34$	VOM	CE8
Curved track. R = 300 m	v = 82 km/h	VOM	CE8
Curved track. R = 600 m	v = 127 km/h	VOM	CE8
Curved track. R = 1200 m	v = 155 km/h	VOM	CE8

Table 5.5: VOM stands for French "Ready-to-go vehicle" ("Véhicule en Ordre de Marche"), CE8 stands for French "Exceptionnal load of 8 passengers per square metre" ("Charge Exceptionnelle de 8 passagers par mètre carré").

The track layout on all the simulations has a length of 2000 metres, with an input signal from a stretch of the Köln-Minden line between Rheda and Oelde (North Rhine-Westphalia, Germany). This input signal is set on all the simulations, be their track straight or curved sections. Straight track sections have a complementary input in the form of a lateral alignment flaw, which provides a lateral impulsion as a switch blade would cause in a real scale case. The wheels conicity has also an influence over the vehicle stability, hence the simulations of two extreme cases (new and worn wheel treads). Therefore, the lateral impulsion is especially set to trigger the train oscillations. Should a critical mode be excited by the combination of speed and the impulsion, it would be easily detectable through the safety indexes and the signals recorded on the simulations. Curve simulations combine the effects of a curved section plus the irregularities of the track, in a wide range of cases: tight (300 metres), medium (600 metres) and large (1200 metres) radii. Curved tracks consist of two straight sections, followed by an S-shaped curve/counter-curve part. All curves have transition sections and a small straight transition between the right-hand and the left-hand curve.

The train configuration is an six-car trainset of the Régio 2N model, with its secondary suspension inflated. Two load cases will be considered: tare load (VOM) and exceptional load (CE8). The response obtained from the simulations on both states will provide an insight on the limits of the vehicle dynamic behaviour. The speeds are set up so that the train rolls at a speed which is 10% higher than the maximum authorised speed for each simulation. This practise grants a safety margin for operations: should the vehicle undergo a critical vibration cycle or have an eigenmode excited at the simulations speeds, it would be triggered over the topmost operational speed. Thus it would be unlikely that it could be triggered under normal operation.

Safety index limits		
Index	**Straight track**	**Curved track**
Y/Q	0,8	1,2
ΣY	68 kN	
sΣY	34 kN	
$\ddot{y}^+$	10,3 m/s^2	
s$\ddot{y}^+$	5,3 m/s^2	
$\ddot{y}^*$	3 m/s^2	3 m/s^2 2,8 m/s^2 (R = 600 m) 2,6 m/s^2 (R = 300 m)
$\ddot{z}^*$	3 m/s^2 or 5 m/s^2 (fault mode)	
s_R	0,21 (pantograph car) or 0,225	

Table 5.6: Safety limits for the simulations of dynamic behaviour of the rolling stock.

The safety indexes which are evaluated under this simulation are the wheels vertical and lateral loads (Q and Y), the derailment coefficient or Nadal's coefficient (Y/Q), the shift effort over the axles (ΣY), the lateral accelerations over the bogie frame ($\ddot{y}^+$) and carbody ($\ddot{y}^*$) and the vertical accelerations of the carbody ($\ddot{z}^*$). Gauge restrictions are not evaluated within these simulations. Furthermore, the simulations over curving sections are performed under clear cant deficiency conditions. Nevertheless, these simulations provide valuable information regarding the dynamic behaviour of the rolling gear, regardless of the gauge performances. The limits for these values are detailed in Table 5.6.

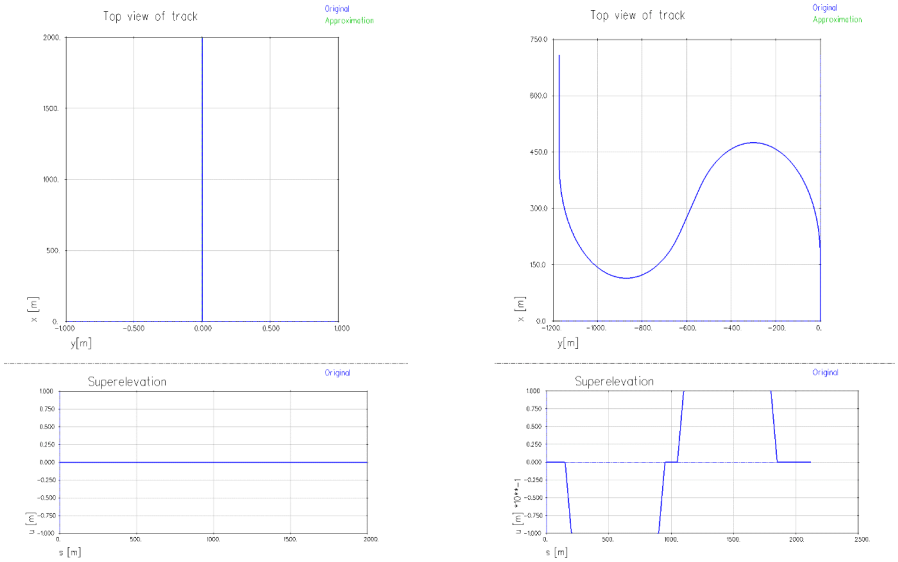

Figure 5.13: The straight track stretches 2 km with a lateral alignment flaw to induce and excitement cycle on the vehicle. The curved track takes two consecutive curves, right and left-hand, both with radii of 300 metres and a superelevation of 100 mm. This "S-shaped" track section is also used for curving behaviour assessment simulations.

5.3 Preliminary tests

Prior to the draft of the set of simulations under variability, it is necessary to tune the models recovered from Bombardier. The objective is to have a better knowledge of the modelling of the trainset and of the software characteristics. A special stress has been put on the management of the inputs for the simulations, to guarantee the likeliness of the simulations with respect to the actual behaviour of a full-scale Régio 2N EMU trainset.

5.3.1 Sensitivity to the wheel-rail contact properties: friction coefficient

The numerical modelling of railway vehicles requires the definition of a wide ensemble of parameters. In order to ensure the vehicle correct behaviour when travelling over the simulated tracks, an accurate modelling of the contact between the rails and each wheel must be performed. The contact between the rails and the wheels does not concern exclusively the wheels' treads (*one-point contact*), but the wheels' flanges as well (*multi-point contact*). Since the wheelsets hunt laterally across the track because of their tapered form, the flange can come into contact with the rails' head. Moreover, the flanges' contact with the rail head is frequent when the rolling stock negotiates curves, as the lateral efforts over the wheelsets tend to shift them against the outer rail.

This is a cause of heavy wear on both the wheels and the rail, as well as being a source of noise. The efforts arising from these interactions have a key role defining the vehicle behaviour, having a topmost importance when assessing derailment conditions.

The definition of the contact problem can be structured through several stages [Bosso et al., 2013]. First, the *evaluation of the contact geometry* allows to obtain the position of the contact patch on both the wheel and the rail profiles. The profiles of the wheels and rails are normatively defined, yet they constitute complex geometries, usually defined point by point. The software SIMPACK manages the contacts through a cross-evaluation of a set of tables of both geometries, thus yielding the point or points where both geometries interact. The resolution of the *normal problem* leads to the definition of the contact patch and the loads' distribution. The final steps solve the kinematic conditions around the contact and the tangential efforts arising from the wheels' adherence, thus involving a friction coefficient at the interface. SIMPACK offers several methods to solve the contact problem, as well as different ways to handle the friction coefficient: *constant* friction, *variable, profile sway (y) dependent* friction, *track, s-coordinate dependent* friction.

Derailment test – $\mu = f(y_{wheelset})$ Derailment test – $\mu = const.$

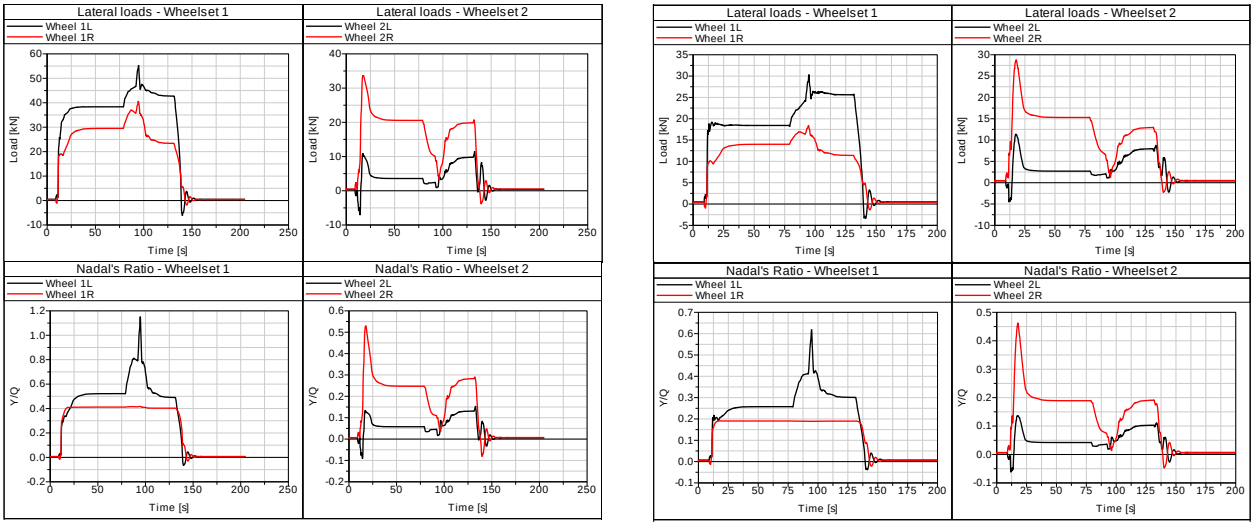

Figure 5.14: Constant friction results in lower peak values and derailment risk, while variable friction coefficients yield a more accurate result, according to real-tests feedback.

Providing an accurate definition of the friction coefficient is a major issue, for it conditions the real-likeliness of the model behaviour. Within the current framework, several simulations were conducted with two different types of friction coefficients: *constant* ($\mu = 0,4$) and *variable, profile dependent*. The latter coefficient is defined as a series of values along the wheel lateral profile. Several control points have an associated friction coefficient, the intermediate values being linearly interpolated between the interval extremities. The variable friction coefficient evolves from $0,36$ at the flange to $0,4$ and $0,45$ at the base and the centre of the wheel tread. Thus, the tangential efforts will be calculated differently depending on the position of the contact patch, as the friction coefficient will not have a single value.

The lateral efforts and the derailment ratio (Nadal) show a strong dependence to the friction coefficient. The results in Figure 5.14 show that, for two equivalent derailment assessment simulations, a constant friction coefficient diminished the peak lateral efforts, as well as Nadal's ratio. However, the feedback provided by Bombardier stated that a simulation of such kind should yield values of Y/Q of around 1, matching full-scale results obtained from tests conducted over a twisted track. Therefore, the profile-variable definition of the friction coefficient will be preferred and kept throughout the rest of the present works.

5.3.2 Sensitivity to single, structural element failures: primary coil spring breakdown

The FLEXX Compact bogies are fitted, as it has been shown previously, with two primary suspension elements on each side of the axle-boxes. The inner axle guiding element, a rubber-to-metal spring (PSi), and a coil spring on the outer part (PSo). The latter vertical stiffness is of most importance to ensure the adequate transfer of vertical efforts to the axle-box and, consequently, to the wheel and the contact patch with the rail. The coil spring structure consists on two concentric coil springs, supplying respectively 76 and 24 % of the global stiffness of the element. Therefore, a lack of mechanical resistance on a primary coil spring could cause hazardous situations on the rolling stock. The breakdown of a single primary coil spring has been modelled on *eight* different scenarios. Each case corresponds to the cracking of the stiffest of the two concentric springs, thus yielding a remaining stiffness of 24 % of the nominal value. The failures are reproduced over the bogie elements of the leading car of the train (bogies B1 and B2). The element references are referenced on the form "PSo + axle # + L(eft)/R(ight)". Each of the eight configurations has been tested through the numerical models for derailment, curving behaviour and dynamic behaviour assessment.

The failure of a primary coil-spring has a *major* impact on the vehicle behaviour under derailment test conditions. The dramatic decrease of stiffness over an element causes a load imbalance on the affected bogie, which turns the rolling stock prone to derailment. When the failing element is

placed over the attack wheel on the outside rail of the curve, the derailment ratio clearly surpasses the limit of 1,2 for curves, transitions and special tracks. Other critical cases relate to the failure of the conjugate suspension element with respect to the leading attack wheel (i.e. opposite wheel on the opposite axle, see Table 5.7). The uneven stiffnesses cause an imbalance of the bogie loads, with the three unaffected element absorbing the excess loads which are no longer withstood by the failing PSo. As a matter of fact, the element failure does not merely affect its immediate environment, but it spreads its effects across the carbody and to the neighbouring bogies. If one takes the trainset attack wheel as the reference point, its safety indexes are especially sensitive to the failures of its fellow element on the bogie diagonal. Furthermore, coil spring failures on the right side of the 2^{nd} trailer bogie shift the attack wheel Y/Q ratio over the limits, replicating the "diagonal" pattern.

Failing element	**Bogie 1**				**Bogie 2**			
	1L	1R	2L	2R	1L	1R	2L	2R
PSo1L B1	3,0935	0,4313	0,173	0,5377	0,7132	0,4159	0,263	0,5312
PSo1R B1	0,8231	0,4144	0,084	0,4449	1,0928	0,4184	0,1911	0,364
PSo2L B1	0,805	0,4173	0,0997	0,3881	0,7126	0,4159	0,2632	0,5348
PSo2R B1	1,3046	0,4159	0,1047	0,7207	0,6861	0,4166	0,1922	0,3658
PSo1L B2	0,9464	0,4153	0,1537	0,5915	2,9745	0,4288	0,2506	0,4602
PSo1R B2	1,315	0,4182	0,1066	0,4334	0,5545	0,4175	0,2162	0,4514
PSo2L B2	0,9975	0,416	0,1519	0,5469	0,7753	0,4186	0,1338	0,2049
PSo2R B2	1,2002	0,4177	0,1243	0,4571	0,9069	0,4168	0,2979	0,9267

Table 5.7: Scores for Nadal's ratio (Y/Q) under derailment conditions for single failures on a 1^{ary} coil spring.

The stiffness decrease reduces the resistance of the first stage of the suspension, thus causing an additional deflection over the affected axle-box. Such effects have a special relevance for the analysis of the train curving behaviour. Lateral efforts are specially concerned, the shift efforts over an affected wheelset raising by more than three times the reference values (see Figure 5.15). The effect of the increased lateral efforts becomes evident on the registers of the lateral acceleration, higher than those of the reference model. We have observed as well that the train overpasses the limits set for the flexibility coefficient, thus overpassing gauge restrictions for this specific rolling stock. As a general rule, this happens when the failing coil spring coincides with the outer side of the curve. The bogie frame sinks when negotiating the curve, lowering the carbody base, which then rolls excessively.

The study of the impact of a coil spring failure on the trainset dynamic behaviour simulations has shown some interesting effects. The numerical simulations over a *straight track* display that the

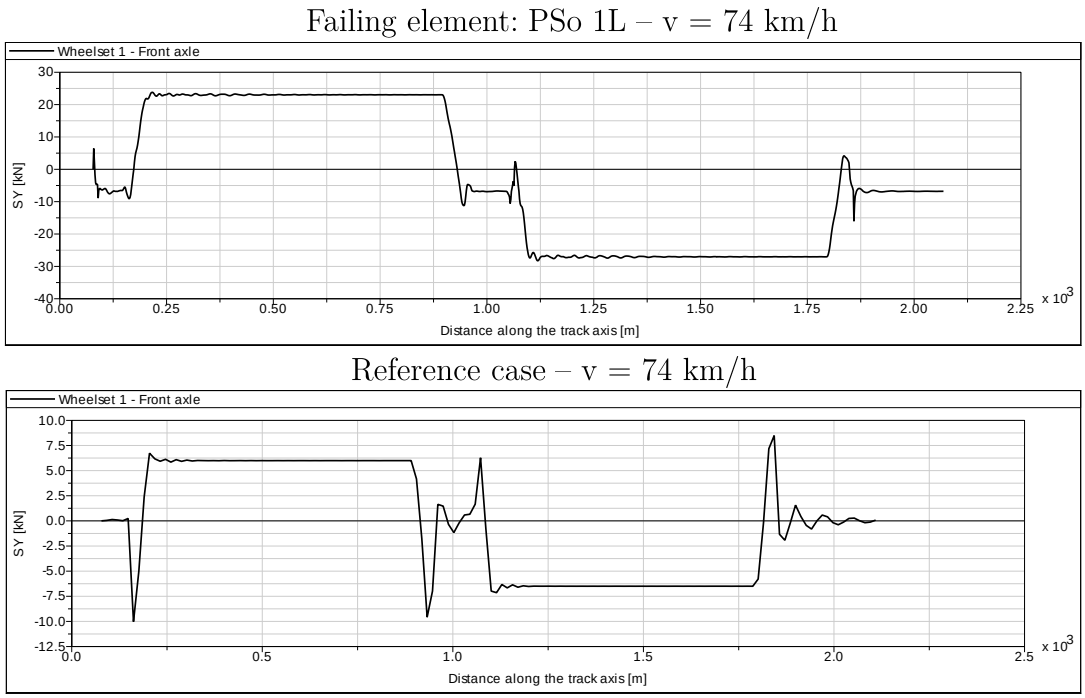

Figure 5.15: The effort increases sharply due to the failing coil spring on the left side axlebox.

load imbalance (see Figure 5.16) over the failing bogie takes generally a cross-shape distribution. Thus, the failing element and its conjugate are unloaded, while the elements on the opposite diagonal endure extra efforts, compared with reference simulations. The effects are transmitted to the other bogie across the carbody, leading to an increase of loads on the side of the failing coil spring (i.e. a right-side failing element on the head bogie leads to an additional overload of the right-side coil springs on the trailing bogie). In addition, several safety indicators such as the shift effort over the bogies and the acceleration over the axle-boxes show an increase of the vibration levels superposed to the reference behaviour. Moreover, shift efforts increase by 2 to 3 kN when presenting a flaw on one coil spring. The carbody placed over the bogie with the failing element undergoes additional roll motion when facing lateral excitation from the track (alignment flaws).

The effects of a coil spring failure can have a stronger impact depending on other concomitant factors, such as the load state of the rolling stock or the wheels conicity. Heavier vehicles are less sensitive to track irregularities because of their higher inertia, yet their curving behaviour becomes critical, as the inertia of the carbodies can cause excessive sway or roll motion. As regards of the wheels conicity, it is directly related to the wheelsets kinematic hunting motion [Wickens, 1965], thus having an influence on the vehicle dynamic performance.

Reference case – v = 176 km/h

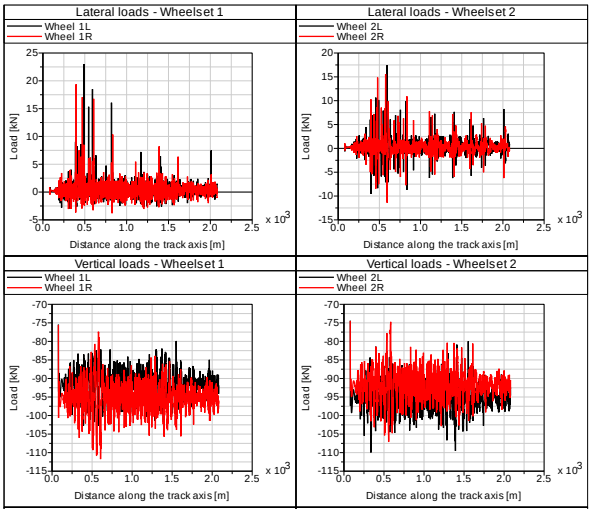

Failing element PSo 1L – v = 176 km/h

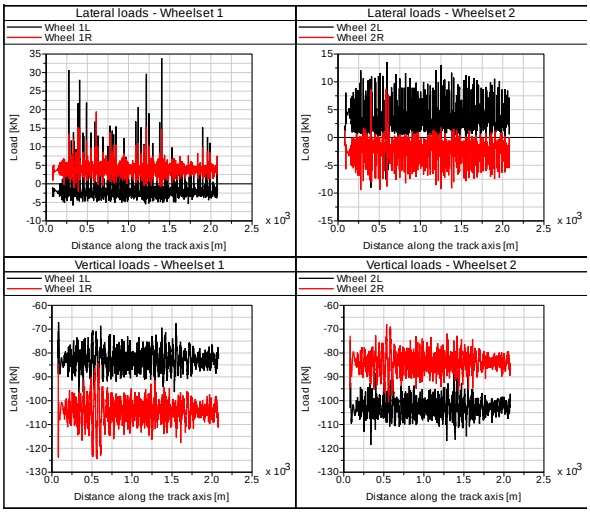

Figure 5.16: Lateral (Y) and vertical (Q) efforts calculated by SIMPACK at the four contact points of the leading bogie for both the reference (left) and one coil spring failure (right) cases. The shift on the quasi-static effort levels for the failure simulation is clearly noticeable.

To summarize, the numerical models that have been provided by Bombardier show a sensitivity to the failure of a suspension element, modelled through the change of its constitutive properties. Moreover, the safety indexes measured during the simulations are affected by the changes on the properties. The model can handle situations of critical risk (for instance, derailment), showing an appropriate score according to the kind of risk. Therefore, the modelling of the chosen rolling stock is suitable for our purposes in terms of sensitivity to single-failure, structural element cases.

5.3.3 Sensitivity to dissipative element failures: lack of damping

FLEXX Compact bogies are equipped with several dashpots which supply dissipative capacities on both the primary and the secondary suspension. Four dampers are placed in parallel to the primary suspension elements around the axle-boxes, while two/four shock absorbers (for extremity/intermediate bogies) link the bogie frame with the vehicle carbody. A lateral dashpot

links the bogie pivot with the bogie frame, damping lateral motion. Yaw dampers are also present on the end bogies and across the whole trainset for the versions rolling at top speeds of 200 km/h. According to the customers feedback and Bombardier internal reviews, it can be expected that a dashpot may lose up to 35 % of its damping capacities. Thus, two kinds of sensibility tests have been analysed preliminarily: the failure of a *single* damper and a *generalized loss* of dissipative capacities over the trainset.

In the case of a sudden loss of damping capacities over an axlebox, the effects are mainly noticeable on the simulations with a dynamic assessment purpose, for the derailment and curving/flexibility coefficient simulations are performed under quasi-static conditions. The lack of damping causes an excess oscillation over the affected axlebox, thus affecting the wheel-rail contact efforts (see Figure 5.17). The peak effort measured on the contact point has almost doubled with respect to the reference calculations. The higher lateral efforts result on an increase of the shift effort over the leading wheelset of almost 2 kN, yet in spite of the strong increase, all safety indicators remain below the normative limits.

As a matter of fact, the effects of a global loss of damping properties (i.e. a shared decrease of dissipative effects of the dashpots) do not imply a strong drift on the safety indicators. It seems that a single failure has a higher impact on some metrics than a commonly-shared degradation across all suspension elements. The failure of dissipative elements has been estimated as an interesting aspect to model, thus being included as a generalized condition in the numerical simulations within these works.

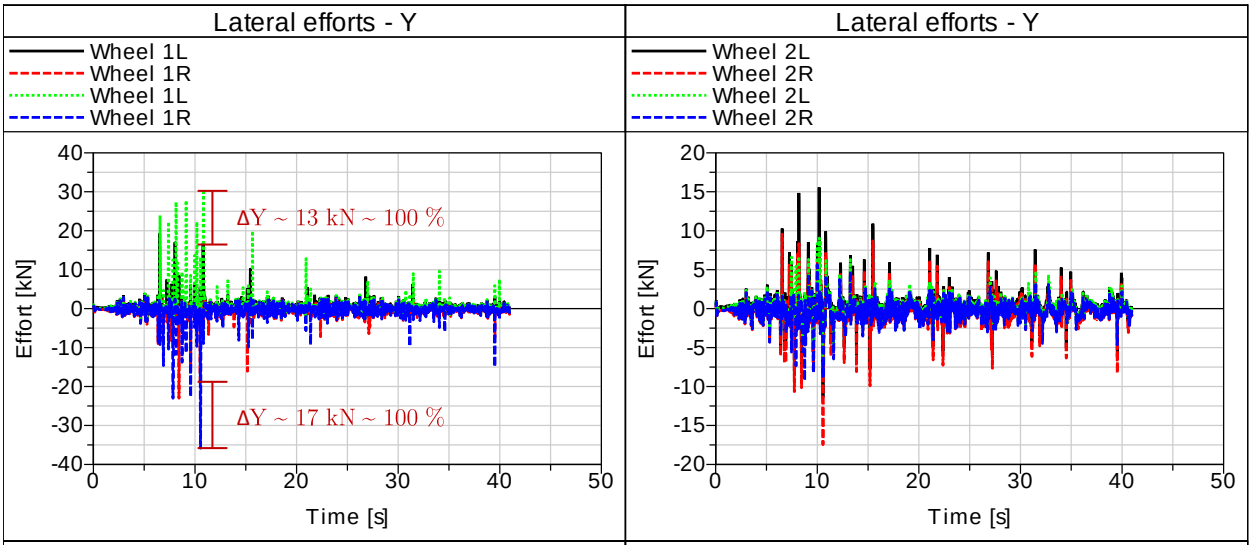

Black/Red → Efforts over the left/right wheels on the reference configuration.
Green/Bleu → Efforts over the left/right wheels with a front, left damper failure.

Figure 5.17: Lateral (Y) efforts calculated by SIMPACK at the leading wheelset contact points of the head bogie for a front, left-side damper failure case. The increase on the peak efforts is clearly noticeable on both sides of the wheelset.

5.4 Simulation on non-deterministic variability

5.4.1 Simulation plan

The suspension elements selected on Chapter 2 are the subject of the fault simulations which have been undertaken with the numerical models presented on the previous paragraph. The mechanical characteristics of the rubber reference described in Chapter 3 have led to the study of the changes on the properties of the *primary rubber spring*. These were determined on Chapter 4, allowing an estimation on the variability levels of the properties, which will be used to set up the dynamic simulations.

The evolution of the properties of the suspension elements can be observed as a *homogeneous change*. The natural ageing of the base materials and the mechanical wear and fatigue, affect all the elements. Since the vehicle does not have a preferential mode of operation, such a change would be evenly distributed on all suspension elements (the train does not run over a loop line, nor in a fixed sense). However, random interventions may appear as the result of a sudden replacement of a faulty suspension element. Since the bogie has a symmetric structure, the organs surrounding a wheelset must have the same properties. Thus, a flaw on a suspension element forces the replacement of the homologue elements to keep the properties balanced. A combination of replaced and aged suspension elements on a bogie would constitute a *heterogeneous change*.

Variation levels - Expected scenarii

The study of the variability in Chapter 4 has shown that the stiffness of the primary rubber springs evolves in a range from its nominal values up to an increase of stiffness of about 25 to 30 % of the nominal value. The intrinsic variability for a single thermal ageing configuration has shown that the stiffness values obtained from the same temperature and times of exposure may vary ± 3 % points around the average increase. Since the variations observed spread over a varied range of increments, a decision was taken to simplify the levels of simulation which were chosen.

- Bombardier specifies in the technical requirements, agreed with the suppliers of suspension elements, a tolerance margin on the element's properties, which can rank up to ± 15 %, but the scatter on the properties is, in practice, much narrower.

  Therefore, a *first stiffness increase level* has been fixed at +15 % of the nominal value, with a tolerance band of ± 1,5 % points centred on the base increase.

- As regards of the higher increments observed in the thermal ageing, they rank between 25 and 30 % of the nominal value. Thus, it was decided to fix an *second stiffness level* at +30 % stiffness with a wider tolerance band of ± 3 % points, centred on the base increment as well.

The two chosen levels have a *reference state* (brand-new train, no variability) added to the analysis. These variability levels constitute the basis for the dynamic behaviour assessment of a trainset equipped with FLEXX Compact bogies.

Variation levels - Complementary scenarii

The robustness assessment of the FLEXX Compact bogie is at the core of Bombardier's interests during these project. Once the base guidelines for dynamic tests had been established, several complementary cases were brought up to explore the behaviour of the system under extreme conditions. Three cases have been retained, *a possible loss of stiffness* and *two extremely stiffened suspensions.*

- The loss of mechanical stiffness of a suspension element can be a consequence of the fatigue and damage of the base materials. Bombardier practises already enforces fatigue tests as part of the supplying process, determining long-cycle tenure of its components. Even though the results on the parts have always been positive, the idea of testing a *degraded operation mode* was retained. A level of -30 % stiffness was retained as a possible (yet unlikely) degraded mode. A tolerance band of ± 3 % points, centred on the base increment, was applied as well.
- A strong increase on the stiffness of the rubber-based compounds appears as an unlikely event. However, the loss of a part of the rubber, forcing the elements to adjust in a degraded, dry-bumpstop situation, could redefine the base stiffness which is declared (steel is much stiffer than rubber). Therefore, there was an interest on testing two complementary situations under very strong stiffness increases:
  - A first stiffness increase level has been fixed at +50 % of the nominal value, with a tolerance band of ± 5 % points centred on the base increase.
  - A second stiffness increase level has been fixed at +80 % of the nominal value, with a tolerance band of ± 8 % points centred on the base increase.

Stiffness increments	
Base increase	Tolerance band
-30 %	-33 % to -27 %
15 %	13,5 % to 16,5 %
30 %	27 % to 33 %
50 %	45 % to 55 %
80 %	72 % to 88 %

Table 5.8: Stiffness increases and tolerance bands to set up the dynamics simulations, based on experimental results and agreed with Bombardier.

The set of new-state simulations was launched at a first stage to recover the vehicle's validated behaviour and to set up the reference state. These simulations have predefined suspension properties, corresponding to a new vehicle and set up by Bombardier's dynamics engineers. Therefore, the calculations were *deterministic*, as the inputs were arbitrarily chosen. The set up of the simulations with increased stiffness has been addressed under a different premise: the inputs would be *non-deterministic*, that is, there would be no arbitrary choice on the definition of the suspension properties. Instead, an algorithm has generated an appropriate ensemble of increase rates, one per each of the suspension elements within the model.

The simulations with *homogeneous changes* were set up by performing *ten random shots* on each global increase level, generating a total of *forty random suspension configurations*. The random increase rates have been applied to their respective suspension elements, thus effectively creating forty train configurations to be tested on each of the eighteen SIMPACK models. The total amount of homogeneous simulations was of **868 individual calculations**. The set up of the ensemble of models and their inputs with the MBS software SIMPACK has required the use of an automatised script, generating the variables and modifying the base models to set up the new inputs. The launching and post-processing of the simulations was controlled by a second script tool, developed by Bombardier and modified to the purpose of these works. A final post-processing script gathered the results from each calculation, preparing their exploitation on a series of Excel templates. For a detailed explanation of the simulation work flow, the reader is invited to refer to [Malo Estepa, 2017].

5.4.2 Derailment aptitude results

The change on the stiffnessess of the primary rubber spring and the auxiliary spring has a direct influence on the vehicle's performance on derailment tests. The test is performed with the secondary suspension of the trainset under *deflated mode*. Therefore, the overall suspension chain is stiffer than in normal operation mode.

Expected variation scenarii

The derailment coefficient Y/Q evolves linearly with the increase or decrease rate of the suspension stiffness, proportionally to the evolution of the stiffness. The increase of the suspension stiffness rises the coefficient, but the increase does not overpass the limits set for this precise simulation (Figure 5.18). Therefore, the current design of the FLEXX Compact can cope with stiffness increases up to +30 % of the components base stiffness, remaining safety-compliant.

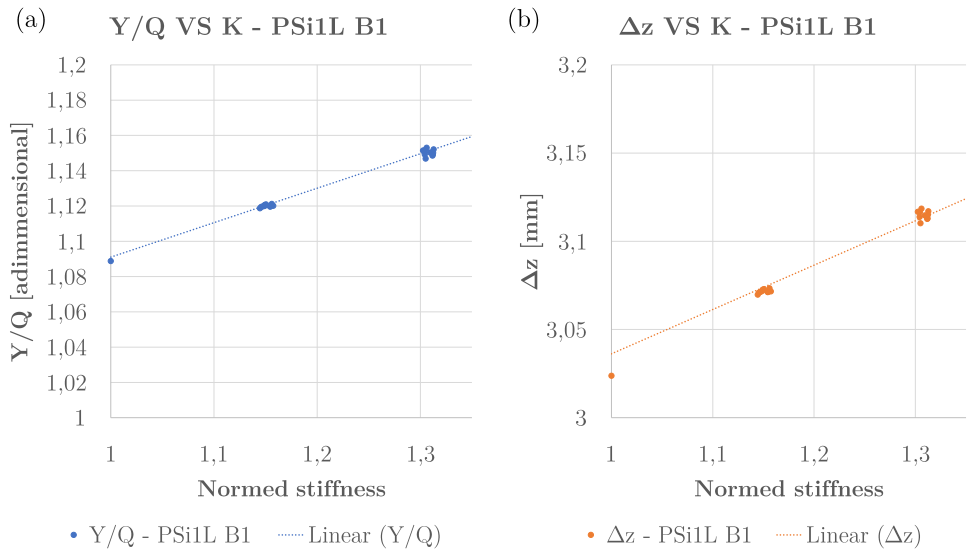

Figure 5.18: (a) Derailment ratio increase with increasing stiffness, measured on the leading attack wheel. (b) Wheel lift increase with increasing stiffness, measured on the leading attack wheel.

Complementary variation scenarii

In the case of the complementary scenarii discussed previously, it appears that softer rubber-to-metal characteristics tend to lower the safety indicators, as observed for the -30 % decrease (Figure 5.19). The increase of the suspension stiffness over +30 % shows some shots which have reached

the safety limit at +50 %. However, the complementary indicator given by the wheel lift (Δz) shows that the wheel does not raise above the rail more than 5 mm at any case, as shown on the orange curves. Moreover, the stiffness increase rate is much higher than reasonably expectable and unlikely. Consequently, the risk of derailment can be considered as partial, but must be controlled to prevent any dangerous situations.

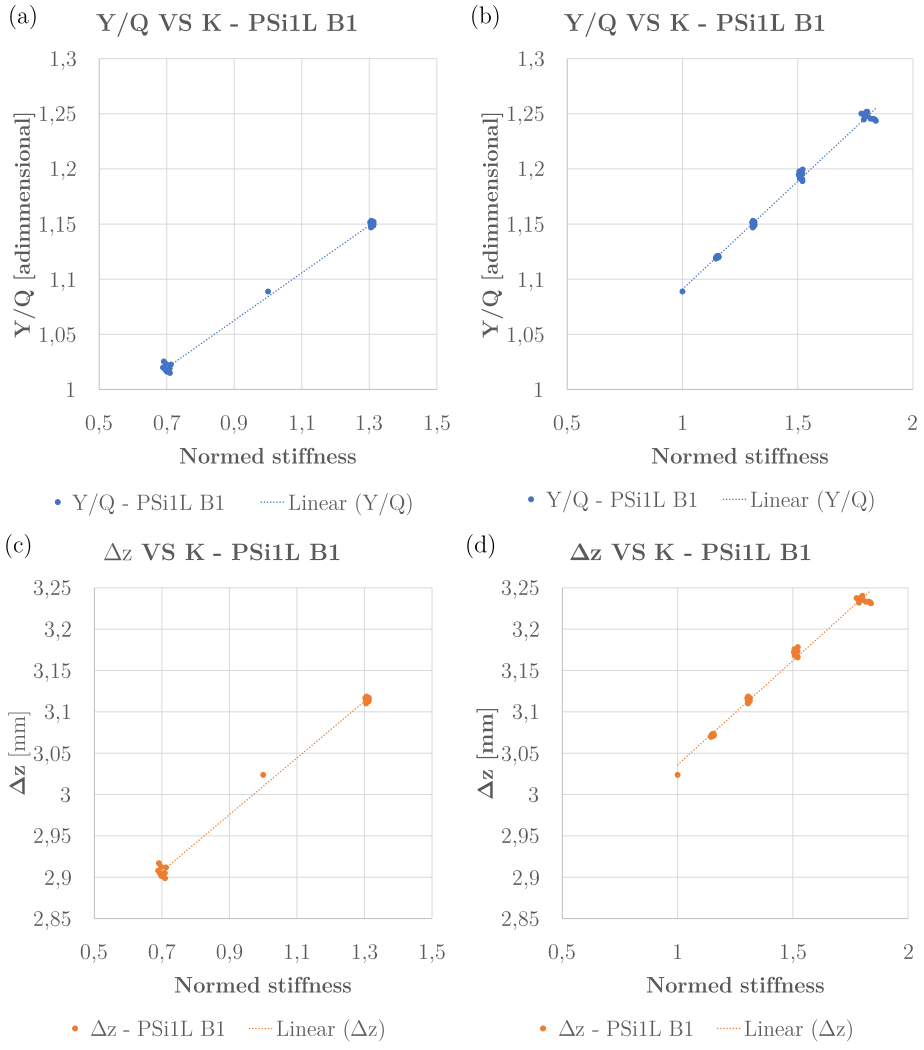

Figure 5.19: (a) Derailment ratio decrease with lower stiffness, measured on the leading attack wheel, compared to its increase counterpart. (b) Derailment ratio increase from brand-new to extremely unlikely increases of stiffness, over the attack wheel (c) Wheel lift decrease with lower stiffness, measured on the leading attack wheel, compared to its increase counterpart. (d) Wheel lift increase with increasing stiffness, measured on the leading attack wheel.

5.4.3 Curving behaviour results

As explained on the definition of the numerical models, seven simulations of curving behaviour have been performed for each stiffness configuration, with an increasing speed. From an operational point of view, the highest speed respecting **gauge constraints** imposed to the rolling stock is the simulation at 73,88 km/h. The *flexibility coefficient* equals 0,21 on this specific case, which is the limit for the pantograph cars on the trainset. Therefore, the results which will be discussed in the next paragraphs will be referred to the simulations performed at such speed, which is understood as the most constraining case.

Expected variation scenarii

The results for the simulations with stiffness increases of +15 and +30 % show that both the *derailment coefficient* and the *shift efforts* on the wheelsets show a very low increase, which grows linearly with the stiffness and remain well beneath the normative limits. Higher stiffnesses appear to cause a dispersive behaviour over the carbody lateral acceleration (Figure 5.20), but all simulations respond within tolerance limits.

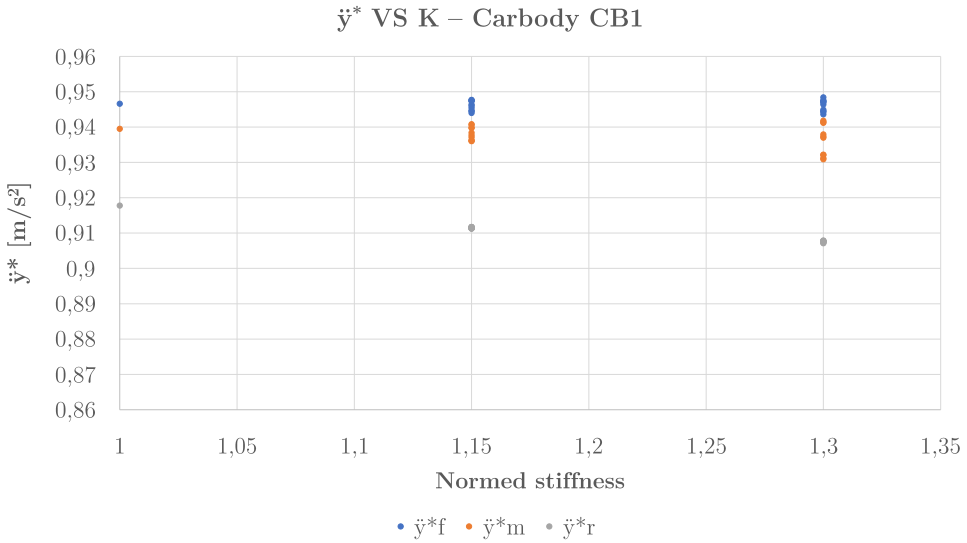

Figure 5.20: Dispersion of the lateral acceleration measurements over the leading carbody.

Complementary variation scenarii

An homogeneous evolution of the stiffnesses on whichever sense causes the *derailment coefficient* and the *shift efforts* to vary linearly with the stiffness. The results obtained are well under the

UIC-518 limits: $Y/Q_{max} \sim 0,4$ and $\Sigma Y \sim 24,5$ kN. Interestingly, the evolution of the *lateral acceleration* on *both the bogie frame and the carbody* show a trend rupture between +30 % and +50 % increases, with a sudden decrease of the acceleration records at strong stiffness increases (Figure 5.21).

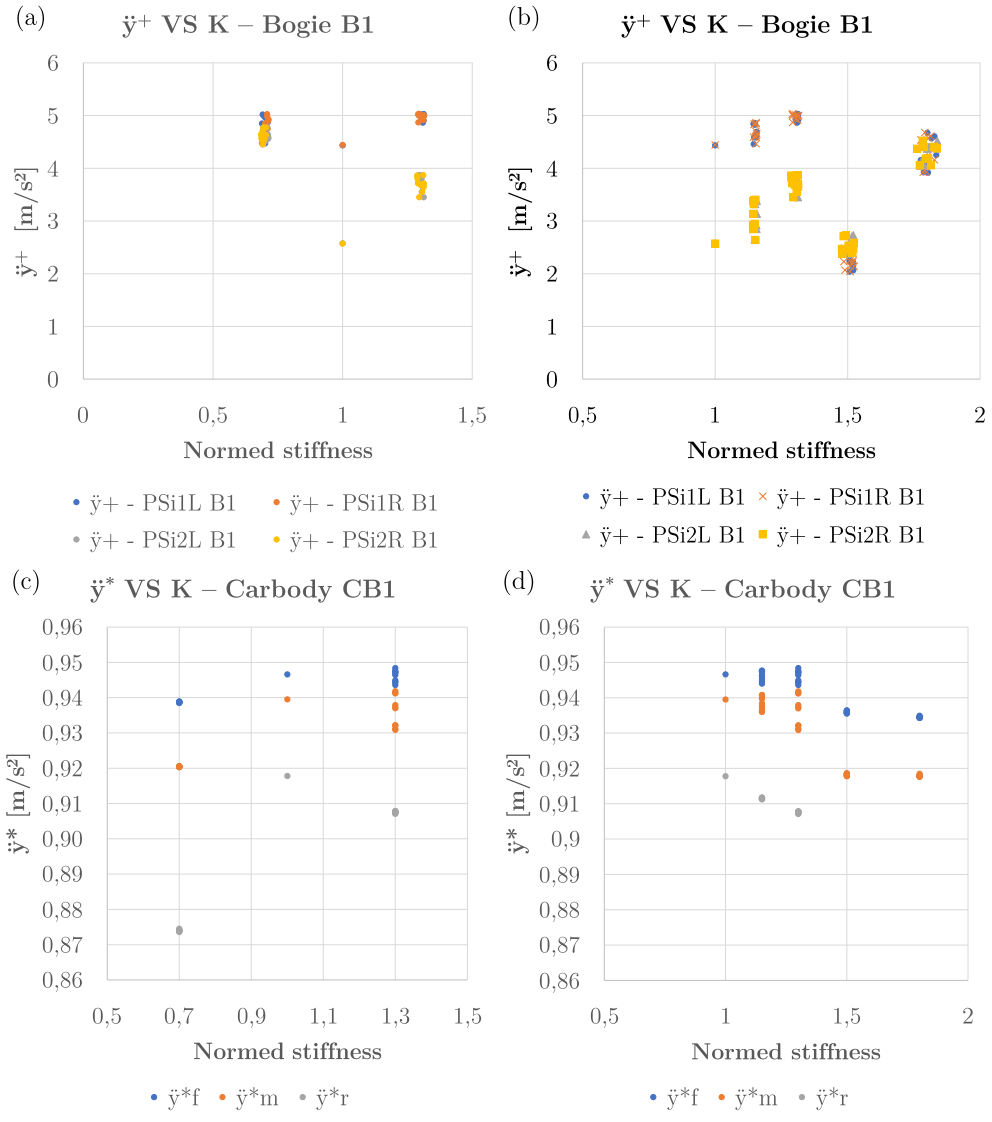

Figure 5.21: (a) and (b) Lateral acceleration over the axlebox position of the leading bogie for various stiffness levels. (c) and (d) Lateral acceleration levels at the front (f), middle (m) and rear (r) of the leading carbody.

A possible explanation for this sudden change can be found upon the bumpstop mechanisms within the bogie, which are usually inactive but can be loaded under some cases. The strong increase of stiffness might have caused an load imbalance within the suspension, thus effectively loading other elements and changing the response of the bogie. Nevertheless, the two cases affected by the change of behaviour fall well beyond the expectable increases of stiffness. The safety indexes remain well below the limit values calculated with the instructions of the UIC-518.

5.4.4 Dynamic behaviour results

The analysis of the dynamic behaviour of the trainset encompasses a wide range of simulations on straight and curved track, with worn and new rolling gear, as well as with empty and crush loads. To facilitate the interpretation of the results, the simulations will be coupled by families of models: the straight tracks with different conicities will be discussed first, the curved tracks being addressed later. Since the vehicles run under two load cases, they will be both discussed model by model, along with the effects of the stiffness changes.

We would like to underline the conditions in which curving tests are performed, for the speed imposed cause the train to roll under *cant deficiency*. The interest of such simulations is to assess the stability and robustness of the system against instabilities, at speeds above the operational limits, thus ensuring the safe behaviour of the rolling stock within its operational conditions. Therefore, the *flexibility coefficient* will clearly overtake the limits for the rolling stock, hence not being useful for any practical purposes.

Straight track, wheel conicity, $\lambda = 0{,}05$, v = 176 km/h

The results from the simulations have shown that the suspension elements have a key role on the dynamic stability of a trainset subjected to a lateral impulsion when rolling on a straight track. The combination of a specific *load case* and a *stiffness variation* could be the source of an non-convergence problem regarding the simulations.

Expected variation scenarii The simulation results for *expectable stiffness configurations* have not shown any non-compliant results. Equivalent simulations show that the load case has an influence on the safety indexes: the *derailment coefficient* decreased for higher payloads, whereas the *shift efforts* and *lateral accelerations increase*. The evolutions of the metrics are directly proportional to the stiffness variation.

Complementary variation scenarii As regards of the complementary changes in the suspension properties, the increase of stiffness beyond the expectable variation range shows that the vehicle remains stable and safe. However, a particular problem has arisen for the simulations under *crush load* with a loss of stiffness around -30 %. The safety indexes of the simulations showed a double plot with two groups of values: one "expectable" and around half of the values grouped at very low results (Figure 5.22). After inspection of the post-processed graphics of these simulations, it appears that the simulations ended abruptly, because of a non-convergence of the calculation.

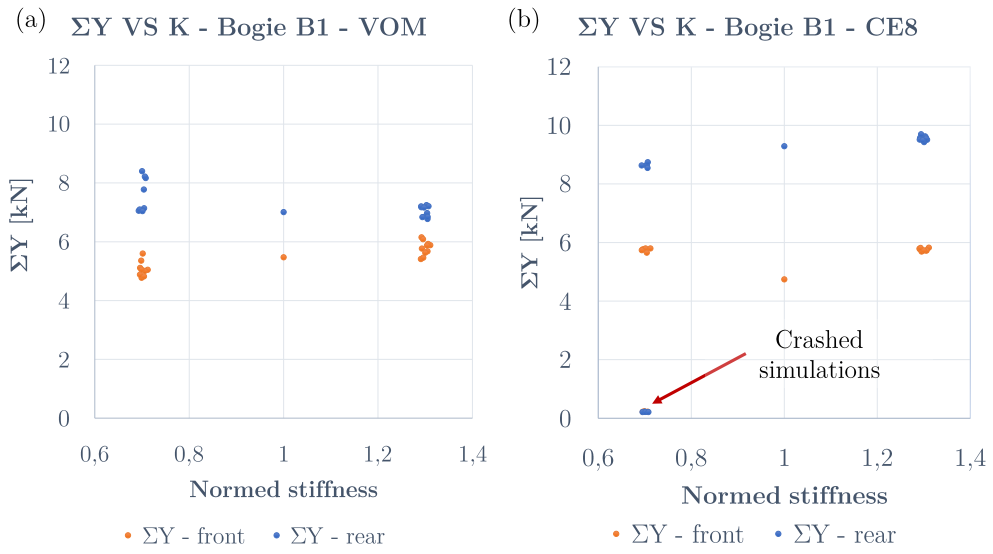

Figure 5.22: (a) Shift efforts over the axles of the leading bogie under tare load. (b) Guiding efforts over the wheelsets of the leading bogie.

Straight track, wheel conicity, $\lambda = 0{,}34$, v = 176 km/h

The simulations with $\lambda = 0,34$ have not undergone any unstable phenomena. The results show that the load state of the train has an influence on the amplitude of the oscillations, which are slightly stronger when the vehicle is on *empty load*.

Expected variation scenarii The variation of the stiffness in the expectable range has a direct proportional effect on the safety indexes, which evolve in a rather linear manner. The *derailment index*, the *shift efforts* and the *lateral accelerations* do not show a strong dependence to the stiffness, while the acceleration on the bogie decreases strongly with increasing stiffness (Figure 5.23). The *flexibility coefficient* remains fairly stable.

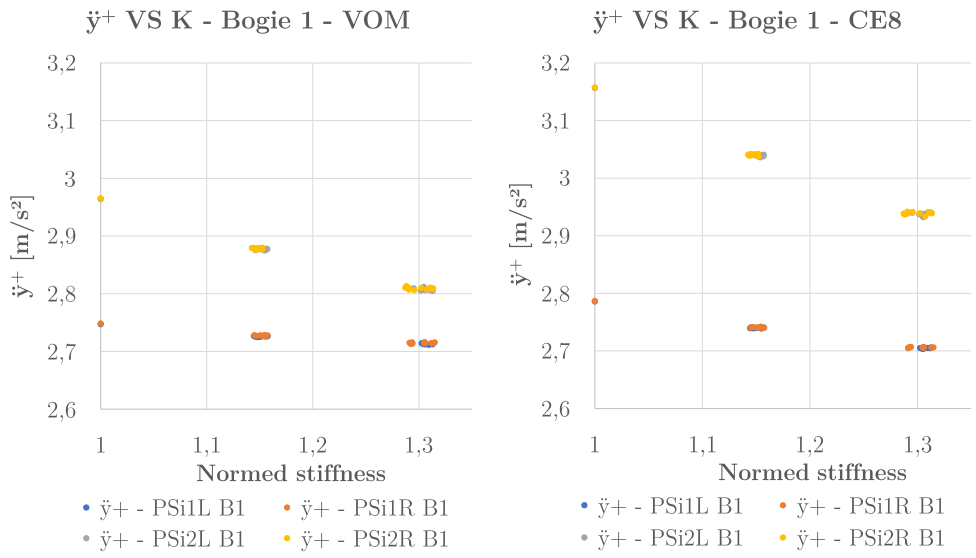

Figure 5.23: Lateral acceleration over the bogie frame, for the vehicle under *tare load* (left) and *crush load* (right).

Complementary variation scenarii Stronger changes on the properties beyond the range of predicted variability have a similar effect, affecting the safety indexes in a direct proportional sense. A lower stiffness increases the acceleration levels on the bogie (Figure 5.24), while the stronger increases reduce it even below the levels reached with a stiffness increase of +30 % (Figure 5.25).

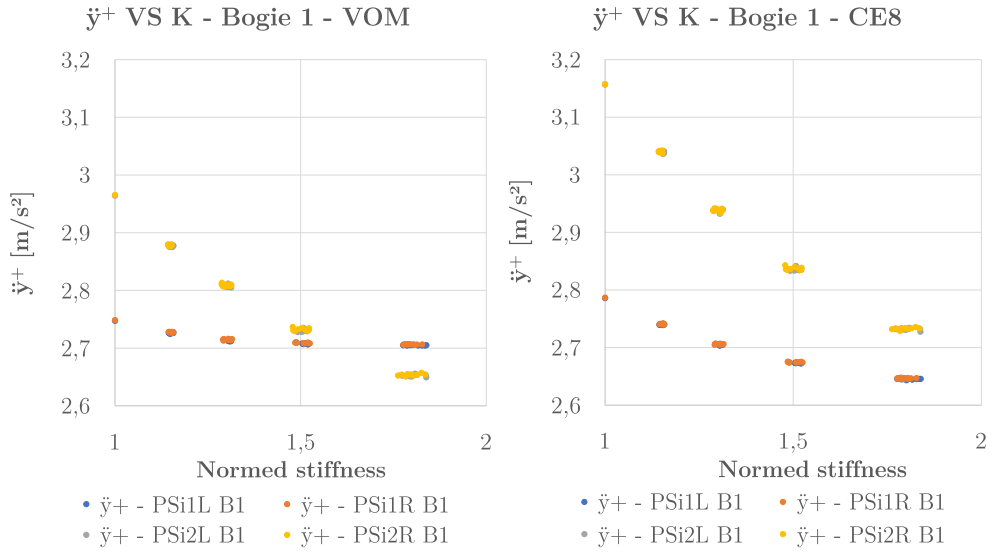

Figure 5.24: Lateral acceleration over the bogie frame, for the vehicle under *tare load* (left) and *crush load* (right).

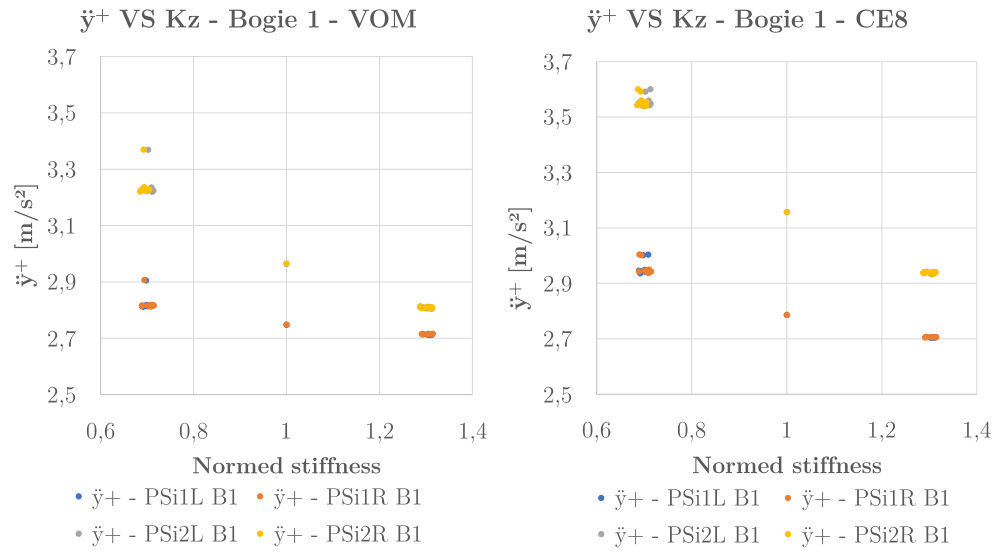

Figure 5.25: Lateral acceleration over the bogie frame, for the vehicle under *tare load* (left) and *crush load* (right).

Curved track, R = 300 m, v = 82 km/h

Regarding the dynamic behaviour of the rolling stock while negotiating a tight curve with cant deficiency, the results have shown that the train remains essentially stable for all the simulated scenarii. The system remains fairly insensitive to the changes on the stiffness, as the indexes vary very little. However, the load of the train has a strong effect on the indexes. For example, the shift efforts can rise up to 5 kN ($\sim +25$ %).

Expected variation scenarii The main remarks on the effects on an expected increase of stiffness concern the *shift efforts* and the *lateral acceleration* on the carbody. The guiding efforts over the front axle of the leading bogie are close to the dynamic limit $s\Sigma Y_{lim} = \Sigma Y_{lim}/2 = 34$ kN (Figure 5.26). The acceleration over the carbody is near to the acceptable limit of 1,5 m/s^2, but since the vehicle runs under *strong cant deficiency*, such values would be lower at normal operation speeds.

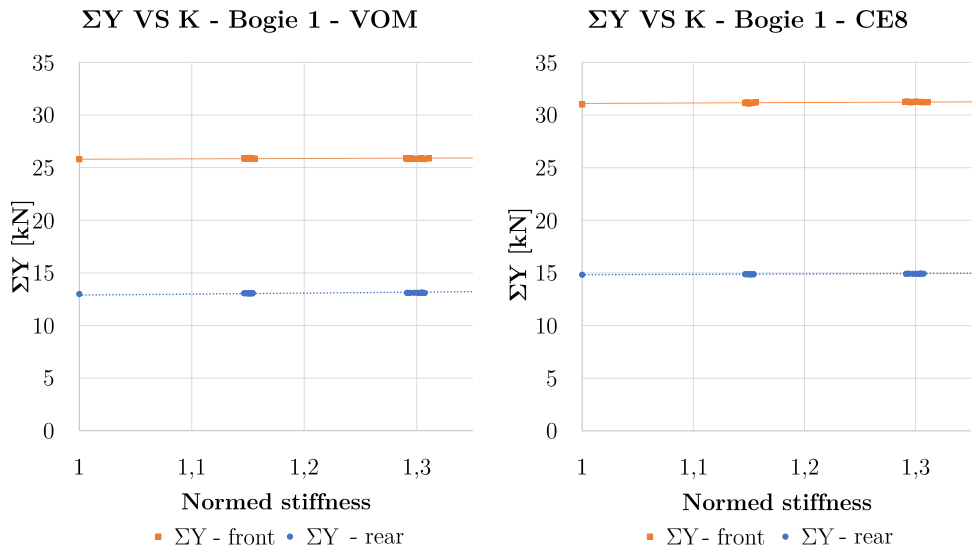

Figure 5.26: Shift efforts over the two leading wheelsets, for the vehicle under *tare load* (left) and *crush load* (right).

Complementary variation scenarii The observations obtained under the probable variation interval remain valid for the complementary scenarii (Figure 5.27). *Shift efforts* are close to the limit, but below. A loss of stiffness tends to reduce slightly the value of the indexes (Figure 5.28).

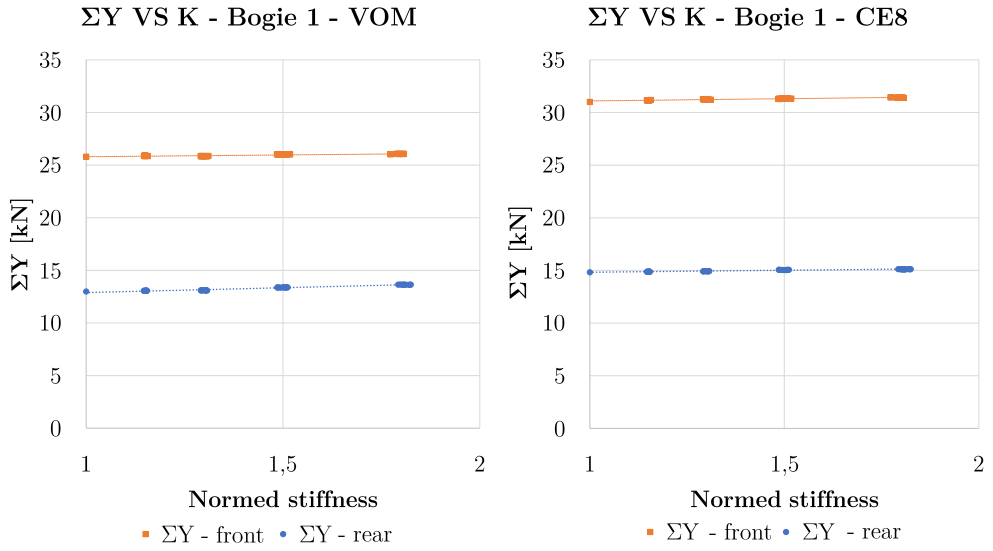

Figure 5.27: Shift efforts over the two leading wheelsets, for the vehicle under *tare load* (left) and *crush load* (right).

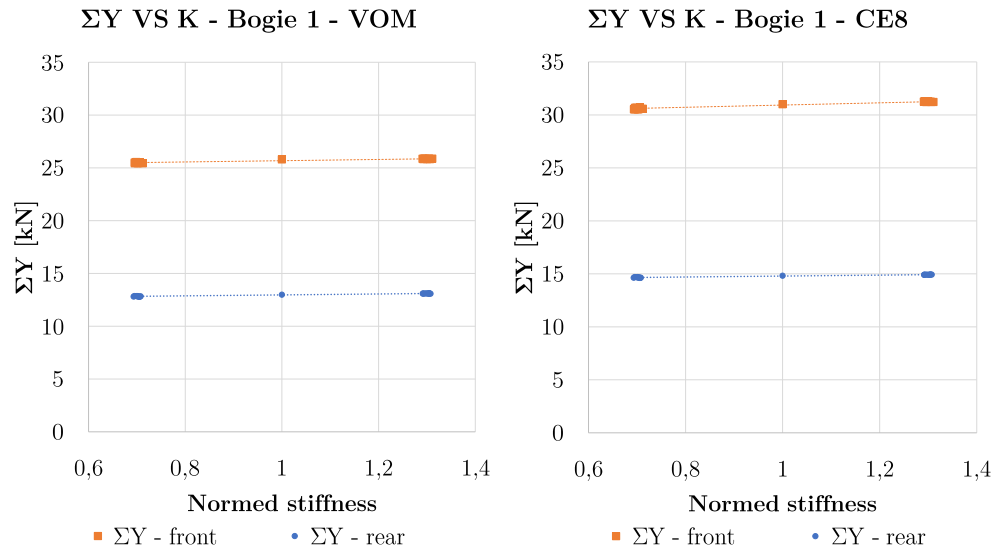

Figure 5.28: Shift efforts over the two leading wheelsets, for the vehicle under *tare load* (left) and *crush load* (right).

Curved track, R = 600 m, v = 127 km/h

The results arising from the simulations of curving behaviour for a medium radius show that the trains is, little to no sensitive to the changes on the stiffness of the suspension elements. Similarly, the model exhibits slightly different scores depending on whether it is empty of fully loaded.

Expected variation scenarii The results evolve in a slightly linear manner, but the indexes remain essentially unchanged for most of the cases and under the normative limits (Figure 5.29). The *lateral acceleration* of the carbody is very close to the limit of 1,5 m/s^2, but remains below it.

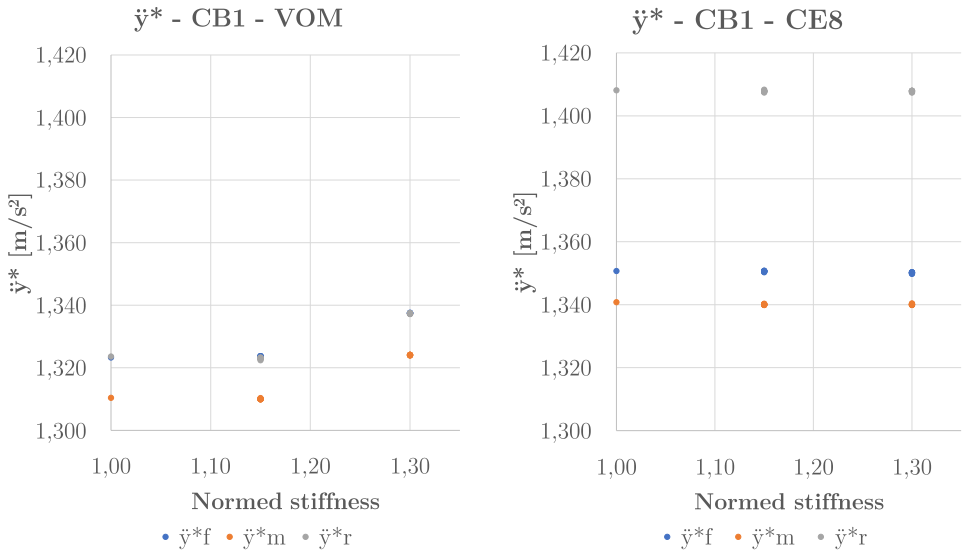

Figure 5.29: Lateral accelerations at the front (f), middle (m) and read (r) of the first car, for the vehicle under *tare load* (left) and *crush load* (right).

Complementary variation scenarii As regards of the complementary scenarii, the safety indexes remain below the limits, although some values are very close to the limit of 1,5 m/s^2. Interestingly, it appears that a loss of stiffness has rising effect on the lateral acceleration of the carbody (Figure 5.31).

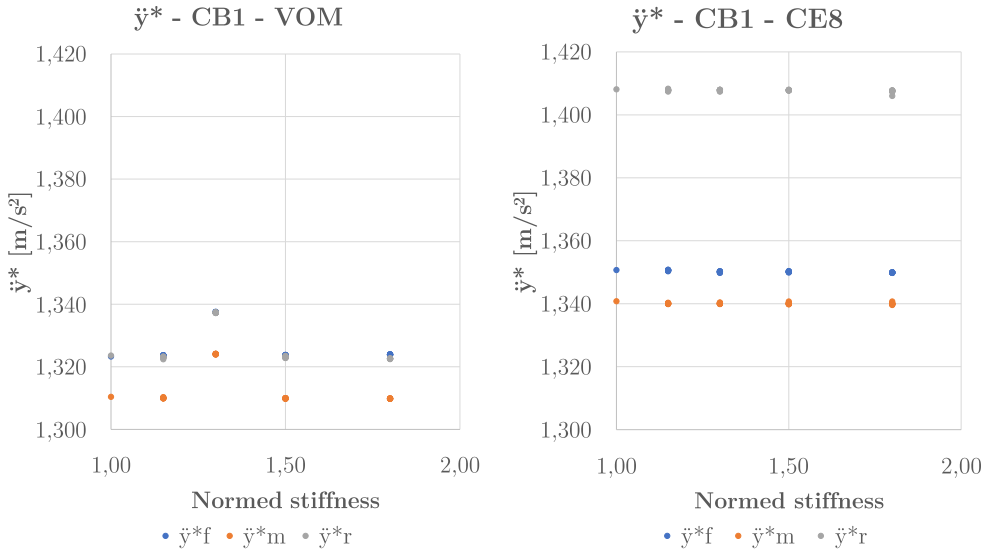

Figure 5.30: Lateral accelerations at the front (f), middle (m) and read (r) of the first car, for the vehicle under *tare load* (left) and *crush load* (right).

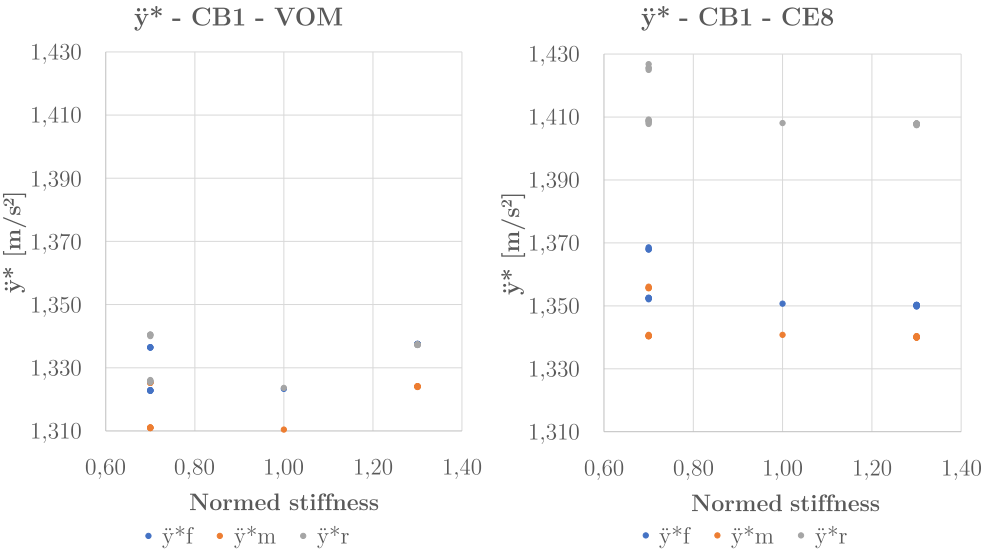

Figure 5.31: Lateral accelerations at the front (f), middle (m) and read (r) of the first car, for the vehicle under *tare load* (left) and *crush load* (right).

Curved track, R = 1200 m, v = 155 km/h

As regards of the trainset's dynamic behaviour when negotiating large radius curves, the simulations have shown that the train may incur in an excess of guiding efforts over the rear wheelset of the leading bogie under certain configurations. The evolution of the safety indexes is proportional to the stiffness variation, increasing in a slightly linear trend.

Expected variation scenarii The scenarii with expected variations of the suspension stiffness have shown that a combination of *crush load* plus an increase of stiffness of +15 or +30 % can cause peak values on the *shift effort* higher than 34 kN (Figure 5.32). Even though the peak limit is 68 kN, the RMS limit is of 34 kN. Both increments show that the shift effort overpasses the limits for sustained distances ($\sim$ 100 metres) (Figure 5.33).

Complementary variation scenarii The dynamic, RMS limit for *shift efforts* is set at 34 kN, and it is again overpassed during long periods in the simulations with an increase of +50 % and +80 % (Figure (Figure 5.34)). On the contrary, a decrease of the stiffness causes a reduction of the shift efforts (Figure (Figure 5.35)).

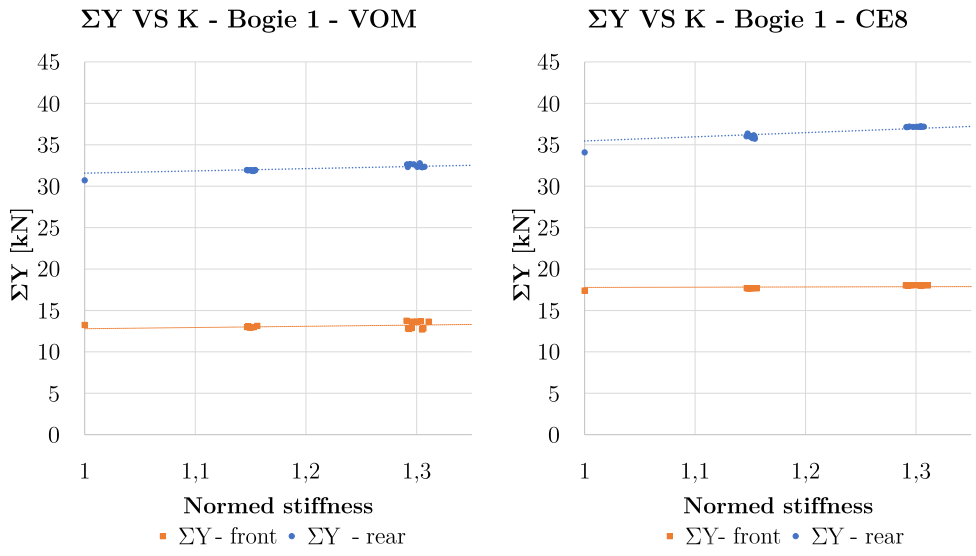

Figure 5.32: Shift efforts on the wheelset of the leading bogie, for the vehicle under *tare load* (left) and *crush load* (right).

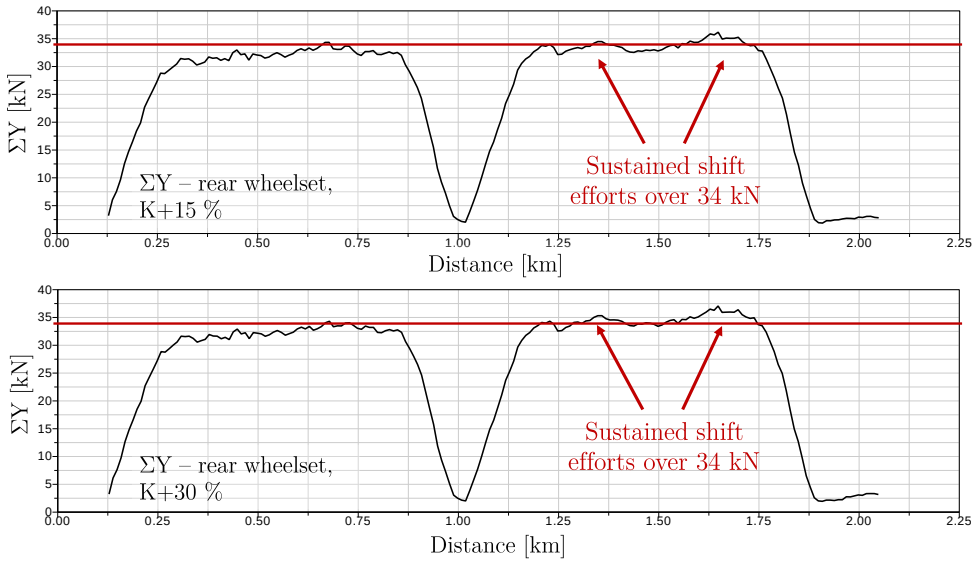

Figure 5.33: Shift effort signal for +15 % stiffness and +30 % stiffness increases, for the vehicle *tare load* (left) and *crush load* (right). The shift effort overcomes the RMS limit during sustained periods, at about 1,6 km of distance.

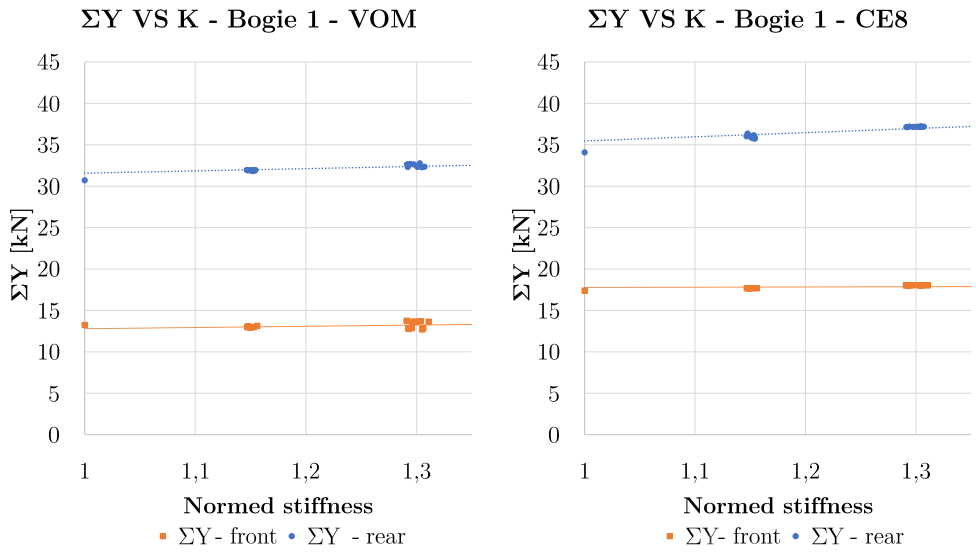

Figure 5.34: Shift efforts on the wheelset of the leading bogie, for the vehicle under *tare load* (left) and *crush load* (right).

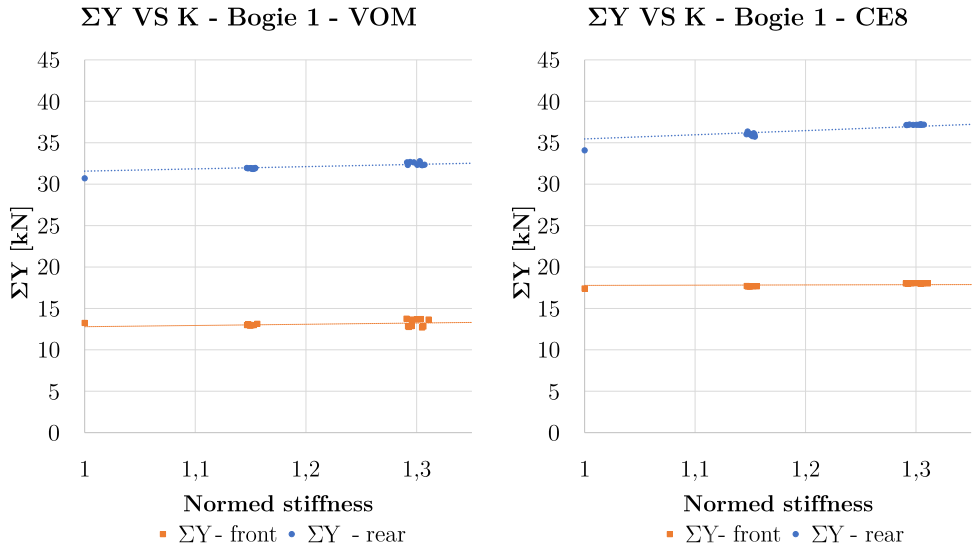

Figure 5.35: Shift efforts on the wheelset of the leading bogie, for the vehicle under *tare load* (left) and *crush load* (right).

5.5 Conclusion

The final chapter of these works has addressed the impact of the variability of the suspension properties on the global behaviour of a trainset. The basis of the study of railway dynamics have been presented, as well as some of the foremost aspects related to the modelling of railway rolling stock: track geometry, the wheel-rail contact and the rolling stock suspension. A brief discussion about the sources of derailment has been presented, along with the aspects related to the rolling behaviour of railway vehicles: kinetically static curving and dynamic behaviour in all kinds of tracks.

Complying with the request of the UIC-518 discussed in the second chapter, the use of numerical models to assess the fault behaviour of rolling stock is justified, since the virtual models have been validated with respect to real-scale tests. The models provided by Bombardier have been recalled, as well as the specific safety indexes applying to all the cases which have been simulated on each particular context. A first insight on the models use has been presented through the preliminary tests. Several aspects around the models sensitivity have been described. The *friction coefficient* in the wheel-rail interface is crucial, for high values can prevent artificially the wheel lift, leading to erroneous results when assessing derailment risk on the rolling stock. Hence, the definition of a variable, y-dependent friction coefficient, μ, is most appropriate. It will ensure a richer input for this variable, as well as the likeliness of the model with respect full-scale official approval results. The model has proved to be sensitive to *single-failure* simulations. The failure of a primary coil-spring has been extensively tested over the model, showing the increased risk of derailment by analysing Nadal's coefficient Y/Q. The results from the simulations show that both the software and the model are able to handle failure situations, and that it is possible to assess the behaviour of the train under degraded situations by virtual means. Finally, the ability of the model to simulate *global failures* or properties changes has been tested, through a change on the global characteristics of the primary dampers. It has been shown that, in spite of a major lack of damping (up to 35 %), the system remains relatively unaffected in terms of measured accelerations and able to cope with a lack of dissipative capacity.

A design of experiments for simulations has been drafted, introducing the notion of variability on the properties of the suspension. Multiple scenarii of variable suspension properties have been generated with a random normal distribution, whose parameters have been presented (average value and scatter interval). A management script has been prepared to ensure the simulations process from the pre-processing of the simulations to their post-processing and result compilation.

The Régio2N and its FLEXX Compact bogies have shown a strong resilience against changes on the properties of the primary rubber spring and the secondary auxiliary spring. As a general principle, the changes on the stiffness can cause a drift on the safety indexes, which evolve linearly with the increase of stiffness applied over the suspension element. **None of the cases whose variation intervals are derived from ageing phenomena have overpassed the safety**

limits enforced by the norm UIC-518. The variation of the safety indexes of these simulations does not appear very prejudicial. However, there are several cases which deserve some attention with regards to the evolution of the stiffness parameters:

- The derailment test might yield non-compliant results when undergone under severe increases of stiffness (+50 % or more). Albeit having a safety margin, as the wheel lift remains lower than 5 mm, and such an increment is fairly unlikely, the design engineer must bear in mind that the derailment test is very sensitive to stiff suspensions.
- When addressing the assessment of curving behaviour, a special attention should be paid to the change on the behaviour of the kinematic paths of the bogie. Under extreme loads or displacements, bumpstops or other elements with an interface clearance (only active under severe condition) may come into use. Some of these elements are rubber-based and were not initially considered within this study (decision discussed in Chapter 2). Therefore, the initial premises of the study and the suspension elements which were initially considered as relevant might not be sufficient to study the behaviour of the vehicle.
- Some dynamic simulations have shown a special sensitivity of this precise design of bogie to the loss of stiffness of the aforementioned elements. A non-negligible loss of stiffness, approaching -30 % of the component's nominal stiffness can trigger, combined with an *exceptional load* and a *conicity* around $\lambda = 0,05$, can cause simulation problems (half of a batch simulations crashed unexpectedly).
- As regards of the dynamic behaviour of the vehicle in curving simulations, no critical cases have been found. The runs on large radius curves showed sustained, high values of *guiding efforts* over the wheelsets on the leading bogie. Since the runs have been performed under strong *cant deficiency*, one could presume that such an event might be unlikely under operational conditions. However, we eagerly encourage a revision of the results by simulations under operational speed.

Bibliography

[Andersson et al.,] Andersson, E., Berg, M., and Stichel, S. *Rail Vehicle Dynamics - Fundamentals and Guidelines*. KTH, Stockholm. (Cited on page 151.)

[Andersson, 2012] Andersson, M. (2012). Derailment in track switches. Master's thesis, Chalmers University of Technology. (Cited on pages ix and 151.)

[Ayasse et al., 2006] Ayasse, J.-B., Chollet, H., and Iwnicki, S. (2006). Wheel-Rail Contact. In *Handbook of Railway Dynamics*, pages 85–120. CRC Press Books, London. (Cited on pages 143, 149 and 150.)

[Berg, 2016] Berg, M. (2016). Model for rubber springs in the dynamic analysis of rail vehicles. *Proceedings of The Institution of Mechanical Engineers - Part F-journal of Rail and Rapid Transit*, 211:95–108. (Cited on page 147.)

[Bosso et al., 2013] Bosso, N., Spiryagin, M., Gugliotta, A., and Somà, A. (2013). Review of Wheel-Rail Contact Models. In *Mechatronic Modeling of Real-Time Wheel-Rail Contact*, pages 5–19. Springer Berlin Heidelberg, Berlin, Heidelberg. (Cited on page 165.)

[Brabie, 2005] Brabie, D. (2005). *On the Influence of Rail Vehicle Parameters on the Derailment Process and its Consequences*. Licenciate thesis, KTH - Stockholm. (Cited on pages 148 and 151.)

[Brabie, 2007] Brabie, D. (2007). *On Derailment-Worthiness in Rail Vehicle Design Analysis of vehicle features influencing derailment processes and consequences*. PhD Thesis, Royal Institute of Technology Aeronautical and Vehicle Engineering Rail Vehicles, Royal Institute of Technology Aeronautical and Vehicle Engineering Rail Vehicles SE-100 44 Stockholm Sweden. (Cited on pages ix and 151.)

[Bruni et al., 2011] Bruni, S., Vinolas, J., Berg, M., Polach, O., and Stichel, S. (2011). Modelling of suspension components in a rail vehicle dynamics context. *Vehicle System Dynamics*, 49(7):1021–1072. (Cited on page 144.)

[Carter, 1922] Carter, F. (1922). *Railway Electric Traction*. Edward Arnold & Co. (Cited on page 140.)

[Carter, 1926] Carter, F. (1926). On the action of a locomotive driving wheel. *Proceedings of the Royal Society of London A: Mathematical, Physical and Engineering Sciences*, 112(760):151–157. (Cited on pages ix, 143 and 144.)

[Carter, 1928] Carter, F. (1928). On the stability of running of locomotives. *Proceedings of the Royal Society of London A: Mathematical, Physical and Engineering Sciences*, 121(788):585–611. (Cited on pages ix and 140.)

[Chamorro and Escalona, 2012] Chamorro, R. and Escalona, J. L. (2012). *Simulación dinámica de ferrocarriles en vías deformables - Métodos avanzados de discretización en dinámica de sistemas multicuerpo flexibles*. Editorial Académica Española, Saarbrücken. (Cited on page 142.)

[Cherniak, 2013] Cherniak, A. Y. (2013). Operational definition of the possible causes of derailment of freight cars. *Prace Naukowe*, Politechniki Warszawskiej(96). (Cited on page 151.)

[EN14363, 2005] EN14363 (2005). *Railway application - Testing for the acceptance of running characteristics of railway vehicles - Test of running behaviour and stationary tests*. CEN. (Cited on page 157.)

[Garg and Dukkipati, 1984] Garg, V. K. and Dukkipati, R. V. (1984). *Dynamics of Railway Vehicle Systems*. Academic Press, 55 Barber Greene Road, Don Mills, Ontario M3C 2A1. (Cited on pages ix, 24, 140 and 142.)

[Jha and Gokhale, 2017] Jha, P. K. and Gokhale, S. S. (2017). Modeling and Validation of Gatimaan Express with Vi-Rail. *Int J Recent Sci Res*, 8(11):21701–21707. (Cited on page 151.)

[Jönsson, 2004] Jönsson, P.-A. (2004). *Modelling and Laboratory Investigations on Freight Wagon Link Suspensions with respect to Vehicle-track Dynamic Interaction*. Licenciate Thesis, KTH - Stockholm, Stockholm. (Cited on page 145.)

[Kalker, 1968] Kalker, J. (1968). The tangential force transmitted by two elastic bodies rolling over each other with pure creepage. *Wear*, (11). (Cited on pages ix and 144.)

[Kalker, 1991] Kalker, J. J. (1991). Wheel-rail rolling contact theory. *Wear*, 144(1):243 – 261. (Cited on pages ix and 144.)

[Malo Estepa, 2017] Malo Estepa, A. (2017). Lot 4 - Livrable ANR Projet DYNABOG - Résultats de simulations sous SIMPACK. Technical report, IRT Railenium, Valenciennes. (Cited on page 174.)

[Morales-Ivorra et al., 2016] Morales-Ivorra, S., Real, J. I., Hernandez, C., and Montalban, L. (2016). Derailment risk and dynamics of railway vehicles in curved tracks: Analysis of the effect of failed fasteners. *J. Mod. Transport*, 24(1):38–47. (Cited on page 148.)

[Park et al., 2009] Park, C., Kim, Y., and Bae, D. (2009). Sensitivity analysis of suspension characteristics for Korean high speed train. *Journal of Mechanical Science and Technology*, 23(4):938–941. (Cited on page 156.)

[Park et al., 2018] Park, C.-K., Lee, K., and Lee, T. (2018). MULTI-CRITERIA OPTIMIZATION OF A TRAIN SUSPENSION FOR KOREAN HIGH SPEED TRAIN USING KRIGING METAMODEL. (Cited on page 156.)

[Presthus, 2002] Presthus, M. (2002). Derivation of Air Spring Model Parameters for Train Simulation. Master's thesis, Lulea University, Västeras. (Cited on pages 147 and 148.)

[Stichel, 1999] Stichel, S. (1999). On freight wagon dynamics and track deterioration. *Proceedings of the Institution of Mechanical Engineers, Part F: Journal of Rail and Rapid Transit*, 213(4):243–254. (Cited on page 146.)

[Suarez et al., 2013] Suarez, B., Mera, J., Martinez, M., and Chover, J. (2013). Assessment of the influence of the elastic properties of rail vehicle suspensions on safety, ride quality and track fatigue. *Vehicle System Dynamics*, 51(2):280–300. (Cited on page 156.)

[TOUMI, 2016] TOUMI, M. (2016). *Numerical modeling of the wheel-rail contact for the study of the parameters influencing Kalker's coefficients : Application to the railway dynamics*. Theses, Université Paris-Est. (Cited on page 143.)

[UIC505, 2006] UIC505 (2006). *Matériel de transport ferroviaire - Gabarit de construction du matériel roulant*. UIC, 1 edition. (Cited on page 157.)

[UIC513, 1994] UIC513 (1994). *Guidelines for evaluating passenger comfort in relation to vibration in railway vehicles*. UIC, 1 edition. (Cited on pages 156 and 157.)

[UIC518, 2009] UIC518 (2009). *Testing and approval of railway vehicles from the point of view of their dynamic behaviour - Safety - Track fatigue - Runnign behaviour*. UIC, 4 edition. (Cited on pages ix, 35, 157 and 162.)

[UIC703, 1989] UIC703 (1989). *Caractéristiques de tracé des voies parcourues par des trains de voyageurs rapides*. UIC, 1 edition. (Cited on page 161.)

[Wickens, 1965] Wickens, A. (1965). The dynamic stability of railway vehicle wheelsets and bogies having profiled wheels. *International Journal of Solids and Structures*, 1:319–341. (Cited on pages ii, ix, 155 and 168.)

[Wickens and Iwnicki, 2006] Wickens, A. and Iwnicki, S. (2006). A History of Railway Dynamics. In *Handbook of Railway Dynamics*, pages 5–38. CRC Press Books, London. (Cited on pages 23, 139, 148, 154 and 155.)

[Xie et al., 2016] Xie, H., Zeng, W., and Lin, G.-m. (2016). Sensitivity analysis of suspension parameters on dynamic performance of a rail vehicle based on a virtual prototype response surface method model. *Advances in Mechanical Engineering*, 8(9):1687814016669636. (Cited on page 156.)

[Zboinski, 1997] Zboinski, K. (1997). Dynamical investigation of railway vehicles on a curved track. *European Journal of Mechanics and Solids*, 17:1001–1020. (Cited on pages ix, 151, 155 and 160.)

[Zboinski and Golofit-Stawinska, 2018] Zboinski, K. and Golofit-Stawinska, M. (2018). The impact of primary suspension stiffness of 2-axle bogie of MKIII passenger car on its dynamical behaviour. *Transport Problems*, 13(1). (Cited on page 156.)

[Zhou et al., 2014] Zhou, H., Xu, B., and Zhang, J. W. (2014). Sensitivity Analysis of the Elastic Properties of Rail Vehicle Suspensions on Vibration Based on the HXN5 Locomotive Model. In *Advanced Design and Manufacturing Technology IV*, volume 635 of *Applied Mechanics and Materials*, pages 201–207. Trans Tech Publications. (Cited on page 156.)

Conclusions and perspectives

The project DYNABOG has been jointly undertaken by Bombardier Transportation, the laboratory LAMIH of the Université Polytechnique Hauts-de-France and the IRT Railenium. The works have spanned from October 2015 until October 2018, having encompassed the subjects which were presented in the previous chapters. It is the purpose of this last section to summarize the initial goals, as well as the conclusions obtained during the project. Several possible openings and perspectives on the area will be addressed as well.

Project aims

Bombardier Transportation proposed the project DYNABOG in the context of a search for the optimization of maintenance cycles and life-cycle costs, regarding the family of bogies FLEXX Compact. The feasibility of the optimization was based on a shift of highly-intrusive overhaul operations, coupling their occurrence by an increase of maintenance periodicity. However, such an operation cannot be addressed without ensuring the safe operation of the rolling stock under extended maintenance conditions. Therefore, several general subjects had to be addressed:

- A choice of suspension elements enabling the extension of overhaul periods had to be addressed. The methodology to pick up the components had to be based on Bombardier's current quality tools and on current safety (RAMS) standards for the railway industry. A special stress was laid on the possibility of several element failures occurring at the same time.
- The study of the chosen components had to assess the evolution of their properties throughout a lifecycle, exploring the mechanisms acting on the material. A characterization of the base materials and of the suspension elements was expected, as well as empirical evidence on the evolution of the components properties. The variability of the main properties is a strong asset for the final step of the works.
- The assessment of the safe operation for railway rolling stock is performed via a series of tests, whose results depend on the suspension properties. Therefore, a series of tests had to

be undertaken to prove the impact of the variability of the suspension on the performances of the vehicle. The limits obtained from the dynamics simulations would orientate the feasibility of overhaul extensions.

Results and perspectives

Quality-based methodology

The selection of the suspension elements having an interest for the aims of the project was conducted via a study of the FMECA documentation for the FLEXX Compact bogie. The failure modes were classified owing to their criticality level, building matrices of occurrence probability of two simultaneous failure modes. It was found that, **according to the failure rates from Bombardier, it is highly improbable that two critical failure modes may occur at the same time**. Therefore, the choice of the suspension element has been addressed not on a failure rate basis, but on a maintenance-based, qualitative approach.

Owing to the wide range of suspension elements and failure modes, the need for a simplification of the document appeared as evident. Therefore, a **decision tree methodology has been developed**. The decision tree allows any engineer to stroll through the FMECA of a bogie and select, via two general stages, the suspension elements and their failure modes which are interesting for an overhaul extension.

The application of the decision tree to the FMECA of the FLEXX Compact bogie equipped on Régio2N trainsets has led to the choice of two suspension elements of interest, the primary rubber spring and the auxiliary spring. Finally, **the former element has been retained to develop our methodology**.

Despite the generality of the approach and the reasoning within the decision tree, it has a main drawback. **The results** of any analysis of a bogie FMECA are case-dependent. Hence the outcome of the study is "biased" by the design of the bogie, and **the chosen components will be different from one model to another**. Moreover, this practise should be transposed on different models to assess its adaptability.

Rubber properties and ageing

In order to determine the properties of the rubber reference which is part of the primary rubber spring, several test campaigns have been launched: an accelerated thermal ageing campaign to simulate the degradation of the properties of the rubber, as well as a mechanical characterization campaign and an exploratory chemical test campaign. The mechanical test results have served to

identify several material models to describe the hyperelastic behaviour of the rubber along the ageing.

A design of experiments encompassing several configurations of time and temperature has been drafted to age standard specimens of rubber in a ventilated oven. The ageing caused a slight shrink and loss of mass on the samples. After the ageing, the specimens underwent standard tensile stress tests, obtaining their mechanical characteristics curve. The metrics recovered from the tests show that the **thermal ageing causes a change in the material properties**. Its breakdown resistance decreases, although the material becomes stiffer. An Arrhenius technique has been successfully deployed to describe the evolution of the rubber properties throughout ageing. **Three master curves for ultimate strain and stress**, as well as **for the secant stiffness (200 %)**, have been calculated.

Moreover, some spare rubber remainders have been used to perform swelling tests in order to evaluate the reticulation rate of the rubber. Upon completion of the tests, it has been observed that **the reticulation rate increases with the thermal ageing**. The Arrhenius technique has been applied as well to obtain an evolution curve of the reticulation rate along time. Samples of naturally aged rubber were recovered from real parts and swelled as well to compare with the laboratory results. **However, the analytical results from the evolution curve did not match accurately the age of the samples from real parts**. The improvement of this approach could be achieved by a richer database of material data, plus a reduction of the uncertainties regarding the real parts history and service conditions.

Next, an **identification of hyperelastic models** was undertaken on the mechanical test results. A five-parameter, generalized Mooney-Rivlin model of third order was used. From each thermal ageing configuration, three out of five test curves were chosen for identification. Thus, 46 sets of five C_{ij} parameters each were recovered from the samples. When plot against the time of exposure, **it appears that the thermal ageing causes an evolution on the coefficients of the model**. However, the mechanism driving the drift on the properties remains unclear. Applying the Arrhenius method to the coefficients did not yield any conclusive results. Plotting some of the C_{ij} versus the reticulation rate of their samples showed that the coefficients evolve in a slightly linear manner with v_e. An evolution model of the C_{ij} parameters depending on the reticulation rate v_e could be developed with larger experimental data on the latter parameter.

A qualitative analysis of a series of averaged curves, one per thermal ageing configuration, was performed. The results show that, for this rubber reference, **the thermal ageing increases the stiffness at low stretch levels up to 70 °C**, stabilizing or slightly decreasing above this temperature. Heat exposure increases neatly the high strain crystallization stiffening of the material. The variability induced by the thermal ageing in the properties of the rubber can rank

up to +40 % of the new-state curves.

A strong dispersion was found on the sample results. The rubber mixture used to prepare the test specimens was not homogeneously stirred during the preparation phase. Therefore, most of the samples exhibited irregular surfaces and inclusions within the material. **A better control of the specimens at fabrication would contribute to reduce the scatter on the material properties**.

Similarly, tests were conducted when the tests facilities were available for the project purposes, which caused **important delays between each test stage**. Moreover, the manufacturer of the pieces sent the all specimens on a single shipment at the beginning of the campaigns. Norms demand strict delays to be met between the sample's vulcanization and testing, especially if further tests such as the ageing are to be conducted. Furthermore, **the storage of the samples must ensure that no external sources disturb the rubber state**. As regards of the test conditions, the effects of imposed strain on samples during ageing tests can affect the properties of the material. The inclusion of such effect could be of interest in further works. Finally, **a review of the design of experiments of the rubber testing** would be highly advisable, to secure the delays between each stage of tests and to reduce the induced variability.

As regards of the mechanical characterization of the material, **the samples supplied by the manufacturer did not permit to perform other tests than standard tensile stress characterization**. Therefore, the characterization of the material remains partial and would require further tests in a complementary configuration (pure shear, for example), to have a global knowledge of the rubber behaviour. The chemical characterization by swelling tests has shown encouraging results. However, since the studied rubber is filled with carbon black, special corrections must be applied to obtain an accurate result. It is strongly possible that an improvement of the storage chain and fabrication would reduce the dispersion of the results as well. Nevertheless, the extrapolation of the reticulation rate by an Arrhenius method requires a better correspondence between the thermal ageing tests and natural ageing, taking into account that real parts exhibit a gradient of properties and ageing rate across the rubber section.

Suspension element: variability on mechanical properties

Kriging model: variability results

The wide database of material properties obtained from the mechanical characterization tests and the thermal ageing has allowed an extensive FE simulation plan. **All the material configurations have been tested**, obtaining three reference stiffnesses which match the same number of load cases on the vehicle. However, thorough test campaigns are rare within the

industry. Therefore, a different focus has been proposed, based on a numerical approach to the determination of the ageing effects.

A **Kriging model** with five inputs has been prepared, time and temperature of ageing plus three control points on rubber curves, related to the three characteristic parts of the hyperelastic curve. An expected output, the part stiffness, has been fed to the model as well. The model was **trained with the experimental results**, and subsequently used with 20,000 datasets generated by a random process. The results have permitted to **obtain the maximum and minimum envelopes of the stiffness value, depending on the ageing configuration**. The Kriging model has highlighted the most unfavourable configurations for the thermal ageing. Interestingly, **the most constraining cases match three thermal ageing configurations whose mechanical characteristics compose the upper envelope of the behaviour curves**. Therefore, in this context one can assume that the highest mechanical properties would yield the strongest mechanical stiffnesses.

Within an industrial context, **it appears legitimate to considerate that the variability can be determined** not by the worst experimental case, but rather **by the most pessimistic expectation**. Therefore, instead of performing vast test campaigns, some few characterizations, coupled with a variability interval setting an increase of decrease of the curve, can be of utmost interest to determine the range of variation of a set of properties. These works have shown that an increment of +40 % stiffness of the rubber characteristics (based on the experimental evidence), would yield a stiffness variability up to +35 %. The results have been comforted by the FE simulation campaign, whose variability levels were of +40 % on the input curves and +27 % for the maximum stiffness.

As regards of the life-cycle evolution, an Arrhenius method has been applied to the three stiffnesses defining the behaviour of the primary rubber spring. On the one hand, three corresponding master curves have been obtained, describing a possible evolution of the properties. On the other hand, some real parts recovered from Deutsche Bahn (DB) were tested in Bombardier's facilities in Siegen. However, the comparison between the experimentally determined stiffness and the prediction curve has yielded a mismatch: the parts, 6-year old, appear as being between new state and 2,5 years old.

Perspectives and improvement

Despite the thorough test campaign which has been undertaken, the characterization of the primary rubber spring remains incomplete: the evolution of its transversal and longitudinal stiffness, as well as other test configurations could be tested. The Kriging principle could be then applied to the new metrics, thus providing a complete view on the evolution of the part properties.

As regards of the thermal ageing tests performed on the standard specimens, further research must be done in order to ensure a maximum resemblance between the sample state and a naturally aged part. **Naturally aged rubber show a gradient of properties from its surface to the core**. Consequently, the properties which we have predicted are more pessimistic than reality, for the bulk of the rubber can be relatively spared from ageing. Moreover, such a property gradient would explain the difference between the reticulation rate in aged specimens and real samples. **A better approach** to model the true state of the rubber **would be the modelling of the varying properties across the rubber**.

The predictability of the master curves retrieved from the FE simulations is subjected to the weaknesses pointed out previously. The stiffness of the parts depend on the properties of a rubber layer which was deemed core-aged. Concerning the adjustment of the master curve to the operational temperature, the shift factor which is used depends on the accuracy of the Arrhenius regression, and on the objective temperature. In this case, Bombardier has pointed out that the average temperature in the geographical area of operations of the real parts might be lower than 20 °C. Therefore, a re-adjustment of the curves by a new shift factor could lead to more accurate results.

Dynamic behaviour of the rolling stock

Simulation results

The variability levels on the suspension element properties have been implemented in a MBS software to evaluate the dynamic behaviour of a Régio2N trainset. An adapted script has generated the random stiffness input values with variability intervals based on the experimental (test) and numerical (FE + Kriging) results. The models have shown a **specific sensitivity to the stiffness increases on the derailment test**. The kinematic-static curving behaviour has shown that the vehicle respects the gauge constraints under the expected levels of variability. As regards of the global dynamic behaviour, **the train appears to be sensitive to an increase of stiffness when negotiating large radius curves**. The shift efforts appeared to have a sustained RMS value over the normative limit, which could accelerate the wear on both the infrastructure and the rolling gear.

Perspectives and results

Despite the two particular cases mentioned previously, it appears probable that the Régio2N could withstand an extension of the lifecycle of the analysed component. However, the extent of **the effects of** such extension is yet unknown. The present works have focused solely on **the ageing-induced stiffness variations**. However, **fatigue and creep effects** are also present

on the part. Their combined effects **must be evaluated in detail to ensure the complete compliance of the rolling stock** under extended overhaul periods.

As discussed previously on the validity of the FMECA analysis and the conclusions which can be extracted from the methodology, the approach is case dependant. The FLEXX Compact bogie which has been analysed comprises a series of metallic elements, whose properties are deemed invariable during a life-cycle. Such elements contribute to the robustness of the design, allowing higher variations on their fellow rubber-to-metal parts. **An analysis on a bogie with full rubber-to-metal suspensions would yield, probably, different results**. Moreover, such cases would have a higher interest from the dynamics point of view, assessing the effect of the variability on the suspension properties.

Appendix A

Example of a rolling stock bid

The content of the present appendix is to provide an exhaustive example on a rolling stock public bid, obtained from information disclosed by the Spanish Ministerio de Fomento (Ministry of Infrastructure). The specific bid regarded the acquisition of up to 30 high-speed trains for the state-owned operator Renfe. The following paragraphs explain in a more detailed manner the requirements for a rolling stock manufacturer to tender for a bid, as well as the demands and scores issues by the operator to bestow the choice of a preferred bidder.

A.1 Rolling stock bids

The mechanism for railway operators to open a process to buy new trains is the call for bids, which is addressed to rolling stock manufacturers. This process encourages the competence between the attending companies, which will try to supply the most adequate offer to the customer. The operator will issue a first document, stating the needs of the company and the requirements that must be fulfilled to be compliant with the call. Usual requirements in offers are the purpose of the train (high-speed, regional, commuter...), the expected capacity (number of passengers) or performances (top speeds and/or accelerations), technical requirements (kind of powering), environmental requirements (CO_2 emissions, green footprint, recyclability) and, more recently, maintenance aspects (costs, expected maintenance delays, etc.). We would like to bring up an example backed with exhaustive information: the last high-speed rolling stock bid issued by the Spanish public operator Renfe, in November 2015 [BOE, 2015]. The technical and economic requirements issued in the call for bids are listed below.

1. Fifteen (15) high-speed passenger trains, with an option for 15 additional trains.
2. Standard UIC gauge.

3. Three-tension electric feed.
4. Maximal operational speed: 320 km/h.
5. Maintenance services to be included for a period of 30 years, with an optional extension for 10 years.
6. Reference cost for the bid: 2.642 B€ .

Rolling stock manufacturers can submit their offers to the company following the procedure which is established in the documentation issued with the public call. The document describes as well the qualification rules for the company to be authorised to present a bid, stating a certain number of scores and calculation methods to attribute the points associated to each score.

1. Economic and financial solvency may account up to 20 points. Companies failing to comply with at least 50% of the score will be automatically disqualified. A zero-point score will be awarded to companies failing to present a global turnover statement. Five points will be awarded for each year with an annual income of 100 M€ or more, during the previous 4 years.
2. Technical characteristics will account up to 80 points. Companies failing to comply with at least 50% of the score will be automatically disqualified. These points will be awarded as follows:
    - Up to 50 points awarded through individual scores of 25 points. Each award accounts for a similar experience on manufacturing and supplying similar rolling stock ($v_{MAX} \geq$ 250 km/h) within the European Union, when such contracts have a minimum cost of 100 M€/project.
    - Up to 30 points awarded through individual scores of 15 points. Each award accounts for a similar experience on maintaining a similar kind of rolling stock ($v_{MAX} \geq 250$ km/h) within the European Union, when such contracts have a minimum cost of 5 M€/year and project.

Once a manufacturer has been accepted as a potential bidder by the operator (public or private), the company's engineering teams begin the work to find the most suitable offer within the product portfolio. Up to the 1990s, rolling stock manufacturers used to work on a tailored fit solution approach for each customer. Although this method can give an precise solution to the railway operator's needs, it is expensive and might need extensive development or re-development of subsystems, sometimes starting from scratch. The search for economical efficiency has led to a new paradigm among manufacturers. Trains and rolling stock are classified within a series of families, named "platforms". For example, Bombardier Transportation has several families of products: Flexity (tramways), Talent and OMNEO (single/double-deck, for both commuter and

regional services), TWINDEXX (double-deck intercity), ZEFIRO (high-speed trains) and TRAXX (locomotives). This principle can be transposed to a deeper level of development, creating families of subsystems, such as Bombardier's FLEXX bogie families.

As described before, each platform is designed to fit a "universe" of services or a certain kind of environment, thus standardizing the most expensive parts of the product's design, while being flexible enough to fit in the customer's needs. Furthermore, the standardization encompasses several efforts, both in engineering and in economic domains, which seek to master all aspects regarding the platform. For example, "hollow" models of the platform are ready-to-use to test the main technical aspects of a potential bid, such as the train's general dynamic behaviour, supplying a quick answer to the customer's needs while ensuring a sound engineering basis. Respectively, economical assessment of production and supply chain costs are conducted during the platform design. This information is a strong asset for the manufacturer when tendering for a bid, as cost calculations will be more exact and eventual cuts to obtain best costs will be easier to evaluate.

A.1.1 Stakes on a rolling stock bid

The development of a specific proposal for a bid requires a compromise between the manufacturer's know-how and capacities and the customers' demands. The first step on the design process is the choice of the most suitable platform according to the bid's requirements, defining the global architecture of the future train and its general characteristics. From this general description, each engineering team (bogie, carbody, power chain, etc.) drafts an equipment proposal to meet the needs that have been cascaded from the global aims and design. Such equipments can come in the shape of a whole predefined subsystem, like the bogie, or have to be defined ad-hoc for the project. The platform architecture is especially fit for this phase, as the subsystem's costs are already defined internally along with the engineering design. As a result, each proposal encompasses an economical evaluation in terms of raw supplies, equipment and workload. Thus, the information is readily handled to the integration team, which will compile the data and produce a tender bid for the customer.

Large offers are usually developed in several stages. After the opening for tenders, all the bids from the manufacturers are collected under sealed envelopes. Offers are studied by the railway operator, which discloses the bids and makes a first choice: offers which do not comply with the exigences of the customer are disqualified. Next, the remaining bids are then subjected to a deeper study. The outcome of this evaluation is a series of recommendations to each tenderer, underlining the critical aspects of their bid(s) to be improved for the final evaluation. A series of scores and critical aspects are transmitted to all participants, which have a fixed period of time to submit an answer. After handling the corrected tenders, the customer may bestow its decision in an open act with all the competing manufacturers.

This procedure was applied for the call for new high-speed trainsets of the Spanish public operator Renfe in November 2015. The process was fairly publicised, with the evaluation of the final proposals being publicly disclosed [Rodríguez, 2016]. The evaluation was assessed with a series of scores up to a global amount of 100 points, which were bestowed as listed below:

1. Technical requirements, up to 35 points.
2. Economical requirements, up to 65 points, according to the following aspects:
    - Global cost of the offer (M € plus M€ /train).
    - Maintenance costs for 30 years (M € plus M€ /km and train).
    - Declared Energy consumption (kWh/km).
    - Number of seated places.
    - Availability rate.
    - Years of warranty.
    - Economic value (€ /seat during the expected life-cycle).

Other aspects which were taken into account were the costs of fitting 10 trainsets with the French signalling system TVM, as well as their safety and operations approval by the French Railway Security Agency (EPSF). The train's exploitation readiness was also an asset for the customer in this offer.

Bibliography

[BOE, 2015] BOE (2015). Anuncio 35996 del BOE núm. 286 de 2015. *Boletin Oficial del Estado*, (286). Published: Online publication on the official journal. (Cited on page I.)

[Rodríguez, 2016] Rodríguez, A. (2016). Informe: nuevo tren de alta velocidad. *Revista Vía Libre*, None(613):3–28. (Cited on page IV.)

Appendix B

Great Deformations and Hyperelasticity

The content of this second appendix develops in a more detailed manner the formal frame of the continuum mechanics and the study of great deformations, which has been introduced on Chapter 3. The study of the mechanical behaviour of rubbery compounds had a strong complexity from its very beginnings. The strongly non-linear material behaviour plus the high-strain levels under loading demanded a combination of existing formalisms (*mechanics formalisms* and (*thermodicanical approach*)) plus a series of new theories to describe the material's constitutive laws (the *hyperelastic models*). Thorough descriptions of the *mechanics formalisms* regarding with great deformations by Sidoroff [Sidoroff, 1982] and Holzapfel [Holzapfel, 2000] provide a deeper insight on the issue to the reader. The academic works from Méo [Méo, 2000] or Lejeunes [Lejeunes, 2006] have addressed these aspects extensively. The following paragraphs intend to present the main aspects regarding the study of hyperelasticity on the various aspects cited above.

B.1 Great deformations in continuum mechanics

The mechanical description of a large strain problem is addressed as part of the description of the solids' mechanics. Be it a solid body Ω, on a reference configuration C_0, undergoing a transformation yielding a body Ω'. The global motion of the body can be described by mean of the the function $\vec{x}(x,t)$. Taking the undeformed metric $\vec{X}$, the transformation is expressed by means of a displacement vector $\vec{u}(x,t)$ (Equation B.1). Therefore, the configuration can be regarded from two reference frames: the original, undeformed configuration (*Lagrangian description*) or the modified configuration (*Eulerian description*). The transformation around a local point can be described by means of the *gradient tensor* (Equation B.2). The tensor $\bar{\bar{F}}$ yields as well the passage from the former reference to the latter, linking effectively both reference frames (Equation B.3).

Because of its definition, $\bar{\bar{F}}$ does not belong to the original configuration, nor to the deformed configuration, but to a *mixed configuration*, in-between both states. As a useful result, the gradient tensor can be used to describe the changes of volume on the material, J, its determinant being the volume change (Equation B.4) of the material (its value equals 1 for incompressible materials such as rubbers).

$$\vec{x}(x,t) = \vec{X} + \vec{u}(X,t) \tag{B.1}$$

$$\bar{\bar{F}} = \frac{\partial \vec{x}}{\partial \vec{X}} \tag{B.2}$$

$$\vec{x} = \bar{\bar{F}}\vec{X} \tag{B.3}$$

$$J = \det(\bar{\bar{F}}) > 0 \tag{B.4}$$

Measuring the deformations endured by the material depends on the chosen configuration reference. The measure is given by the *scalar product* of the displacements, observed on each reference frame. Therefore, the Lagrangian representation in Equation B.5 has associated the right Cauchy-Green tensor $\bar{\bar{C}}$ as a metrics of the changes endured by the material, plus the Green-Lagrange tensor $\bar{\bar{E}}$ as a metrics of the deformation in an more "engineering sense" (Equation B.8). Equivalently, the Eulerian representation given by Equation B.10 gives the measure of the deformation at the current configuration, with the Euler-Almansi tensor yielding the metrics of the deformation (Equation B.12).

$$\begin{aligned} d\vec{x} \cdot d\vec{x} &= \bar{\bar{F}}d\vec{X} \cdot \bar{\bar{F}}d\vec{X} \\ &= d\vec{X} \cdot \bar{\bar{F}}^T\bar{\bar{F}}d\vec{X} \\ &= d\vec{X} \cdot \bar{\bar{C}}d\vec{X} \end{aligned} \tag{B.5}$$

$$\bar{\bar{C}} = \bar{\bar{F}}^T\bar{\bar{F}} \tag{B.6}$$

$$d\vec{x} \cdot d\vec{x} - d\vec{X} \cdot d\vec{X} = 2d\vec{X}\bar{\bar{E}}d\vec{X} \tag{B.7}$$

$$\bar{\bar{E}} = \frac{1}{2}(\bar{\bar{C}} - \bar{\bar{I}}) \tag{B.8}$$

$$\begin{aligned} d\vec{X} \cdot d\vec{X} =& \bar{\bar{F}}^{-1} d\vec{x} \cdot \bar{\bar{F}}^{-1} d\vec{x} \\ & d\vec{x} \cdot \bar{\bar{F}}^{T} \bar{\bar{F}} d\vec{x} \\ & d\vec{X} \cdot \bar{\bar{B}}^{-1} d\vec{X} \end{aligned} \tag{B.9}$$

$$\bar{\bar{B}} = \bar{\bar{F}} \bar{\bar{F}}^{T} \tag{B.10}$$

$$d\vec{x} \cdot d\vec{x} - d\vec{X} \cdot d\vec{X} = 2 d\vec{x} \bar{\bar{A}} d\vec{x} \tag{B.11}$$

$$\bar{\bar{A}} = \frac{1}{2} (\bar{\bar{I}} - \bar{\bar{B}}^{-1}) \tag{B.12}$$

The description of the efforts and stresses takes a similar dualism with respect to the reference frames. Should a body Ω undergo a transformation leading to a deformed body Ω', one can represent the stresses on a point of the surface by the stress vector $\vec{s}$, obtained from the Equation B.14 where $\bar{\bar{\sigma}}$ is the *Cauchy stress tensor*, which arises from the classic definition in continuous mechanics and is symmetric. The definition of the stress state at the current state with respect to the initial configuration (Equation B.15) yields an intermediate tensor, the *1^{st} Piola-Kirchhoff stress tensor* (PK1), which does not belong to neither of the configurations and is not symmetric. Transporting the vector $d\vec{f}$ to the reference configuration one can obtain the *2^{nd} Piola-Kirchhoff stress tensor* (PK2), $\bar{\bar{S}}$, which is, as the Cauchy stress tensor, symmetric. From all of these, only the two first tensors, Cauchy and 1^{st} Piola-Kirchhoff, define the actual efforts over the material and are therefore useful on the definition of the mechanical problem.

$$\vec{s} = \frac{d\vec{f}}{dS} \tag{B.13}$$

$$d\vec{f} = \bar{\bar{\sigma}} \vec{n} dS \tag{B.14}$$

$$d\vec{f} = \bar{\bar{\Pi}} \vec{n} dS_0 \tag{B.15}$$

$$d\vec{f_0} = \bar{\bar{F}}^{-1} d\vec{f} \tag{B.16}$$

$$\bar{\bar{F}}^{-1} \bar{\bar{\Pi}} \vec{n} dS_0 \tag{B.17}$$

$$\bar{\bar{S}} \vec{n} dS_0 \tag{B.18}$$

The definition of a constitutive relation between the deformations observed on the material and the applied efforts can be done, consequently, under three different reference frames. However, it appears necessary that such a relation should be independent of the observer's point of view, i.e. *objective*. Therefore, the law's constituent metrics will necessarily be objective as well. For instance, the objective metrics related to the current/transformed configuration are $\bar{\bar{S}}$ and $\bar{\bar{E}}$, which would be suitable to define a constitutive relation *on the current/actualized configuration* solely. Furthermore, the material's characteristics such as the (an)isotropy need to be taken into account as well. The tensors describing an isotropic material belong to the class of *orthogonal tensors*, which are invariant with respect to the rotation of the reference frame. Consequently, the behaviour law involving the tensors will be invariant as well. A further step into determining a set of objective metrics to describe the rubber's behaviour involves the mathematical *invariants of the deformation tensors*. Two-dimensional tensors have three associated metrics, whose expressions are given by Equations B.21 ($\bar{\bar{X}} = \bar{\bar{B}}$ *or* $\bar{\bar{C}}$) and which remain unchanged regardless of the chosen reference. This specific property makes them interesting to study the material's behaviour.

$$I_1(\bar{\bar{X}}) = tr(\bar{\bar{X}}) \tag{B.19}$$

$$I_2(\bar{\bar{X}}) = \frac{1}{2}(tr(\bar{\bar{X}})^2 - tr(\bar{\bar{X}}^2)) \tag{B.20}$$

$$I_3(\bar{\bar{X}}) = \det \bar{\bar{X}} \tag{B.21}$$

B.2 Hyperelastic models

The formal frame for the analysis of a hyperelastic material involves the thermodynamics of continuum solids. Within its postulates, it defines the *first and second* principles of thermodynamics. The addition of Helmholtz's Free Energy function combined with both principles yields the *Clausius-Duhem inequality*, which states the nullity or positivity of the dissipation of energy within the material. The inequality relates the mechanical work within the material with the dissipative and thermal effects and can be written for each of the reference frames discussed previously (Equations B.24) [Boukamel, 2006].

$$\Phi = \bar{\bar{\sigma}} : \bar{\bar{D}} - \rho(\dot{\psi} + s\dot{T}) - \frac{1}{T}\vec{q} \cdot \vec{grad}_x T \geq 0 \quad \text{Eulerian configuration} \tag{B.22}$$

$$\Phi_0 = \bar{\bar{\Pi}} : \dot{\bar{\bar{F}}} - \rho_0(\dot{\psi} + s\dot{T}) - \frac{1}{T}\vec{q} \cdot \vec{grad}_X T \geq 0 \quad \text{Intermediate configuration} \tag{B.23}$$

$$\Phi_0 = \bar{\bar{S}} : \dot{\bar{\bar{E}}} - \rho_0(\dot{\psi} + s\dot{T}) - \frac{1}{T}\vec{q} \cdot \vec{grad}_X T \geq 0 \quad \text{Lagrangian configuration} \tag{B.24}$$

Hyperelastic environments are a specific case of non-linear elasticity which are characterised by the material having a reference configuration which is free of stress, an absence of energy dissipation and the material's behaviour being described by a specific free energy density function which is dependent on the material's strains and temperatures [Boukamel, 2006]. Under such conditions, the inequality of Clausius-Duhem (Equations B.24) can be rewritten without its dissipative terms, thus yielding the Equation B.27.

$$\Phi = \bar{\bar{\sigma}} : \bar{\bar{D}} - \rho\dot{\psi} = (\bar{\bar{\sigma}} - 2\rho\bar{\bar{B}}\frac{\partial\psi}{\partial\bar{\bar{B}}}) : \bar{\bar{D}} = 0 \quad \text{Eulerian configuration} \tag{B.25}$$

$$\Phi_0 = \bar{\bar{\Pi}} : \dot{\bar{\bar{F}}} - \rho_0\dot{\psi} = (\bar{\bar{\Pi}} - \rho_0\frac{\partial\psi}{\partial\bar{\bar{F}}}) : \dot{\bar{\bar{F}}} = 0 \quad \text{Intermediate configuration} \tag{B.26}$$

$$\Phi_0 = \bar{\bar{S}} : \dot{\bar{\bar{E}}} - \rho_0\dot{\psi} = (\bar{\bar{S}} - \rho_0\frac{\partial\psi}{\partial\bar{\bar{E}}}) : \dot{\bar{\bar{E}}} = 0 \quad \text{Lagrangian configuration} \tag{B.27}$$

If one takes the *energy's density function* $\mathcal{W} = \rho_0\psi$, the expressions of the constitutive relation between the metrics for deformations and stresses can be written in their generalized forms given on Equations B.30. Nevertheless, the formulation of the hyperelastic behaviour law is not yet complete, as further considerations must be taken into account. Rubbery materials are generally considered as *incompressible* (i.e. the efforts engaged to changes their volume are tremendous compared to any other deformation modes [Sidoroff, 1982]). The incompressibility condition is translated by the Equation B.4 being equal to 1, which in turn imposes a condition on the *deformation rate tensors*, $\bar{\bar{D}}$ and $\dot{\bar{\bar{E}}}$, that $D_{ii} = 0$. On the current configuration, the latter condition adds a *spheric part* to the stress tensor, which is modulated by an arbitrary parameter "p", associated to the *hydrostatic pressure*. The condition is transportable to the intermediate and initial configurations, yielding the three equalities in Equation B.33. The *deviatoric part* of the stress tensor is thus defined by the material properties, while the *spheric part* with the hydrostatic pressure is obtained from the particular boundary conditions on each configuration.

$$\bar{\bar{\sigma}} = 2\bar{\bar{B}}\frac{\partial\mathcal{W}}{\partial\bar{\bar{B}}} \quad \text{Eulerian configuration} \tag{B.28}$$

$$\bar{\bar{\Pi}} = \frac{\partial\mathcal{W}}{\partial\bar{\bar{F}}} \quad \text{Intermediate configuration} \tag{B.29}$$

$$\bar{\bar{S}} = \frac{\partial\mathcal{W}}{\partial\bar{\bar{E}}} \quad \text{Lagrangian configuration} \tag{B.30}$$

$$\bar{\bar{\sigma}} = 2\bar{\bar{B}}\frac{\partial \mathcal{W}}{\partial \bar{\bar{B}}} - p\bar{\bar{I}} \quad \text{Eulerian configuration} \tag{B.31}$$

$$\bar{\bar{\Pi}} = \frac{\partial \mathcal{W}}{\partial \bar{\bar{F}}} - pCof\bar{\bar{F}} \quad \text{Intermediate configuration} \tag{B.32}$$

$$\bar{\bar{S}} = \frac{\partial \mathcal{W}}{\partial \bar{\bar{E}}} - pJ\bar{\bar{C}}^{-1} \quad \text{Lagrangian configuration} \tag{B.33}$$

Bibliography

[Boukamel, 2006] Boukamel, A. (2006). Modélisations mécaniques et numériques des matériaux et structures en élastomères. Memoire d'habilitation à diriger des recherches, Université de la Méditerranée - Aix-Marseille II. (Cited on pages iv, v, 49, 55, 65, X and XI.)

[Holzapfel, 2000] Holzapfel, G. (2000). *Nonlinear Solid Mechanics : A Continuum Approach for Engineering / G.A. Holzapfel.* John Wiley & Sons, Chichester. (Cited on pages iv, 64 and VII.)

[Lejeunes, 2006] Lejeunes, S. (2006). *Modélisation de structures lamifiées élastomère-métal à l'aide d'une méthode de réduction de modèles.* PhD thesis, Université de la Méditerranée - Aix-Marseille II. (Cited on pages iv, 49, 58, 64, 67, 85 and VII.)

[Méo, 2000] Méo, S. (2000). *Modélisation numérique du comportement mécanique de structures en élastomère : de l'élasticité à la thermo-visco-hyperélasticité.* PhD thesis, Université de la Méditerranée - Aix-Marseille II. (Cited on pages 64 and VII.)

[Sidoroff, 1982] Sidoroff, F. (1982). Cours sur "Les Grandes Déformations". (Cited on pages iv, 64, 65, VII and XI.)

Prise en compte de la variabilité des caractéristiques de suspension d'un bogie pour l'optimisation des opérations de maintenance

Résumé: La réduction des coûts de maintenance est l'un des enjeux majeurs auquel doit faire face l'industrie ferroviaire pour rester concurrentielle. Parmi les organes de suspension nécessitant un entretien périodique fréquent, les éléments à base métal-caoutchouc jouent un rôle clé dans le fonctionnement du bogie. Les variations des propriétés mécaniques de ces éléments sont étudiées au travers de techniques de vieillissement accéléré pour représenter leur comportement tout au long du cycle de vie. Par ailleurs, des outils de description des variabilités observées sont proposés afin d'établir une stratégie de simulations dynamiques en considérant différents modèles d'un matériel roulant homologué. L'objectif est de quantifier leurs effets sur des indicateurs sécuritaires préconisés par les normes du secteur ferroviaire. Finalement, cette étude permet de justifier la pertinence d'une stratégie d'allongement de cycle de vie en maintenant le niveau de sécurité inhérent au matériel roulant ferroviaire.
Mots-clés: Suspension de bogie, vieillissement élastomère, variabilité, sécurité dynamique.

A consideration of the variability on the characteristics of a bogie's suspension elements, towards the optimisation of maintenance operations

Abstract: The reduction of maintenance costs is a key stake for the competitivity of railway rolling stock manufacturers. The optimization of maintenance operations can be addressed by less, better-planned overhaul operations, through an increase of the life-cycle of some components. Among the most frequently checked suspension organs, rubber-to-metal elements have a key role on the bogie performance. The change on the mechanical properties of these elements are studied by accelerated ageing techniques, so as to represent their behaviour throughout their lifecycle. Several hyper-elastic laws, associated with the characterization of the rubber ageing, have been proposed in these works. These models have been used to simulate the behaviour of the real components. Hence, a set of tools describing the variability observed on the parts is proposed, allowing the design of a strategy for dynamics simulations considering several models of an already approved rolling stock model. The aim is to quantify the variability effect on the safety indexes demanded by standard norms. Finally, this study justifies the pertinence of a strategy aiming life-cycle extensions while ensuring the intrinsic safety levels required on railway rolling stock.
Keywords: Bogie suspension, elastomer ageing, variability, safety dynamics.